2001

Molecular organization and mixing in thin solid films of novel perylene tetracarboxylic dianhydride derivatives: Infrared and surface enhanced Raman studies.

Alicia Patricia. Kam
University of Windsor

INFORMATION TO USERS

This manuscript has been reproduced from the microfilm master. UMI films the text directly from the original or copy submitted. Thus, some thesis and dissertation copies are in typewriter face, while others may be from any type of computer printer.

The quality of this reproduction is dependent upon the quality of the copy submitted. Broken or indistinct print, colored or poor quality illustrations and photographs, print bleedthrough, substandard margins, and improper alignment can adversely affect reproduction.

In the unlikely event that the author did not send UMI a complete manuscript and there are missing pages, these will be noted. Also, if unauthorized copyright material had to be removed, a note will indicate the deletion.

Oversize materials (e.g., maps, drawings, charts) are reproduced by sectioning the original, beginning at the upper left-hand corner and continuing from left to right in equal sections with small overlaps.

Photographs included in the original manuscript have been reproduced xerographically in this copy. Higher quality 6" x 9" black and white photographic prints are available for any photographs or illustrations appearing in this copy for an additional charge. Contact UMI directly to order.

ProQuest Information and Learning
300 North Zeeb Road, Ann Arbor, MI 48106-1346 USA
800-521-0600

MOLECULAR ORGANIZATION AND MIXING IN THIN SOLID FILMS OF NOVEL PERYLENE TETRACARBOXYLIC DIANHYDRIDE DERIVATIVES. INFRARED AND SURFACE ENHANCED RAMAN STUDIES.

BY

ALICIA PATRICIA KAM

A Dissertation
Submitted to the Faculty of Graduate Studies and Research through the
School of Physical Sciences in partial fulfillment of the
requirements for the Degree of Doctor of Philosophy at
The University of Windsor.

Windsor, Ontario, Canada
2001

National Library of Canada
Acquisitions and Bibliographic Services
395 Wellington Street
Ottawa ON K1A 0N4
Canada

Bibliothèque nationale du Canada
Acquisitions et services bibliographiques
395, rue Wellington
Ottawa ON K1A 0N4
Canada

Your file Votre référence

Our file Notre référence

0-612-62324-6

Canada

ABSTRACT

The present work focuses on the fabrication and spectroscopic characterization of submicron thin solid films of novel organic dyes. The synthesis, thin film fabrication, electronic and vibrational spectra of neat materials are described. The main group of organic dyes studied here are novel perylene tetracarboxylic derivatives. The fabrication of thin solid films on a variety of substrates is demonstrated and the long-range molecular organization in the films, extracted using mainly infrared techniques, is illustrated. The starting point in using vibrations as structural probes, is the vibrational assignments of the characteristic perylene tetracarboxylic fundamentals for each dye under study. The assigned vibrational spectra are employed as references to extract the molecular organization in the vacuum evaporated films using data from the complementary techniques: transmission infrared and reflection-absorption infrared spectroscopy. The understanding of the molecular organization opens the door to changing and controlling the molecular film structure with thermal annealing, and these studies are illustrated for bis(n-propylimido) perylene films. It is shown that reorientation can be induced in thin films of bisPTCD dye. The factors that may determine reorientation on thermal annealing are investigated.

Surface-enhanced spectroscopic studies of metal island films coated with the dyes were carried out. The surface-enhanced vibrational spectroscopy (SEVS) used encompasses spectral data obtained from surface-enhanced Raman scattering (SERS), surface-enhanced-resonance Raman scattering (SERRS) and surface-enhanced infrared (SEIR).

The first systematic study of mixed thin solid films of PTDC materials and phthalocyanines, using vacuum co-evaporation, is presented. Mixed films of perylene and phthalocyanine derivatives were fabricated and investigated using SERS, SERRS and SERRS imaging. It is demonstrated that SERRS global imaging is a powerful analytical tool that permits one to distinguish the degree of mixing in mixed films using 1 mW of laser power at the sample. For the first time, global images of mixed films consisting of PTCD and ClInPc, ClGaPc, CuPc and CoPc are reported. The point to point mapping and wide field imaging of the mixed films permits chemical imaging that shows the average distribution of both perylene and phthalocyanine derivatives. SERRS studies indicate minimal molecular interaction between the phthalocyanine and perylene constituents of the fabricated mixed films.

This thesis is dedicated to Aaron, my parents, and my sisters.
Thanks for your love and support.

ACKNOWLEDGEMENTS

"Discovery consists in seeing what everyone else has seen and thinking what no one else has thought"
- ***Albert Szent-Gyorig***
1937 Nobel Prize in Physiology and Medicine

I wish to extend my sincere gratitude and thank you to Dr. Ricardo Aroca for his support, encouragement and direction during my four years at Windsor. Your insight and patience was very much appreciated.

A special thanks to Dr. Carl Tripp. You have enlightened me in new approaches to research and our inspirational "debates" will always be cherished.

" A teacher affects eternity; he can never tell where his influence stops"
-Henry Brooks Adams

To Dr. Jim Duff and Xerox Research Center of Canada, thank you for the great opportunity you have provided through our extensive research collaborations.

The past and present members of the Materials and Surface Science Group, especially Dr. Bob Berno, Dr. Santiago Rodriguez-Llorente, Dr. Carlos Constantino, Tibebe Lemma and Nik Pieczonka, thanks for the good food, advice, ideas and company. It was a pleasure and an honor working with you.

" The important thing is not to stop questioning. Curiosity has its own reason for existing"
-Albert Einstein (1879-1955)

To Aaron, my family and Samantha: I owe my perseverance in this endeavor to you. Your love and support throughout the years has carried me through both the good and bad times.

THANK YOU!

TABLE OF CONTENTS

List of Figures

List of Tables

List of Abbreviations

AFM: Atomic Force Microscopy

SEVS: Surface Enhanced Vibrational Spectroscopy

RRS: Resonance Raman Spectroscopy

SERS: Surface Enhanced Raman Spectroscopy

SERRS: Surface Enhanced Resonance Raman Spectroscopy

RAIRS: Reflection Absorption Infrared Spectroscopy

LB: Langmuir Blodgett

UHV: Ultra High Vacuum

OTS: octadecyltrichlorosilane

BisPTCD : Bis (n-propylimido)perylene

ThioPTCD: Thio(n-propylimido)perylene

TrithiaPTCD: Bis(n-propylimido)trithiaperylene

2sPTCD : n-propyl- mercaptopropylimido perylene

3sPTCD: n-propyl-3 mercaptopropylimido perylene

2(3s)PTCD: Bis(methyl mercaptopropylimido) perylene

Chapter 1

INTRODUCTION

An overview of the Thesis

1.1. INTRODUCTION

Organic photoconductive materials have, in the last thirty years, enjoyed much scientific attention. This interest comes on the heals of the quest for and harnessing of alternative sources of clean energies, such as solar energy. Though initial attention was focused on inorganic photoconductive materials for solar energy conversion, the advantages of organic materials have been recognized [1]. Solar energy conversion, however, is just one of many potential uses of organic photoconductive materials, others include electrophotography and xerography. Moreover, the vast availability of molecular photoconductive materials, low production costs, immense diversity, lower toxicity as compared to their inorganic counterparts, and the ability to synthetically optimize these materials for a specific set of desired properties has fuelled this interest [2]. Perylene bis-dicarboximides are a type of such organic materials that are also distinguished by a high quantum yield of fluorescence that makes them highly promising materials for dye lasers [3]. Table 1.1 lists a few of the applications for perylene materials.

Table 1.1-1: Applications of perylenes.

Perylene	Applications
Perylene Violet 29 Perylene Red 179 Perylene Red 190 Perylene Red 123 Perylene Red 149 Perylene Red 178 Perylene Red 224	Printing inks and xerography[4] Paints and coatings[4] Pigmentation of plastics[4]
Perylene tetracarboxylic derivatives	Solar cells[5] Electroluminescent devices[6] Photoconductors[2, 7] Dye lasers[3]

The study of the photo physical and electrical properties of organic photoconductors is essential to determining important chemical and physical factors that influence, and in some cases govern, the characteristics of these materials. These factors include molecular structure and solid-state morphology, and it has been generally assumed that the structural order of the material is a determinant factor in the understanding and control of their inherent photo physical and electrical properties [8]. In many cases correlations have been established between the value of a certain property as a function of the degree of molecular orientation, such as the change in photoconduction [1]. Polymorphism is a common occurrence in molecular photoconductors. Polymorphism in perylene pigments [2] and phthalocyanine derivatives [9] has been extensively documented. The formation of different spatial structures is thought to be due to the intermolecular forces between the perylene molecules that may give rise to

molecular stacking arrangements where different minima for the interaction energies are possible [10]. This phenomenon alludes to the fact that thin film properties are a function of phase transformations. The physical properties of the material are strongly dependent on the various types of crystal structures a polymorph may assume.

Thin films of organic photoconductive materials can be fabricated by using a variety of techniques such as chemical vapor deposition, physical vapor deposition and Langmuir Blodgett deposition. Vacuum evaporation is a physical vapor deposition technique used in this thesis to acquire thin molecular films of perylene derivatives. Perylene materials are known to be thermally stable and can be thermally evaporated without chemical or thermal deformation of the starting material. In fact, perylene and phthalocyanine are purified by gradient sublimation technologies. The advantages of the vacuum evaporation technique are: wide adjustability in substrate temperature, access to surface during deposition, and lower contamination. In vapor phase techniques, the deposition is determined by the source, the transport factors and three principal surface factors: substrate surface condition; reactivity of the arrival material and the energy input. The energy input is possibly the most important influencing surface factor and may be applied in situ or post-deposition. These factors determine the structure and composition of the deposited film and in turn the various film properties: optical, electrical, magnetic, chemical, mechanical and thermal [11].

Bis (N-propylimido) perylene, bisPTCD, is a highly conjugated planar structure consisting of a perylene chromophore backbone and two propyl side chains. It is the first in a series of novel perylene monomers studied in the scope of this thesis. This molecule is characterized and analyzed for its potential opto-electronic applications. Moreover it

provides the basis on which similar molecules in this thesis are chemically engineered to facilitate optimization of their chemical and physical properties. The ultimate goal of this research is to enable an educated choice of materials to be used as a platform for a variety of molecular device applications. An array of interesting optical properties result when highly ordered films of perylene molecules are produced with well defined molecular architectures which optimizes the excitonic interactions in excited states of these molecules [12-14]. Thus, the successful manufacture and characterization of thin molecular films of these pigments are essential. The ability to control molecular orientation and morphology of fabricated thin films, and in turn their molecular, physical and chemical properties is fundamental to understanding their potential as well as their limitations. Bulk samples are also characterized to establish a reference point that will enable a comprehensive investigation.

The physical properties and structural stability of thin organic films are dependent on both molecular structure and orientation/morphology. Synthetic routes define molecular structure whereas orientation/morphology are dependent on molecular structure and organization, deposition/processing protocols and other less understood effects. Moreover, changes in morphology of the organic films with time are common and often lead to a drop in device performance and eventually device failure. As such, much emphasis is placed on identifying the factors that induce change on a molecular scale. For example, it is well known that the performance degradation of electroluminescence devices is accelerated at higher operating temperatures [15] and that this can be slowed by encapsulation of the device in a protective coating [16]. Using optical microscopy, it has been shown that both the temperature and encapsulation

dependence correlated with the appearance and growth of crystalline domains in the film arising from humidity induced change in morphology [17]. Furthermore, reflection infrared spectroscopy, *Vida infra*, is used to show that a change in orientation of perylene films occurs with thermal annealing [18]. The infrared study provides the link between molecular detail and morphological changes in these films, which in turn, has been correlated to device performance [19]. As a result, a study into the environmental factors that influence molecular orientation in perylene films and ways of controlling such orientation, such as encapsulation of the thin films, is undertaken in the scope of this thesis.

The ability for molecular orientation to be altered by thermal and vapour annealing is demonstrated. Furthermore, control of molecular orientation via encapsulation is also investigated. Unfortunately, encapsulation has its limitations and may not be appropriate for all molecular systems. Other means of controlling molecular orientation must be sought, as it is the control of both molecular orientation and morphology that enables molecular engineering. In this thesis a chemical modification of the bis (n-propylimido) perylene (Table 1.1-2) is attempted, to form a new class of perylene dyes that contain sulfur atoms attached to the chromophore core: thio-bis (n-propylimido) perylene, thioPTCD, and bis (n-propylimido) trithia perylene, trithiaPTCD (Table 1.1-2). The intention is to anchor the molecule to the surface of the substrate through a silver-sulfur bond. There have been a number of reports involving vibrational characterization of various thiols and the elusive S-metal bond [20-22]. The importance of these investigations has lead to a greater understanding of the molecular packing and orientation of these derivatives in both bulk and thin molecular films. Moreover, these

reports suggest that the control of molecular orientation of thin films may be facilitated. The second aspect of the study of this new class of thio derivatives of bisPTCD includes the physical modelling and the measurement of the properties of the metal-organic interfaces [23-25].

The effect of atom substitution in the perylene chromophore on the optical properties and the ability to form organized thin solid films is investigated. Substituents may provide one path to tuning their optoelectronic and photo physical properties. Optimization of such properties via chemical modification has already enabled the utilization of these materials in various applications: optoelectronic, filters and electroluminescent devices. Though there have been a number of publications on various atom substitutions in perylene derivatives, the impact on sulfur substitution has not been extensively investigated [26], especially substitution in the alkyl chains of perylene. Thus, the effect of molecularly engineering the perylene chromophore to contain a sulfur substituent in its alkyl side chain is investigated. This new class of perylene dyes: N-propylimido -(2-methylmercaptoethylimido) perylene (2sPTCD), N-propylimido -(3-methylmercaptoethylimido) perylene (3sPTCD), and bis (methylmercaptoethylimido) perylene (2(3s)PTCD) (Table 1.1-2), is formed and characterized to complement that of thioPTCD and trithiaPTCD, as potential dyes in which molecular orientation and morphology may be controlled via chemisorption of the dye to the substrate.

The applications of perylene derivatives in mixed molecular films have been well studied. In particular, perylene tetracarboxylic acid (PTCD) dyes and phthalocyanine materials are being tested in thin film devices as thin film molecular semiconductor bilayers [27], or forming organic photovoltaic cells [28]. Several templates for device

manufacture have been presented throughout the past decade. The most successful and efficient has employed perylene derivatives as an n-type semiconductor and phthalocyanine as the opposing p-type semiconductor. The first thin film, two-layered organic molecular system comprising of thin molecular films of metal phthalocyanine and perylene tetracarboxylic acid derivative was reported by C.W. Tang [28]. A similar work utilizing copper phthalocyanine and perylene tetracarboxylic dianhydride and perylene tetracarboxylic bisbenzimidole, in which the current-voltage characteristics of the cell were discussed, was reported by Forrest *et al.* [29]. Several reports were published in the early part of the decade, most of which concentrated on optimizing the conditions presented by Forrest and Tang, by varying the constituents of the cell. J. Danziger *et al.* [30] investigated the electrical properties of the heterojunctions formed between copper phthalocyanine and vanadylphthalocyanine with perylene tertracarboxylic dianhydride. Hiramoto *et al.* [31] reported the first three layered organic solar cell with a photoactive interlayer of codeposited metal free phthalocyanine and a perylene tetracarboxylic derivative (Me-PTC). More recently, characterization of molecular thin films of perylene and phthalocyanine derivatives has been the main focus of research [27, 32-38].

Vibrational spectroscopy provides four observables that may be used to extract physical information from thin molecular films: the resonance band position, the band shape, the selection rules and the band intensity. It is this wealth of information that makes vibrational spectroscopy a unique optical probe for determination of the overall structure, chemical, mechanical and localized intermolecular interactions in thick and submicron thin solid films [39, 40]. In particular, the simple surface polarization selection

rules operating in the specular reflection absorption infrared spectroscopy (RAIRS) have been extensively used to determine the orientation of nanometric organic films thermally deposited on a reflecting metal surface. Transmission and reflection spectroscopic techniques can be used complementarily to enable a definitive account of the molecular orientation of perylene molecules [41, 42].

Surface-enhanced vibrational spectroscopy (SEVS) is presently a well developed branch of Vibrational Spectroscopy and the giant enhancement in Raman cross sections of fundamental vibrations on certain rough metallic surfaces (surface-enhanced Raman scattering-SERS [43]) has proven to produce signals of competitive intensity with fluorescent signals or even stronger [44, 45]. The largest enhancements are found using dyes that, due to their large absorption coefficients in the visible region, provide surface-enhanced resonance Raman (SERRS) under excitation with visible lasers. In this thesis, the first study of codeposited MPc-PTCD mixed films using the methods of surface-enhanced vibrational spectroscopy is presented. The mixing trends associated with co-evaporated mixed films of phthalocyanine and perylene (bisPTCD and thioPTCD) derivatives, in equimolar amounts, as determined using SER(R)S and micro-Raman imaging are also reported. Furthermore, it is demonstrated that SERRS can be successfully used to obtain Raman imaging where irradiance of the sample is 60 W/cm^2 or less. SERRS imaging as applied to phase separation studies is also shown.

This thesis is divided into ten chapters. The first chapter introduces the scope of the thesis. The objectives and justifications are discussed in detail. The second chapter encompasses the techniques and experimental conditions used in this thesis, from properties, synthesis and preparation of the materials to the spectroscopic techniques

employed in the characterization of such materials. The third chapter is a detailed and theoretical description of the spectroscopic technique of reflection absorption infrared spectroscopy (RAIRS) that was one of the primary spectroscopic tools used in this thesis. Chapters 2 and 3 are aided with specific examples of results obtained to enable a more in-depth understanding of the results presented in following chapters, and to avoid repetition.

The results of this thesis are presented in six chapters and each aspect of the work performed is analyzed and discussed within. The characterization, molecular orientation and thermal annealing of thin films of bisPTCD are presented in Chapter 4. Chapter 5 reveals the effect of solvent vapors on molecular orientation of thin films of bisPTCD. The control of molecular orientation via encapsulation is also presented in Chapter 5. The spectroscopic characterization and orientation studies of thin films of thioPTCD and trithiaPTCD are presented in Chapter 6 and the effect of sulfur substitution into the core perylene chromophore on molecular packing and orientation was investigated. Chapter 7 investigates sulfur atom substitution in the alkyl side chains of bisPTCD. Similar to Chapter 6, the spectroscopic characterization and molecular orientation of 2sPTCD, 3sPTCD and 2(3s)PTCD were studied with particular interest in the control of molecular orientation. The fabrication and spectroscopic characterization of vacuum evaporated mixed films of perylene (bisPTCD and thioPTCD) and phthalocyanine derivatives (copper phthalocyanine and cobalt phthalocyanine) are presented in Chapter 8. Chapter 8 emphasizes the homogeneity, or lack of, in PTCD-MPc mixed films. The trends associated with mixed films formed between perylene and phthalocyanine derivatives are revealed in Chapter 9. The following perylene and phthalocyanine derivatives were

utilized in this study: bisPTCD, thioPTCD, chloro indium phthalocyanine, chloro gallium phthalocyanine, cobalt phthalocyanine, copper phthalocyanine, zinc phthalocyanine and metal free phthalocyanine. Surface (enhanced) Raman spectroscopy, electronic studies and Raman imaging provided the tools from which this investigation was accomplished. Chapter 10 reiterates the main conclusions of this thesis.

Table 1.1-2: Names and molecular formula of perylene derivatives studied.

Compound	Formula	Structural Formula
Bis(N-propylimido) perylene **bisPTCD**	$C_{30}H_{22}N_2O_4$ (474.51)	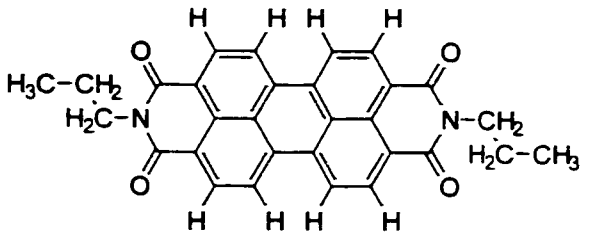
Bis-thio(n-propylimido) perylene, **thioPTCD**	$C_{30}H_{20}N_2O_4S$ (504.56)	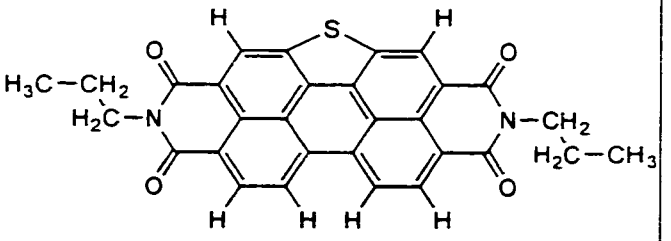
Bis-(N-propylimido)trithia perylene **trithiaPTCD**	$C_{30}H_{18}N_2O_4S_3$ (566.67)	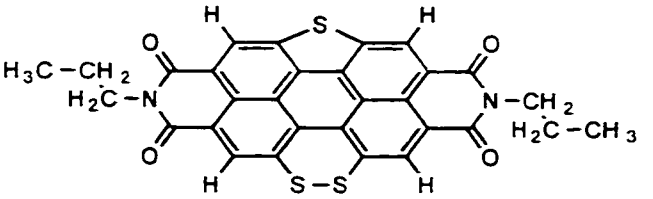
n-propyl-mercaptoethylimido perylene **2sPTCD**	$C_{30}H_{22}N_2O_4S$ (506.57)	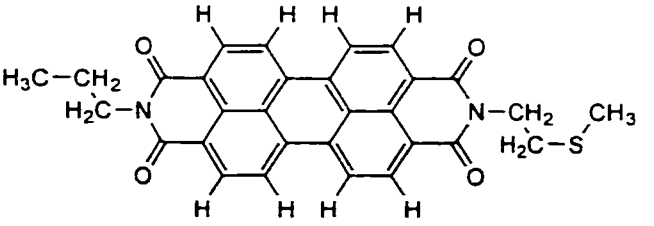

Compound	Formula	Structural Formula
n-propyl-3 mercaptopropylimido perylene **3sPTCD**	$C_{31}H_{24}N_2O_4S$ (520.60)	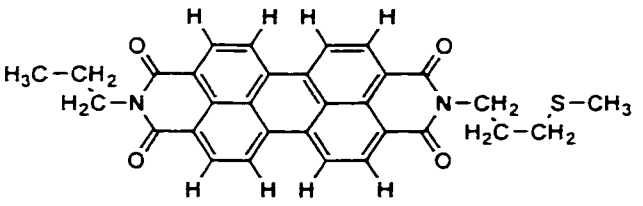
Bis(methyl mercaptopropylimido) perylene **2(3s)PTCD**	$C_{32}H_{26}N_2O_4S_2$ (566.69)	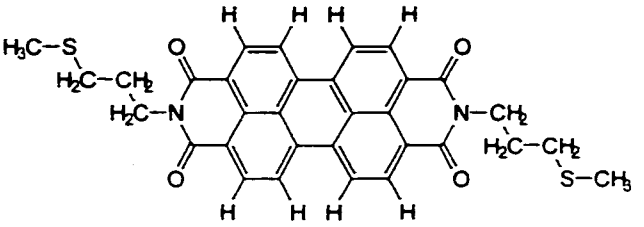

Chapter 2

EXPERIMENTAL AND TECHNIQUES

Description of experimental procedures and instrumentation

2.1. Thin Films

Thin films and thin film technology is an extremely active area of research. The scope of the research in this area is quite remarkable. Applications of thin films range from optics, electronics and microelectronics to mirrors, filters and antireflection coatings. Additional functionality in thin films can be realized by depositing a multilayer of different materials, as such, these materials are influenced by the periodicity in the multilayer rather than their atomic periodicity. The multilayered thin films formed in this fashion can behave as completely newly engineered materials unknown in the bulk form.

The distinguishing factor between bulk material and thin films is the surface-volume ratio. In bulk, the characteristic physical properties are assumed to be volume independent and this assumption is valid as long as it is within macroscopic limits. However, thin films display considerable anomalies in their properties due to the asymmetry of the forces that act upon the surface.

2.2 Thin Film Techniques

Various methods for preparing thin films exist and they can be essentially divided into two main groups: chemical methods and physical methods.

2.2.1 Chemical Methods

Chemical and electrochemical methods consist of several types of deposition which include, but are not limited to, electrolytic deposition, electroless deposition, anodic oxidation, and chemical vapour deposition. However the most important and relevant chemical deposition method to this research is the Langmuir-Blodgett technique, due to its applicability to high molecular weight compounds.

2.2.1.1. Langmuir-Blodgett

In the Langmuir technique a small amount of a high molecular weight substance which has polar functional groups, such as perylene tetracarboxylic derivatives, is dissolved in a volatile solvent and drops of this solution are spread on the surface of water. The monolayer formed in this fashion is then transferred to a solid substrate to form a Langmuir-Blodgett film. In research presented in this thesis, this technique was used as a tool to acquire thin films, to monolayer degrees, of the perylene tetracarboxylic diimide derivatives (PTCDA). Thus, only a brief overview of this method will be given.

2.2.1.2. Monolayer

The surface of a liquid always has excess free energy which is due to the difference in environment between the surface molecules and those in the bulk. In particular, hydrogen-bonding forces in water tend to set up loosely defined networks that will inevitably be modified near the surface. From thermodynamics, the surface tension, γ, of a plane interface is given by:

$$\gamma = \left(\frac{\partial G}{\partial A}\right)_{T,P,n_i}$$

Where G is the Gibbs free energy of the system, A is the surface area, and the temperature, T, pressure, P, and the composition n_i are held constant. The surface tension of water is 73 mNm^{-1} at 20 °C and atmospheric pressure. Thus, due to its high surface tension, water is the preferred subphase used for study of floating monolayers.

A standard monolayer forming material may have two distinct regions in the molecule: a hydrophilic headgroup, which is easily soluble in water, and an insoluble hydrophobic or oleophilic tail. When a solution of this material in a water immiscible

solvent, such as dichloromethane, is placed on a water surface, the solution spreads rapidly to cover the available area. As the solvent evaporates, a monolayer is formed as dictated by the amphiphilic nature of the material.

For large areas per molecule, molecular interactions are small, and the molecules may be regarded as forming a two dimensional gas. Under these conditions the surface monolayer has relatively little effect on the water's surface tension. If a barrier system is used to reduce the area of surface available to the monolayer, the surface tension of the subphase is changed significantly. For a plane surface at equilibrium, the relationship for surface pressure, Π is:

$$\Pi = \gamma_0 - \gamma$$

Where γ_0 is the surface tension in the absence of a monolayer, and γ the value with the monolayer present. Thus the maximum possible surface pressure for a monolayer on a water surface at 20 °C is 73 mNm^{-1}, and normally encountered values are much lower. [46]

2.2.1.3. Isotherms

The most important indicator of the monolayer properties of a material is given by the surface pressure-area isotherm, performed at constant temperature. The most common isotherm mapped is the pseudo equilibrium isotherm, acquired by compressing the film at a constant rate while continuously monitoring the surface pressure. Depending on the materials being studied, repeated compressions and expansions might be necessary to uncover hysterisis and monolayer collapse behavior.

There are many characteristic regions of an isotherm. As the surface area is reduced there is a gradual onset of surface pressure until an approximately horizontal

region is reached. In this region, the hydrophobic part of the molecule is being lifted away. The surface pressure at which this occurs is usually very small due to the weakness of the interaction between the water and the tailgroups. As a result, this portion of the isotherm is often not resolved by the apparatus. This region is followed by a sudden transition to a steep linear slope where compressibility is approximately constant. At a surface area of just over 0.50 nm^2 $molecule^{-1}$, for bisPTCD, there is an abrupt increase in the slope, a result of the transition to an ordered solid-like arrangement of the two-dimensional array of molecules. The compressibility in this region is also constant and thus a linear slope. If this second slope is extrapolated to zero surface pressure, the intercept gives the area per molecule of the material that would be expected for the theoretical state of an uncompressed close-packed layer. Collapse of the monolayer occurs at smaller surface areas and the compressibility approaches infinity. The onset of collapse depends greatly on the past history of the film and the rate at which the film is being compressed. In this type of collapse, the molecular layers are believed to be riding on top of each other and disordered multilayers are being formed [46].

2.2.1.4. Langmuir-Blodgett Deposition

Although the Langmuir-Blodgett (LB) method is one of the classical techniques of surface chemistry, the detailed mechanism by which floating monolayer are transferred to solid substrates is still poorly understood [47]. The molecular interactions involved in the deposition of the first layer may be quite different than those that are responsible for the transfer of subsequent layers. For some materials, film deposition may also be associated with a distinct phase change: from a two dimensional liquid crystalline phase on the water surface, to a closer packed solid crystalline form on the substrate.

The most common LB film deposition is illustrated in Figure 2.2.1.4-1. In this example the substrate is hydrophilic and the first monolayer is transferred as the substrate is raised through the subphase, thus the substrate may be placed in the subphase before the monolayer is spread, or may be lowered in the subphase through the uncompressed monolayer. Subsequently a monolayer is deposited on each traversal of the surface. These stack in a head to head and tail-to-tail configuration, this deposition mode type being referred as the Y-type. However if the substrate is hydrophobic a monolayer will be deposited as it is first lowered into the subphase. A hydrophilic substrate can generate a multilayered structure containing only an odd number of layers, while a hydrophobic substrate generates an even number of monolayer.

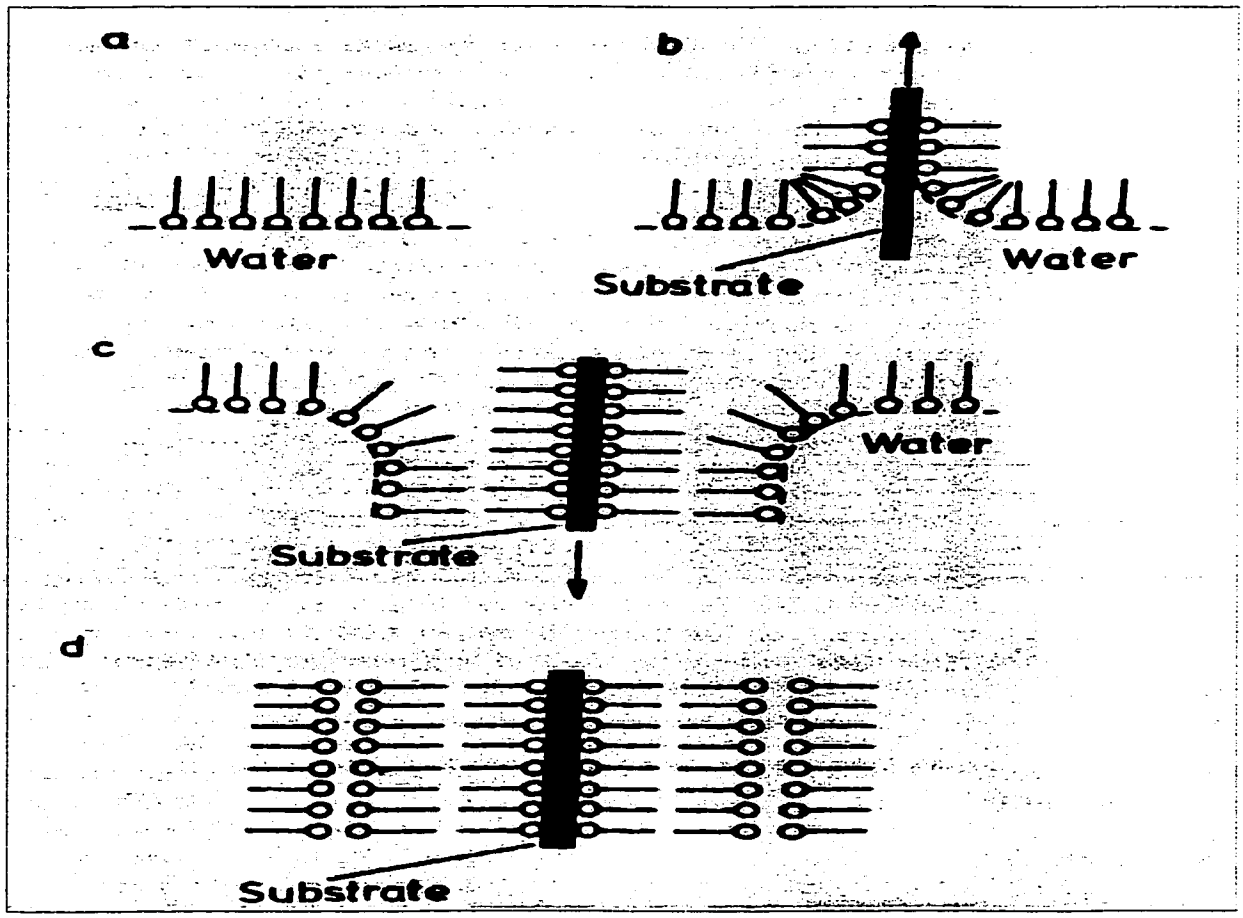

Figure 2.2.1.4-1. : Illustration of the common Y-type LB film deposition

Although Y-type layers are the most easily produced multilayers, monolayers that deposit only as the substrate is being inserted into the subphase or only as the substrate is being removed have been reported. These deposition modes are referred to as X-type and Z-type, respectively. These deposition modes are illustrated in Figure 2.2.1.4-2. . The most relevant type of deposition to this research is the Z-type. There are a number of reports of Z-type deposition, most of which concerned aromatic materials with relatively short or no carbon chains, such as phthalocyanines and perylene tetracarboxylic acid derivatives [48].

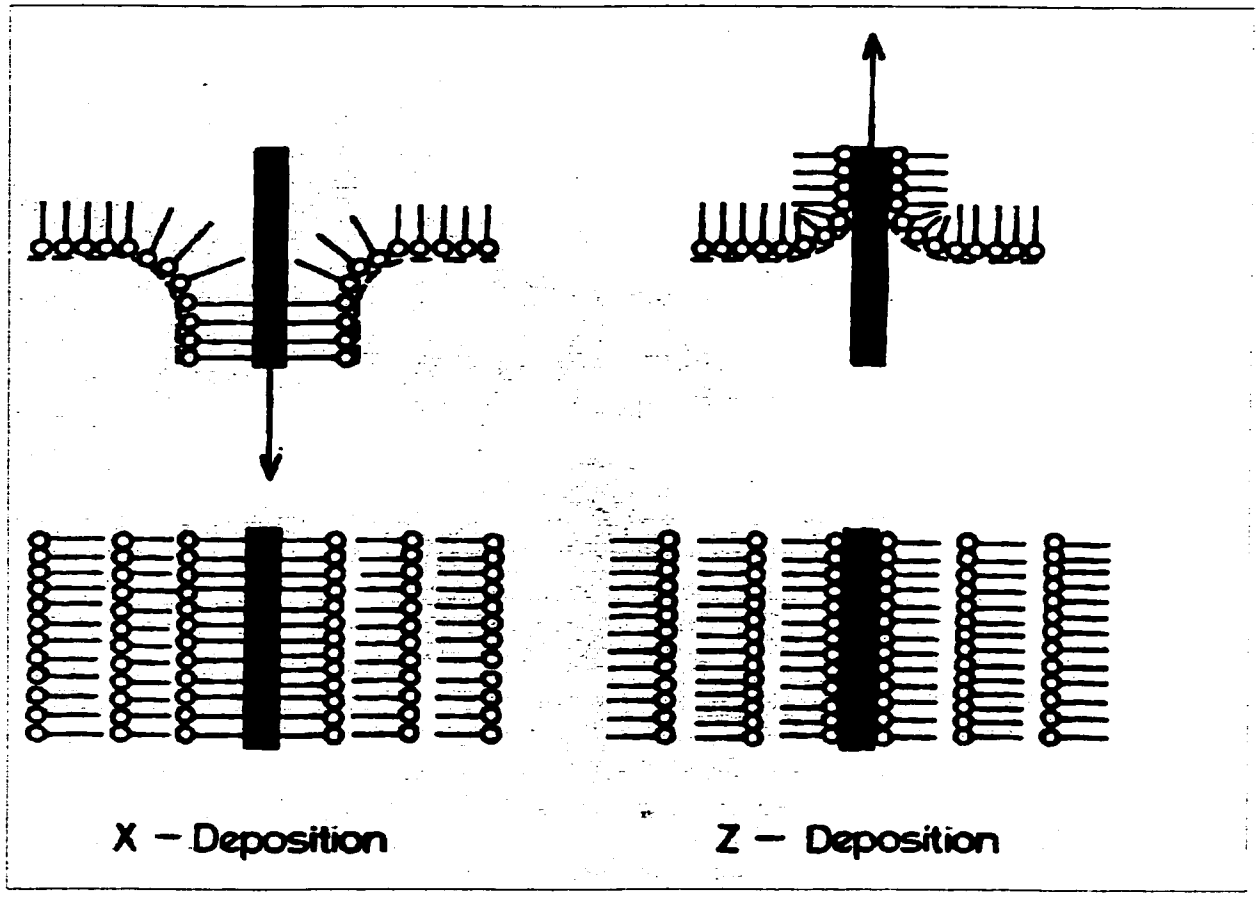

Figure 2.2.1.4-2. : Illustration of X and Z-type deposition.

Film deposition may be characterized by reference to deposition transfer ratio, τ :

$$\tau = \frac{A_L}{A_s}$$

where A_L is the decrease in the area occupied by the monolayer on the water surface, held at constant pressure, and A_S is the coated area of the solid substrate [46].

2.2.1.5. Experimental Apparatus

The apparatus for Langmuir-Blodgett film deposition consists primarily of a trough. A single movable barrier executes the compression of the monolayer and a piston coupled to a low speed electric motor performs the deposition of the monolayer. The surface pressure is constantly monitored with the Langmuir balance.

2.2.1.5.1. Trough

The requirements of a trough material for monolayer studies of film deposition are: the material must be inert, it should be hydrophobic to enable easy cleaning, it should withstand organic solvents and inorganic acids and finally, it should be easily shaped. The work presented in this thesis was done using a trough constructed from polytetrafluoroethylene (PTFE). PTFE is hydrophobic, oleophobic, and resists almost all chemicals. Unfortunately, the materials possess pores that may pick up and slowly release surface active materials. Thus, meticulous cleaning with acetone and deionized water is necessary to avoid contamination.

Furthermore, to reduce factors that may disturb the regular array of molecules in a compact floating monolayer, the trough is isolated. To avoid excessive vibrations that may cause ripples in the subphase, the trough is placed on commercially bought antivibration tables that have four damped pneumatic springs supporting a rigid table top. To reduce air-bound contamination, the trough is enclosed in an in-house clear polyethylene box. Surrounding the subphase with circulating water, in which the

temperature is controlled with a thermostat, minimizes discrepancies due to thermal fluctuations [46].

2.2.1.5.2. Barrier

In this thesis, a single movable barrier is used in the compression of the formed monolayers. In troughs of this type, the container that holds the subphase forms an integral part of the boundary of the compression system, thus a good seal is required between the edges of the trough and the movable barrier. The barrier is moved via a gearing system to an electric motor to enable compression [46].

2.2.1.5.3. Langmuir Balance

The surface pressure is measured using the Langmuir balance. This is a differential technique with a sensitivity in the 10^{-3} mNm^{-1} range [49]. A clean portion of the subphase surface is separated from the monolayer-covered area by a partition and the force acting on this is measured. The partition usually consists of a movable float connected to a conventional balance with which the magnitude of the force is determined. A PTFE float is used connected by thin PTFE foils to the edges of the trough, in order to prevent leakage. Torsion systems are used extensively for the measurement of forces in Langmuir film balances. The force due to film packing displaces the float until the reaction force of a flat spring is equal. This displacement of the float is usually very small. It is then measured using a displacement transducer.

2.2.1.5.4. Deposition Components

The movement of the substrate into and out of the air-monolayer surface is accomplished by using a dipping mechanism. This is constructed from a driving arm and a slave arm or piston rotating through a common axis. The driving arm is controlled by a

motor-sensor system, and the slave arm is guided by the driving arm but remains free for large manual displacements. The speed of dipping was normally set at 0.5mm/min. The dipping speed and the displacement distance, as well as the number of monolayers required, were controlled by the Lauda lift [50-52]. The usual method for monitoring the deposition process of an LB film is the plot of area as a function of time.

2.2.1.6. Langmuir Blodgett Experimental

Meticulous attention to experimental detail is necessary for all monolayer and LB film work. This requires frequent and thorough cleaning for all components; especially before a new monolayer material is to be used. Careful calibration is also important to ensure the precision of the mechanical arrangements of the barrier and the dipping device.

The Lauda trough and the barrier were thoroughly cleaned with deionized water, with a specific resistance of 18.2 MΩm, acquired from the Millipore system. The system was then cleaned with acetone. These steps were repeated approximately three times before the system was finally flushed with deionized water and wiped dry with Kimwipes. The trough was then refilled with deionized water and the barrier calibrated for its movements.

The monolayer forming material, in particular thioPTCD and trithiaPTCD, was dissolved in a solution of 90% HPLC grade dichloromethane and 10% spectroscopic grade trifluoroacetic acid from Aldrich. This solution (10^{-3} – 10^{-4} M) was then carefully spread in small droplets over the trough, via a micro syringe held a few centimeters away from the surface of the aqueous subphase, until a fixed number of molecules was spread. Milli-Q purified water with a measured resistivity of 18.2 MΩ/cm was used as the

subphase. The spread solution was then left for approximately thirty minutes so that the solvent evaporated. Once the solvent had evaporated, compression of the monolayer began.

The surface pressure-area isotherm of the PTCD derivatives was recorded by compressing the trough area at 19.5 cm^2/min. The preparation of floating monolayers at the air-water interface was successful and reproducible isotherms were recorded at 15 °C where the area/molecule extrapolated to zero surface pressure was found to be ca. 0.50 nm^2. LB films were transferred to a variety of substrates in order to explore the surface enhanced vibrational phenomena. The LB monolayers of PTCD derivatives were prepared at 15 °C through z-deposition in a Lauda Langmuir film balance Film. Transfer pressure was 25 mN/m and transfer ratios were all near unity.

2.2.2. Physical Vapour Deposition

The most widely adopted methods of preparation of thin films remain the physical methods such as vacuum deposition. Vacuum deposition has several main advantages over chemical techniques, including applicability to any substance, high purity, in some circumstances preselected structure, variable substrate temperature and access to the surface during deposition. The process of film formation by vacuum deposition consists of several physical stages:

1. transformation of the material to be deposited by evaporation or sublimation into the gaseous state;
2. transfer of atoms from the evaporation source to the substrate;
3. deposition of these particles on the substrate;

4. their rearrangement or modifications of their binding on the surface of the substrate.

Subsequently, the film may be annealed during deposition or post-deposition either to activate grain growth, alter stoichiometry, introduce dopants or cause oxidation.

Analysis of the films lends insight into the deposition process and is often used to evaluate the process. The results of the analysis may then be used to adjust the conditions of the other steps for film property modification.

In physical vapour deposition, the source of the film forming material is a solid, which needs to be vaporized so that it may be transported to the substrate. This may be accomplished by heat or by an energetic beam of electrons, photons or positive ions. The supply rate and contamination of the source are important concerns. The supply rate is important because film properties are influenced by both deposition rate and the ratio in which the particles are supplied to the films. The possibility of contamination, however, extends far beyond the source and are also issues in both transportation and deposition processes.

The major concern in the transport step is the uniformity of the arrival rate over the substrate area. In a high vacuum system, molecules travel from the source to the substrate in straight lines, and the uniformity is controlled for the most part by the geometrical configuration of the system. The deposition step, on the other hand, is determined by both source and transport factors, together with the conditions at the deposition surface. There are three principal surface factors which determine the deposition behavior:

1. substrate surface condition, which includes roughness, level of contamination, degree of chemical bonding with arriving material, and crystallographic parameters in the case of epitaxy;
2. reactivity of the arriving material, i.e. the probability of arriving molecules reacting with the surface and becoming incorporated into the film, also know as the sticking coefficient;
3. energy input to the surface, mainly influenced by substrate temperature, has a profound effect on both the reactivity of arriving material and on the composition and structure of the film.

These three factors work together to determine the structure and composition of the deposited film. This means that for the formation of films with reproducible properties, it is necessary that these parameters be constant and measurable. As a result monitoring is important at all steps in the thin film process [53].

2.2.2.1. Thin Film Evaporation Apparatus

A schematic diagram of a typical vacuum system for thin film deposition is shown in Figure 2.2.2.1-1

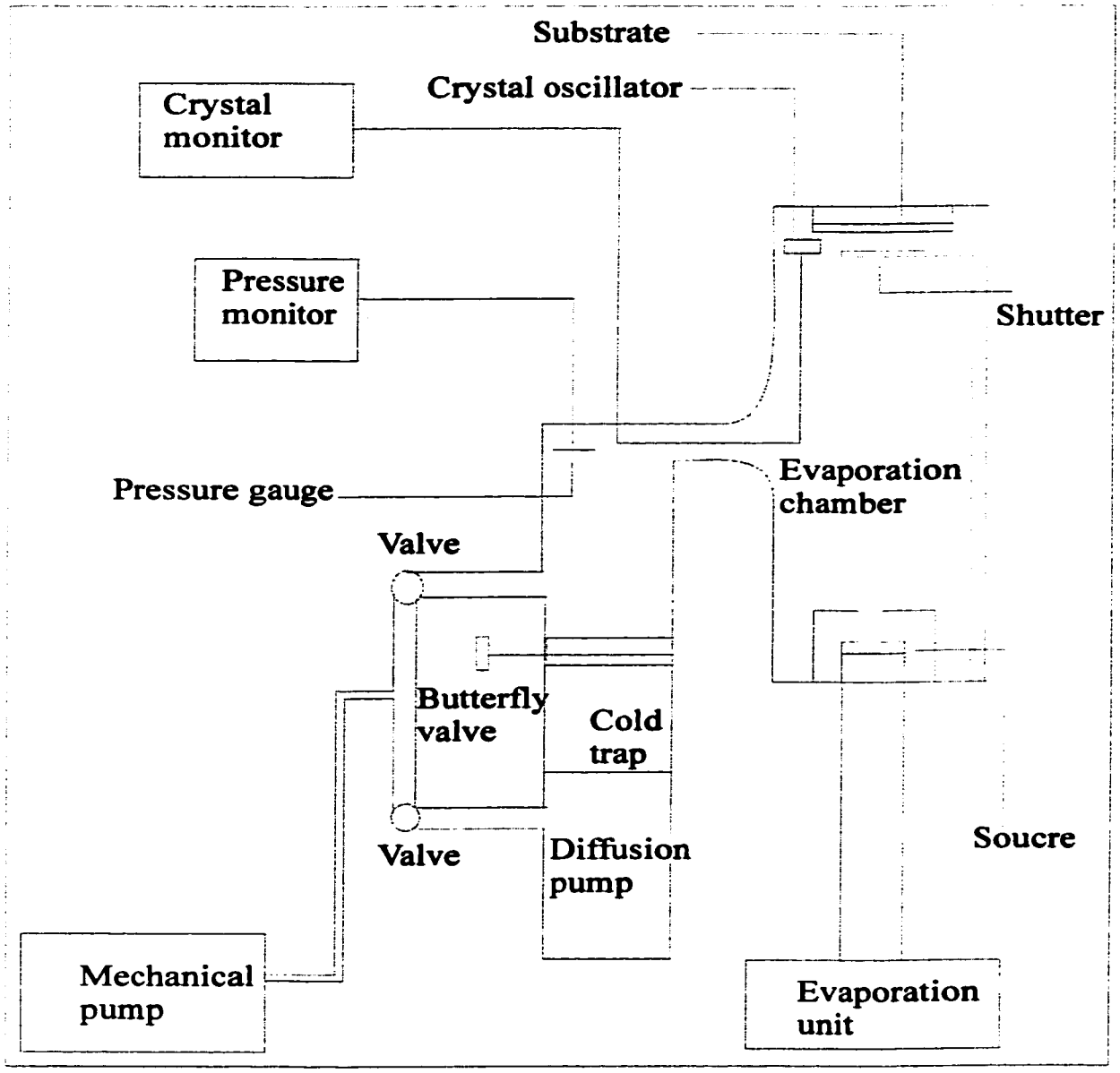

Figure 2.2.2.1-1: An illustration of a typical evaporation system.

In determining the components needed in making vacuum evaporation systems, some special requirements must be met and should be considered. They are as follows:

1) Sufficiently low threshold pressure.

2) Sufficiently fast achievement of threshold pressure from atmospheric.

3) Working chamber uncontaminated by organic vapors.

4) Spacious and easily accessible working chamber.

2.2.2.1.1. Pump Selection and Threshold Pressure

The first two requirements necessitate the use of high vacuum pumps with sufficient pumping speeds and the shortest and widest possible connecting tubing between the pump and the exhausted space. The most widely used, and that used in this research, are metal-oil-diffusion pumps, in particular the Edwards diffusion pump, with a high-quality mineral oil as a working fluid, pre-exhausted by the Edwards E2M2 rotary vacuum pump. The penetration of oil vapors into the working chamber is prevented by insertion of suitable traps, baffles cooled by water or liquid nitrogen, above the pump. By placing a valve between the pump and the exhausted chamber the working cycle can be shortened, especially when there is a direct by-pass, but only at the price of increased vacuum resistance and thus lowered pumping speed.

Low threshold pressures may be achieved by sufficient tightness of the system and the use of low-vapour pressure materials that can be degassed, the best construction material being stainless steel. In ordinary apparatus, such as that of the system used in this research, rubber or silicon rubber gaskets are used. In a more demanding apparatus the seals are made from Vitron, which can be degassed at temperatures up to 150 °C; in ultrahigh vacuum apparatus only metal seals should be used.

2.2.2.1.2. Pressure Measurement

Both the diffusion and roughing mechanical pump can achieve the consistent high level of vacuum in the process chamber as required by this research. This vacuum pressure may be measured by various vacuum gauges. However, the most relevant to this research is the Balzers TPR 010 Pirani gauge that was used to measure the vacuum created by the roughing pump. These gauges are simple and inexpensive instruments.

Their operation is based on heat removal by the gas. The gauge consists of a resistive wire that has a constant current flowing through it. This wire heats up and its temperature is monitored as a millivolt reading on the thermocouple attached to it. When no gas is present, the wires reach a steady state temperature that is determined by radiative heat loss and by conduction through the wires. These gauges, however, have their limitations, which include nonlinearity and calibration dependence on gas composition. Lower vacuum pressures as attained in the process chamber, were measured by using a Balzers IKR 020 cold cathode ion gauge. Here, the pressures are measured by ionizing the gas and measuring the collected ion current, which is proportional to gas concentration.

2.2.2.1.3. Contamination

Contamination of the system may arise from many factors, as aforementioned, and can be introduced in all steps of the deposition process: source, transport, and deposition. Contamination of the substrate, before placement into the evaporation system, was limited for the most part by cleaning with analytical grade ethanol and drying under a continuous flow of nitrogen gas. Two distinguishable evaporation systems were used to further contain impurities. One was specifically used for metal evaporation and the other for organic materials. In the closed system, however, contaminants may enter the vapour environment between the source and the substrate. They absorb on the substrate before film deposition commences and mix with the transporting source material during deposition. Their reduction requires good vacuum practice. The main sources that contribute to contamination of the process vapour environment are: oil backstreaming from the pumps, gas evolution from the chamber materials, and dust stirred from surfaces.

Oil backstreaming into the process chamber can occur whenever oil is used as the pump operating fluid or lubricant. The rate at which this occurs is higher than predicted, since such pumps usually run hot and thereby increase the vapour pressure of the oil. Backstreaming occurs because oil molecules bounce freely backward, from the oil diffusion pump, toward the process chamber without encountering any resistance from countercurrent gas flow. This may be corrected and reduced if a baffle, or trap, is placed in the tube connecting the diffusion pump to the process chamber. This baffle must allow no line of sight path for an oil molecule through it, without at least encountering one surface. The trap is cooled with liquid nitrogen so that the oil condenses and stays there. Another precautionary measure is the use of a valve to block off the diffusion pump from the process chamber, in the advent that the trap is warmed. In this research, both the roughing mechanical pump and the diffusion pump were separated from the process chamber by a valve. The diffusion pump used had a liquid nitrogen cooled trap.

Out gassing of the process chamber material occurs constantly. Contributions to the out gassing contaminants come from both the surface and bulk. The two main surface contaminants are water and oil, due to exposure from air and excessive handling, such as machine shop work and personal handling. In the bulk, such as process containment materials: elastomers and polymers, the most common contaminants are water, solvent vapors and oxygen. A typical and noteworthy example of bulk out gassing is that of the elastomer O-ring. O-ring seals, used in vacuum evaporation systems, are always in contact with the atmosphere; as a result water is continuously leached into the process chamber. Thus, even in a clean elastomer-sealed vacuum chamber, water is the dominant

background gas and limits the vacuum level to the 10^{-6} Torr range, as observed in the vacuum system used in this research.

Out gassing from the metal chamber may contain both high vapour pressure alloying elements and dissolved gases, depending on the materials used to make the chamber. The choice of chamber material is important in limiting out gassing. A stainless steel chamber was used in this research, since stainless steel is comparatively inert and the out gasses consist primarily of CO, H_2 and CO_2. These gases come mainly from the reactions of dissolved oxygen and with the hydrogen and carbon in the steel. They can be reduced significantly by baking. Similarly, out gassing from the substrate was reduced by baking or heating the substrate prior to evaporation.

Dust is a major concern in thin film processing as it has many detrimental results in thin film applications, such as electrical shorts between levels of integrated circuitry and excessive light scattering in optical coatings. Dust arises from the build up of film on the chamber and the eventual flaking off of this build up due to poor adhesion and/or stress build-up. The resulting dust can now be easily transferred to the substrate, before and during deposition. We combated this problem by thoroughly cleaning the chambers with organic solvents prior to each type of evaporation and using a metal shield around the source to reduce deposition on the chamber walls.

Contamination due to impurities in the organic dyes used, namely perylene tetracarboxylic acid derivatives, is very common in this research. These impurities are usually starting material in the synthesis of the dyes and are of lower molecular weight than the target source material. As a result, contamination by these impurities is prevented from depositing on the substrate by thermally evaporating the dyes while

leaving a shutter over the source for a few minutes. After this time all of the lower molecular weight impurities have evaporated and deposited on the lower part of the shutter, the shutter is then opened to allow the target material to be deposited on the substrate. [53]

2.2.2.1.4. Chamber

A sufficiently spacious and easily accessible working chamber usually consists of a metal bell jar mounted on a metal base plate. The base has the form of a collar with branches for connections to vacuum gauges and optional electrical circuitry. The bell jar usually has a copper pipe welded to the outer jacket through which cold water is driven.

2.2.2.1.5. Evaporation Sources

The most commonly used materials for evaporation sources are refractory metals such as, W, Ta and Mo. They are used in the form of wires or specially shaped boats. These are heated by passing current through them. However, the heat generated is nonuniform because of heat conduction down the current contacts. As a result, the evaporation rate control is important and continuous deposition monitoring is necessary. In this research work, dimpled boats were used in the evaporation of metals. Evaporation sources for the organic materials were limited to closed capsules with one relatively small exit hole which fine-tuned the direction and ease of evaporation. [53]

2.2.2.1.6. Physical Foundations for Deposition.

In order that a given molecule may leave the surface of a material, it is necessary that the kinetic energy corresponding to the component of velocity perpendicular to the surface be higher than the energy needed to overcome attracting intermolecular forces. The kinetic energy is determined by the thermal motion of the molecules and as a result

the number of particles fulfilling the inequality increases with temperature. The evaporation therefore occurs at the expense of the internal energy of the body. To prevent a decrease in its temperature, heat has to be supplied and in this research the Balzers BSV 080 glow evaporation control unit enabled the control of heat required. Moreover, there is additional work done during evaporation in consequence of the expansion of volume occurring during the transition into gaseous form.

In a state of equilibrium, that is when the vapour pressure equals the saturated vapour pressure, the basic quantities are interrelated by the Clapeyron-Clausius equation:

$$\frac{dp}{dT} = \frac{L_v}{T\Delta v}$$

Where L_v is the energy needed to overcome attracting intermolecular forces, p is the pressure, Δv the volume change and T the absolute temperature.

If the system is not in equilibrium and there is a relatively lower temperature in some part of it, the vapour will condense in this part and a condition will thus be established for a transfer of material from evaporation source to a colder substrate. The deposition of a film by evaporation is thus essentially a nonequilibrium process.

The liberated particles travel in space with their kinetic velocities along a straight path until a collision with another particle. To ensure a straight path for them between the source and substrate, particle concentration in the space must be low, i.e. the space must be sufficiently exhausted. As a result, at normal geometrical configurations of the apparatus, it is necessary to use pressures of at least 10^{-5} Torr if a considerable dispersion of evaporated particles is to be prevented. [53]

2.2.2.1.7. Deposition Monitoring

Thickness is one of the most important thin-film parameters since it largely determines the properties of a film. On the other hand, almost all properties of thin films depend on the thickness and can therefore be used for thickness measurements. As a result there is a great diversity in methods of measurement.

A thin film is normally not perfectly smooth and has therefore different thickness at different places. If the method employed measures the mass per unit area, from which the average thickness is calculated using a given mass density, then the thickness obtained is called mass thickness. Other methods, in particular optical and electrical techniques usually produce a different result for thickness.

Some methods can only be used for finished films, while others enable the thickness of the film during deposition to be monitored. Monitoring methods are valuable since they allow the preparation of a thin film of selected thickness. Moreover, they can be used for measurement of deposition rate by measuring the thickness increment of unit time.

The most widely used technique for thickness monitoring is the vibrating quartz method. This is a mass thickness method that employs a quartz crystal microbalance, for this research purposes a XTC Inficon quartz crystal oscillator was used, which uses resonant crystalline quartz wafers. Crystalline quartz is piezoelectric, so a quartz wafer generates an oscillating voltage across itself when vibrating at its own resonant frequency, and this voltage can be amplified and fed back to drive the crystal at this frequency. Electrical coupling is done with thin film metal electrodes deposited on opposite faces of a thin quartz wafer having the proper crystallographic orientation. For

deposition monitoring, one electrode is exposed to the vapour flux and proceeds to accumulate a mass of deposit. This mass loading reduces the crystal's resonant frequency. A comparison of this frequency with that of the reference crystal, located in the instruments control unit, is used to calculate the mass deposit. The time derivative of the difference in frequency gives the evaporation rate.

The most important factor is the temperature of the crystal. The fundamental frequency of the crystal may change appreciably with temperature. The temperature during evaporation is affected by the heat radiation of the evaporation source along with the heat liberated directly during the condensation of vapour on the crystal. The heat of condensation may significantly influence the local temperature. Since neither of these two sources of heat can be eliminated and the relationship between frequency and temperature varies for different crystals, a crystal with the smallest temperature dependence is often used. Another contributing factor to thickness measurement is the tooling factor. This factor takes into consideration and accounts for the geometrical parameters of the process chamber and the fact that the crystal and the substrate are at different positions relative to the source. Other parameters that have a profound affect on the measured thickness are the source material density and the z-correction factor that accounts for the acoustic impedance of the crystal and deposit.

2.2.2.2. Physical Vapor Deposition Experimental

For the research presented in this thesis, both the metal and organic deposition were performed in the Balzers high vacuum system. The substrate was introduced through a load lock chamber to allow the main process chamber to remain under vacuum, thereby reducing contamination. For most experimental purposes the substrates used

were transparent and precleaned borosilicate slides (Baxter Cat. M6145), cleaned by rubbing with absolute ethanol and subsequent drying under a continuous flow of dry nitrogen gas. The Edwards E2M2 rotary roughing pump evacuated the load-lock chamber from atmospheric pressure after the substrate had been loaded into it and before the valve was opened into the process chamber. The pressure of the load and lock chamber was measured by the Balzers TPR 010 Pirani vacuum gauge. Once the substrate was in the process chamber, it was heated and controlled at the film deposition temperature. For organic deposition the substrate was left at room temperature. The process and impurity gases were evacuated through an Edwards diffusion pump followed by an Edwards E2M2 backing pump that also served to rough out the process chamber from atmosphere. The process pressure was then measured by the Balzers IKR 020 cold cathode gauge and was nominally 10^{-6} Torr. Both the metal and organic materials were thermally evaporated from cupped tungsten boats using the Balzers BSV 080 glow evaporation control unit. The evaporation rate was allowed to stabilize before the shutter was opened. The mass thickness of the thin films and deposition rate were monitored with a XTC Inficon quartz crystal oscillator.

On borosilicate slides preheated to 200 °C, silver was deposited at a rate of 0.05 nm/s to a total mass thickness of 100 nm, for RAIRS substrates, and to a total mass thickness of 6 nm for silver island films. Similarly, silver was also evaporated on KBr discs to a mass thickness of 6 nm. The bulk density of silver employed was 10.5 g/cm^3, the tooling factor, 105%, and the Z-ratio, 0.529. For surface-enhanced infrared experiments silver and tin were evaporated on ZnS substrates. Both silver and tin were deposited on preheated ZnS substrates, 200 °C for Ag and 80 °C for Sn, at a rate of 0.05 nm/s to a total

mass thickness of 10 nm and 18 nm respectively. The aforementioned evaporation parameters for silver were used. The bulk density of tin employed was 7.30 g/cm^3, the tooling factor, 105%, and the Z-ratio, 0.724.

The perylene tetracarboxylic diimide, PTCDA, derivatives used in the research presented in this thesis were: bisPTCD, thioPTCD, trithiaPTCD, 2sPTCD, 3sPTCD and 2(3s)PTCD. BisPTCD, thioPTCD and trithiaPTCD were individually deposited to a mass thickness of 20 nm onto continuous silver films (mass thickness of 100 nm) and silver island films (mass thickness of 6 nm) in turn supported on a glass substrate. 2sPTCD, 3sPTCD and 2(3s)PTCD were deposited to a mass thickness of 10 nm onto silver island films (mass thickness of 6 nm). ThioPTCD was deposited to a mass thickness of 20 nm onto the SEIR substrates. BisPTCD, thioPTCD and trithiaPTCD were all deposited onto KBr discs to a mass thickness of 20 nm. The deposition rate for PTCDA derivatives was 0.2 nm/s. The bulk density employed for perylene derivatives was 1g/cm^3, the tooling factor, 92%, and the Z-ratio, 1.

Mixed films of perylene and phthalocyanine derivatives were fabricated by mixing both dyes in equimolar ratios, as detailed in Table 2.2.2.2-1.

Table 2.2.2.2-1: Formulation of perylene, Pc, and phthalocyanine, MPc, mixtures.

Perylene	Phthalocyanine	Molar Ratio
bisPTCD	Chloro indium phthalocyanine, ClInPc Chloro gallium phthalocyanine, ClGaPc Cobalt phthalocyanine, CoPc Copper phthalocyanine, CuPc Zinc phthalocyanine, ZnPc Metal free phthalocyanine, H_2Pc	50:50
thioPTCD	ClInPc ClGaPc CoPc CuPc ZnPc H_2Pc	50:50

The Pc-MPc mixtures formed were then co-evaporated from tantalum boats to a mass thickness of 10 nm onto silver island films (mass thickness 6 nm) in turn supported on glass substrates.

2.2.2.2.1. **Encapsulation.**

Encapsulation of the Ag/glass or bisPTCD/Ag/glass was done by placing the sample into a freshly prepared 10^{-3} M octadecyltrichlorosilane (OTS) solution in cyclohexane for 10 minutes, rinsing with cyclohexane and then drying in a N_2 stream.

The OTS reacts with the adsorbed water on the surface of the film to produce an ill-defined cross-linked polysiloxane coating.

2.3. Thin Film Analysis and Spectroscopic Techniques

Thin films have four distinct and characteristic properties: mechanical, electrical, magnetic and optical. These properties can be probed experimentally and are essential in determining the applications in which the thin films are utilized. The most relevant property of thin films to our research is its optical properties. The fundamental physical properties investigated by thin film optics are reflectance, transmittance and polarization of light at various wavelengths and angles of incidence of the beam. These properties are determined from the electromagnetic theory of light as a function of the complex refractive index and thickness of the film and a detailed investigation into these properties will be given in the proceeding chapter. The spectroscopic techniques used in probing the optical and vibrational characteristics of thin films in this research will be discussed in this chapter, with emphasis on instrumentation and practical methods.

2.3.1. Electromagnetic Spectrum

The electromagnetic spectrum encompasses a large range of wavelengths and frequencies, as seen in Figure 2.3.1-1. It is divided into major spectral regions, based upon the methods required to generate and detect the various kinds of radiation and some overlaps are evident. The region of most concern to our research is the ultraviolet, 10^6 cm^{-1}, to the infrared region, 10^2 cm^{-1} [54].

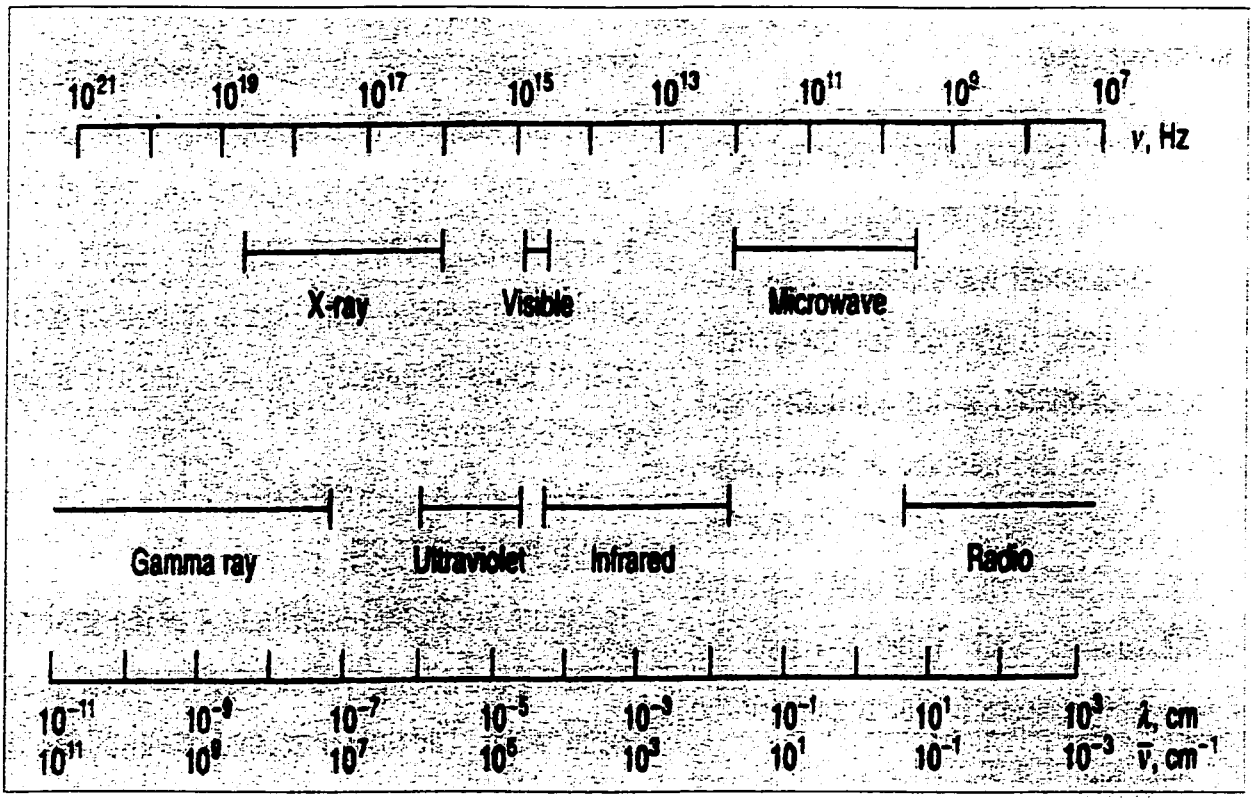

Figure 2.3.1-1 : Illustration of the electromagnetic spectrum.

2.3.2. Instrumentation

Optical spectroscopic methods relevant to this research are based on three phenomena: absorption, scattering, and fluorescence. While the instruments for measuring each differ in configuration, most of their basic components are similar. Moreover, the requirements for these instruments are the same, regardless of the region under investigation: ultraviolet, visible or the infrared portion of the spectrum.

Typical spectroscopic instruments contain five components:

1. a stable source of radiant energy;
2. a transparent container for holding the sample;
3. a device that isolates a restricted region of the spectrum;

4. a radiation detector which converts radiant energy to a usable signal, such as an electrical signal;
5. a signal processor and readout which displays the transduced signal on a meter scale.

In absorption spectroscopy, the beam from the source passes directly through the sample to the wavelength selector, though in some instruments the position of the sample and the wavelength selector are reversed. However, in Raman scattering and fluorescence spectroscopy, the source induces the sample, held in a container, to emit characteristic fluorescent or scattered radiation that is measured at an angle with respect to the source. [54].

2.3.4. Electronic Spectroscopy

Electronic spectroscopy is the study of transitions, in absorption or emission, between electronic states of an atom or molecule. Atoms are unique in this respect as they have only electronic degrees of freedom, apart from translation and nuclear spin, whereas molecules have, in addition vibrational and rotational degrees of freedom.

2.3.4.1. Ultraviolet-Visible Absorption

Absorption of light that causes electronic transitions simultaneously promotes vibrational and rotation transitions. Unfortunately, the absorption bands of most solution phase spectra are so broad that the vibrational and rotational information is totally obscured. However, at low temperature and in the gas phase, the presence of vibrational structure in an electronic absorption spectrum can be resolved, while the rotational fine structure is not generally resolved for polyatomic molecules. This research was

performed primarily in the liquid and solid phase at room temperature, thus only the broad absorption bands due to electronic transitions were observed and considered.

The electronic transition resulting from the absorption of ultraviolet or visible radiation by a molecular species occurs between a ground electronic state and an excited electronic state. A molecular electronic state in which all electron spins are paired is called a singlet state. When one of a pair of electrons of a molecule is excited to a higher energy level, a singlet or a triplet state is permitted. In the excited singlet state, the spin of the promoted electron is still paired with the ground state electron; in the triplet state, however, the spins of the two electrons have become unpaired and are thus parallel. The properties of a molecule in the excited triplet state differ significantly from those of the excited singlet state. More importantly, is the fact that a singlet/triplet transition is less probable event than a singlet/singlet transition.

The absorption of ultraviolet or visible radiation generally results from the excitation of bonding electrons, as a result the wavelengths of absorption peaks and band structure can be correlated with the types of bonds that exist in the species under investigation. In organic molecules, such as perylene tetracarboxylic derivatives, electronic excitation occurs between three classes of electrons: the bonding sigma, σ, and pi, π, electrons and the nonbonding, n, electrons. As a result, four types of electronic transitions are possible: $\sigma \rightarrow \sigma^*, n \rightarrow \sigma^*, n \rightarrow \pi^*$ and $\pi \rightarrow \pi^*$. The most relevant of these is the $\pi \rightarrow \pi^*$ transition that is apparent as three distinct bands in the ultraviolet spectra of aromatic molecules, such as the PTCD derivatives studied in this thesis [54].

2.3.4.1.1. UV-VIS Absorption Instrumentation

UV-VIS absorption spectra were routinely collected on the Varian Cary 50 UV-VIS single beam spectrometer, Figure 2.3.4.1.1-1 [55]

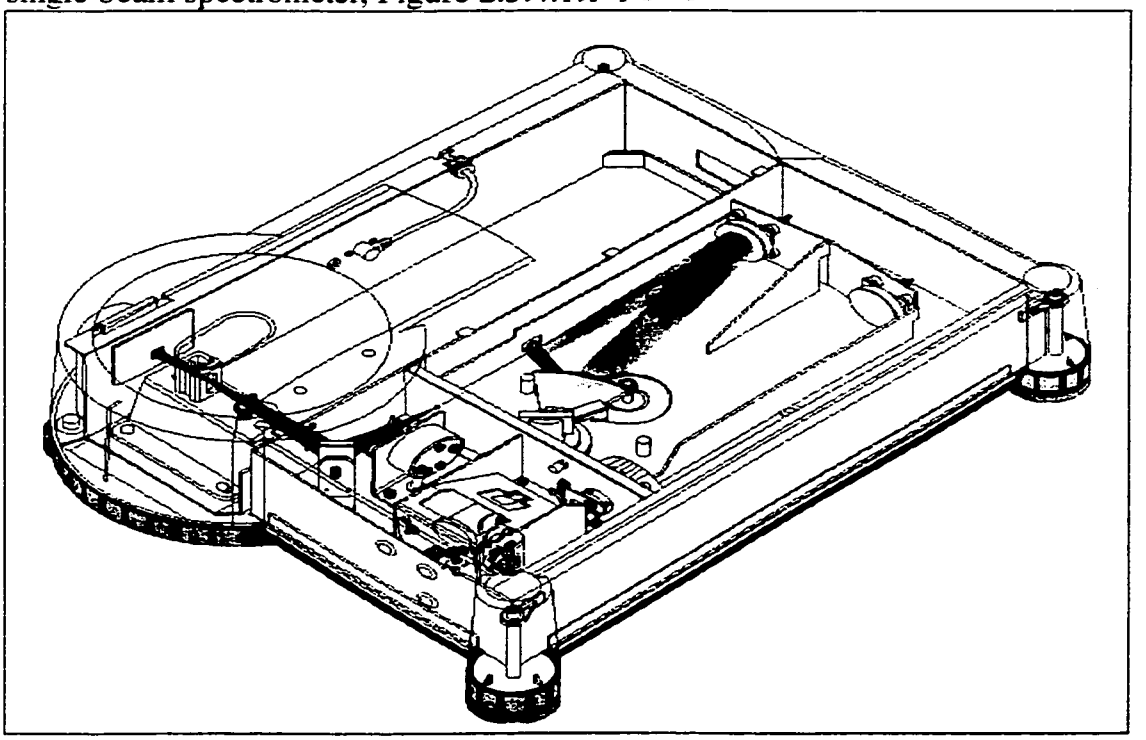

Figure 2.3.4.1.1-1: Illustration of the Cary 50 UV-VIS spectrometer.

This instrument is an example of a temporal dispersive instrument and operates via a sequential linear scan. It contains a continuous Xenon lamp light source that flashes only when acquiring a data point thereby preventing degradation of photosensitive samples and allowing a collection rate of 80 data points per second. The wavelength selector consists of a monochrometer with a motor driven reflection-grating system that sweeps the spectral region of interest at a constant rate. A photoelectric detector enables detection of the radiant energy and the detection is synchronized with the motion of the grating allowing a wavelength scale based upon time to be recorded. A beam splitter is employed to enable simultaneous reference beam correction. The spectral range for this instrument is 190-1100 nm. Data acquisition is performed on the Cary WinUV software

for Windows, while data analysis is executed using the Galactic Industries GRAMS/32^{TM}C software.

2.3.4.1.2. UV-VIS Absorption Experimental

Two types of solid samples were prepared: bulk KBr pellets and thin films of the PTCDA derivative deposited onto precleaned borosilicate slides, KBr discs or silver island films. Solution samples were also prepared by dissolving the PTCDA derivatives in 90% HPLC grade dichloromethane solution and 10% spectroscopic grade TFA solution, and making up to concentrations in the range of 10^{-3} to 10^{-9}M. These samples were investigated using two UV-VIS instruments: the Response single beam spectrophotometer interfaced with an IBM personal computer for data collection and the Varian Cary 50 single beam spectrometer. Spectra were routinely taken in the 200-1100 nm region.

2.3.4.2. Fluorescence

Electromagnetic radiation absorbed by a molecule may be degraded into thermal motion or re-emitted. Light emitted from an excited molecule is called fluorescence if the emission mechanism does not require the molecule to pass through a state of different spin multiplicity from that of the initial state. Fluorescence generally ceases almost immediately after the exciting radiation is removed and has a lifetime of approximately 10^{-7} s for strongly absorbing systems and 10^{-5} s for weakly absorbing systems.

The mechanism of fluorescence is illustrated in Figure 2.3.4.2-1. The incident radiation excites a singlet ground state, S_0, molecule into an excited singlet state, S_1. The molecule is also excited vibrationaly, as aforementioned. Collisions with the surrounding medium induce non-radiative vibrational transitions; these occur because the surrounding

molecules are able to carry away the vibrational energy of the molecule, and hence cause it to step down the ladder of vibrational states in the upper electronic state.

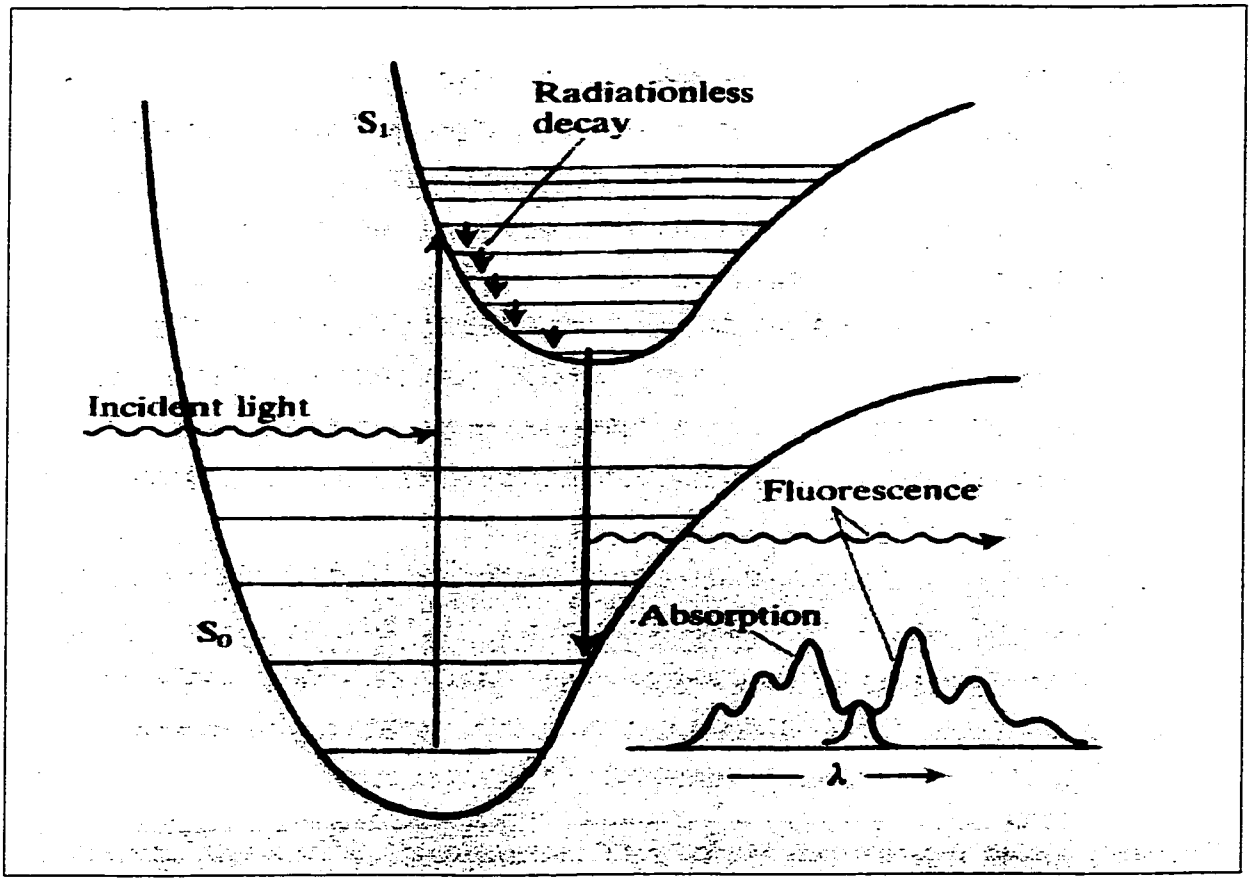

Figure 2.3.4.2-1: The mechanism for fluorescence.

Either of two processes can occur when the molecule has reached its lowest vibrational state. In one, the solvent carries away the electronic excitation energy. The solvent may achieve this de-excitation if its molecules have energy levels that match the energy of the excited molecule, for there may be a resonant transfer of radiation to the solvent. This is known as external conversion. An alternative mode of decay is the radiative decay of the excited electronic state. In this process, the molecule loses its electronic excitation energy by emitting a photon and collapsing back into the lower electronic state. This emitted light is fluorescence.

Whether or not fluorescence occurs depends on a competition between radiative emission and the radiationless de-excitation by energy transfer to the surrounding medium. If the interaction between the excited molecule and its surroundings is strong, radiationless decay will dominate. If the interaction is ineffective at achieving the large energy transfer needed to take the molecule to a lower electronic state, it may still be able to lower the electronically excited molecule down its ladder of vibrational states until it is vibrationally silent. The molecule discards its remaining electronic excitation energy only as radiation. In this case the radiative decay dominates and the molecule fluoresces.

Furthermore, if the initial absorption is not in the lowest excited singlet state of the molecule, internal conversion occurs in which collisions cause the higher singlet states to make a radiationless transition into the lowest excited singlet, S_1, which then fluoresces. Internal conversion appears to be particularly efficient when two electronic energy levels are sufficiently close for there to be an overlap in vibrational energy levels.

Two characteristics of the fluorescence should be noted. The first is that the fluorescence should appear at lower frequency than the incident light. This is due to the fact that the energy of the emitted photon differs from the energy absorbed by the amount of vibrational energy lost to the surroundings. Secondly, there may be vibrational structure in the fluorescence spectrum and as a result the fluorescence spectrum of a molecule should resemble the electronic absorption spectrum of a molecule.

Although fluorescence is generally extinguished as soon as the incident illumination ceases, because all the transitions of interest are allowed and therefore occur very quickly, there is also the phenomenon of delayed fluorescence. One mechanism of delayed fluorescence, and that of particular interest to this research, involves the

excitation $S_0 \rightarrow S_1$ and the subsequent migration of the excited molecule to another molecule. When the two molecules are in contact they form an excited dimer, called an excimer if the molecules are identical and an exciplex if they are different. The excimer/exciplex rapidly falls apart with the emission of fluorescence [56].

2.3.4.2.1. Fluorescence Emission Instrumentation

Fluorescence measurements were routinely performed on the Renishaw Research Raman Microscope System RM2000 equipped with a computer controlled 3-axis encoded (XYZ) motorized stage, with a minimum step of 0.1 μm, and Leica microscope (DMLM series), Figure 2.3.4.2.1-1 [57]. The excitation source is the 514.5 nm laser line of a Spectra-Physics argon ion laser. The wavelength selector system consists of a 1200 grooves/mm grating with additional angle-tuned bandpass filter optics. The spectra are measured using a Peltier cooled (-70 °C) CCD array detector. The laser power at the sample surface is nominally in the range of 1-100mW laser power. The spectral range for fluorescence measurements for this spectrometer is 400-1000 nm. Data acquisition and analysis are carried out using the WiRE software for windows and Galactic Industries GRAMS/32^{TM}C software including the 3D package.

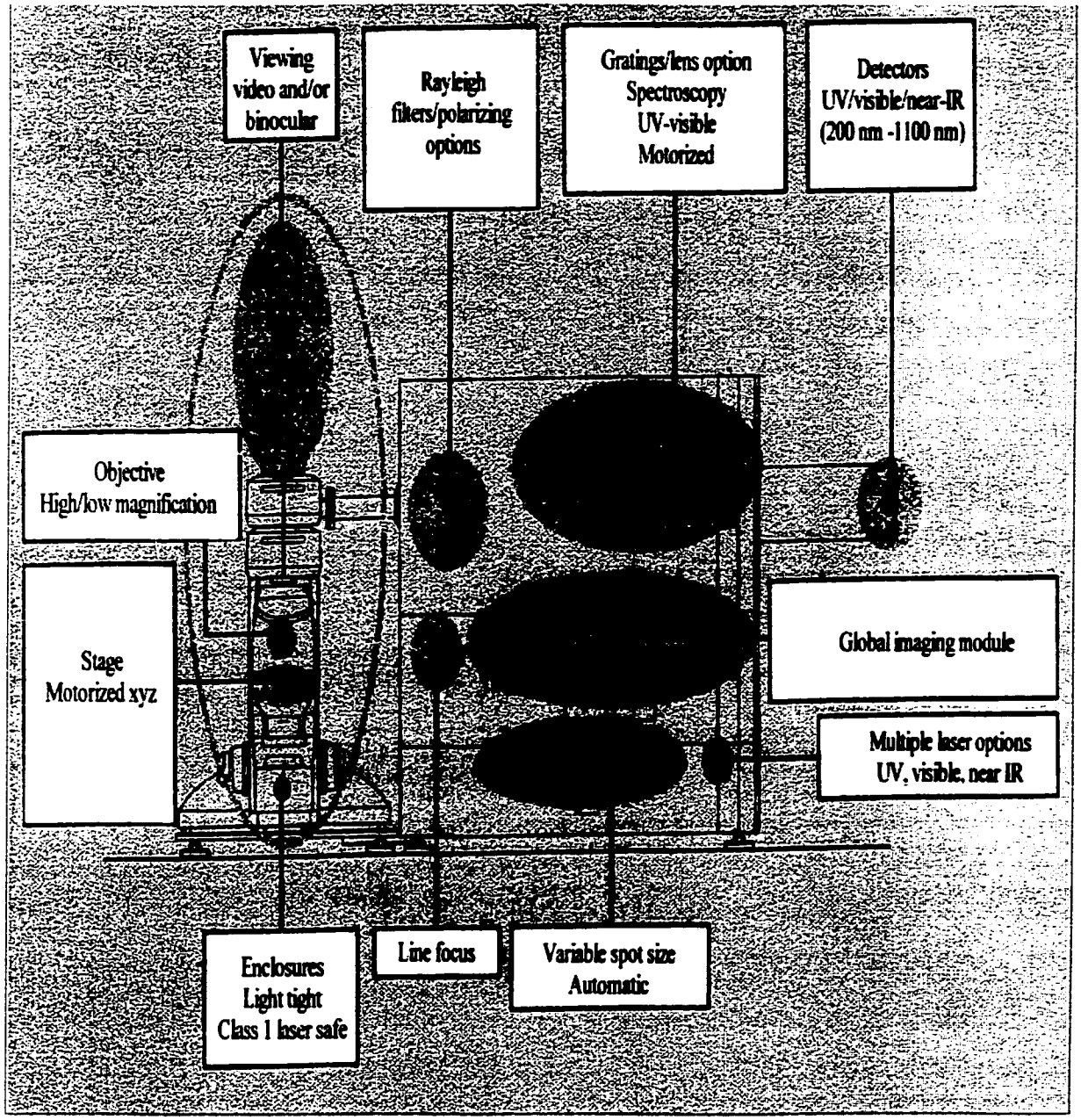

Figure 2.3.4.2.1-1: Illustration of the Renishaw Research Microscope Raman 2000 Instrument.

2.3.4.2.2. Fluorescence Emission Experimental

Samples used in fluorescence measurements were the same as those used in UV-VIS measurements.

Two instruments were used in acquiring fluorescence measurements. For the first part of the research presented in this thesis, a S-1000 spectrograph equipped with a holographic notch filter, a liquid nitrogen cooled CCD detector and a microscope

attachment was used. The excitation source was the 514.5 nm laser line of a Spectra-Physics argon ion laser. For the latter half of the research, Renishaw Research Raman Microscope System 2000, equipped with a microscope attachment and using the 514.5 nm line as the excitation source was used to collect fluorescence data. All spectra were recorded in the back scattering geometry using the microscope's x 50 objective lens. The laser power, number of accumulations, and integration time were set according to the sample under investigation.

2.3.5. Vibrational Spectroscopy

In vibrational spectroscopy, the energy of light which is sufficient to excite vibrations of the molecules which absorb it are found in the infrared region of the electromagnetic spectrum, typically 100-5000 cm^{-1}. Rotational energies of the molecules are characteristically smaller than vibrational energies, thus rotations are simultaneously excited with the molecular vibrations. Vibrational spectra are usually measured by two distinguishable techniques, infrared spectroscopy and Raman spectroscopy. In infrared spectroscopy, the light absorbed by molecules is in the infrared region of the spectrum, as aforementioned. However, in Raman spectroscopy, the difference in incident radiation and that inelastically scattered by molecules is measured and corresponds to the infrared region.

Infrared and Raman spectroscopy are complimentary techniques and are both necessary in obtaining the complete vibrational spectrum of a compound. The symmetry selection rules of a molecule determine whether vibrational modes are Raman or IR active. IR active vibrational modes occur if there is a change in the dynamic dipole

moment, while Raman active modes are due to a change in the molecular polarizability of a molecule.

2.3.5.1. Infrared Absorption

In infrared spectroscopy light of all different frequencies is passed through a sample and the intensity of the transmitted light is measured at each frequency. At frequencies corresponding to vibrational energies of the sample, some light is absorbed and less light is transmitted than at frequencies that do not correspond to vibrational energies of the molecule.

Two geometries for infrared absorption spectroscopy were used in this research: transmission and reflection absorption (RAIRS). Both are complementary methods used to probe molecular orientation in prepared thin films of the samples. The theoretical background for infrared spectroscopy is given in the proceeding chapter (Chapter 3).

2.3.5.1.1. Infrared Absorption Instrumentation

Infrared spectra were routinely recorded with the Bomem DA3 Fourier Transform Infrared Spectrophotometer. This spectrophotometer is an example of a multiplex instrument, in particular the Michelson interferometer. In this device a beam of radiation from the globar source is collimated and impinges on a KBr beam splitter, which transmits approximately half of the radiation and reflects the other half. The resulting twin beams are then reflected from mirrors, one of which is fixed and the other of which is movable. The beams then meet again at the beam splitter, with half of each beam being directed toward the sample and MCT liquid nitrogen cooled detector and the other two halves being directed back toward the source. Only the two halves passing through the sample to the detector are employed for analytical purposes. The optical configuration of

the Bomem DA3 FT-IR spectrophotometer is shown in Figure 2.3.5.1.1-1 [58]. The entire system is evacuated and held under vacuum while infrared spectra are recorded. The spectral range and resolution for mid-infrared measurements on this instrument is 400-4000 cm^{-1} and $1cm^{-1}$ respectively. Data analysis is carried out using Galactic Industries GRAMS/32^{TM}C software.

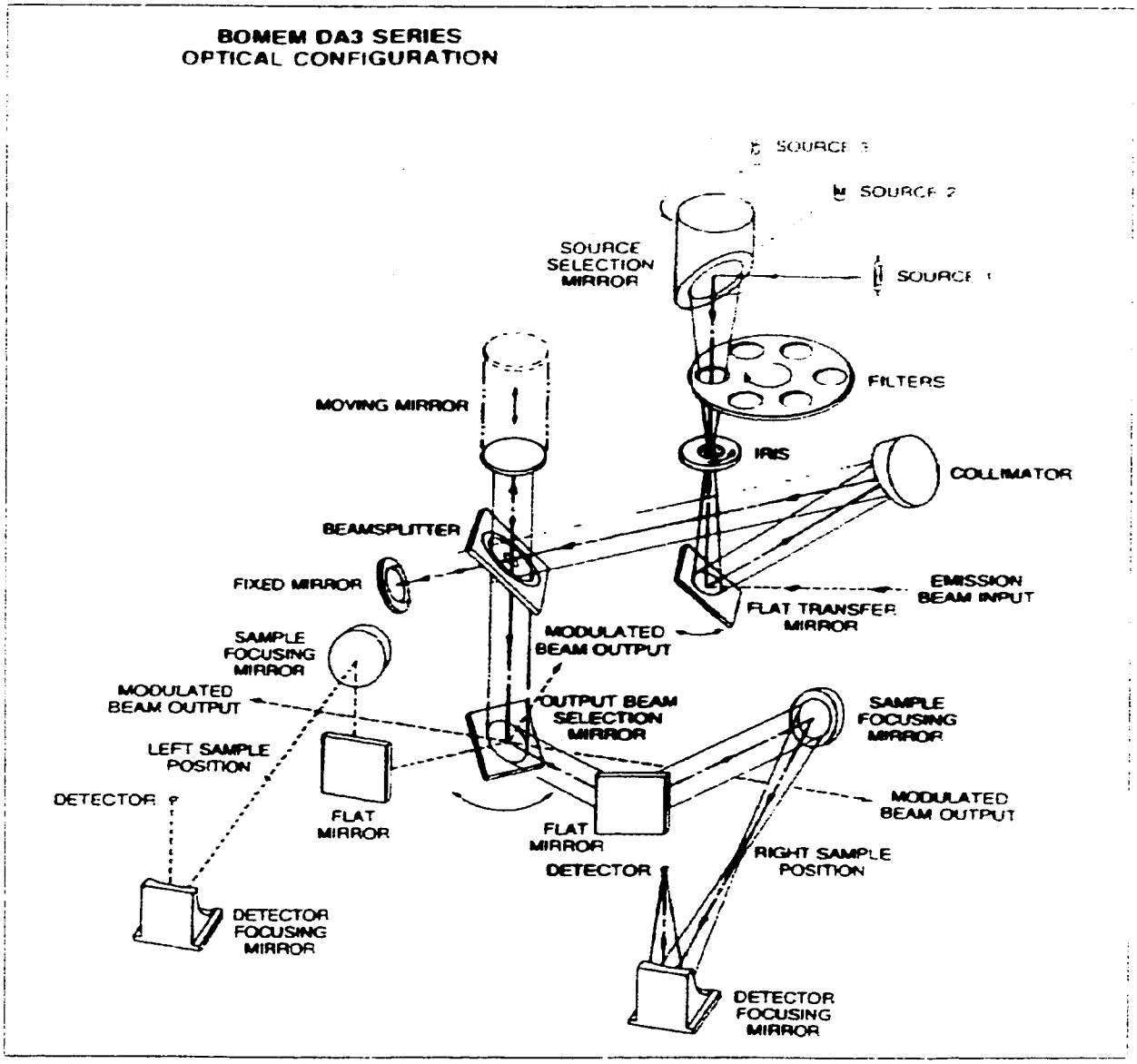

Figure 2.3.5.1.1-1:Optical configuration of the Bomem DA3 FT-IR instrument.

2.3.5.1.2. Infrared Absorption Experimental

Infrared absorption spectroscopy in the transmission geometry was routinely done on several types of samples; bulk KBr pellets, evaporated thin films deposited on KBr discs and on silver island films in-turn deposited on infrared transparent substrates, such as ZnS, and Langmuir-Blodgett (LB) films deposited on infrared transparent substrates. The Bomem DA3 Fourier transform infrared spectrometer, with 1 cm^{-1} resolution, was employed in obtaining spectra of these samples. Spectra were routinely recorded under vacuum in the region of 400-4000 cm^{-1}.

RAIRS samples were nominally thin evaporated films of PTCDA derivatives deposited on a 100 nm thick smooth silver film. RAIRS spectra were recorded using an in-house modified Bomem 110-E equipped with a Judson mid range (650 cm^{-1}) 1 mm x 1 mm MCT detector [59], with a 4 cm^{-1} resolution. The entire system was purged and maintained under a closed cell of dry air. The sample holder was adapted to include four concave mirrors that focused the IR beam onto the substrate at an 80 degree angle of incidence [60]. The substrate holder consisted of a flat aluminum-heating element, which was thermally controlled by a 100V variastat. The temperature of the substrate was monitored using a thermocouple. Annealing of the sample under dry air was done in-situ, while recording the RAIRS spectra. Vapor annealing of the sample under various atmospheres was done at the specified temperature for 30 minutes using standard vacuum line techniques and cells. RAIRS spectra were recorded in the region of 200-4000 cm^{-1} with 4 cm^{-1} resolution.

2.3.5.2. **Raman Scattering**

The Raman process is the inelastic scattering of a photon by a molecule. An inelastic process is one in which energy is transferred between the two colliding systems. In Raman scattering the incident photon may lose energy to the molecule by exciting its rotation or vibration, in which case it emerges from the collision with a lower frequency. Alternatively, the photon may acquire energy from the molecule if a mode is already excited and hence emerge with a higher frequency. Since the molecular rotation and vibration are quantized, the energy transfer can occur only in packets, and so the scattered light contains frequency components that are shifted from the incident frequency by discrete amounts. The magnitude of these shifts is independent of the wavelength of excitation. The frequency composition of the scattered radiation is the Raman spectrum of the molecule.

It is important to note that the energy change of the molecule when it interacts with a photon, is equal to the energy of the photon, hν. Thus depending on the frequency of radiation from the source, the energy of the molecule can assume any of an infinite number of virtual states between the ground electronic and first excited electronic state.

In Raman spectroscopy, an intense, monochromatic beam of incident radiation from a laser passes through the sample and the radiation scattered perpendicular to the propagation direction is detected and analyzed. The spectrum consists of a strong Rayleigh component at the incident frequency, which arises from elastic collisions between the photons and the sample, and a series of lines to high and low frequency of that component. The lines to low frequency are the Stokes lines. They arise from collisions in which photons lose energy to the molecule. The lines to high frequency are

the anti-Stokes lines, and are due to collisions in which photons gain energy from the molecule. The Stokes lines are generally more intense than the anti-Stokes lines because the latter require the presence of a pre-existing population of excited molecules. However as temperature increases, a larger fraction of the molecules will be in the first vibrationally excited state and the ratio of anti-Stokes to Stokes intensity increases [56].

2.3.5.2.1. Raman Theory

When a molecule is irradiated with light, a small portion of it may be scattered either elastically or inelastically. Light scattering arises from dipole moments induced in atoms or molecules by the incident field, through the polarizability of electrons. The static polarizability leads to Rayleigh scattering, while modulation of the polarizability by electronic, vibrational or rotational motion leads to Raman scattering.

A simple classical model illustrates most of the essential features of Raman scattering. A laser illuminates the sample at frequency ν_0; the amplitude of the electric field of the light is:

$$E = E_0 \cos(2\pi\nu_0 t)$$

Suppose the polarizability of the molecule is modulated at the vibrational frequency ν_1,

$$\alpha = \alpha_0 + \alpha_0 \cos(2\pi\nu_1 t)$$

where α_0 is the polarizability at the equilibrium nuclear geometry. Since the electric field induces a dipole moment in the molecule according to:

$$\mu = \alpha E$$

Substituting both the time dependant equations for α and E into the definition of the induced dipole moment results in

$$\mu = \alpha_0 E_0 (1 + \cos 2\pi \nu_1 t)(\cos 2\pi \nu_0 t)$$

$$\mu = \alpha_0 E_0 \cos 2\pi \nu_0 t + \tfrac{1}{2}\alpha_0 E_0 \cos 2\pi(\nu_0 + \nu_1)t + \tfrac{1}{2}\alpha_0 E_0 \cos 2\pi(\nu_0 - \nu_1)t$$

The scattered light has been modulated by the oscillating polarizability and sidebands appear in the spectrum. The first term is the Rayleigh scattering at the unshifted frequency ν_0, the second term is the anti-Stokes Raman scattering, and the third term is the Stokes Raman scattering. This model provides the selection rule for Raman scattering: molecular polarizability must change during a vibration for that vibrational mode to be Raman active. As a result molecular symmetry determines whether a vibration is Raman active or forbidden [61].

2.3.5.2.2. Raman Instrumentation

Raman scattering, resonance Raman and surface enhanced Raman studies were routinely recorded on the Renishaw Research Raman Microscope System RM2000 equipped with a computer controlled 3-axis encoded (XYZ) motorized stage, with a minimum step of 0.1 μm, and Leica microscope (DMLM series), as detailed in Chapter 2-section 2.3.4.2.1. This instrument contains a 1200 grooves/mm grating with additional angle-tuned bandpass filter optics. The excitation source included the 514.5 nm laser line of a Spectra-Physics argon ion laser, the 633 nm He-Ne laser line and the 780 nm diode laser line. Spectra are measured using a Peltier cooled (-70 °C) CCD array detector. The laser power at the sample surface is nominally in the range of 1-100 mW laser power. The Raman spectra were usually recorded in the 100-3500 cm^{-1} spectral region. Data acquisition and analysis are carried out using the WiRE software for windows and Galactic Industries GRAMS/32^{TM}C software including the 3D package.

2.3.5.2.3. Raman Experimental

Three instruments were used in acquiring Raman measurements. The FT-Raman spectra were recorded with a Bruker RFS100 provided by J. Hellman of Bruker Canada. Similar to fluorescence studies. two instruments were used in recording the Raman scattering measurements. For the first part of the research, the S-1000 spectrograph equipped with a holographic notch filter and a liquid nitrogen cooled CCD detector was used. The Renishaw Research Raman Microscope System RM2000 equipped with a microscope was used for the latter part. The excitation source for both instruments was the 514.5 nm laser line of a Spectra-Physics argon ion laser. Additionally, the 633 nm He-Ne laser line and the 780 nm diode laser line were used to obtain Raman data on the Renishaw System. All spectra were recorded in the back scattering geometry using the microscope's x 50 objective lens. The laser power, number of accumulations, and integration times were set according to the sample under investigation.

Samples were prepared according to the technique applied. For FT-Raman and Raman scattering, the samples were powders and KBr pellets of the PTCDA derivatives under investigation. The samples for resonance Raman spectroscopy were thin evaporated films, nominally 200 Å in thickness, LB films and KBr pellets. Similarly, for surface enhanced Raman spectroscopy, samples were thin evaporated films and LB films of the material deposited on island films of silver (60 Å).

2.3.5.2.4. Raman Microscopy

There are at least two distinct Raman imaging concepts based on Raman Microscopy. The first is point-to-point sampling, carried out as a line scanning analysis of areas of the sample. In this technique, the laser spot size or the collection optics

defines the spatial resolution of the image. As the image consists of a sequence of single point Raman spectrum acquisitions, the collection time is usually on the order of a few minutes to a few hours depending on the sample area.

The second concept, global imaging, is based on the light distribution in a wide field. The spatially resolved spectra are collected over the entire illuminated area. The result is a sample image based on spectroscopic information and from which the spatial distribution of a particular component may be extracted [62]. It is possible to obtain a chemically selective two-dimensional image from the global imaging technique if an optical filter, which allows transmission of a characteristic Raman frequency of one component of the sample, is used to capture the global image. Unlike, point-to-point sampling, the acquisition of a two-dimensional image at one Raman shift is rapid (in the order of 10s), as a large number of samples spots are observed simultaneously. Further, since global imaging uses a weakly defocused laser, the power density is much lower than a single point acquisition and reduces the risk of sample damage.

Point-by-point line scanning and area mapping, and global images were obtained with the Renishaw Research Raman Microscope System RM 2000, as detailed in Chapter 2-section 2.3.4.2.1. Two lasers were used to obtain point-by-point maps and global images: 514.5 nm and 633 nm laser lines. The laser power at the sample was varied between 20 μW and 2 mW. The maps were recorded using a Leica microscope and a 50 x microscope objective to focus the laser beam to a spot ca. 1.0 μm^2. Global imaging was recorded using the angled tuned dielectric filters at a given Raman wavenumber of the surface enhanced resonance Raman spectrum. For the PTCDA derivatives studied, this wavenumber corresponded to the ring-stretching vibration at 1297 cm^{-1}. The laser spot

size was defocused and the Raman scattered light from a large surface area was collected. An area of 40 μm^2 was used to facilitate a visual comparison of the resulting images and mapping plots. Data acquisition and analysis were carried out using the WiRE software for windows and Galactic Industries GRAMS/32^{TM}C software including the 3D package.

2.3.6. Atomic Force Microscopy

Atomic force microscopy (AFM) is a technique for analyzing the surface morphology of a rigid material, such as a thin film, to the level of that of an atom. AFM uses a mechanical probe to magnify surface features up to 100,000,000 times, and it produces 3-D images of the surface.

Atomic Force Microscopy is a scanned probe technique, which relies on a very sharp probe positioned within a few nanometers above the surface of interest. [63, 64] [65-68].

An atomic force microscope senses interatomic forces that occur between a probe tip and a substrate. The AFM probe tip is normally integrated into a microfabricated, thin film cantilever. Once contact between the probe tip and the sample surface has been established, the sample is translated laterally relative to the probe tip, while the vertical position of the cantilever is monitored. Variations in sample height cause the cantilever to deflect up or down, which changes the position sensor output, thus generating the error signal that the feedback circuit uses to maintain a constant cantilever deflection (constant force). Detection of cantilever deflections is often the optical lever method, as illustrated in Figure 2.3.6-1 [69]. In this method, a laser beam is trained on the back surface of the cantilever, and the reflected beam is sent to a photodiode that is divided into two sections, A and B. Due to the macroscopic length of the reflected light path, any deflection of the

cantilever causes a magnified lateral displacement of the reflected laser spot on the photodiode. The relative amplitudes of the signals from the two segments of the photodiode change in response to the motion of the spot. The difference signal (A-B) is very sensitive to cantilever deflection; detection of deflections of <0.1 nm is readily achieved. Normal imaging forces are in the 1 - 50 nanoNewton range and cantilever deflections of less than 0.1 nm can be detected.

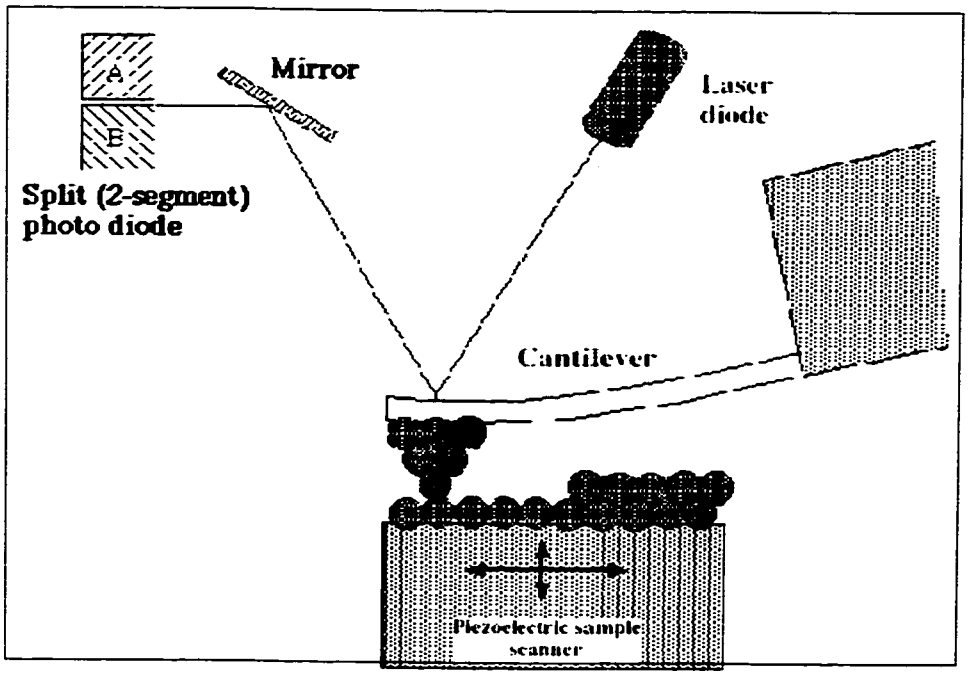

Figure 2.3.6-1: Optical lever detection of cantilever deflection.

To create a 3-dimensional map of surface height, the probe is scanned horizontally along a series of parallel lines, while the height at each point along each line is recorded. Probe signals that have been used to sense surfaces include electron tunneling current, interatomic forces, photons, capacitive coupling, electrostatic force, magnetic force, and frictional force. In AFM, the probe signals depend so strongly on the probe-substrate interaction that changes in substrate height of as little as 0.01 nm can be

detected. In addition, AFM probes can interact with regions of the substrate that are of atomic-scale lateral dimensions, which allows the substrate height to be measured with sub-nm lateral resolution as well.

2.3.6.1. AFM Experimental

AFM images were performed in contact mode by Rick MacAloney at the Department of Chemistry, University of Toronto, Toronto Ontario, Canada.

2.4. Model Calculations

Geometry optimization and vibrational calculations, for the PTCDA derivatives, performed to help the assignment were executed using Hyperchem 4.5, utilizing semi-empirical AM1 and PM3 methods, and Gaussian at RHF/3-21G level of theory.

2.5. Properties of Perylene Tetracarboxylic Derivatives

Perylene tetracarboxylic derivatives are generally solid and red, however bluish black, maroon and black derivatives are also known. Many of the red colored derivatives display a red solid-state fluorescence and relationships between the solid-state color and the N-substituents have been investigated [70].

Absorption spectra of perylene derivatives have been, on average, very difficult to obtain, due to their low solubility in organic solvents. However, by increasing the N-alkyl chain, solubility increases for some perylene dyes and they form red purple solutions with intense yellow to green fluorescence. Perylene dyes are readily soluble in concentrated sulfuric acid via protonation. The protonated perylene pigment causes a red-shift of the absorption of 80 nm compared to the free perylene pigment. Similarly, the relatively low solubility of perylene derivatives in most solvents hinders high fluorescence quantum yield. This may be likewise rectified by substitution of long or branched alkyl chains.

The excellent lightfastness, photostability and thermal stability makes perylene derivatives prime candidates for various applications. Thermal decomposition and lightfastness of most perylene derivatives initiate above 400 °C. A correlation between the length of N-alkyl chains and decomposition temperatures has been established for monoamides of perylene [71], and indicates that for longer or branched alkyl chains thermal stability decreases. Decomposition of the monoamides is considered to be initiated by the degradation of the N-alkyl substituents.

Perylene derivatives have recently been investigated for their opto-electric properties due to their highly conjugated molecular structure. Most applications of perylene derivatives are as thin molecular films either vacuum deposited or monolayers

deposited via Langmuir Blodgett. The dimensions of such films facilitate the fabrication of molecular devices, such as electroluminescent diodes, electrochemical cells and organic semiconductors.

Tang's report on the n-type semiconductor properties of perylene in the p/n junction organic solar cells was the first acknowledged application of perylene [28, 72]. Since its publication, the synthesis and properties of perylene tetracarboxylic derivatives have been widely studied with the aim of improving their molecular functions. In this fashion, Gregg *et al.* have investigated the energy transfer process in perylene bis(phenethylimide) films for semiconductors [73]. In this report, they suggest that the close packing and correspondingly strong electronic coupling between the perylene molecules and the relatively high degree of structural order in the films may account for the long range and rapid exciton transfer. Other published applications have included the Alcácer *et a.l* report on the synthesis and growth of modified perylene molecular conductors derived from 1,2,7,8-tetrahydrodicyclopenta-(cd-lm)perylene and from perylothiophene with the counter ions I_3^- and nickel dimaleonitriledthiolate [74]. Hiramoto *et al.* observed a large photocurrent multiplication in various organic films such as a series of perylene pigments [75]. They later followed this report by a proposal of a model that can explain the large photocurrent multiplication phenomenon at the perylene/metal interface. Studies on light emitting diodes was done by Ostrick *et a.l*, where they revealed the complexity of transport in a molecular thin film by investigating the substantial anisotropies in the electronic transport properties of thin polycrystalline films of perylene tetracarboxylic dianhydride as observed in field effect transistors and

light emitting diodes [76]. These reports only add to the continuously growing number of papers on the applications of perylene derivatives.

The electrical and optical spectra of individual perylene molecules are dominated by their electronic structure, which may be modified by molecular tailoring. Moreover, the color of perylene dyes in the solid state is influenced by their crystalline structure. Therefore it is important to control the solid-state structure of the molecular materials in order to improve their designed molecular functions for practical applications [77].

The electronic characterization of various perylene derivatives is fundamental in determining future applications. To date, electronic spectroscopy of perylene has been an active research area and has encompassed both theoretical and experimental aspects of the technique. One of the first electronic studies of perylene crystals was undertake by Hochstrasser, where he reported that the electronic spectrum was unusually diffuse [78]. He later followed this investigation with a report in which he studied the absolute intensity of the lowest energy electronic state of perylene [79]. The theoretical and experimental facets of electronic spectroscopy were bridged in a report by Adachi *et al.*, in which the electronic absorption spectra of perylene tetracarboxylic dianhydride, naphthalenetetracarboxylic dianhydride and their derivatives were investigated. Theoretical studies of the electronic structures were performed, and the relationship between the size of π-conjugation and the absorption spectra formulated [80]. Alternatively, electronic emission studies of perylene bis(phenethylimide) films were completed by Gregg *et al.*, in which long range singlet energy transfer in the films were investigated [73]. Electronic studies of Langmuir Blodgett films have also been accomplished. Weiss *et al.* have studied both the E-Excimer and Y-type luminescence of

perylene dimers at 1.5 K [81]. A comparative analysis of the results obtained to that from α-perylene crystal showed that luminescence of perylene dimers in disordered Langmuir Blodgett film appears to be much closer to the predictions of theoretical models for excimer formation in isolated perylene dimers.

The importance of electronic spectroscopy in perylene characterization has been exemplified by Adachi *et al.*, in which they approached the design of near infrared dyes by theoretically elucidating the electronic absorption spectra of arylimidazole introduced into 3,4,9,10-perylenetetracarboxylic dianhydride and its imide derivatives, via molecular orbital calculations [82]. Such modifications in the molecular structure of the perylene moiety has a profound effect on the dipole moment transition, which is characterized as a charge transfer property rather than the π-π^* excitation of the perylene chromophore. The molecular packing of mixed Langmuir Blodgett films of N, N'-bis(2,5-di-tert-butylphenyl)-3,4,9,10-perylenedicarboximide and steric acid have also been studied. Dutta *et al.* have studied the changes in the molecular packing in these mixed films via electronic absorption and emission spectroscopies. They report well-organized mixed films whose eximer emission and excitation profile changes with time [83].

2.6. Synthesis of Novel Perylene Tetracarboxylic Derivatives

Dr. Jim Duff, at Xerox Research Center of Canada, performed all syntheses of the perylene tetracarboxylic derivatives.

2.6.1. Bis(n-propylimido)perylene,*bisPTCD*

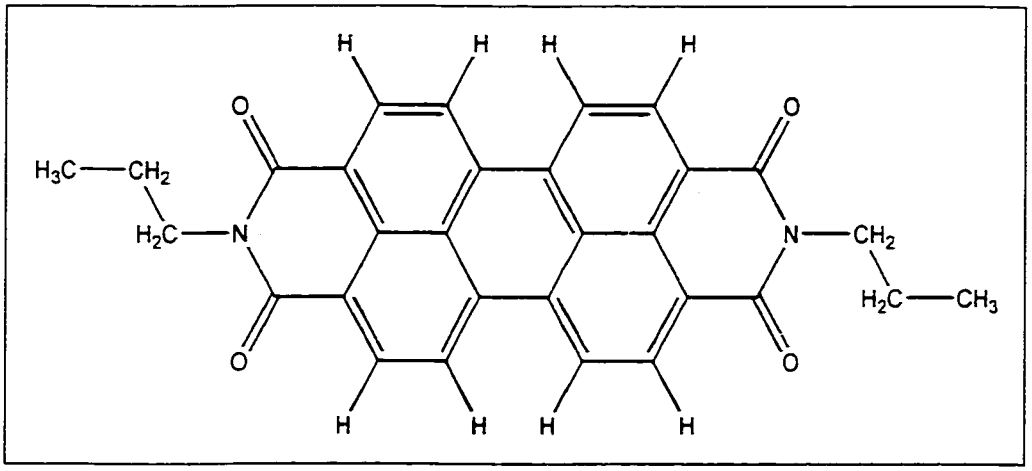

Figure 2.6.1-1: Molecular structure of bisPTCD

The molecular structure of BisPTCD, Figure 2.6.1-1, consists of a backbone of perylene tetracarboxylic acid dianhydride with one propyl chain attached to each end of the imide. It was prepared by condensing perylene-3, 4,9,10-tetracarboxylic acid with propylamine in an appropriate solvent [84]. The product was then purified by temperature gradient sublimation.

2.6.2. Thio-bis(n-propylimido)perylene, *thioPTCD*

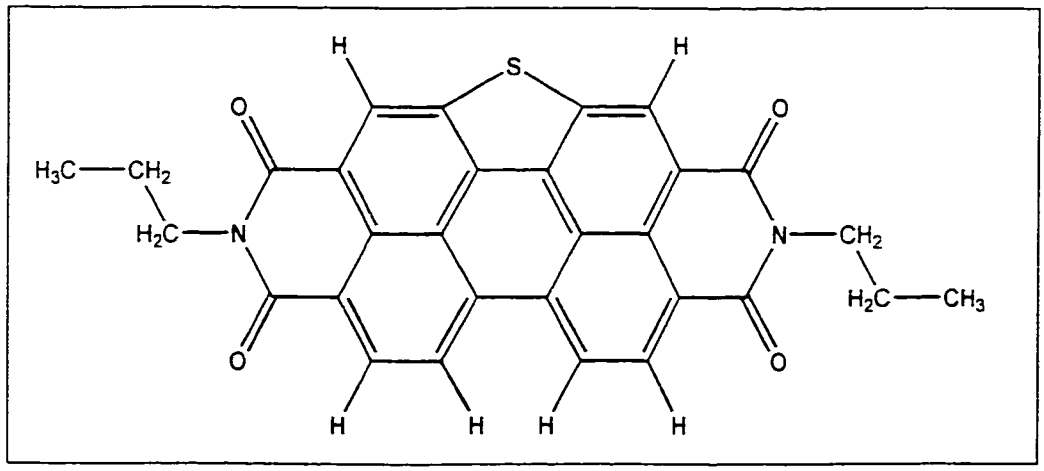

Figure 2.6.2-1: Molecular structure of thioPTCD

The molecular structure of ThioPTCD, Figure 2.6.2-1, is similar to its parent molecule, BisPTCD, with the exception of the incorporation of a sulfur atom in the backbone chromophore structure. The starting tetracarboxylic anhydride for the ThioPTCD was prepared by sulfonation of the perylene-3,4,9, 10-tetracarboxylic acid dianhydride with chlorosulfonic acid. Subsequent deoxygenation and dehydration results in the synthesis of perylo-thiophene-3,4,9,10-tetracarboxylic dianhydride [85]. Condensation with propyl amine in appropriate solvent yields thio-bis(n-propylimido)perylene [86].

2.6.3. Bis(n-propylimido)trithiaperylene, *trithiaPTCD*

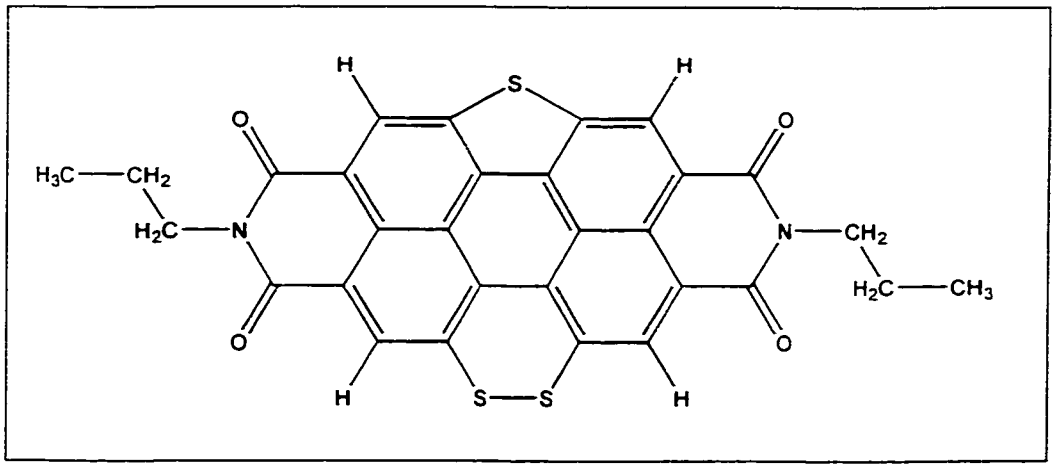

Figure 2.6.3-1: Molecular structure of trithiaPTCD

This molecule, Figure 2.6.3-1, consists of three bridging sulfur atoms in the perylene chromophore. It is prepared by refluxing a mixture of thieno(2,3,4,5-ikl)perylo(6,6a,6b,7-cde)-1,2-dithiin-4,5,9,10-tetracarboxylic dianhydride and n-propylamine in DMF. The mixture was stirred at the boiling point. The resulting suspension was filtered. The solid was washed with boiling DMF until the filtrate became light yellow-green. The solid was then washed with methanol and then dried at 70 °C.

2.6.4. N-Propylimido-methylmercaptoethylimidoperylene, *2sPTCD*

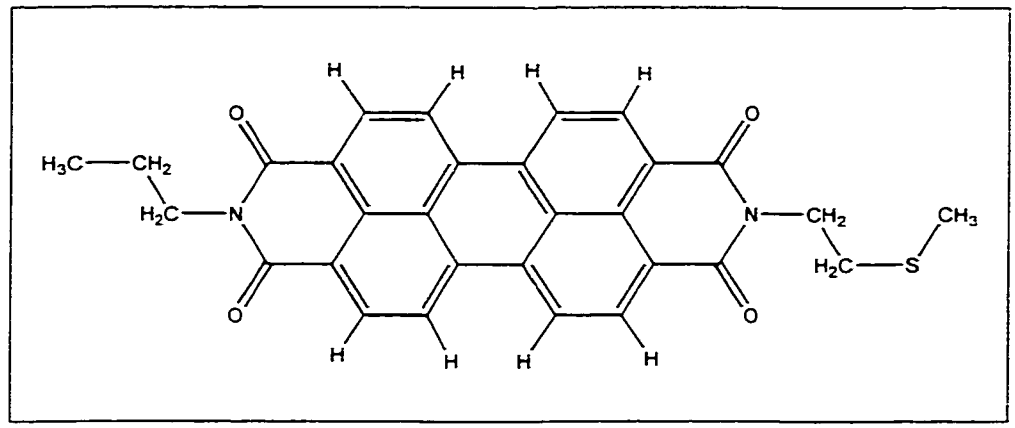

Figure 2.6.4-1: Molecular structure of 2sPTCD

The chemical structure of this molecule, Figure 2.6.4-1, consists of the main perylene chromophore with an alkyl side chain on one end and an alkyl thiol side chain on the other. It was synthesized by stirring 3,4,9,10-Perylenetetracarboxylic acid monoanhydride mono-n-propylimide (3.03 g, 0.0070 mole) in 150 ml of DMF under an argon atmosphere. 2-(methylmercapto)ethylamine (2.0 g (0.022 mole) was added and the mixture was stirred for 10 min at room temperature then was heated for 2 h at 140 °C. The dark brown suspension was filtered through a preheated sintered glass funnel and was washed with 3 X 50 mL portions of boiling DMF followed by 25 mL of cold DMF and 3 X 20 mL of methanol. The product was dried at 60 °C to give 3.2 g (90%) of shiny brown solid. DSC: 324 (endotherm), 414 °C (strong, sharp endotherm).). ^{1}H-NMR (300 MHz, 1:3 V/V $CF_3CO_2D/CDCl_3$, internal TMS): 1.06 (t, 3H, CH_3), 1.82 (m, 2H, C-CH_2-CH_3), 2.31 (s, 3H, S-CH_3), 3.01 (t, 2H, CH_2-S), 4.24 (t, 2H, N-CH_2), 4.56 (t, 2H, N-CH_2), 8.77 (m, 8H, Ar-H). *Anal.* Calcd. for $C_{30}H_{22}N_2O_4S$: C 71.13, H 4.38, N 5.53. Found: C 70.45, H 4.48, N 5.47.

2.6.5. N-Propylimido-(3-methylmercaptopropyl)imidoperylene, *3sPTCD*

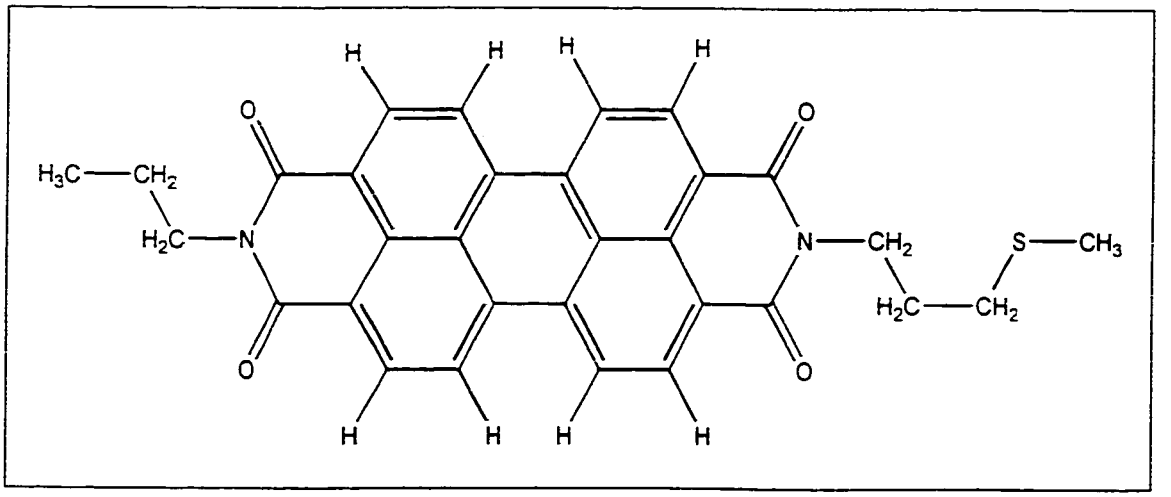

Figure 2.6.5-1: Molecular structure of 3sPTCD

Similar to 2sPTCD, this molecule has both an alkyl and thio alkyl chain, Figure 2.6.5-1. It was prepared by stirring 3,4,9,10-Perylenetetracarboxylic acid monoanhydride mono-n-propylimide [87, 88](4.33 g, 0.010 mole) in 150 ml of water under an argon atmosphere. 3-methylmercaptopropylamine (5.25 g, 5.4 mL) was added and the mixture was stirred for 30 min at room temperature and 2 h at reflux. The resultant black suspension was cooled to about 80° C then was filtered and washed with 4 x 50 mL portions of water at 80 °C. The initial filtrate was dark red. The final wash was colorless. The solid was then washed with 3 x 25 mL of methanol then was dried at 60 °C to give 4.3 g (83%) of black solid. DSC: 313 (weak endotherm), 356 (endotherm), 375 °C (strong endotherm). ^{1}H-NMR (300 MHz, 1:3 V/V $CF_3CO_2D/CDCl_3$, internal TMS): 1.05 (t, 3H, CH_3), 1.82 (m, 2H, C-CH_2-CH_3), 2.14 (m, 2H, C-CH_2-C), 2.18 (s, 3H, S-CH_3), 2.73 (t, 2H, CH_2-S), 4.24 (t, 2H, N-CH_2), 4.40 (t, 2H, N-CH_2), 8.81 (AB, 8H, Ar-H). *Anal.* Calcd. for $C_{31}H_{24}N_2O_4S$: C 71.52, H 4.65, N 5.38. Found: C 71.99, H 4.44, N 5.42.

2.6.6. Bis (3-methylmercaptopropylimido) perylene, *2(3s)PTCD*

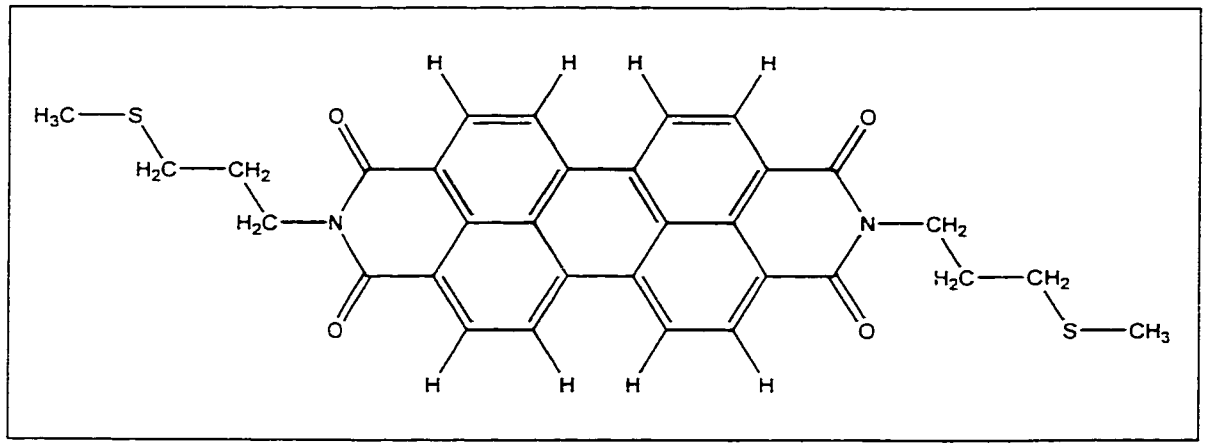

Figure 2.6.6-1: Molecular structure of 2(3s)PTCD

The chemical structure of this molecule, like 2sPTCD and 3sPTCD, contains the perylene chromophore, Figure 2.6.6-1. However it differs from the aforementioned by having two alkyl thiol chains attached to the main backbone. It was prepared by adding 5.25 g (5.27 mL, 0.05 mole) of 3-methylthiopropylamine to a dispersion of 3,4,9,10-perylene tetracarboxylic acid dianhydride (PTCDA. 3.92 g, 0.01 mole) in 200 mL of 1-methyl-2-pyrrolidinone (NMP). The mixture was stirred under an argon atmosphere for 15 min at room temperature then was heated to reflux (ca. 202 °C) for 30 min. The resultant dark brown suspension was cooled with stirring to about 155 °C, then was filtered through a 300 mL, medium porosity sintered glass funnel that had been preheated with 100 mL of boiling N,N-dimethylformamide (DMF). The solid was washed in the funnel with 3 x 40 mL portions of boiling DMF, then with 40 mL of cold DMF followed by 3 x 20 mL portions of methanol. The initial filtrate and first boiling DMF wash were black the third DMF wash was orange. The product was dried at 60 °C for 16 h to give 4.2 g (74%) of shiny black needles. The compound showed sharp, endothermic transitions at 237, 363 and 373 °C by Differential Scanning Calorimetry (DSC). ^{1}H-NMR (300 MHz, 1:3 V/V

$CF_3CO_2D/CDCl_3$, internal TMS): 2.15(m, 4H, CH_2), 2.20 (s, 6H, S-CH_3), 2.76 (t, 4H, CH_2-S), 4.41 (t, 4H, N-CH_2), 8.83 ppm (m, 8H, Ar-H). *Anal.* Calcd. for $C_{32}H_{26}N_2O_4S_2$: C 67.82, H 4.62, N 4.94. Found: C 67.61, H 4.47, N 4.64.

Chapter 3

REFLECTION ABSORPTION INFRARED SPECTROSCOPY

Theory and interpretation

3.1. Reflection Absorption Infrared Spectroscopy

The absorption of infrared radiation by thin solid molecular films, deposited on to smooth metal surfaces, can be described within the realm of Maxwell's equations, and the corresponding technique is called reflection-absorption infrared spectroscopy (RAIRS). There are indeed a number of acronyms [39] found in the literature for this particular technique; however, RAIRS is perhaps the most common and it has been adopted in all our work. Here, the properties of reflected light would be described first followed by the spatial directionality of molecular vibrations, leading to surface selection rules and the RAIRS experiment.

In the macroscopic theory, space averages of all field quantities are performed over large distances and long time intervals compared to the characteristic atomic and molecular sizes and periods, respectively. Moreover, the space averages performed are significantly smaller than both the space and time resolution of the device employed to probe such field quantities [89]. Macroscopic Maxwell-Lorentz Theory is applied to various physical problems; however, of particular interest here is the absorption and scattering of electromagnetic waves by particles and films. The macroscopic Maxwell-Lorentz equations for a charged material medium are tabulated in Table 3.1-1 [89].

Table 3.1-1: Macroscopic Maxwell-Lorentz equations for a charged material.

$\nabla \bullet \vec{D} = \rho$	Gauss's electric law
$\nabla \bullet \vec{B} = 0$	Gauss's magnetic law
$\nabla \times \vec{E} = -\frac{\partial \vec{B}}{\partial t}$	Faraday's law
$\nabla \times \vec{H} = \vec{J} + \frac{\partial \vec{D}}{\partial t}$	Ampère's law
$\vec{F} = q\vec{E} + q\vec{v} \times \vec{B}$	Lorentz law

The field vectors are the electric displacement, $\vec{D}$, magnetic flux density, $\vec{B}$, current density, $\vec{J}$, electric field, $\vec{E}$, and magnetic field intensity, $\vec{H}$. In order to solve these equations the field vectors must be related to each other. This is accomplished with the constitutive equations,

$$\vec{J} = \sigma \vec{E} \qquad (3.1\text{-}1)$$

$$\vec{B} = \mu \vec{H} \qquad (3.1\text{-}2)$$

$$\vec{P} = \varepsilon_0 \chi \vec{E} \qquad (3.1\text{-}3)$$

$$\vec{D} = \varepsilon_0 (1 + \chi) \vec{E} \qquad (3.1\text{-}4)$$

where σ is the conductivity, μ is the permeability, ε_0 is the permittivity in vacuum, and χ is the electric susceptibility. These relations are dependant on the medium under investigation but will be assumed to be independent of fields, position and direction.

In an isotropic, non-magnetic and non-radiative material, Maxwell's relations provide a wave equation that holds for each component of the electric field $\vec{E}$.

$$\nabla^2\vec{E} = \frac{1}{\varepsilon_0 c^2}\frac{\partial^2\vec{P}}{\partial t^2} + \frac{1}{c^2}\frac{\partial^2\vec{E}}{\partial t^2} \qquad (3.1\text{-}5)$$

Consider a plane wave solution of the form:

$$E = E_0 e^{i(kz-\omega t)} \qquad (3.1\text{-}6)$$

where t is time, $\omega(=2\pi\nu)$ is the angular frequency of the wave and z is the direction of propagation. The wavevector is,

$$k = \frac{2\pi}{\lambda} = \frac{\omega}{c} \qquad (3.1\text{-}7)$$

In materials the wavevector is a complex number,

$$k = \frac{\omega}{c}\eta = \frac{\omega}{c}(n + i\kappa) \qquad (3.1\text{-}8)$$

where η is the complex refractive index.

The most productive and simple model for the material medium is the Lorentz oscillator model. It postulates that Hooke's Law can describe the force binding the electron to the nucleus of an atom,

$$F(x) = kx \qquad (3.1\text{-}9)$$

where x is the displacement from equilibrium. If the Lorentz system comes into contact with an electric field, then the electron will simply be displaced from equilibrium. The oscillating electric field of the electromagnetic wave will set the electron into harmonic motion. Thus, the dipole moment, p = ex, of each atom in the medium can be defined. If the density of atoms in the media is denoted as N, then the polarization density, $\overline{P}$, induced in the medium by the field may be defined as:

$$P = Np = Nex \qquad (3.1\text{-}10)$$

The magnetic field effects, however, are miniscule compared to the electric field and can be ignored. The equation for Lorentz force oscillations in an electric field which is polarized in the x-direction and which takes damping effects into consideration has the following form:

$$\frac{\partial^2 x}{\partial t^2} + \gamma \frac{\partial x}{\partial t} + \omega_0^2 x = \frac{e}{m} E \qquad (3.1\text{-}11)$$

where γ is the damping factor, ω_0 is the frequency, e is the electron charge and m is the electron mass. Furthermore, assuming an oscillating electric field and that the displacement follows the oscillations of the electric field:

$$x = x_0 e^{-i\omega t} \qquad (3.1\text{-}12)$$

$$\frac{\partial x}{\partial t} = -i\omega x_0 e^{-i\omega t} \qquad (3.1\text{-}13)$$

$$\frac{\partial^2 x}{\partial t^2} = -\omega^2 x_0 e^{-i\omega t} \qquad (3.1\text{-}14)$$

Substituting equations (3.1-12) - (3.1-14) into equation (3.1-11) and solving for x_0:

$$x_0 = \frac{\frac{e}{m} E_0}{\omega_0^2 - \omega^2 - i\gamma\omega} \qquad (3.1\text{-}15)$$

The dipole moment may now be defined as:

$$p_0 = e x_0 = e \times \frac{\frac{e}{m} E_0}{\omega_0^2 - \omega^2 - i\gamma\omega} = \frac{\frac{e^2}{m} E_0}{\omega_0^2 - \omega^2 - i\gamma\omega} \qquad (3.1\text{-}16)$$

Thus, the polarization density can be written as:

$$P_0 = Np_0 = N[\frac{\frac{e^2}{m}}{\omega_0^2 - \omega^2 - i\gamma\omega}] \cdot E_0 = N\alpha(\omega)E_0 \qquad (3.1\text{-}17)$$

where $\alpha(\omega)$ is the atomic polarizability. The oscillating density takes the following form:

$$P = Np = N\frac{\frac{e^2}{m}}{\omega_0^2 - \omega^2 - i\gamma\omega}E_0 e^{i(kz-\omega t)} \qquad (3.1\text{-}18)$$

Using the polarization density in the wave equation and solving for ***k***:

$$k^2 = \frac{\omega^2}{c^2}\left(1 + \frac{N\frac{e^2}{m}}{\varepsilon_0(\omega_0^2 - \omega^2 - i\gamma\omega)}\right) = \frac{\omega^2}{c^2}\varepsilon(\omega) \qquad (3.1\text{-}19)$$

$\varepsilon(\omega)$ is the dielectric function connecting the external field with the dielectric displacement in matter:

$$D = \varepsilon(\omega)\varepsilon_0 E \qquad (3.1\text{-}20)$$

Let the plasma frequency, ω_p^2, be defined as:

$$\omega_p^2 = \frac{Ne^2}{\varepsilon_0 m} \qquad (3.1\text{-}21)$$

Then the dielectric function can be written as:

$$\varepsilon(\omega) = \eta^2 = 1 + \frac{\omega_p^2}{\omega_0^2 - \omega^2 - i\gamma\omega} \qquad (3.1\text{-}22)$$

Furthermore,

$$\eta^2 = (n + i\kappa)^2 = n^2 - \kappa^2 + i2n\kappa = \varepsilon_1(\omega) + i\varepsilon_2(\omega) \qquad (3.1\text{-}23)$$

Extracting the real and the imaginary parts from equation (3.1-23):

$$\varepsilon_1(\omega) = n^2 - \kappa^2 = 1 + \frac{\omega_p^2(\omega_0^2 - \omega^2)}{(\omega_0^2 - \omega^2)^2 + \gamma^2\omega^2} \tag{3.1-24}$$

whilst the imaginary part of the dielectric function is:

$$i\varepsilon_2(\omega) = i2n\kappa = \frac{i\omega_p^2\gamma\omega}{(\omega_0^2 - \omega^2)^2 + \gamma^2\omega^2} \tag{3.1-25}$$

The real and imaginary part of the complex refractive index are given by

$$n = \left(\frac{1}{2}\{\varepsilon_1(\omega) + [\varepsilon_1^2(\omega) + \varepsilon_2^2(\omega)]^{1/2}\}\right)^{1/2} \tag{3.1-26}$$

$$\kappa = \left(\frac{1}{2}\{-\varepsilon_1(\omega) + [\varepsilon_1^2(\omega) + \varepsilon_2^2(\omega)]^{1/2}\}\right)^{1/2} \tag{3.1-27}$$

When $\omega_0 = \omega$, the external frequency reaches the value of the natural frequency of the molecule, the system is in resonance. The absorption of energy at the resonant frequency is discussed in terms of a number defined in forced oscillations, the quality factor $Q = \frac{\omega_0}{\gamma}$.

The relative intensity of the absorption is directly proportional to the quality factor.

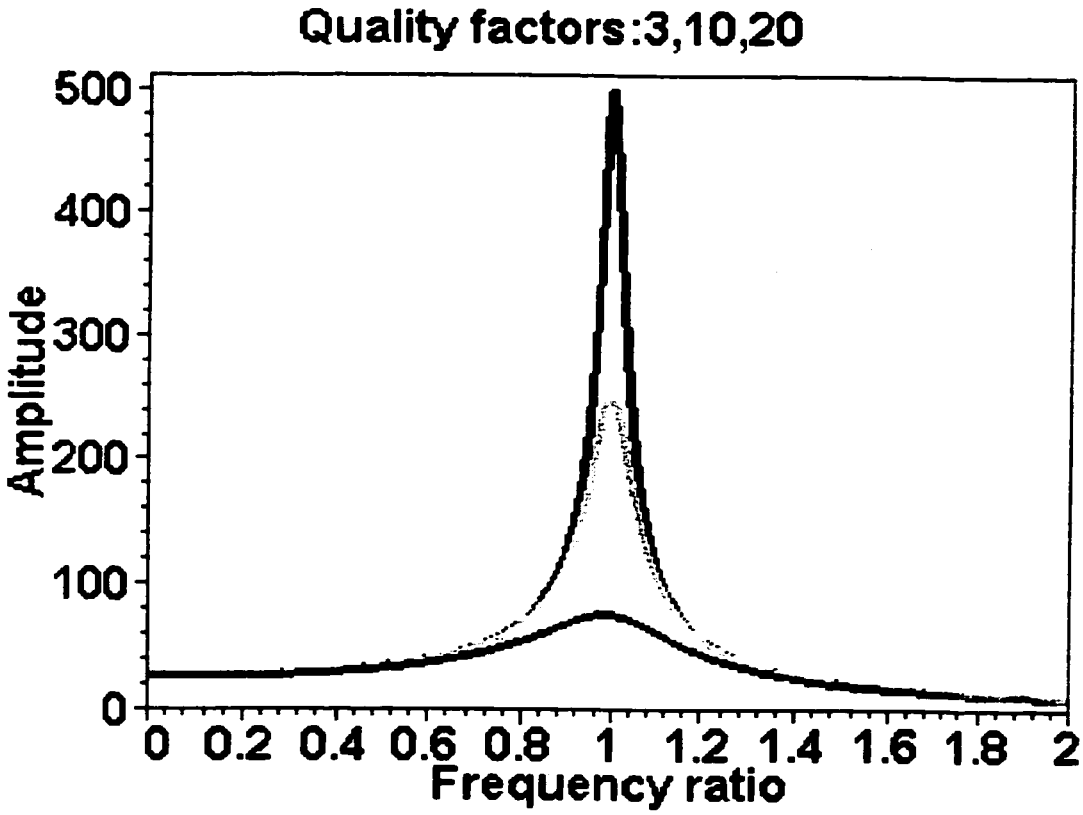

Figure 3.1-1: Illustration of the relationship between relative intensity and quality factor.

The effect of the quality factor in the absorption spectrum is illustrated in the figure using three values of Q = 3,10 and 20. The maximum is observed in resonance, i.e., at

$$\frac{\omega}{\omega_0} = 1, \textit{for the resonance condition}.$$

The model of a single oscillator or that of an ensemble of uncoupled oscillators allows one to discuss the optical properties of some matter. It is demonstrated that the amplitude of these driven oscillators is maximum in resonance and it depends on the damping, where a low damping corresponds to a high quality factor and vice versa. However, the amplitude strongly depends on a factor that is not included in (3.1-22), the strength of the coupling between electromagnetic field and oscillator called the oscillator

strength. In quantum mechanics this is the transition matrix squared. The resonances of oscillators permit one to describe molecular resonances in the visible or infrared spectral region as well as other resonances in solid such as optical phonons, plasmons and excitons. The case of strong coupling between the electromagnetic wave and the polarization wave gives rise to the world of polaritons and quasiparticles.

In summary, the simple model of force oscillator is a powerful tool to discuss the spectra of matter interacting with an external electromagnetic field. The absorption is well defined in terms of the natural frequency (resonance frequency), the damping that determines the quality factor and the imaginary part of the electric susceptibility.

3.2. Reflection at smooth metal surfaces.

The first study of reflection-absorption infrared radiation on smooth metal surfaces was that of Francis and Ellison [90], who studied LB of stearates on silver mirrors. This work was promptly followed by Pickering and Eckstrom's report [91] on CO absorption on rhodium mirrors. However, it was Robert Greenler [92] who developed both the experimental aspects and theory of reflection absorption infrared spectroscopy. He investigated the problem of obtaining the infrared spectrum of a molecular monolayer adsorbed on a bulk metal, while adjusting the optical constants of the adsorbed layer and the metal, various thicknesses of the absorbed layer, the angle of incidence and both states of polarization of the incident radiation.

The problem of determining the light reflected and transmitted at a boundary separating two media is dealt with by applying boundary conditions to the solutions of Maxwell's equations. The laws governing the optical properties of light dictate that a light wave is reflected and refracted on encountering a boundary between two media.

Light is refracted and propagated into the second medium, while it is reflected in the first. This phenomenon is explicitly defined in Snell's and Fresnel laws. Consider the reflection of infrared radiation from a clean and highly reflecting metal surface. The incident beam impinges at an angle θ relative to the surface normal: the incident and reflected beam and the surface normal lie in the incident plane, Figure 3.2-1.

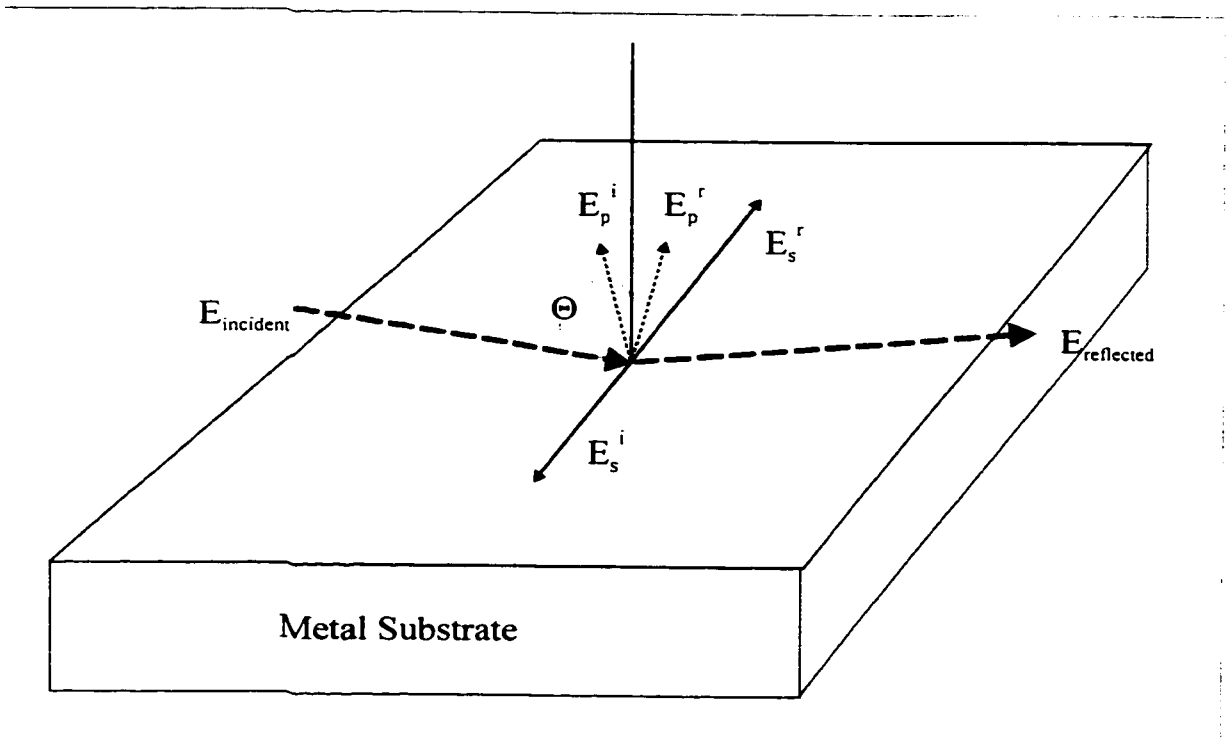

Figure 3.2-1: Reflection geometry showing the s and p components of the electric fields of the incident, E^i, and the reflected, E^r, radiation.

The Fresnel law for reflected light on a boundary between two media is a conservation law, where the sum of the components of the electromagnetic field must be equal for the two media at the interface [93].

$$\frac{r_p}{a_p} = \frac{\tan(\theta - \theta_1)}{\tan(\theta + \theta_1)} \qquad (3.2\text{-}1)$$

$$\frac{r_s}{a_s} = \frac{\sin(\theta - \theta_1)}{\sin(\theta + \theta_1)} \qquad (3.2\text{-}2)$$

where a and r are the amplitudes of the incident and reflective wave respectively, and s and p refer to the polarization. The angle of refraction is given by θ_1 and the angle of incidence is given by θ. Snell's law states that at the media interface the phase of both the reflected and refracted wave must equal that of the incident wave [94]. Thus,

$$\frac{\sin\theta}{v} = \frac{\sin\theta'}{v_1} = \frac{\sin\theta_1}{v_2} \qquad (3.2\text{-}3)$$

where θ' is the angle of reflection [95] and v_1 and v_2 are the velocities of light in the two media. The angle of incidence and the angle of refraction may then be defined in terms of the refractive index:

$$\sin\theta = \left(\frac{v_1}{v_2}\right)\sin\theta_1 = n\sin\theta_1 \qquad (3.2\text{-}4)$$

where $\theta_1 = \pi - \theta$

The intensity for the reflected radiation, in a non-absorbing material, is the square of the real amplitudes. As a result,

$$R_p = r_p^2 = 0 \qquad \text{when } \theta + \theta_1 = \frac{\pi}{2} \qquad (3.2\text{-}5)$$

Furthermore, since

$$\cos^2\theta_1 = 1 - \sin^2\theta_1 \qquad (3.2\text{-}6)$$

$$\cos\theta_1 = \pm\sqrt{1-\frac{\sin^2\theta}{n^2}} \qquad (3.2\text{-}7)$$

However, the refractive index is complex and $\cos\theta_1$ may be written as

$$\cos\theta_1 = \pm i\sqrt{\frac{\sin^2\theta}{n^2}-1} \qquad (3.2\text{-}8)$$

where n is the complex refractive index of the medium. For unit amplitude of incident light, the amplitude of s-polarized reflected wave is given by:

$$r_s = -\left(\frac{\sin\theta\cos\theta_1 - \cos\theta\sin\theta_1}{\sin\theta\cos\theta_1 + \cos\theta\sin\theta_1}\right) \qquad (3.2\text{-}9)$$

After algebraic rearrangements, the amplitude of the reflected wave is defined as:

$$r_s = -\left[\frac{-\cos\theta + i\sqrt{\sin^2\theta - n^2}}{\cos\theta + i\sqrt{\sin^2\theta - n^2}}\right] \qquad (3.2\text{-}10)$$

Similarly the amplitude of the p-polarized reflected wave is given by:

$$r_p = \left[\frac{n^2\cos\theta - i\sqrt{\sin^2\theta - n^2}}{n^2\cos\theta + i\sqrt{\sin^2\theta - n^2}}\right] \qquad (3.2\text{-}11)$$

The reflectance, R, of a non-absorbing opaque medium for a given polarization is completely described by the absolute value of the square of the amplitude of the reflected wave for that polarization and with unit amplitude of the incident light.

$$R = |r|^2 \qquad (3.2\text{-}12)$$

Thus, the reflectance for a smooth metal for p-polarised and s-polarised reflected wave can be defined as:

$$R_p = r_p^2 \qquad (3.2\text{-}13)$$

Figures 3.2-2, 3.2-3, and 3.2-4 illustrate the amplitudes and reflectance for the s- and p-polarized reflected wave for silver, gold and aluminum in the UV region and IR region of the electromagnetic spectrum respectively.

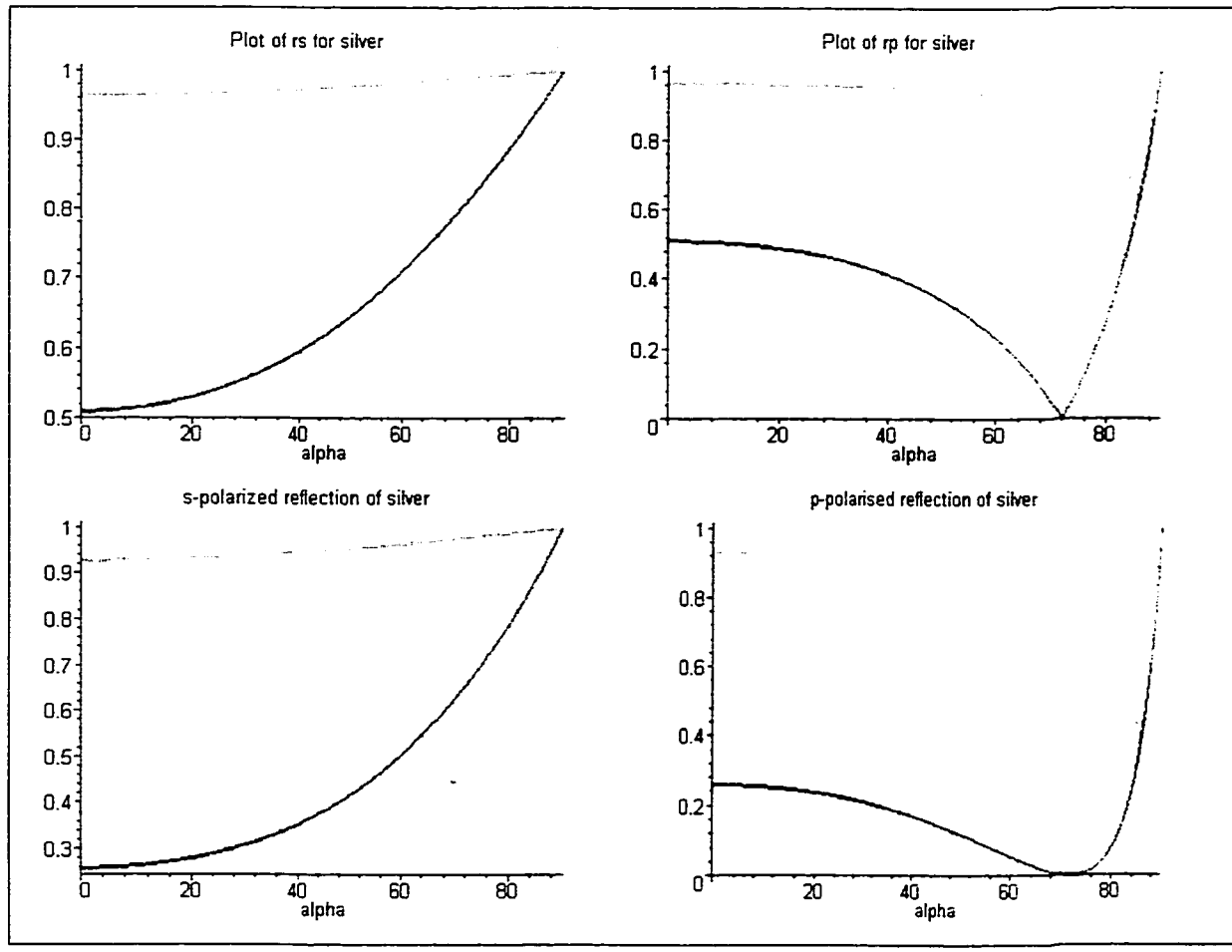

Figure 3.2-2: Amplitudes and reflectance for s- and p-polarized reflection wave for silver at 516.6 nm (red) and 9.537 μm (green).

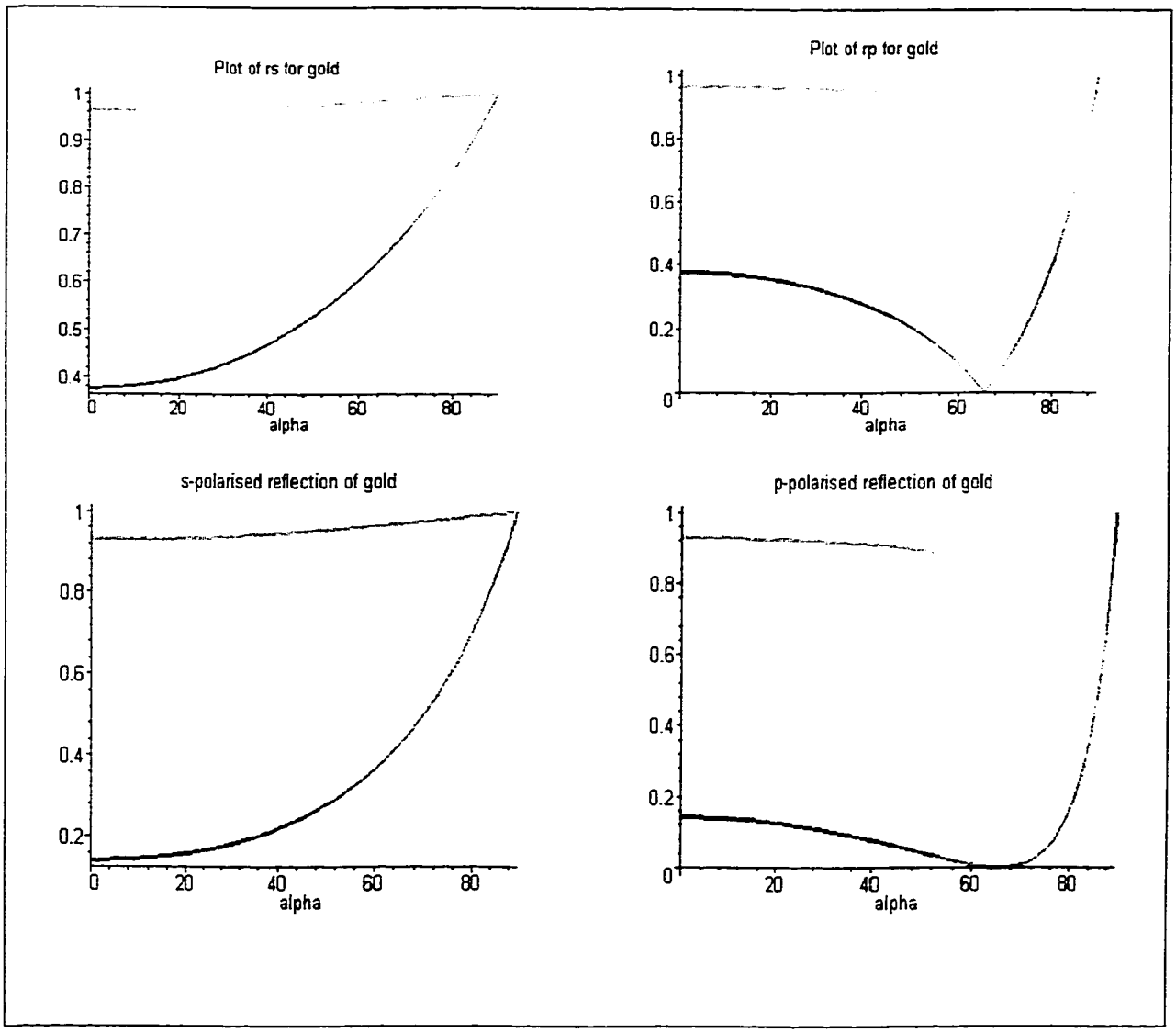

Figure 3.2-3: Amplitudes and reflectance for s- and p-polarized reflection wave for gold at 516.6 nm (red) and 9.537 μm (green).

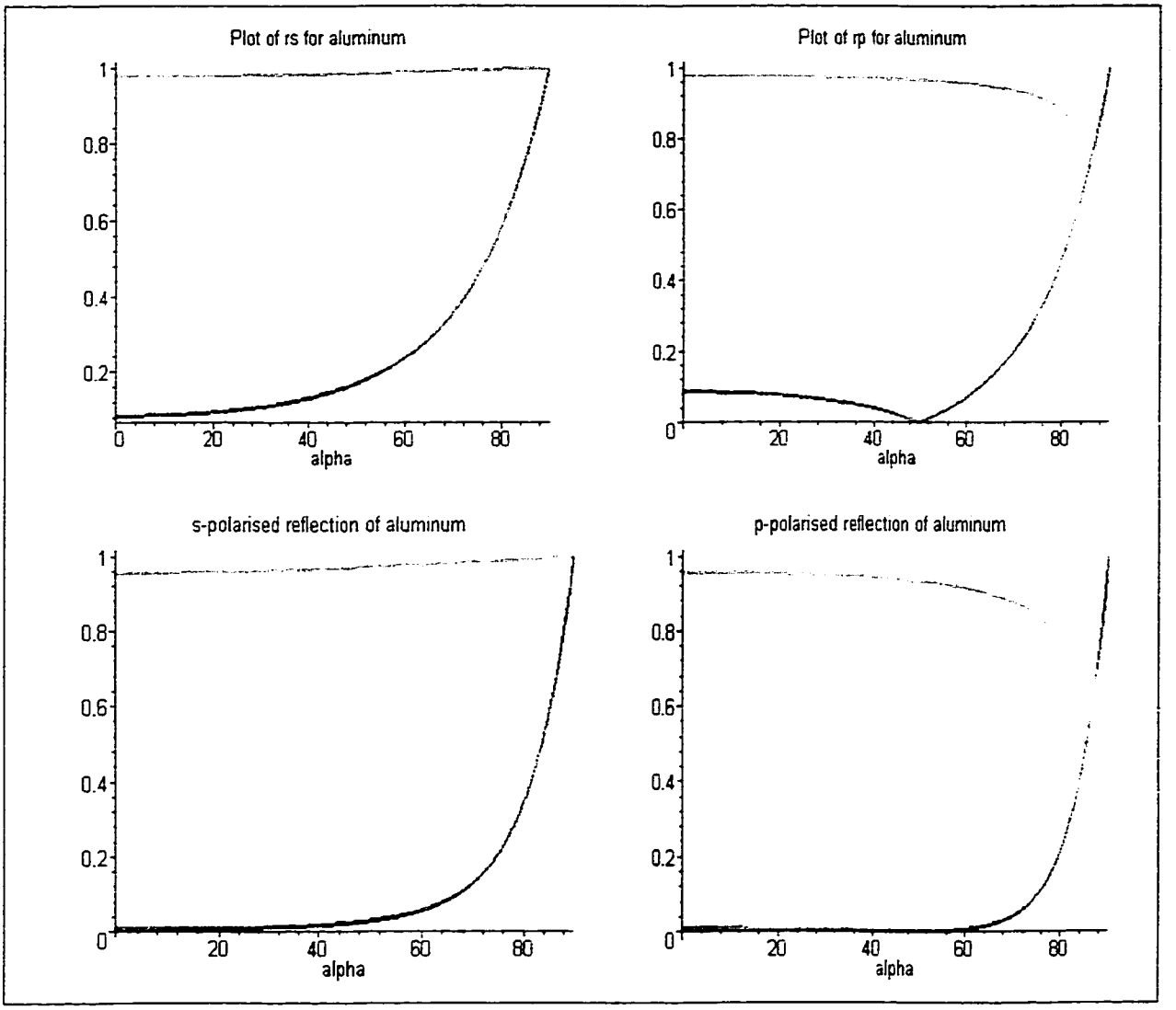

Figure 3.2-4: Amplitudes and reflectance for s- and p-polarized reflection wave for aluminum at 516.6 nm (red) and 9.537 μm (green).

The interference of the incident and reflected electric fields are now considered. If the amplitude of the incident electric field is equal to that of the reflected electric field, since the reflection coefficients are themselves complex quantities, the amplitudes of the incident and reflected fields are related by the Fresnel coefficients:

$$R_p = r_p A_p \qquad (3.4-7)$$

$$R_s = r_s A_s \qquad (3.4-8)$$

Where A_p and A_s are the amplitudes of the incident electric fields.

3.3. Molecular Vibrations in Films

The interaction of IR electromagnetic radiation with matter, illustrated in Figure 3.3-1, can be described as a linear dipole coupling due to the atomic vibrational motion. This motion may be resolved into a superposition of a limited number of fundamental motions called normal modes of vibration. In general, a molecule with N atoms will have 3N-6 modes of vibration, while a linear molecule will have 3N-5 modes of vibration. For each such mode, the periodic displacement of the atoms involved in that mode can be represented by a normal coordinate, Q. The dipole moment of the molecule, μ, is in general a function of Q and will change from its static value if that mode is energized by the absorption of IR radiation.

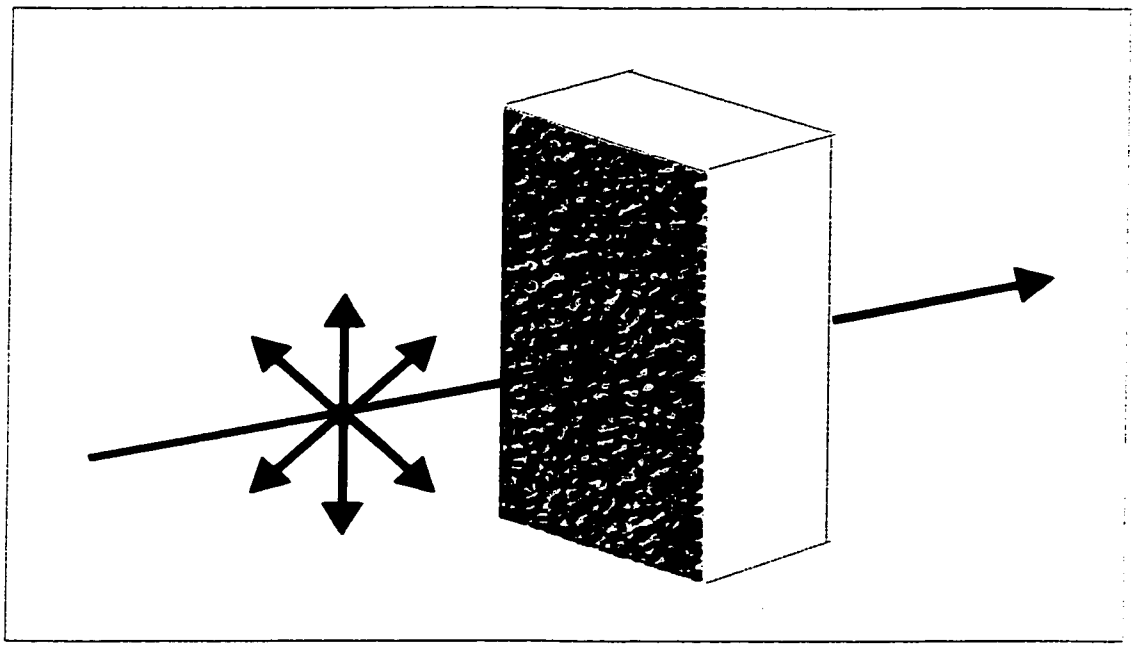

Figure 3.3-1: Polarization effects associated with transmission infrared spectroscopy of thin films.

A vibrational transition is IR active if the electric dipole moment of the molecule changes during a vibration. The interaction of the IR photon with a molecule is described by adding an interaction Hamiltonian, H_{int}, to the ground state Hamiltonian, H_0 in the Schrodinger equation for a stationary state. The form of $H_{int} = \bar{E} \bullet \mu$, the dot product of the optical electric field and the transition dipole moment. The transition moment for a transition between lower and upper states with vibrational wave functions ψ_k and ψ_m respectively is given by:

$$\int \psi_m^*(\tau) H_{int}(\tau) \psi_k(\tau) d\tau = \langle m | \mu \bullet \bar{E} | k \rangle \qquad (3.3\text{-}1)$$

where $d\tau$ is a volume element in configuration space. The total dipole moment can be expanded in a Taylor series about the equilibrium configuration. However, because ψ_m and ψ_k are orthogonal wavefunctions, and the transition probability is given by the square of the transition moment, the probability is defined by:

$$P_{mk} \propto \left(\frac{\partial \mu}{\partial Q} \bullet \bar{E} \right)^2 |\langle m | Q | k \rangle|^2 \qquad (3.3\text{-}2)$$

Due to the orthogonality of ψ_m and ψ_k, the integral $\langle m|Q|k \rangle$ is non-zero only if $k = m+1$. This is the spectral selection rule for fundamental modes. It should be noted that from the preceding equation, the absorption probability depends on the dynamic dipole moment, that is the change in the dipole moment during the vibration. Thus, $(\frac{\partial \mu}{\partial Q})_0$ should be different from zero to have an infrared active mode. Furthermore, the probability of observing an IR absorption band is easily determined using the symmetry properties of the molecule. Each molecule can be assigned to a specific point group, which in turn

possesses a certain number of symmetry elements. The symmetry operations associated with the individual symmetry elements, when performed on a molecule, must leave at least one atom (or point) indistinguishable. The total molecular matrix can be reduced to their respective irreducible representations. The important group theoretic properties of a point group are summarized in the form of a character table, which gives the characters of the irreducible representations or symmetry species for each symmetry operation. It is important to realize that not all possible vibrational modes are IR active and that the wavefunctions ψ_m and ψ_k have symmetry properties represented by symmetry species. Thus, the selection rules indicating which transitions are allowed in the IR spectra are readily derived when the symmetries of ψ_m, ψ_k and $\frac{\partial \mu}{\partial Q}$ are known. If the product:

$$\Gamma[\psi_m] \times \Gamma\left[\frac{\partial \mu}{\partial Q}\right] \times \Gamma[\psi_k] \qquad (3.3\text{-}3)$$

contains the totally symmetric irreducible representation of the point group, the transition is IR active [96].

According to (3.3-2), the absorption further depends on the square of the cosine of the angle between the change in the dipole moment, $\frac{\partial \mu}{\partial Q}$, and the electric field, $\vec{E}$. Therefore, when the direction of the electric field is known (fixed polarization), molecular orientation can be probed as it can be done in solids: crystals and films where molecules have fixed spatial orientations. In infrared transmission spectroscopy, the origin of the technique sensitive to light polarization is illustrated in Figure 3.3-2.

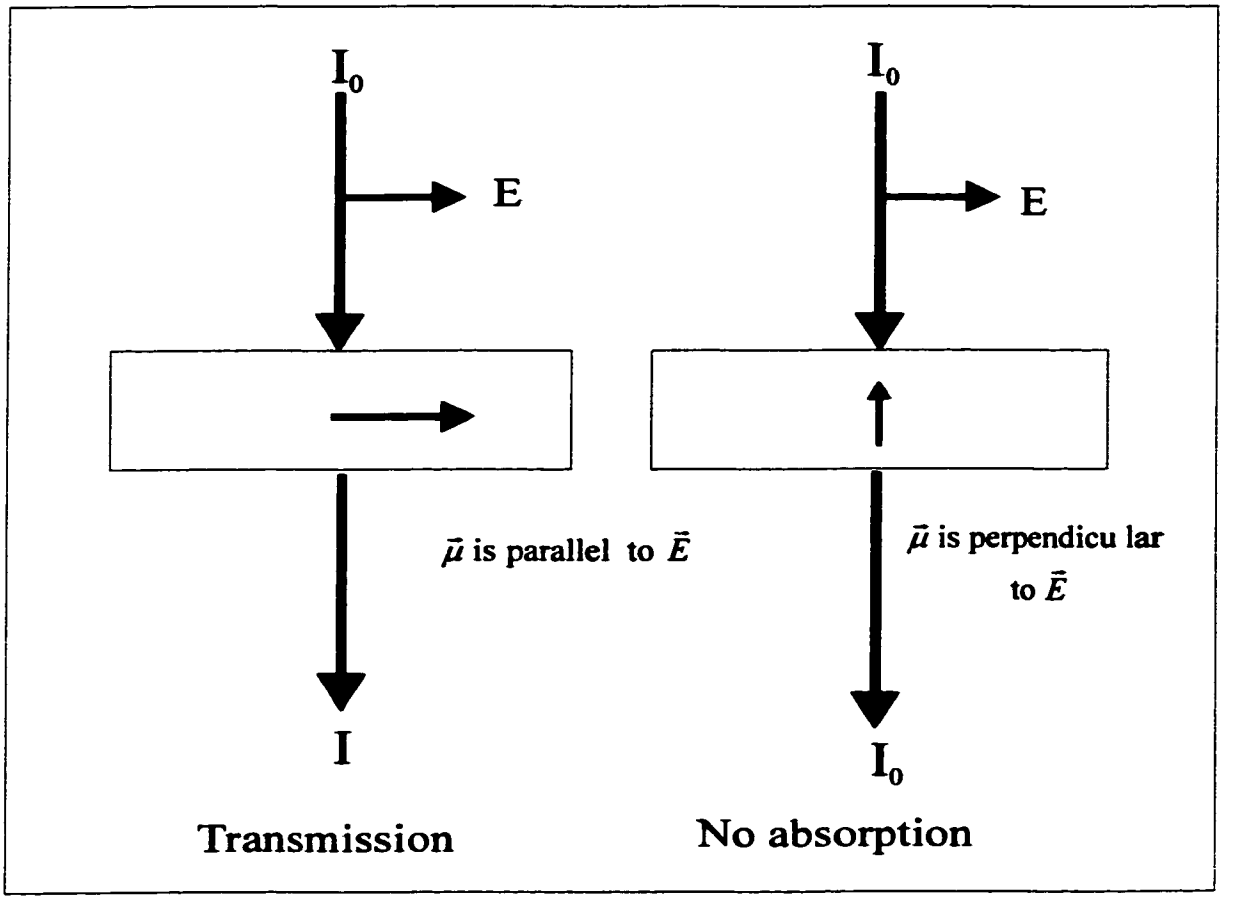

Figure 3.3-2: Polarization effects due to dipole orientation

3.4. The RAIRS experiment

Reflection absorption IR spectroscopy probes the interface region above a metal surface by measuring the absorption of a specularly reflected IR beam, incident at glancing angles, as a function of wavenumber. From the previous discussion it is evident that the absorption of radiation by a thin film on a smooth metal surface depends on two **spatial** factors: the polarization of the beam of light at the surface and the molecular orientation in the film.

The first application for reflectivity for the s and p-polarized components of an electromagnetic wave incident at an angle θ on a metal surface from air, was developed

by Greenler [92]. It was shown that light at a reflecting surface is highly polarized and that at an appropriate angle of incidence the p-polarized component of the electromagnetic wave is three orders of magnitude greater than the s-polarized or parallel component [97]. The intensity of the absorption of an IR allowed transition in a molecule is determined by

$$I = \left|\frac{\partial \mu}{\partial Q}\right| \bullet \vec{E} \cos\theta \qquad (3.4\text{-}1)$$

Thus, a molecule oriented such that the change in the dynamic dipole moment of one of its normal vibrational modes is parallel to the electric field ($\cos\theta=1$) will demonstrate a maximum intensity. However, if the change in the dynamic dipole moment of the same vibrational mode is oriented perpendicular to the electric field ($\cos\theta = 0$), the resulting intensity would be negligible, and as a result the molecular orientation of a molecule on a metal surface can be determined. This is widely known as the surface selection rules [98]. These surface selection rules further restrict the selection rules given by the irreducible symmetry species, due to the constraints introduced by molecular orientation and light polarization.

Both the polarization effects of reflection and interference at metal surfaces and molecular symmetry provide the tools required to extract molecular orientation and distinguish between vibrationally allowed modes from observed spectral intensities in terms of local surface selection rules. For large molecules, such as bis-(N-propylimido) perylene (bisPTCD), the local symmetry arguments may be used to find the directionality of the dipole moment derivatives that may allow molecular orientation determination, thus further discussion of perylene molecule is limited to the perylene tetracarboxylic

diimide (PTCD) moiety. The molecular groups that are largely responsible for the change in the dipole moment, as well as the directionality of the dynamic dipole of the PTCD moiety are identified as the carbonyl stretching modes in the plane of the PTCD chromophore observed at 1662 cm^{-1} and 1697 cm^{-1}, and the C-H wagging modes out of the plane of the chromphore observed at 810 cm^{-1} and 746 cm^{-1} [42]. Molecular organization in a film creates a spatial anisotropy that can be extracted using the change in the relative intensity observed in the spectra of the film recorded in the transmission geometry and in RAIRS. In the transmission geometry, the polarization of the incident light lies parallel to the surface and absorption intensity is maximum for normal vibrational modes that have a change in their dipole moment parallel to the substrate (as illustrated in Figure 3.3-2). On the other hand, in RAIRS, the vibrational modes with a change in dipole moment perpendicular to the substrate will demonstrate maximum absorption intensity. Hence, the orientation of the bisPTCD molecule on the surface of a metal can be determined by the changes in ratio of the in-plane C=O stretching band intensity to the out-of-plane C-H stretching band intensity.

In a reflection absorption infrared spectrum of a vacuum evaporated film of bisPTCD, in which the molecular orientation of the perylene chromophore is head-on the metal substrate, the in-plane carbonyl stretching modes of the bisPTCD molecule appear relatively more intense than the out-of-plane C-H wagging modes. Furthermore the symmetric in-plane C=O stretching mode will be more intense than the antisymmetric carbonyl stretching mode for this orientation. This is determined by the fact that a large band intensity for the in-plane C=O stretch indicates that the dynamic dipole for this vibration is parallel to the electric field and therefore perpendicular to the metal substrate.

Conversely, weak band intensity for the out-of-plane C-H wag indicates that the dynamic dipole for this vibration is perpendicular to the electric field but parallel to the metal substrate, as illustrated in Figure 3.4-1.

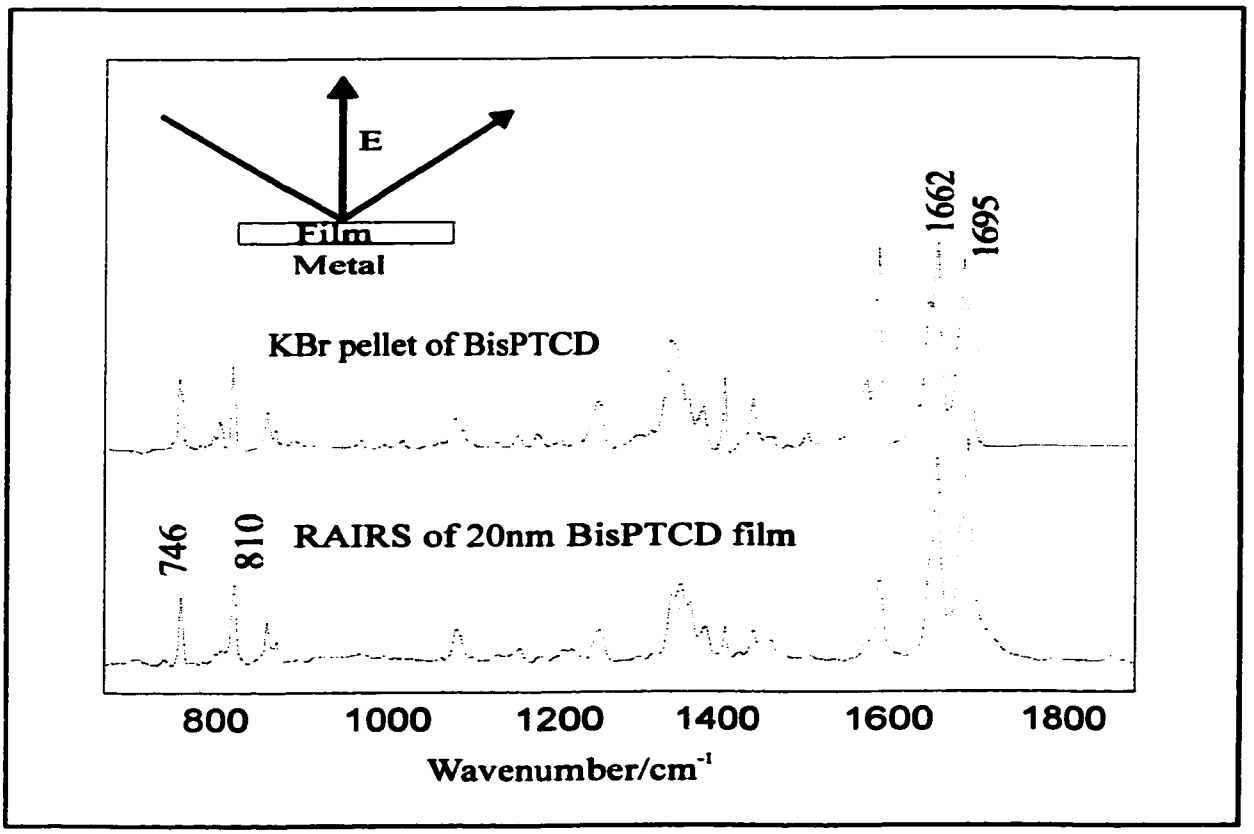

Figure 3.4-1: Transmission spectrum of bisPTCD pellet and RAIRS spectrum of an evaporated 20 nm film of BisPTCD on silver mirror.

Chapter 4

BIS(N-PROPYLIMIDO) PERYLENE

Spectroscopic characterization and orientation studies

4.1. Electronic Characterization

The electrical and optical spectra of individual perylene molecules are dominated by their electronic structure. In the solid state, the electronic interactions between the closed-packed planes of the perylene chromophore are influenced by various steric effects, and are easily altered by molecular tailoring. These differences in interactions are reflected by shifts in the absorption spectra corresponding to the π-π^* transition and physically, by variations in color of different perylene dyes [77]. Similarly, artifacts in the emission spectra of perylene dyes characterize their degree of aggregation in thin solid films.

The electronic absorption of bis (N-propylimido) perylene, bisPTCD, in solution displays the characteristic vibronic progression of the perylene molecules, in which the vibronic structure corresponds to a constant wavenumber of 1407 cm^{-1} [80]. This is the difference between the 0,0 band at 539 nm and the 501 nm band, and the difference between the 0,1 band at 501 nm and the 468 nm band. The same components are seen in the electronic spectrum of the 20 nm film, however the effect of band broadening in the solid produces an overlapping as shown in Figure 4.1-1. The broadening observed in the spectrum of the film is even more pronounced in the electronic absorption spectrum of the isotropic KBr pellet. The electronic absorption spectra of bisPTCD in solution and that of a 20 nm thin film evaporated onto KBr substrate are shown in Figure 4.1-1.

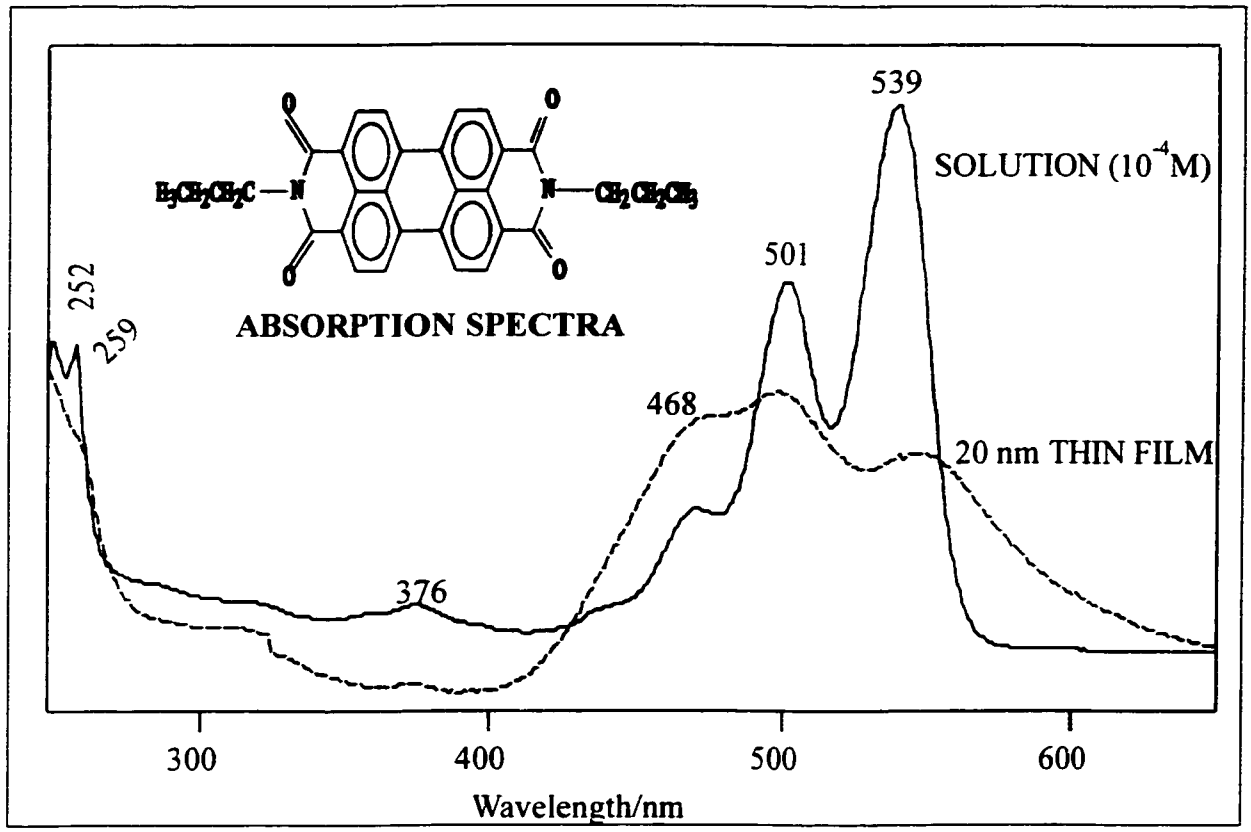

Figure 4.1-1: Absorption spectra of bisPTCD in solution and of a 20 nm thin solid film.

The steady state fluorescence spectrum of a solution of bisPTCD was identical with that of other members of the monomer perylene tetracarboxylic acid dianhydride series [8, 99]. It resembles the mirror image to that observed in the electronic absorption spectrum of a solution of bisPTCD, with a pronounced red shift in the vibronic structure. A characteristic broad excimer emission was observed for the evaporated 20 nm film at 686 nm and for the KBr pellet at 696 nm. The emission spectra of the solution, thin film and KBr pellet of bisPTCD are shown in Figure 4.1-2.

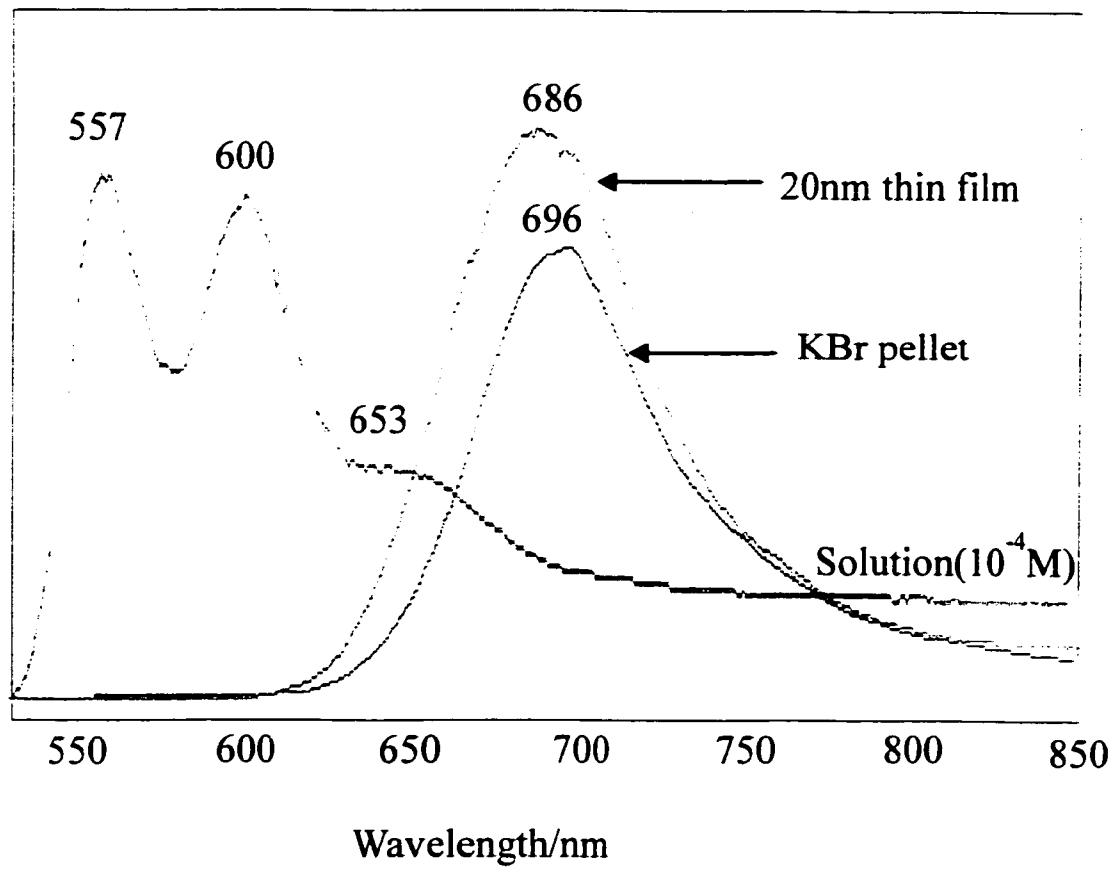

Figure 4.1-2: Electronic emission spectra of bisPTCD

4.2. Vibrational Characterization

Vibrational spectroscopy provides four observables that may be used to extract physical information from thin solid films: the resonance band center position, the band shape, the selection rules and the band intensity. It is this wealth of information that makes vibrational spectroscopy a unique optical probe for determination of the overall structure, chemical and localized intermolecular interactions in thick and submicron thin solid films [39, 40]. In particular, the simple polarization selection rules operating in the specular reflection absorption infrared spectroscopy (RAIRS) have been extensively used to determine the orientation of submicron organic films thermally deposited by vacuum

vapor deposition on a reflecting metal surface. Transmission and reflection spectroscopic techniques can be used complementarily to enable a definitive account of the molecular orientation of perylene molecules via the surface selection rules [41, 42].

The bis- (N-propylimido) perylene molecule has 168 fundamental vibrational modes, however analysis will be limited to only the assignment of characteristic fundamental vibrational wavenumbers of the PTCD moiety, such as those belonging to the carbonyl stretching, ring stretching and C-H wagging vibrations. For large molecules the local symmetry arguments may be used to find the directionality of the dipole moment derivatives that may allow molecular orientation determination. Therefore, the goal here is the identification of normal modes and local symmetry assignments, i.e., the identification of the molecular group largely responsible for the change in the dipole moment as well as the directionality of the dynamical dipole. For instance, the infrared active vibrations of the PTCD moiety may be classified into in-plane and out-of-perylene-plane fundamental vibrational modes. Further, the normal modes of bisPTCD are expected to correlate with the vibrational spectra of N-pentyl-N'-propyl-perylenebis (dicarboximide)(PPTCDPr) that has been previously reported, as only those normal modes of the core PTCD moiety are investigated and the chemical structure of bisPTCD is similar to PPTCDPr [8].

The most significant and relevant group frequencies for molecular orientation considerations in bisPTCD films are the carbonyl stretching vibrations, the in-plane C=C and ring vibrations of perylene and the out-of-perylene-plane C-H wagging vibrations. The antisymmetric and symmetric in-plane C=O stretching vibrations for bisPTCD are observed at 1662 cm^{-1} and 1697 cm^{-1} respectively, while the C=C stretches are at 1595

cm^{-1} and 1580 cm^{-1}. The two out-of-plane vibrational modes, the C-H wags, are observed at 810 cm^{-1} and 746 cm^{-1} [42]. It is essentially the changes in the band intensity ratio between the in-plane and out-of-plane vibrations, C=O/C-H, from which molecular orientation can be determined. The infrared spectrum of the KBr pellet and that of the 20 nm thin solid film on KBr are shown in Figure 4.2-1. The transmission spectra of the 20 nm evaporated film of the bisPTCD, shown in Figure 4.2-1, reveals that the out-of-plane C-H wagging bands, at 746 cm^{-1} and 810 cm^{-1} and the carbonyl stretching observed at 1662 cm^{-1} and 1697 cm^{-1} have the same relative intensity as found in the isotropic KBr pellet.

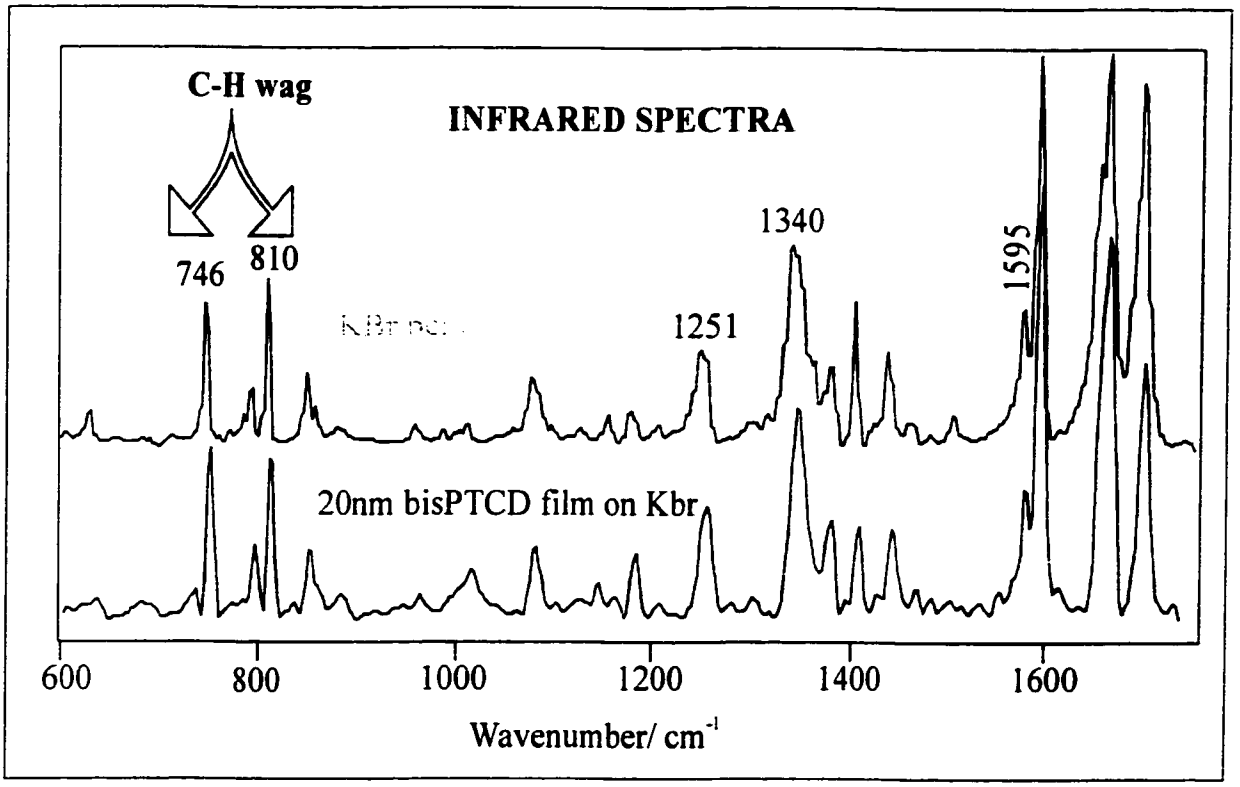

Figure 4.2-1: FTIR transmission spectra of an isotropic KBr pellet and a 20 nm thin solid film of bisPTCD on KBr.

The differences in relative intensities between the infrared spectra of bisPTCD dispersed in KBr (isotropic reference sample), and the evaporated thin film are minimal, indicating that anisotropies in the thin film structure are not detectable. It may be concluded that the film formed on KBr does not present a large degree of molecular organization. The full bandwidths at half maximum (FWHM) are also very similar for the two samples. Since FWHM are sensitive to changes in the intermolecular interactions due to molecular alignment, it is a confirmation of minimal organization in the evaporated film. Relative intensities, FWHM and the corresponding wavenumbers for all the infrared spectra are listed in Table 4.2-1.

Table 4.2-1: Observed infrared wavenumbers for bisPTCD. Relative intensity (RI) and the full width at half maximum (FWHM in cm^{-1}) are given for each spectrum. RAIRS-1: room temperature. RAIRS-2: spectrum at 200 °C.

cm^{-1}	KBr Pellet		Film		RAIRS -1		RAIRS-2		Assign.
	RI	FWHM	RI	FWHM	RI	FWHM	RI	FWHM	
746	16	6	33	6	16	6	100	6	C-H wag
810	13	5	28	5	17	5	78	5	C-H wag
850	4	5	4	5	7	5	24	5	C-H wag
1077	15	9	14	9	12	8	15	8	C-H bend
1083	20	11	3	9			5	7	C-H bend
1251	24	12	25	12	15	11	19	10	C-H bend
1343	61	14	57	16	6	12	20	10	C-N str
1404	13	6	15	6	7	6	5	6	ring str
1440	24	9	21	7	6	10	5	9	ring str
1580	6	11	12	8	2	8	2	7	C=C str
1595	38	8	50	8	21	8	25	7	C=C str
1652	62	12	30	10	10	9	18	9	C=O str
1662	100	9	100	9	84	10	30	7	C=O str
1688	60	8	7	11	30	8	7	8	C=O str
1697	66	11	51	11	100	11	25	8	C=O str

4.3. RAIRS AND THERMAL ANNEALING OF THIN FILMS.

Molecular orientation of bisPTCD on a metal substrate may be determined by the selection rules referred to in Chapter 3. The RAIRS spectra of 20 nm bisPTCD deposited onto a smooth 100 nm silver surface are shown in Figure 4.3-1. The vibrational probes used here for molecular orientation on the surface are the C-H wags at 810 cm^{-1} and at 746 cm^{-1} and the in-plane C=O stretching vibrations. The reference spectrum is the KBr spectrum given in Figure 4.2-1. The spectrum labeled before annealing is the original film evaporated onto the silver surface held at room temperature. The C-H wagging modes have a dynamic dipole, $\vec{\mu}$, perpendicular to the plane of the chromophore while the C=O modes have a $\vec{\mu}$ in the plane of the perylene moiety. Therefore, as the molecule becomes oriented with the perylene ring flat-on the silver surface, the dynamic dipole of the C-H wagging bands becomes more parallel to the electrical field component which results in the enhancement of these C-H bands, as observed.

The correlation between thermal annealing and molecular orientation in PTCD derivatives has not been investigated to date. There are many consequences of thermal annealing, and they include re-evaporation of the dye from the substrate, decomposition, oxidation of the metal substrate, and polymorphism. Experimentally, to guard againstthe water effect, the thermal annealing of the thin films was performed in a cell purged with dry air. The perylene studied was established to be thermally stable within the temperature range employed for annealing, with decomposition temperatures above 450 °C.

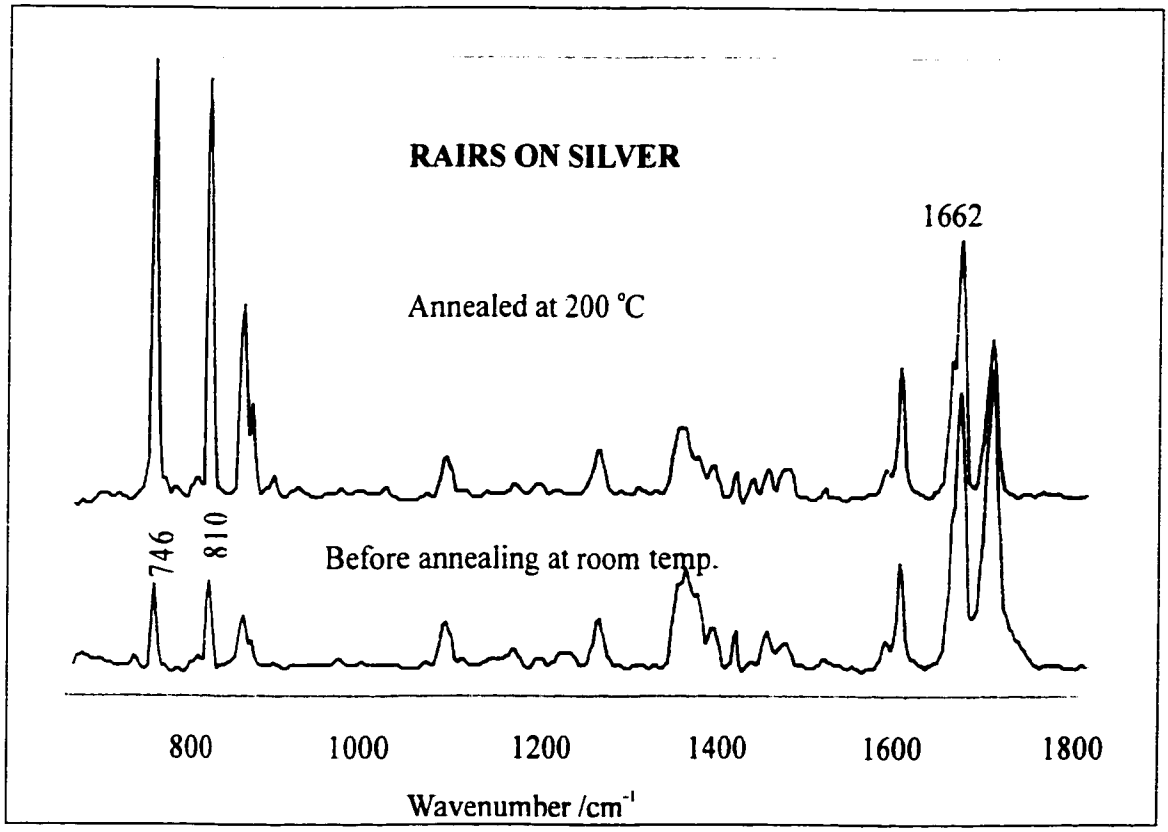

Figure 4.3-1: Reflection absorption spectra of 20 nm bisPTCD film on 100 nm Ag at room temperature and after annealing at 200 °C.

A study of bisPTCD spectra, indicated that the overall intensity of the vibrational bands has not decreased on annealing, therefore ruling out the possibility of re-evaporation. A close inspection reveals that there are four carbonyl components at 1652 and 1662 cm^{-1}, 1688 and 1697 cm^{-1}. The high wavenumber bands are the locally symmetric stretches ($\bar{\mu}$ along the long perylene axis) and the middle is the locally antisymmetric vibrations. Thus, the strong absorption at 1697 cm^{-1} points to a certain degree of head-on molecular orientation of the perylene moiety on the surface of the substrate. On thermal annealing the relative intensity of the 1662 cm^{-1} is the strongest in the C=O stretching group. Since the effective dynamic dipole of this C=O modes is along

the short perylene axis it indicates an edge-on molecular orientation of the perylene chromophore. The band intensity ratio, C=O/C-H, is therefore smaller after annealing than it is before annealing. In summary, the RAIRS spectra of the annealed bisPTCD film reveals a large increase in relative intensity for the C-H out-of-plane wagging that is consistent with a predominant perylene flat-on molecular orientation (face-on orientation). The analysis of the C=O bands further points out an intensity contribution from a fraction of molecules with an edge-on orientation. Furthermore, as can be seen in Table 4.2-1, annealing is characterized by a smaller FWHM in some bands. This provides evidence for a reduction in the amorphous content of the sample as the sample adopts a more crystalline configuration.

4.4. FT-Raman and SERRS

Raman spectroscopy is a unique surface analytical tool that provides a probe for surface structure and dynamics. The Raman process itself is inherently weak, however the discovery of surface enhanced Raman spectroscopy (SERS) conferred unprecedented sensitivity and selectivity to surface Raman spectroscopy. Moreover, this technique provides spectra that are complementary to those obtained by infrared spectroscopy. As Raman scattering depends upon the change in the molecular polarizability during a molecular vibration while infrared absorption upon the change in the dipole moment, no mode is both infrared and Raman active in centrosymmetric molecules [61]. In molecules of reasonably high symmetry, such as perylene dyes, there is still a partial exclusion. Thus both spectroscopies are necessary to obtain the complete vibrational spectrum.

The selection rules for infrared and Raman are extracted from a comparison of the FT-Raman and FT-IR spectra of bisPTCD presented in Figure 4.4-1. It can be seen that

although the relative intensities are very different, the Raman active bands are also observed in the FTIR spectrum.

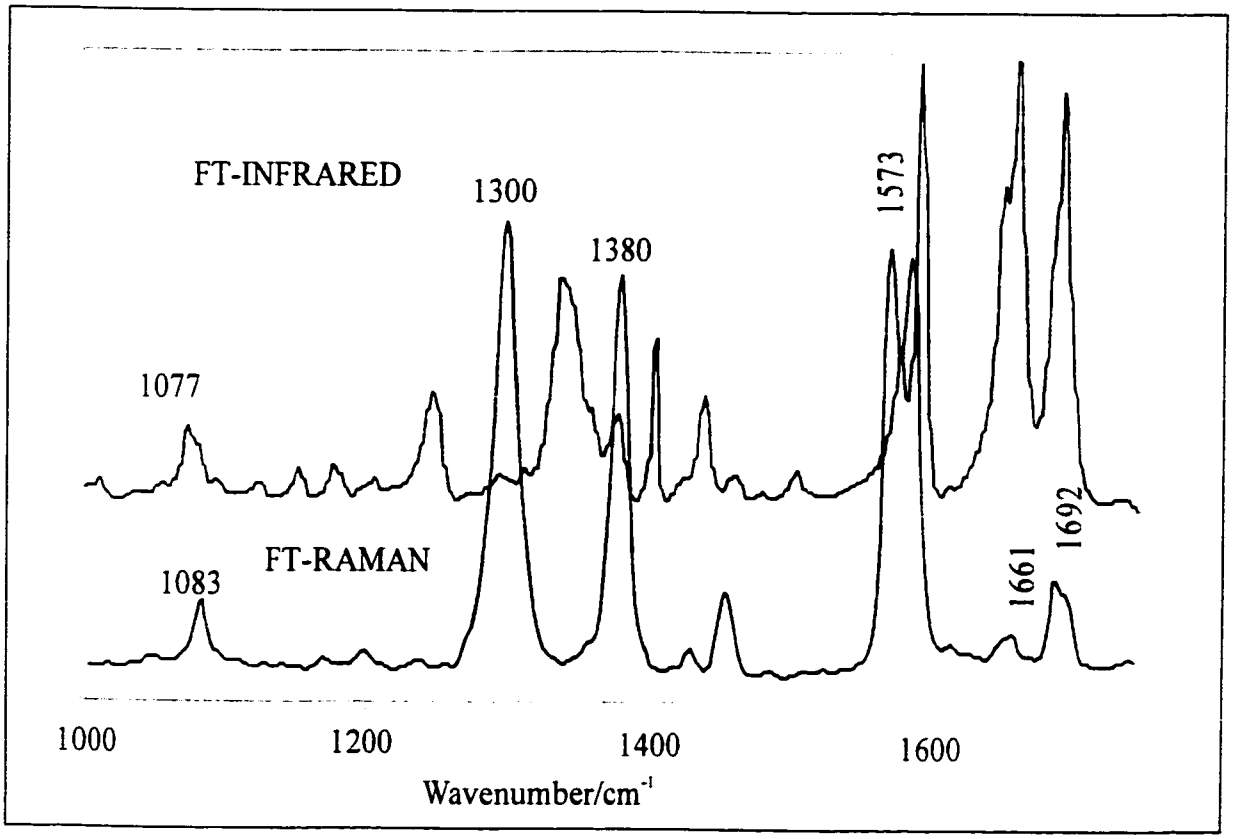

Figure 4.4-1: FT-Raman and FTIR spectra of the isotropic KBr pellet of bisPTCD.

The absorption spectrum of bisPTCD has a region of maximum absorption in the 300-500 nm range. Thus, the 1064.1 nm laser line is off resonance with this absorption band and results in spontaneous Raman scattering. On the other hand, the 514.5 nm laser line is in resonance with the region of maximum absorption and would give rise to resonant Raman spectra (RRS). Correspondingly, a surface-enhanced Raman scattering (SERRS) effect is initiated for bisPTCD deposited on silver islands and excited with the 514.5 nm laser line. The off-resonance FT-Raman excited at 1064.1 nm shows the main

peaks of the chromophore that are also seen in the resonance Raman effect and surface-enhanced resonance Raman scattering (SERRS) as shown in Figure 4.4-2.

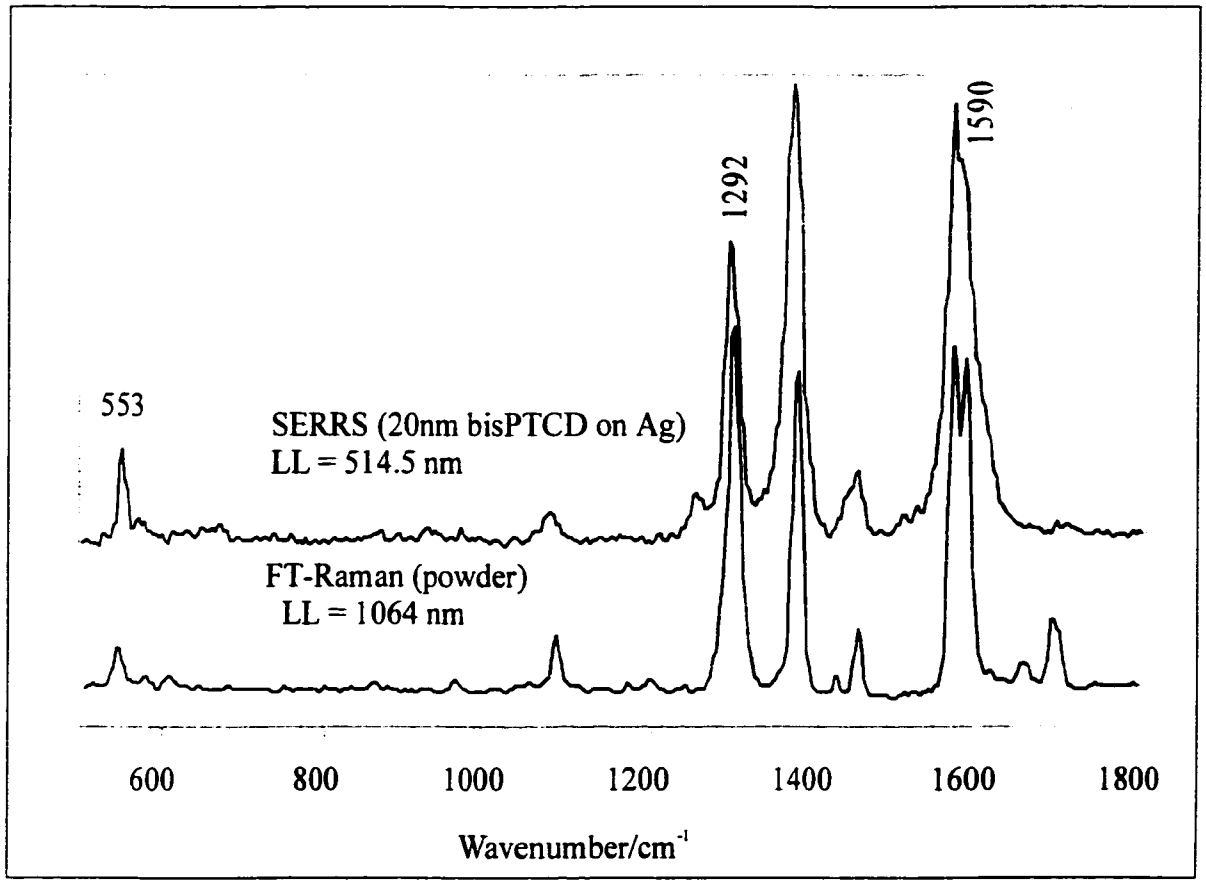

Figure 4.4-2: Enhanced inelastic light scattering in resonance with the electronic transition (SERRS) at 514.5 nm and the off resonance spectrum at 1064.1 nm.

The most important difference between the FT-Raman and SERRS is the absence of the carbonyl stretching vibrations in SERRS due to the surface selections rules observed in surface enhanced vibrational spectroscopy. The relative Raman intensities, FWHM and the corresponding wavenumbers are listed in Table 4.4-1.

Table 4.4-1: Raman wavenumbers, relative intensities (RI) and FWHM (in cm^{-1}) for bisPTCD.

FT-Raman(1064 nm)			SERRS (514.5 nm)			Assignment
cm^{-1}	(RI)	FWHM	cm^{-1}	(RI)	FWHM	
545	(6)	12	553	(9)	12	Per. Ring def.
1084	(10)	12	1076	(2)	12	C-H bendings
			1255	(8)	16	C-H bend
			1292	(34)	11	C-H bend
1300	(100)	19	1300	(27)	11	Per. ring stretch
			1372	(100)	17	Per. ring stretch
1380	(63)	15	1381	(17)	10	Per. ring stretch
1431	(1)	10	1442	(7)	15	Per. ring stretch
1456	(10)	12	1456	(10)	13	Per. ring stretch
1573	(47)	11	1572	(60)	11	C=C stretch
			1581	(41)	11	C=C stretch
1588	(60)	14	1590	(30)	17	C=C stretch
1653	(1)	9				C=O stretch
1661	(3)	11				C=O stretch
1692	(8)	10				C=O stretch
1701	(6)	9				C=O stretch

4.5. Summary

Thin films of bisPTCD have been successfully fabricated by high vacuum vapor deposition. Both the UV-VIS absorption and fluorescence spectra of solution and thin films of bisPTCD show characteristic profiles of the PTCD moiety. Comparison of the transmission and reflection absorption infrared spectra reveals an on average head-on orientation of bisPTCD in the thin films. Furthermore since FWHM and band positions are sensitive to changes in intermolecular interactions, analysis of the FWHM and band positions in both the films and RAIRS samples show no apparent changes or band shifts. This suggests that bisPTCD is physisorbed in thin evaporated films. A change in the molecular orientation and increased molecular organization in the evaporated films, in which bisPTCD molecules are physisorbed on to the substrate, can be initiated by thermal annealing, as was demonstrated. On thermal annealing the molecular orientation of bisPTCD becomes face-on. Harnessing this tool to produce films of a certain molecular architecture is industrially important. In conclusion, the spectroscopic characterization of the new material has been carried out to determine molecular symmetry and fundamental vibrations of the chromophore.

Chapter 5

THE ROLE OF WATER IN THE MOLECULAR RE-ORIENTATION ON THERMAL ANNEALING OF BIS(N-PROPYLIMIDO)PERYLENE FILMS

Application of RAIRS in solvent induced orientation investigations

5.1. Introduction

Changes in orientation are deduced from the well-known surface selection rules for reflection spectroscopy from a smooth metal surface. The description of infrared experiments on molecules adsorbed onto reflecting metal surfaces follow the surface selection rules outlined in Chapter 3. The bisPTCD chromophore is planar and thus changes in orientation can be easily determined from a comparison of modes with dynamic dipoles located within the plane of the chromophore (i.e., within the plane of the aromatic moiety) to fundamental vibrational modes with dynamic dipole moments perpendicular to the aromatic plane. Specifically, orientational changes are deduced from a comparison of the in-plane C=O stretching vibrational bands at 1662 and 1697 cm^{-1} relative to the out-of-plane C-H wagging vibrational band associated with the aromatic ring located at 810 cm^{-1}. For brevity, this band intensity ratio is abbreviated as C=O/C-H. In the previous chapter [18], it was shown that the C=O/C-H band intensity was higher in the RAIRS spectrum of the unannealed 20 nm bisPTCD film on a silver mirror than the same ratio obtained for the transmission spectrum of bisPTCD dispersed in a KBr pellet. This intensity difference is the result of the sublimed bisPTCD having, on average, a preferred orientation in which the aromatic rings extend perpendicular from the surface (head-on adsorption). Heating the sample of 20 nm bisPTCD films on a silver mirror in air at 125 °C or below did not alter the spectrum. However, when heated to 200 °C in air, the C-H out-of-plane modes increased in intensity by a factor of seven, as shown in Figure 5.1.1-1. This has been interpreted as a change in orientation where the bisPTCD assumes an orientation where, on average, the aromatic rings are face-on relative to the surface.

In this chapter the nature and origin of the induced change in the molecular organization of bis (n-propylimido) perylene films described in the previous chapter [18], are explored using reflection infrared experiments as a sensor for detecting the onset in reorientation due to solvent vapor annealing. In this manner, the change in the spectrum could be used as a probe in testing strategies for improving film robustness. In essence, a film that was more resistive to changes in morphology would likely exhibit a higher transition temperature or require longer heating times to produce a detectable band intensity change in the reflection infrared experiment. Furthermore, the role of a protective coating is investigated by using temperature as a probe and by observing the subsequent orientational change of bisPTCD films.

5.1.1. The origin of molecular reorganization

The origin of the induced re-orientation under thermal annealing was assumed to stem from external factors in this case environmental conditions. The primary step in determining the factors which influence and induce reorientation on thermal annealing was the exclusion of those factors found in the matrix of air, that are nominally, nitrogen, oxygen, carbon dioxide and water vapor. To determine whether re-orientation originated from one or a combination of these factors, a thin 20 nm film of bisPTCD on smooth silver was annealed in vacuum, employing a range of annealing temperatures, 50-200 °C. Results indicate that there was no molecular re-orientation as no significant changes were observed in the RAIRS spectra obtained both prior to and after annealing, in contrast to the findings shown in Figure 5.1.1-1 [18]. This experiment was then repeated in dry air concluding in a similar result as obtained in vacuum, that is, no re-orientation was observed as shown in Figure 5.1.1-1.

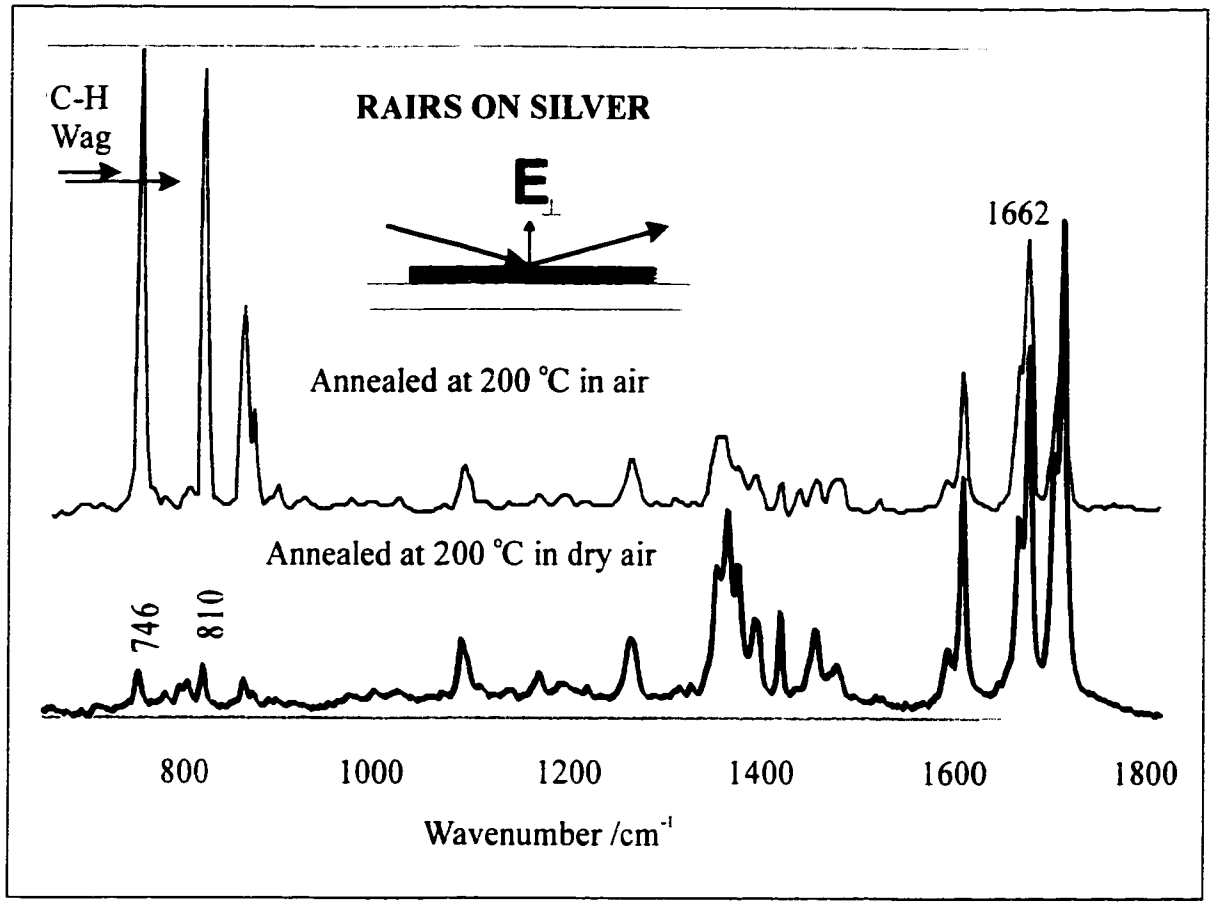

Figure 5.1.1-1: Reflection-absorption spectra of bisPTCD film before and after thermal annealing. Notice the change in relative intensity of the out-of-plane wagging mode.

The latter results suggest that the origin of the re-orientation was due to the presence of water in the atmosphere. To validate this theory, the thermal annealing of a thin film of bisPTCD was performed solely in the presence of water vapour. A comparison of the RAIRS spectra taken of the film both prior and post water vapour-annealing showed the out-of-plane C-H bands, at 746 and 810 cm^{-1}, increased in intensity as annealing progressed. This indicated an average re-orientation of the molecules on the surface to a face-on organization on the substrate. The source of molecular reorientation with thermal vapour annealing would appear to be the penetration of water molecules

from the air/film interface into the layered structure of the bisPTCD film. Supporting evidence for the water effect in the bisPTCD layers was provided by thermal vapour annealing the films using several organic solvents. Solvent vapour annealing of the bisPTCD films at 200 °C using methylene chloride, tetrahydrofuran, thionyl chloride, and carbon tetrachloride did not produce spectral changes in the RAIRS spectra. However, RAIRS spectral changes did occur when the samples were vapour annealed in the presence of alcohols such as methanol, ethanol, propanol, butanol, and isopropanol. The effect observed with methanol and 1-propanol is shown in Figure 5.1.1-2. The RAIRS spectrum of a bisPTCD film annealed in vacuum at 150 °C is also included for comparison. It can be seen that the relative intensity of the out-of-plane C-H bands increases for films annealed in the presence of methanol and 1-propanol.

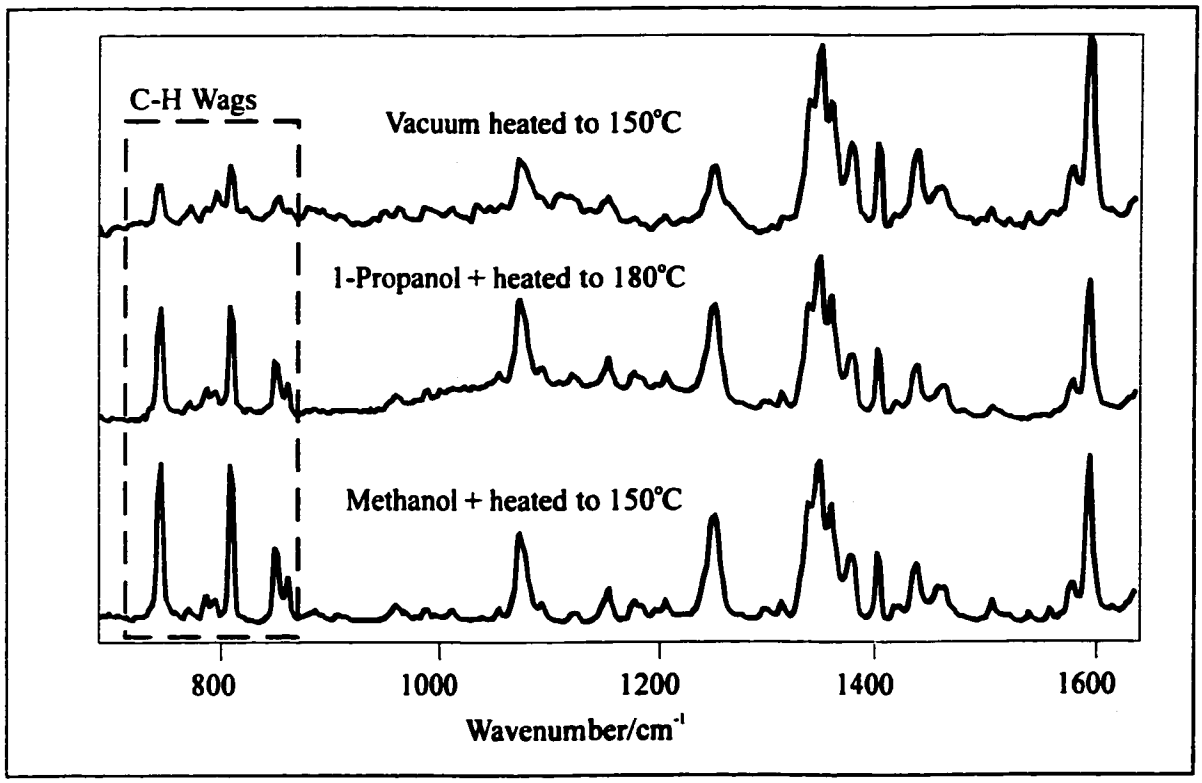

Figure 5.1.1-2: Reflection-absorption spectra of bisPTCD films in presence of methanol and 1-propanol vapors.

The vibrational bands observed above 1300 cm^{-1} are securely assigned to in-plane modes of the chromophore PTCDA ring [100, 101]. Therefore, the increase in the C-H wags confirms the average reorientation (higher face-on contribution) produced by solvent annealing. Furthermore, an interesting trend was observed with the size of the alcohol. The onset of spectral change was dependent on the size of the alcohol. A higher temperature or longer incubation time was needed to cause a change in the spectrum and both increased as the size of the alcohol increased. A reorientation requiring alcohols or water and not observed with other solvents suggests a mechanism involving hydrogen-bonding interactions whereas the alcohol size dependence is indicative of a process where water is more efficiently intercalated into the bisPTCD layers.

The most likely occurrence of hydrogen bonding is with the polar imido moieties. Aziz *et al.* have observed humidity-induced crystallization in electron transporting layers and not in the hole transporting layers of electroluminescence devices [17, 19]. It is noted that the electron-transporting molecules contain polar functionalities whereas the hole transporting molecules are generally, non-polar in nature. The intercalation of water via hydrogen bonding with the imido group would increase the spacing between perylene molecules and thus decrease the π-π ring overlap. This decrease in π-π interaction (or increase in intermolecular spacing) would weaken the coupling between molecules enabling a reorientation to occur more readily. The atomic force microscopy (AFM) images of 20 nm bisPTCD films were recorded in the contact mode and were kindly provided by Rich MacAloney from the University of Toronto. The AFM images of the 20 nm bisPTCD film before and after annealing revealed a substantial change in the film morphology as can be seen in Figure 5.1.1-3. A vacuum evaporated bisPTCD film of 20

nm mass thickness on glass is not a smooth film. It is an island film as can be seen in the AFM image where the size and height are shown. Direct comparison of the island size is possible since the spatial dimensions represented in the Figure 5.1.1-3 are kept constant. The cross section in Figure 5.1.1-3 shows that the island or disk type structures of the film surface after annealing are greater than 300 nm in width. Conboy *et al.* also performed an analogous study on the effect of vapour annealing on thin-film molecular semiconductor bilayers (TiOPc/PPEI, titanyl phtahlocyanine and perylene phenethylimide) [27]. The spectroscopic work was conducted in the visible region of the spectrum and there is no report of the infrared spectra. However, the AFM data also show that treatment of the vacuum deposited films results in the crystalline transformation of the materials and severely alters the contact between the TiOPc/PPEI layers.

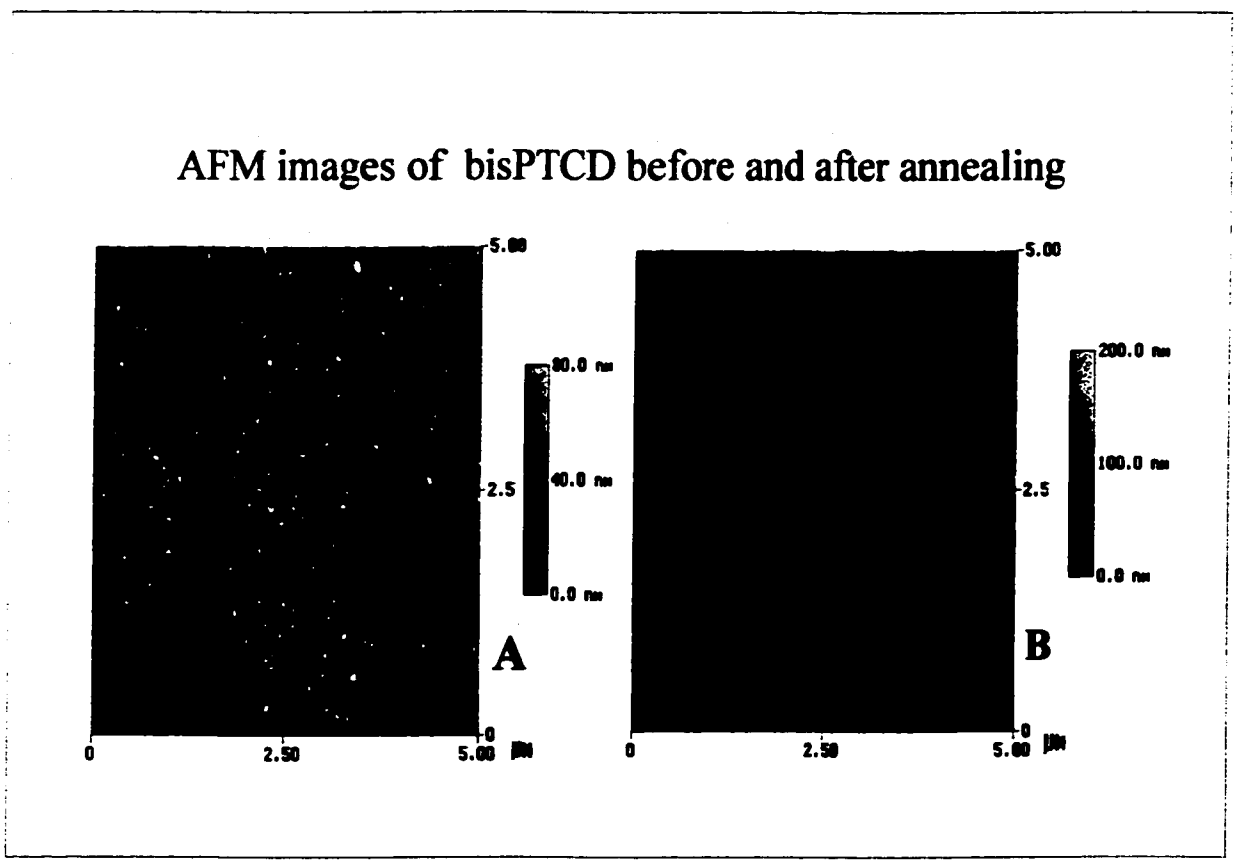

Figure 5.1.1-3: AFM images for bisPTCD film before annealing (A) and after heating at 200 °C in air (B).

5.1.2. Film encapsulation

A series of experiments were carried out in order to study the annealing of protected "encapsulated" bisPTCD films from the effect of atmospheric gases. Therefore, the reflection-absorption infrared spectra of bisPTCD films before and after coating with a hydrophobic octadecyltrichlorosilane (OTS) film were recorded. The presence of a polymerized OTS layer is evidenced by the methylene modes at 2920, 2850 and 1466 cm^{-1}. It is important to note that the C=O/C-H ratio for bisPTCD is the same in both spectra; the OTS treatment did not cause a change in the orientation of the underlying bisPTCD film. More importantly, no change in orientation of the bisPTCD is observed

when the OTS coated sample was heated in air up to 200 °C. The fact that no spectral change is observed is consistent with the expected suppression of morphological changes by encapsulation. The RAIR spectra obtained for an encapsulated sample annealed at four different temperatures are presented in Figure 5.1.2-1.

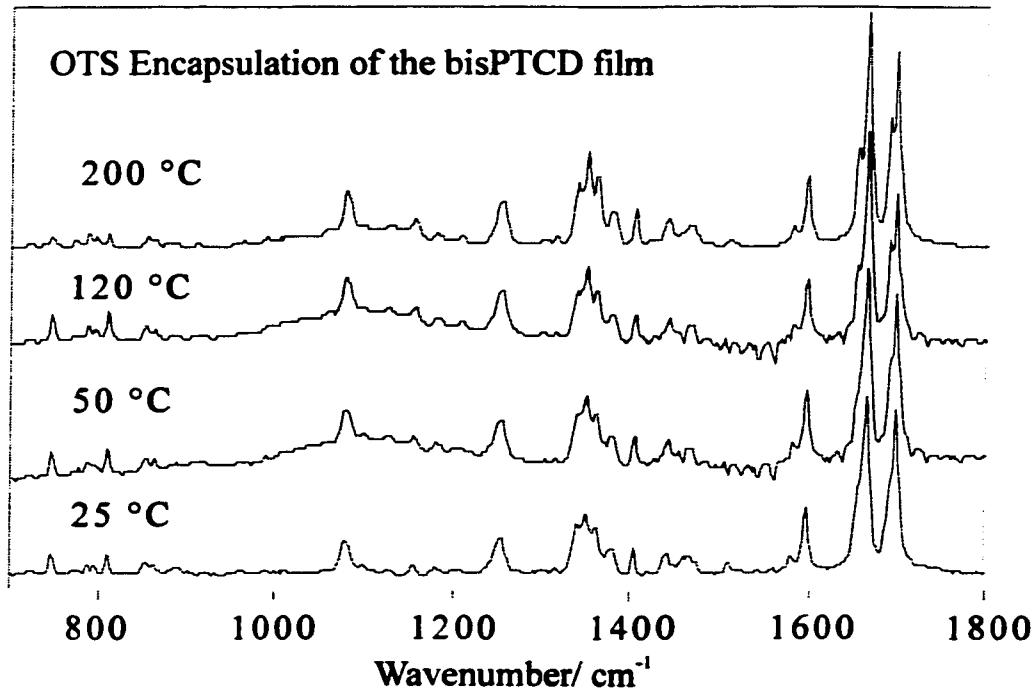

Figure 5.1.2-1: Reflection absorption spectra of a bisPTCD film on smooth silver coated with OTS. Spectra taken after annealing the sample at 25, 50, 120 and 200 °C.

One possible explanation is that the OTS overlayer freezes the location of the bisPTCD molecules hindering any possible reorientation. A second explanation is that the protective coating prevents a component found in the vapor phase from interacting

with the bisPTCD layer. To test these two possibilities a second series of experiments was conducted in which the bisPTCD films were annealed under varying atmospheric conditions. In the first experiment, the bisPTCD film was annealed under vacuum (10^{-6} Torr). No spectral changes were observed when the sample was heated to 150 °C or 200 °C. Next, the bisPTCD was heated in dry air (water vapor and CO_2 removed). Again, there were no spectral changes at 150 or 175 °C. Finally, a bisPTCD film was heated solely in the presence of water vapor (2 Torr), as shown in Figure 5.1.2-2. In this case, spectral changes occurred at 150 °C akin to those observed when the sample is heated at the same temperature in air. These experiments showed that water vapor was needed for reorientation of the film and that the role of the OTS film is to prevent water from penetrating into this layer.

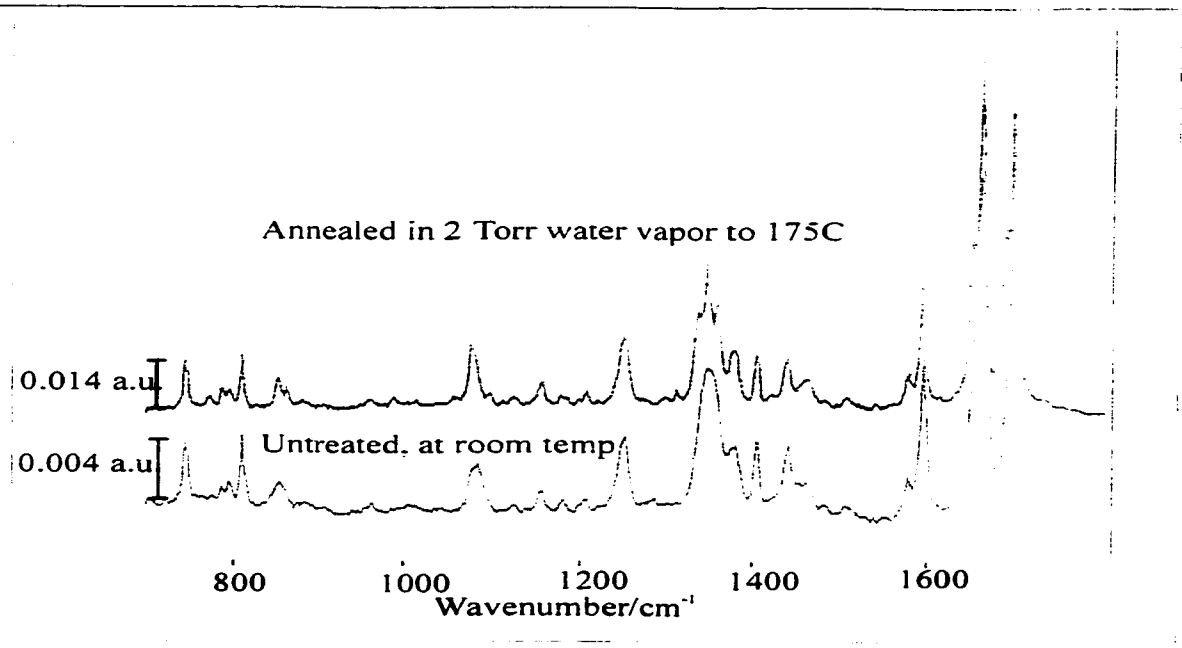

Figure 5.1.2-2: RAIRS spectra of 20 nm bisPTCD film on smooth silver annealed in the presence of water vapor. Spectra are not scaled.

While water is clearly needed to induce reorientation, a molecular basis for this change has yet to be determined. One possibility is that the water reacts with the bisPTCD at 150 °C. However, this is highly unlikely because the DSC decomposition temperature reported for this compound is above 450 °C. Furthermore, we did not detect any reaction when bisPTCD powder was heated at 150 °C in a high humidity chamber for a period of one hour, as shown in Figure 5.1.2-3.

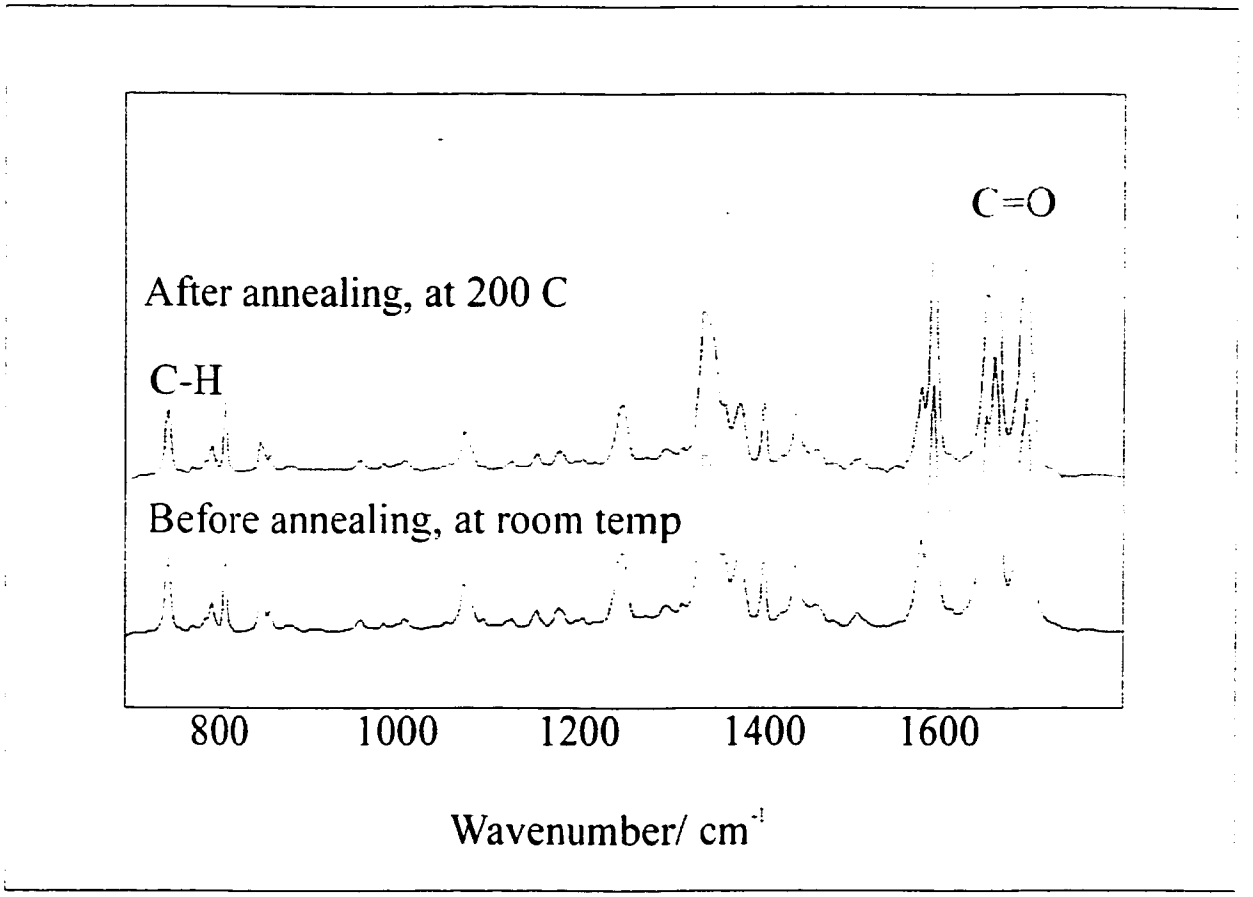

Figure 5.1.2-3: Reflection absorption spectra of a bulk bisPTCD. Spectra taken at room temperature and after annealing the sample at 200 °C.

A second possibility is that the water does not interact with the bisPTCD but rather modifies the metal/organic interface. Water penetrating at this interface could either oxidize the metal or interpenetrate at the metal/organic interface resulting in the delamination of the bisPTCD from the surface. To test this possibility, OTS was again used. An OTS film was deposited on silver prior to bisPTCD deposition. This has two effects. First, it is unlikely that water is penetrating at the OTS/bisPTCD interface and secondly, the OTS isolates the bisPTCD from direct contact with any oxidative changes to the metal surface. On thermal annealing of this modified film in air, reorientation occurred at the same temperature as that of a non-OTS coated substrate. This suggests that the origin of molecular reorientation is not due to the penetration of water at the silver/bisPTCD interface resulting in oxidation of the metal surface or delamination of bisPTCD from the surface.

5.1.3. Summary

The effect of water and alcohol vapor annealing on thin solid film of bisPTCD has been identified using vibrational spectroscopy. The well-known surface selection rules of reflection-absorption infrared spectroscopy provided the basis to show that water, methanol and 1-propanol induced molecular reorientation on bisPTCD films under thermal annealing. The bisPTCD films (20 nm mass thickness) were fabricated on reflecting silver substrates and the most likely cause of the reorientation caused by water is a hydrogen bonding mechanism with the polar moieties of the bisPTCD that disrupt the packing in molecular solid film. It was further shown that film organization might be protected by encapsulation. Experiments of solvent vapor annealing of bisPTCD films

with a silane protective coating have shown that the molecular organization of the evaporated films is preserved.

Chapter 6

THIN SOLID FILMS AND SURFACE ENHANCED VIBRATIONAL SPECTRA OF THIO-BIS (n-PROPYLIMIDO) PERYLENE AND BIS (n-PROPYLIMIDO) TRITHIAPERYLENE

Spectroscopic characterization, molecular orientation and morphology studies

6.1. Introduction

The successful formation of a floating monolayer and the fabrication of thin solid films of thio-bis (n-propylimido) perylene (thioPTCD), Figure 6.1-1A, and bis (n-propylimido) trithiaperylene (trithiaPTCD), Figure 6.1-1B. have been achieved and their chemical structures are shown in Figure 6.1-1. Surface-enhanced Raman scattering (SERS) and Surface-enhanced resonance Raman scattering (SERRS) spectra of LB monolayers and of vacuum evaporated films have been obtained and are discussed. SERRS imaging is also reported. Infrared reflection-absorption spectroscopy was used to study the long-range organization in thin solid films and the organic–metal interactions of the new PTCD materials.

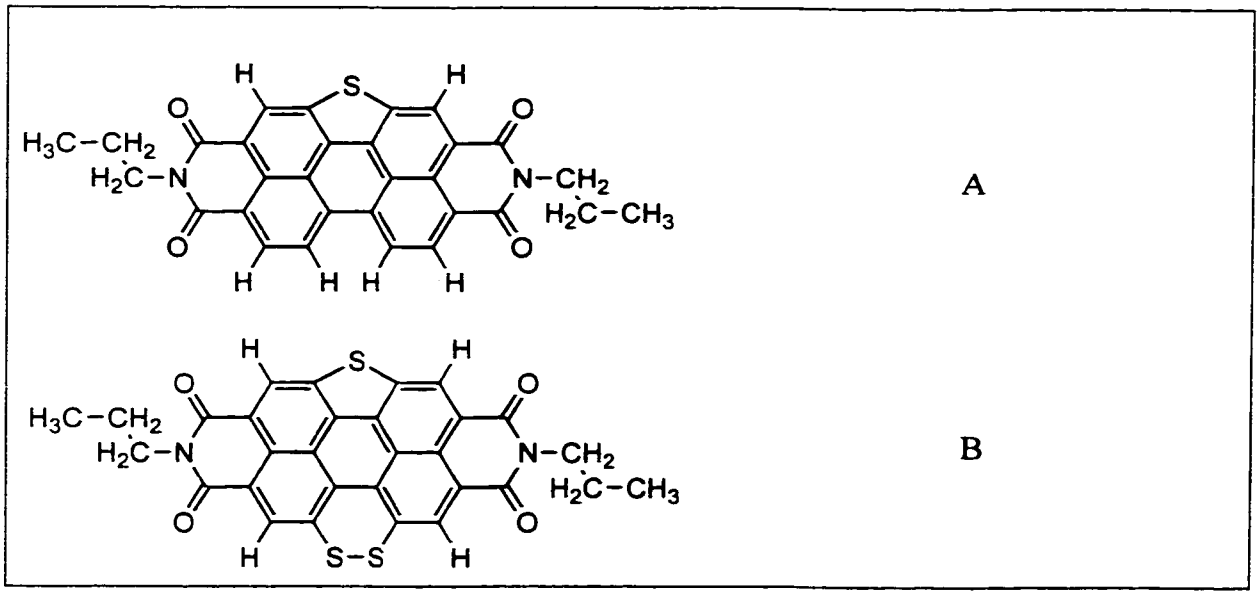

Figure 6.1-1. : Molecular Structure of thio-bis (n-propylimido) perylene (A) and bis (n-propylimido) trithiaperylene (B).

6.2. *THIO-BIS (n-PROPYLIMIDO) PERYLENE*

6.2.1. Electronic spectra

The absorption spectra of PTCD derivatives in solution are essentially identical and they correspond to the electronic spectrum of the aromatic core [80]. The absorption spectrum of thioPTCD in solution, shown in Figure 6.2.1-1, is not an exception in spite of the presence of a sulfur atom attached to the perylene chromophore. The vibronic structure shows equally spaced maxima with a constant separation of ca. 1416 cm^{-1}. The absorption spectra of the solid KBr pellet and that of the evaporated film, as seen in Figure 6.2.1-1, are more sensitive to the presence of substituent groups in the chromophore [102]. The differences between the spectra of the bulk and that of the thin solid films speak to the fact that the absorption spectra of these materials were strongly dependent on the morphology of the solid. The absorption spectrum of the KBr pellet is broad and extends into the red with considerable absorption at 600 nm. The evaporated film, as compared to the KBr pellet, shows a strong absorption with maxima similar to the solution spectrum in wavelength but different intensities. The result is an indication of the higher degree of crystallinity observed in the evaporated film. The emission spectrum of the 20 nm film of thioPTCD on KBr pellet is characteristic of excimer formation observed in PTCD materials due to a monomer [102, 103] with a broad, unresolved red shifted emission band at 634 nm.

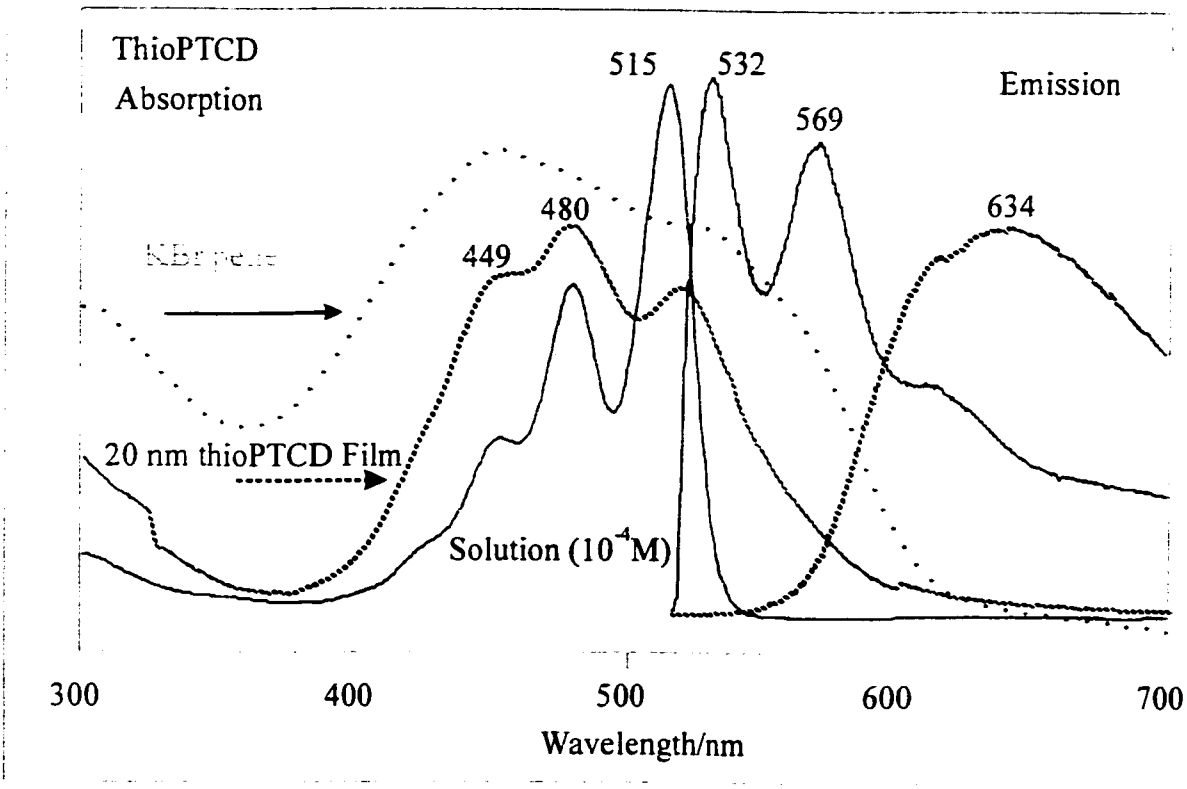

Figure 6.2.1-1: Electronic absorption and emission spectra of ThioPTCD. The intensity is in arbitrary units. The emission spectrum of the 20 nm thioPTCD on KBr pellet was obtained using the 514.5 nm excitation laser line.

6.2.2. Vibrational analysis

ThioPTCD contains 51 atoms and 147 fundamental normal modes of vibration. The discussion can be reduced to characteristic vibrational modes that serve as probes for analytical characterization and applications to molecular organisation studies and molecule-metal surface interactions. The assignment of observed vibrational bands is mainly reduced to the fundamental vibrations of the chromophore. The vibrational modes of the propyl moiety are well known and do not require a separate discussion. The local symmetry of the chromophore (planar moiety) allows the separation of normal modes according to the direction of their dynamic dipoles, helping the assignment of

infrared active vibrations. As mentioned in Chapter 3, for molecular orientation determination the most relevant normal modes are the in-plane carbonyl stretching vibrations, ring stretching vibrations and the out-of plane C-H wagging modes. The assignment of characteristic vibrational wavenumbers observed in the infrared spectra and the computed wavenumbers and intensities are given in Table 6.2.2-1.

Table 6.2.2-1. Calculated and observed IR wavenumbers, and relative intensities for thioPTCD. * S.F. = 0.9.

Cal.*	Intensity Km/mole	Pellet cm^{-1}	RAIRS cm^{-1}	SEIR cm^{-1}	Assign.
706	30	737 w			C-H wag
737	9	742 m	741 w	735 m	C-H wag
804	12	810 m	807 w	803 m	C-H wag
826	67	837 w			Ring def
839	34	846 w			Ring def
867	39	859 w	851 vw		C-H wag
869	29	888 vw	886 vw		C-H wag
1009	26	1046 vw			C-H wag
1088	11	1078 m	1078 m	1073 w	C-H bend
1109	27	1108 vw	1109 w		Ring str
1133	250	1143 vw			C-H bend
1146	68	1150 w	1146 w		Ring str
1168	108	1177 w	1178 vw		C-H bend
1232	131	1239 m	1238 m	1233m	C-H bend
1272	65	1248 m			C-H bend
1294	1060	1303 sh	1302 w		Ring str
1312	27	1315 s	1315 m	1308 m	C-N str
1330	183	1338 w	1337 w	1334 w	Ring str
1340	306	1346 w	1354 w		Ring str
1369	122			1350 w	C-N str
1381	155	1377 w	1379 w	1373 w	C-H bend
1401	253	1397 w	1396 vw		C-H bend
1425	7		1426 m	1420 m	Ring str
1442	4	1433 s	1433 w		Ring str
1463	5		1460 w	1456 w	Ring str
1574	215	1560 m	1560 w	1556 w	Ring str
1588	323	1597 s	1596 m	1589 s	C=C str
1675	758	1660 vs	1663 vs	1651 vs	C=O str
1713	760	1695 vs	1697 vs	1687 vs	C=O str

Vibrational assignments were helped by animation of the atomic displacements obtained from the solution of the vibrational problem in Gaussian at RHF/3-21G level of theory. The mid-infrared spectrum and the calculated wavenumbers are illustrated in Figure 6.2.2-1. Considering that the calculated intensities are for the isolated molecule, and the experiment corresponds to a solid dispersion in KBr, it can be seen that the calculated IR intensities follow the general pattern of the observed spectrum.

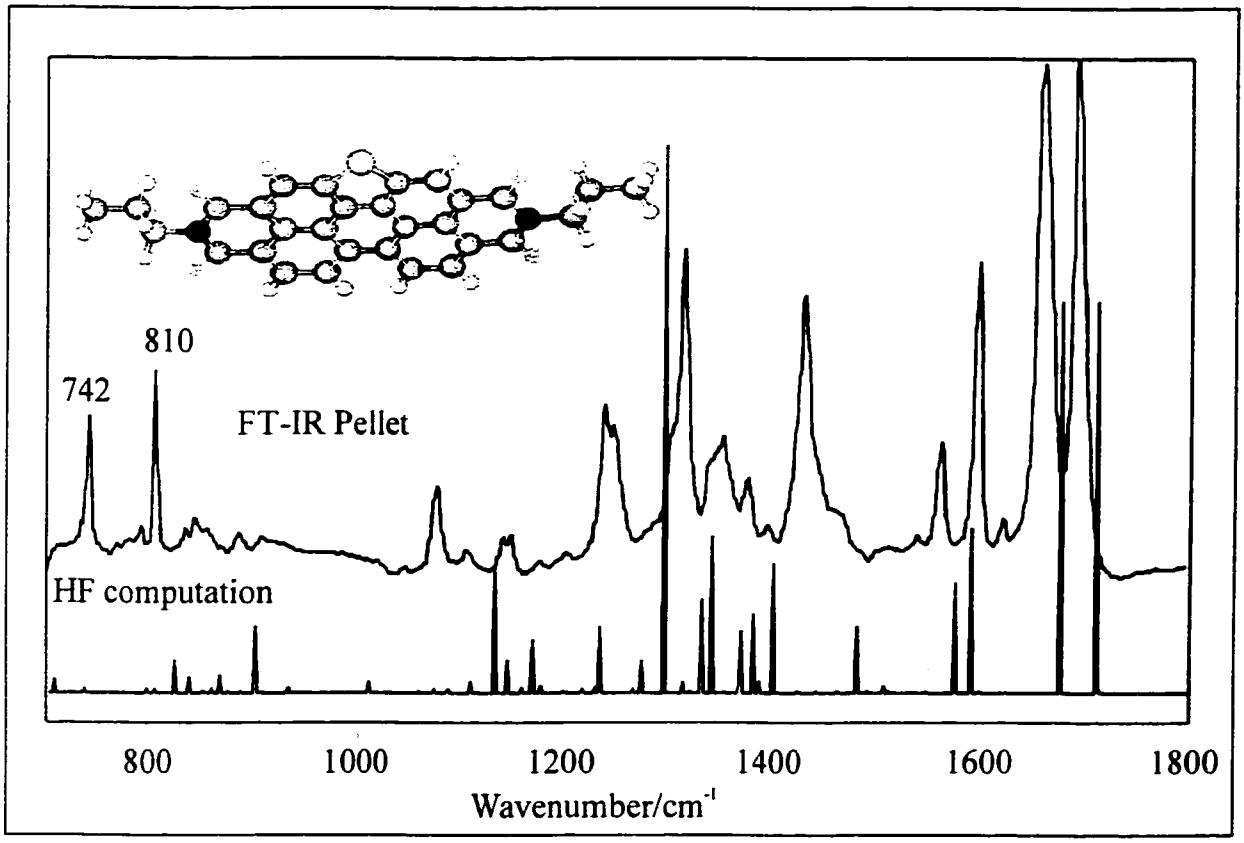

Figure 6.2.2-1: Calculated and observed infrared spectrum of thioPTCD in a KBr pellet. Intensity units are arbitrary.

Similar observations can be made for the calculated Raman intensities and the most intense observed bands. The Raman wavenumbers and intensities are listed in Table

6.2.2-2. Clearly, quantum computations are now an essential part of the most common analytical tools used for materials characterization.

Table 6.2.2-2: Calculated and observed Raman wavenumbers and relative intensities for thioPTCD. * S.F. = 0.9

Cal.*	Int.	FT-Raman Powder		Powder 514.5 nm		LB-SERRS 514.5 nm		LB SERS 633 nm		Assign
cm^{-1}	$Å^4$/ a.m.u	cm^{-1}	FW HM	cm^{-1}	FW HM	cm^{-1}	FW HM	cm^{-1}	FW HM	
519	63	519 (7)	10	520 (9)	5	522 (6)	15			Ring def.
1066	118							1054 (4)	8	C-H bend
1073	471	1081 (3)				1076 (1)	12	1076 (5)	26	C-H bend
1088	78		12							C-H bend
1133	196	1109 (7)	11	1109 (16)	5	1097 (1)	15	1107 (10)	11	C-H bend
1159	105							1160 (4)	12	Ring Str.
1263	1617	1246 (8)	16	1246 (10)	14	1240 (7)	14	1245 (11)	12	C-H bend
1272	213	1275 (7)	12	1275 (8)	9	1274 (6)	16	1275 (7)	8	C-H bend
1318	336									
1335	605	1315 (25)	13	1314 (3)	7	1311 (22)	21	1314 (41)	13	Ring Str.
1340	4186							1380 (23)		C-H bend
1347	1781	1396 (100)	14	1397 (100)	8	1393 (100)	16	1396 (100)		Ring Str.
1367	96								17	Ring Str.
1481	39					1472 (2)		1467 (3)	7	Ring Str.
1506	39							1506 (5)	16	Ring Str.
1547	2134	1538 (12)	9	1539 (12)	6	1536 (10)	7	1537 (14)	12	Ring Str.
1581	1295	1555 (5)	7	1553 (4)	5	1550 (5)	11	1555 (5)	9	Ring Str.
1598	5118	1579 (18)	12	1580 (14)	6	1574 (8)	13	1575 (25)	14	C=C str.
1618	309	1621 (48)	13	1622 (36)	6	1619 (36)	20	1620 (32)	10	C=C str.
1676	109	1661 (6)	13					1668 (3)	7	C=O str
1717	358	1695 (13)	10	1697 (8)	8	1698 (2)	13	1699 (9)	12	C=O str.

The infrared spectrum is characterized by the PTCD vibrations: in-plane carbonyl modes at 1697 cm^{-1} and 1662 cm^{-1}, ring stretching modes at 1597 cm^{-1} and 1560 cm^{-1}, out-of-plane C-H wagging modes at 742 cm^{-1} and 810 cm^{-1}. The term out-of-plane is used here to indicate the local planar structure of the chromophore. There are also a number of intense infrared bands that can be assigned to "in-plane" C-H bending modes and ring stretching vibrations in the 1000-1450 cm^{-1} spectral region. The far-infrared spectrum of thioPTCD was also recorded and the agreement between calculated and observed wavenumbers is illustrated in Table 6.2.2-3. The vibrational modes active in the far-infrared region of the spectrum are highly coupled with important contributions from skeletal deformation, ring deformations and ring torsions.

The FT-Raman spectrum of thioPTCD contains a group of medium intensity bands at 1695 cm^{-1}, 1661 cm^{-1} (carbonyl stretching vibrations), 1621 cm^{-1}, 1579 cm^{-1}, 1555 cm^{-1} and 1538 cm^{-1} (ring stretching vibrations). The strongest band in the FT-Raman spectrum is observed at 1397 cm^{-1} and can be assigned to the perylene ring stretching vibration. The FT-Raman and the Raman spectrum of a thioPTCD powder excited at 780 nm are shown in Figure 6.2.2-2. The Raman spectrum simulated using calculated Raman intensities is also given in Figure 6.2.2-2 for comparison. It can be seen that the calculated spectrum gives a general pattern of relative intensities that is in fairly good agreement with the observed spectra of the solid and it is a good guide for the interpretation of the observed spectra.

Table 6.2.2-3. Far-infrared wavenumbers for thioPTCD.

Calc. cm^{-1}	Km/mol	Observed cm^{-1}	FWHM
114	1	115	4
131	1	138	4
154	10	153	12
196	3	185	16
218	5	215	5
222	1	222	7
247	1	244	5
265	13	264	13
311	9	317	8
331	13	338	9
379	15	363	9
383	47	388	12
413	24	419	14
441	4	448	12
440	4	483	14
510	34	512	14
528	27	537	17
583	3	589	18
641	8	627	15

The FT-Raman and Raman of the bulk, with the 1064 nm and 780 nm laser line respectively, should be considered the reference spectra of the dye material. The typical chromophore fundamental modes are observed in the film spectrum at 1380 cm^{-1} and 1394 cm^{-1}, a very strong pair of ring stretches at 1571 cm^{-1} and a shoulder at 1580 cm^{-1}, followed by a very strong ring stretching-C-H with bending mode contribution at 1291 cm^{-1} as reported in Chapter 4 [8, 18, 80, 101]. The characteristic vibrational frequencies are given in Table 6.2.2-2.

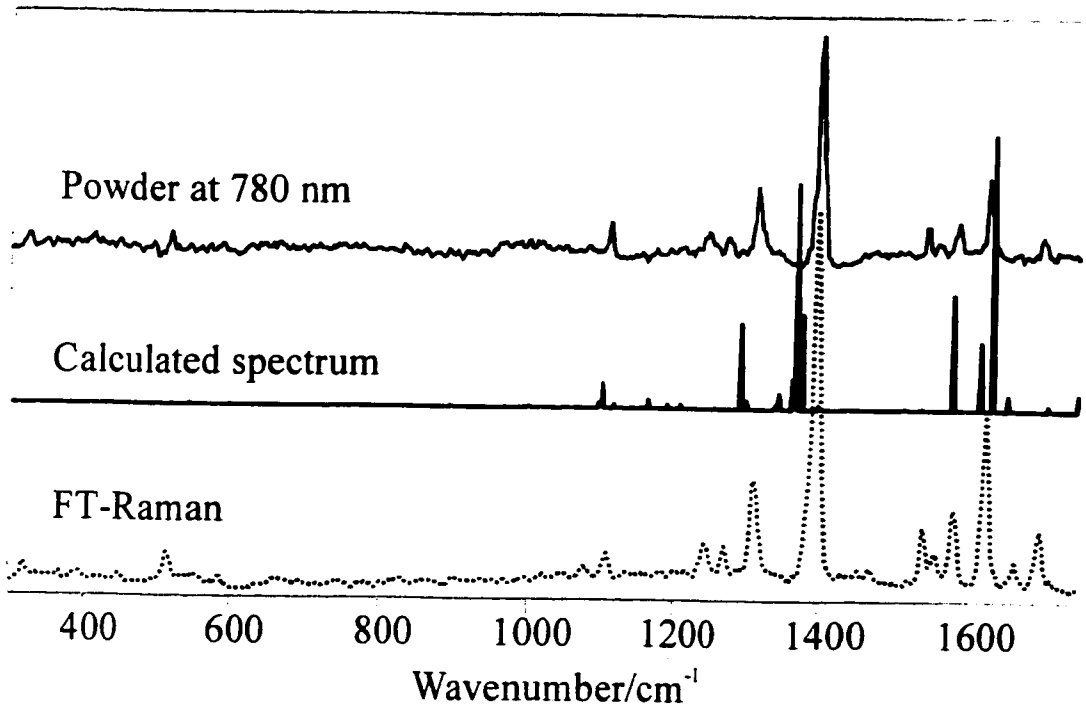

Figure 6.2.2-2: Calculated and observed Raman spectra of thioPTCD. FT-Raman excited at 1064 nm and Raman spectrum of the KBr pellet of thioPTCD recorded with the 780 nm. The y-axis is in arbitrary intensity units.

6.2.3. Surface-enhanced infrared and Surface-enhanced-Raman scattering and imaging

6.2.3.1. SEIR

Surface-enhanced vibrational spectroscopy (SEVS) comprises the study of molecular vibrations of molecules adsorbed on surfaces that can enhance the absorption and the emission of electromagnetic radiation. SEVS has two complementary techniques: surface-enhanced infrared and surface-enhanced Raman scattering spectroscopies. The first report by Hartstein *et al.* [104] showed that silver films could also be used for the observation of SEIR. According to the electromagnetic mechanism used in the interpretation and evaluation of the enhancement factor, the enhancement factors in the observed intensities may be described as the product of two contributions: the electromagnetic enhancement produced by certain rough metal surfaces, in which the enhancement activity of the substrate depends on the shape and size of surface protrusions, and the dielectric function of the adsorbed material in the spectral region of interest (chemical effect). They may be written as follows:

$$SERS \propto |A(\omega_L)|^2 |A(\omega_E)|^2 \left|\frac{\partial \alpha}{\partial Q}\right|^2$$

$$SEIR \propto |A(\omega)|^2 \left|\frac{\partial \mu}{\partial Q}\right|^2$$

Where A (ω_L) is the enhanced-absorption term at the frequency ω_L and A (ω_E) is the enhanced-emission factor at the frequency ω_E. Since both contributions are wavenumber dependent, the enhancement factors are characteristic for each normal mode [105].

Silver and gold have been commonly used in SEIR experiments [100, 106]. Recently, tin island films have been added as substrates for SEIR [107]. In this chapter the results of SEIR experiments on tin and silver island films are presented. SEIR was achieved for both substrates. The transmission SEIR spectra of 20 nm film of thioPTCD on silver islands (10 nm thickness) and tin islands (18 nm thickness) fabricated onto a ZnS substrate are shown in Figure 6.2.3.1-1. The spectrum of KBr pellet of thioPTCD (middle spectrum) is also included in Figure 6.2.3.1-1 for direct comparison. The spectrum of a KBr pellet of thioPTCD provides the absorptions due to infrared resonances with a random spatial distribution of molecules and aggregates that should closely follow the spatial averages directly obtained from the character tables of the point group symmetry. Notably, the observed relative intensities in the SEIR spectra of thioPTCD on tin and silver are very close to that of the solid matrices. They are, however, slightly different from those observed in RAIRS of thin solid films of the neat material on smooth metal surfaces. The actual enhancement factors were very modest, about 10 for silver and no more than 5 for tin. The wavenumbers for the observed bands have been included in Table 6.2.2-1.

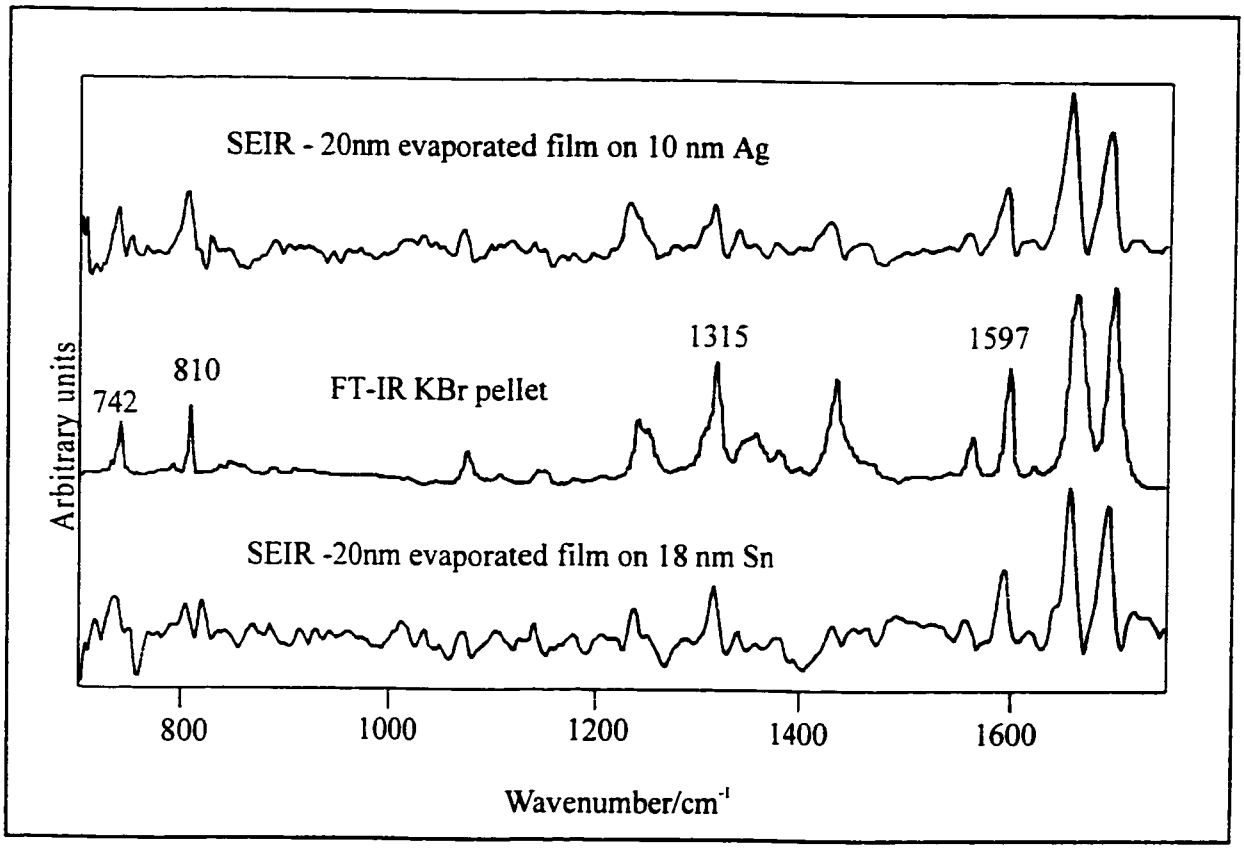

Figure 6.2.3.1-1: Surface-enhanced infrared of thioPTCD on Ag island (top), reference spectrum of KBr pellet (middle) and SEIR on 18 nm Sn island film (bottom).

6.2.3.2. SERRS and SERRS point-to-point line scanning

Langmuir-Blodgett (LB) monolayers and evaporated films were fabricated onto silver island films in order to obtain the surface-enhanced vibrational spectra. The surface-enhanced resonance Raman scattering of a single LB monolayer on silver is shown in Figure 6.2.3.2-1 for two excitation laser lines. To facilitate transfer and ensure a homogeneous cover of the silver islands (6 nm mass thickness of silver on glass), mixed LB monolayers were fabricated using a 1:5 molar ratio of thioPTCD and arachidic acid (AA). The addition of fatty acids makes the monolayer more flexible, facilitating transfer to solid substrates. The formation of the Ag-S bond at the metal-organic interface was a possibility; similar to the formation of the Ag-S bond in thiolate complexes that has been

reported by several groups [22, 108, 109]. The Ag-S bond in silver thiolate complexes is observed within the 150-250 cm^{-1} range [108]. The Ag-S bond found in the SERS spectrum of benzenethiol in silver sol is reported at 240 cm^{-1} [109]. The Ag-S stretching vibration observed in the SERS spectrum of benzyl phenyl sulphide is at 215 cm^{-1} [22]. Ulman *et al.* [110] have studied the Raman spectra of alkanethiolate monolayers on silver and gold. The work was carried out using about 2 mW of the 633 nm laser line. Unfortunately, the authors do not show the SERS spectra below 800 cm^{-1}. The SERRS spectra shown in Figure 6.2.3.2-1 do not provide evidence of chemisorption, as the Ag-S was not observed. The SEIR spectrum is limited to the mid-infrared and does not provide any direct evidence of chemisorption. However, the out-of-plane modes are observed with some relative intensity. The latter intensity of out-of-plane modes should be minimal for a chemisorbed configuration forming a Ag-S bond, since the out-of-plane modes are perpendicular to the electric field. Since the SEIR enhancement factor is modest, the contribution from physisorbed layers to the spectrum is significant in the case of evaporated films. This is in contrast with SERS where the first layer may dominate the spectrum.

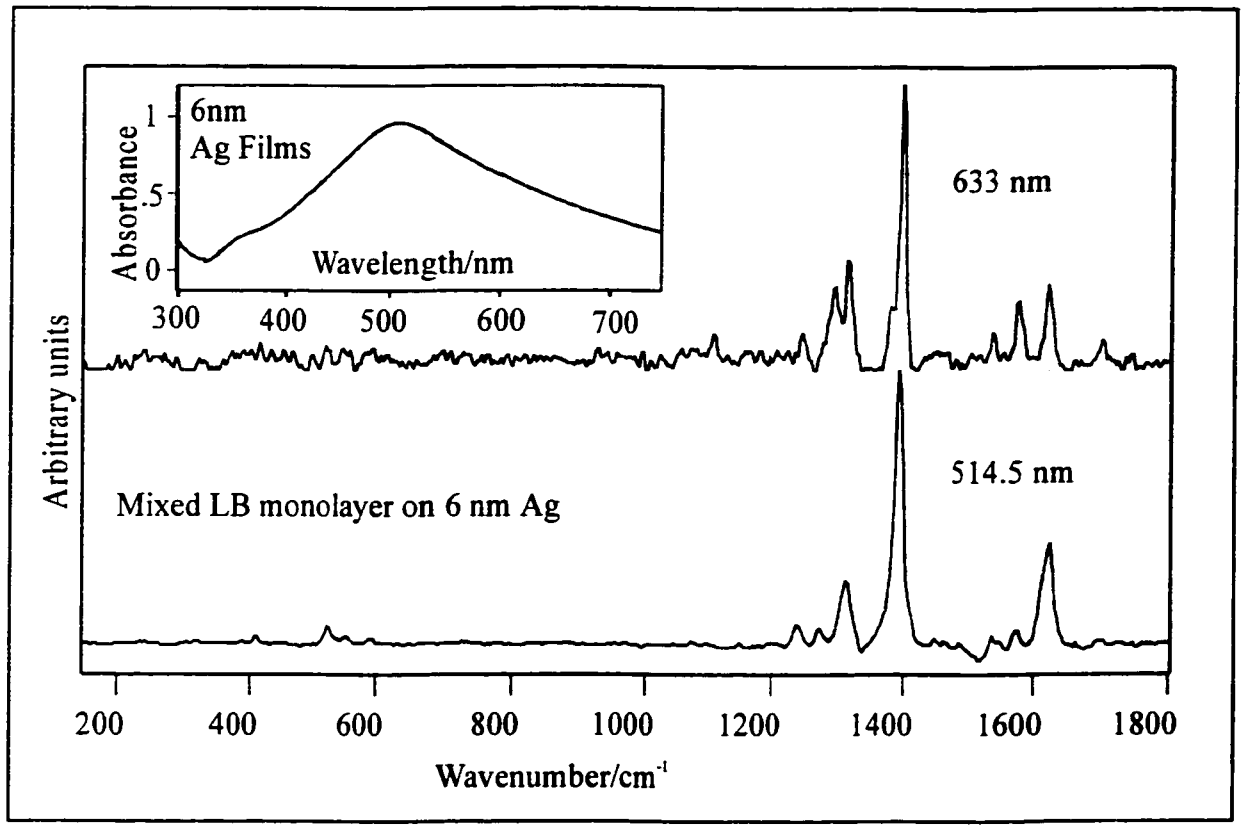

Figure 6.2.3.2-1: Surface-enhanced resonance Raman scattering of a single LB monolayer film deposited on silver islands excited with 0.5 mW of the 633 nm and the 514.5 nm laser lines. Inset: plasmon absorption of a 6 nm mass thickness silver film.

Point-to-point line scanning of SERRS spectra for a vacuum evaporated film of thioPTCD onto silver was recorded using 1 μm intervals with a spot size of ca. 1μm^2. The sample was prepared by evaporating 10 nm mass thickness of thioPTCD onto 6 nm silver island film. The SERRS spectra for the evaporated film, taken with the 633 nm laser line, and that of the mixed LB monolayer, acquired with the 514.5 nm laser line, given in Figure 6.2.3.2-1 are practically identical. The results for a line of 40 points are shown in Figure 6.2.3.2-2. It can be seen that apparently, there is homogeneous SERRS activity throughout the line on the surface. The laser power at the sample was 250 μW.

A photodecomposition is observed with the 514.5 laser line when power at the sample is higher than 2 mW.

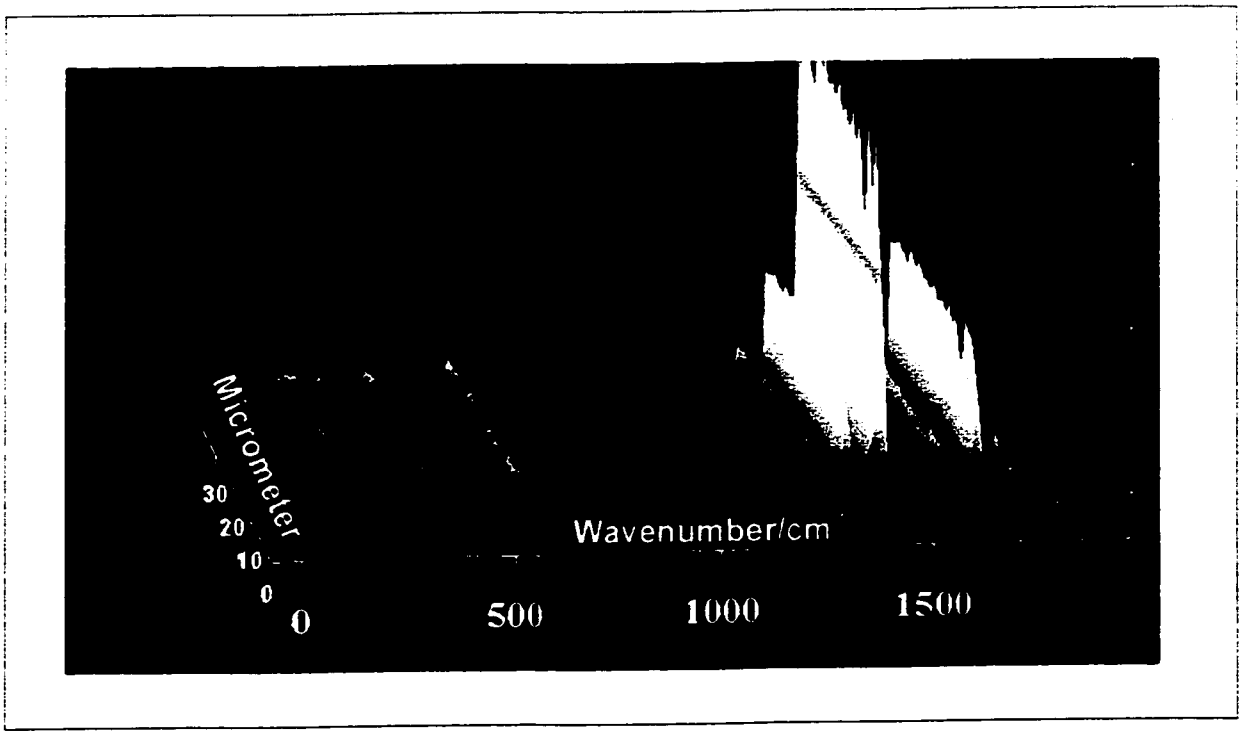

Figure 6.2.3.2-2: Point-to-point line scanning of the SERRS spectra of thioPTCD forming a 10 nm mass thickness evaporated film onto silver islands.

6.2.4. Thin solid films, organization and molecular orientation

Molecular orientation of a film on a metal surface may be interpreted from the specular and refection absorption infrared spectroscopy. Determination of molecular orientation is facilitated by the selection rules as defined in Chapter 3. The RAIRS spectrum of ThioPTCD acquired at room temperature, 25 °C, is shown in Figure 6.2.4-1. Analysis of spectra indicates that the C-H wagging bands at 742 cm^{-1} and 808 cm^{-1} are observed with minimal relative intensity compared to reference spectrum of the isotropic sample (Figure 6.2.2-1). Furthermore, the relative intensity of the C=O bands have remained constant thereby confirming the presence of an "edge-on" molecular

orientation.

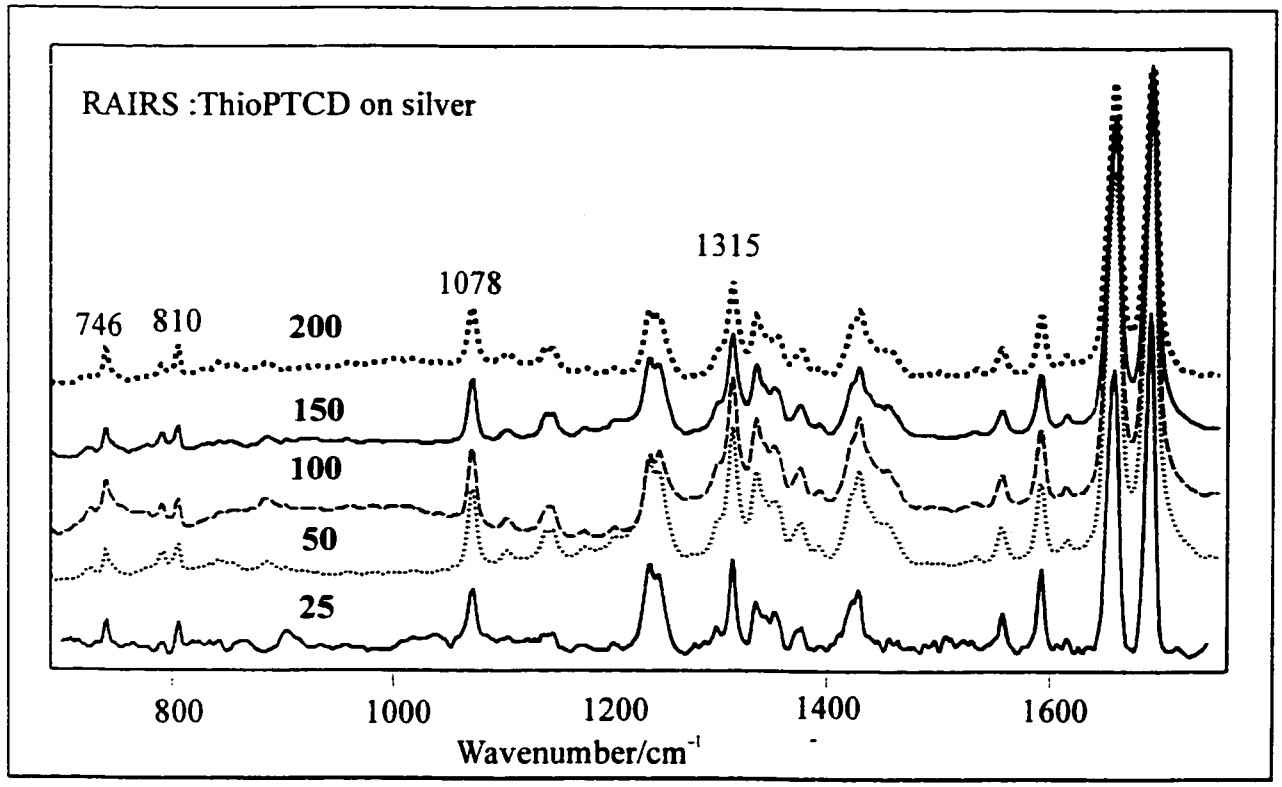

Figure 6.2.4-1: Infrared reflection-absorption of an evaporated thioPTCD film on a reflecting silver film. The first spectrum recorded at room temperature is followed by spectra of the annealed sample starting at 50 °C and further annealed at 100, 150 and 200 ^{0}C.

The thermal annealing of bisPTCD has been previously reported in Chapters 4 and 5 [18]. The main conclusions from the bisPTCD work were that thermal annealing in the presence of water vapour or small alcohols can induce a change in molecular orientation and may in fact produce a phase transition. The RAIRS spectra of the thioPTCD dye annealed at 50, 100, 150 and 200 °C in air are shown in Figure 6.2.4-1. The bottom spectrum was obtained at room temperature and is included as a reference. A comparative study of the untreated and annealed films of thioPTCD indicates no apparent change on

annealing. The film morphology was obtained by contact mode AFM before and after annealing, Figure 6.2.4-2. The morphology of the films follows the spectral trends of no change under thermal annealing. It is concluded thermal annealing does not induce phase changes in thioPTCD films. The results indicate that the smooth silver substrates, induce a molecular orientation for upper layers that does not change significantly under thermal annealing. Furthermore, annealing studies in which a layer of octadecyltrichlorosiliane (OTS) was first deposited on silver followed by thioPTCD indicates that reorientation occurs like that of bisPTCD. These results seem to suggest that the orientation could be driven by the formation of Ag-S bonds. However, this assumption is not supported by the surface-enhanced data.

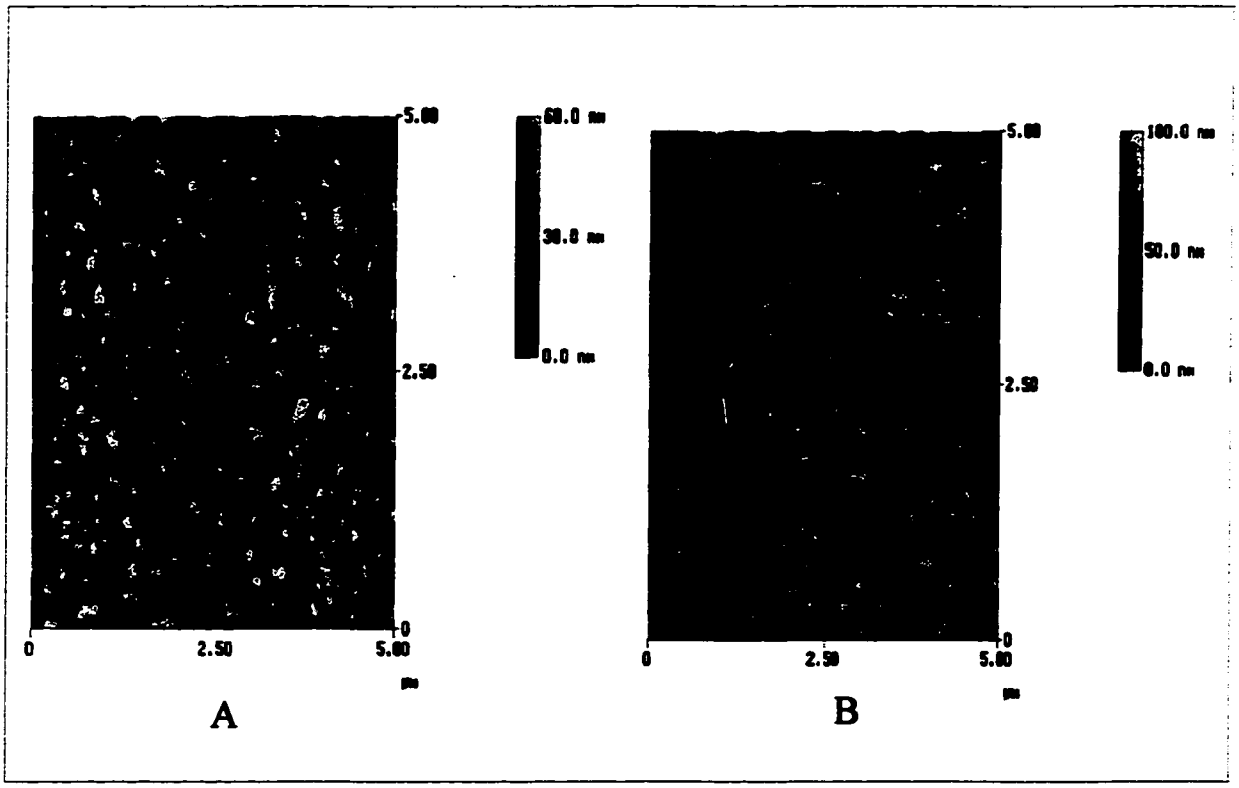

Figure 6.2.4-2: Tapping mode AFM images of thioPTCD at room temperature (A) and after annealing at 200 °C.

6.2.5. Summary

Langmuir-Blodgett films and vacuum evaporated films of a new material, thioPTCD have been fabricated onto metal and dielectric substrates. The vibrational infrared and Raman spectra including computer-aided assignment of fundamentals were reported. The surface-enhanced vibrational spectra, SEIR and SERRS were obtained for vacuum evaporated films on metal island films and SERRS of LB monolayers were also recorded. The surface-enhanced vibrational spectra gave no conclusive evidence for the formation of the Ag-S bond between thioPTCD and substrate. Point-by-point line scanning of SERRS on silver islands reveals a fairly homogeneous SERRS activity at 1 micron intervals. Using RAIRS, it was found that solid films formed on smooth silver surfaces are not affected (structural change and molecular orientation) by thermal annealing as has been previously observed for other PTCD materials. Aided by the studies with OTS, the thermal annealing results suggest that orientation could be driven by the formation of Ag-S bonds.

6.3. BIS (n-PROPYLIMIDO) TRITHIAPERYLENE

Bis (*n*-propylimido) trithiaperylene, trithiaPTCD, may be envisioned as a bis (*n*-propylimido) perylene molecule with three bridging sulfur atoms in its backbone, unlike thioPTCD that contains one bridging sulfur. The main conclusions from the thioPTCD study were the successful fabrication of submicron films via vacuum deposition and Langmuir-Blodgett techniques. In addition, the preferential edge-on orientation of thioPTCD sulfur analogue with respect to the surface of the substrate was demonstrated. Thus, the relationship between molecular structure and both molecular organization and orientation is a key interest of the characterization of bis (n-propylimido) trithiaperylene.

6.3.1. Electronic Spectra

The electronic absorption spectrum of trithiaPTCD in solution is shown in Figure 6.3.1-1.

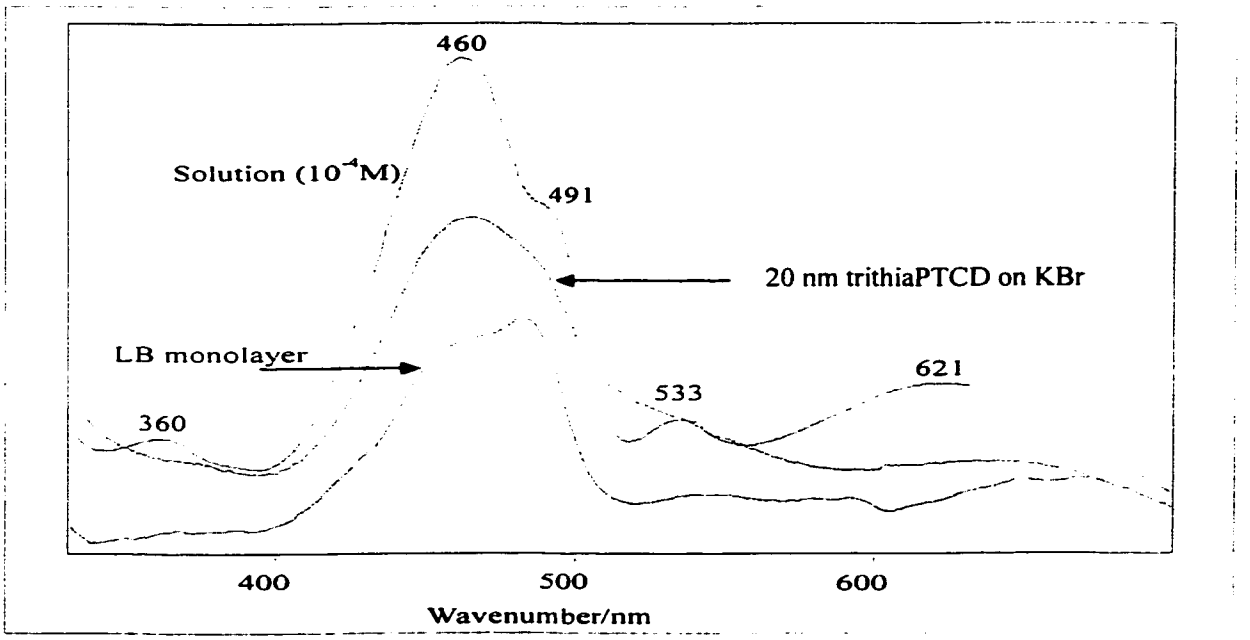

Figure 6.3.1-1: Absorption spectra for trithiaPTCD.

The absorption spectrum of the solution displays the characteristic vibronic structure of the perylene chromophore. The absorption bands corresponding to the three distinct electronic states of the perylene chromophore were observed at 460, 491 and 533 nm. A secondary band similar to that of bisPTCD was observed at 360 nm. The most notable feature of the solution absorption spectrum is the broad red-shifted band at 621. which indicates a degree of aggregation in the solution. The absorption spectrum of a 20 nm trithiaPTCD evaporated film on KBr disc and a LB monolayer film of trithiaPTCD are also shown in Figure 6.3.1-1. Both spectra display strong resemblances to the solution absorption spectrum. The evident presence of the broad red-shift absorption band in each spectrum is a strong indication of aggregation and also suggests that thin molecular films of trithiaPTCD are influenced to a greater degree, by the sulfur substituents in the perylene chromophore, than that of thioPTCD. The broad emission band of the trithiaPTCD thin film, similar to that of thioPTCD, indicates excimer formation.

6.3.2. Vibrational Analysis

TrithiaPTCD is a member of the perylene tetracarboxylic 3,4,9,10-dimide (PTCDI) family. Using local symmetry arguments the discussion on the vibrational assignments of trithiaPTCD can be restricted to that of the perylene chromophore, as a result important molecular information may be obtained. Since PTCDI is a planar molecule, infrared active normal modes may be characterized by the direction of their dynamic dipole moments: in-plane and out-of-plane. The characteristic vibrational infrared wavenumbers of trithiaPTCD and their assignment are given in Table 6.3.2-1.

Table 6.3.2-1: Calculated and observed IR frequencies and relative intensities for trithiaPTCD. * S.F. = 0.9

Calc. *	Wavenumber	KBr Pellet		Film		RAIRS		RAIRS (Annl)		Assignment
cm^{-1}	cm^{-1}	Rel. Int.	FWHM	Rel. Int.	FWHM	Rel Int.	FWHM	Rel Int.	FWHM	
766	746	6	5	8	12	9	16	5	13	C-H wag
801	792	3	10	6	32	5	12	4	9	C-S str.
810	810	20	5	20	8	17	5	12	4	C-H wag
867	869	4	7	6	27	3	8	3	21	C-H wag
911	908	3	9	4	12	3	11	4	32	Ring str.
929	930	1	11	4	69	2	17	2	15	Ring str.
997	998	1	7	5	35	1	40	1	22	C=C str.
1110	1097	9	13	9	26	6	19	6	10	Ring str.
1160	1153	13	7	10	8	8	8	6	6	C=C str.
1248	1243	40	14	31	13	23	12	27	15	C-H bend
1283	1287	53	10	43	10	25	8	34	11	C-H bend
1340	1340	14	16	11	9	18	12	21	13	Ring str.
1369	1357	13	9	12	11	7	12	7	10	Ring str.
1425	1392	13	30	20	9			8	19	Ring str.
1426	1405	8	7	10	2	9	32	4	8	Ring str.
1426	1434	52	17	48	14	25	19	20	8	Ring str.
1453	1461	13	17	9	10	10	20	10	15	Ring str.
1558	1543	10	7	6	9	5	7	6	8	Ring str.
1573	1586	33	8	30	10	20	9	18	10	Ring str.
1642	1662	71	17	84	17	81	15	74	15	C=O str.
1714	1697	100	13	100	14	100	11	100	10	C=O str.

The most relevant vibrational modes of the PTCD moiety are the in-plane C=O stretching modes at 1662 and 1667 cm^{-1}, the ring stretching vibrations at 1586 and 1543 cm^{-1} and the out-of-plane C-H wagging modes at 746 and 810 cm^{-1} for molecular orientation determination. The infrared spectra of trithiaPTCD KBr pellet and a 20 nm evaporated film of trithiaPTCD on KBr disk are shown in Figure 6.3.2.1. Though the relative intensities of both spectra appear to be comparable, in the thin film the relative intensity of the band corresponding to the out-of-plane C-H wagging vibration has increased relative to that observed in the KBr pellet. In addition, the relative intensity of the in-plane antisymmetric C=O stretching vibration has also increased in the thin film as compared to the KBr pellet. These results indicate an on average head-on tilt molecular organization in the thin film. Furthermore, a comparison of the full width at half maximum (FWHM) for the isotropic KBr pellet and thin film, show an increase in FWHM for the thin evaporated film. As intermolecular interactions can be gauged by changes in FWHM, this expounds the fact that there is molecular organization in the thin molecular film.

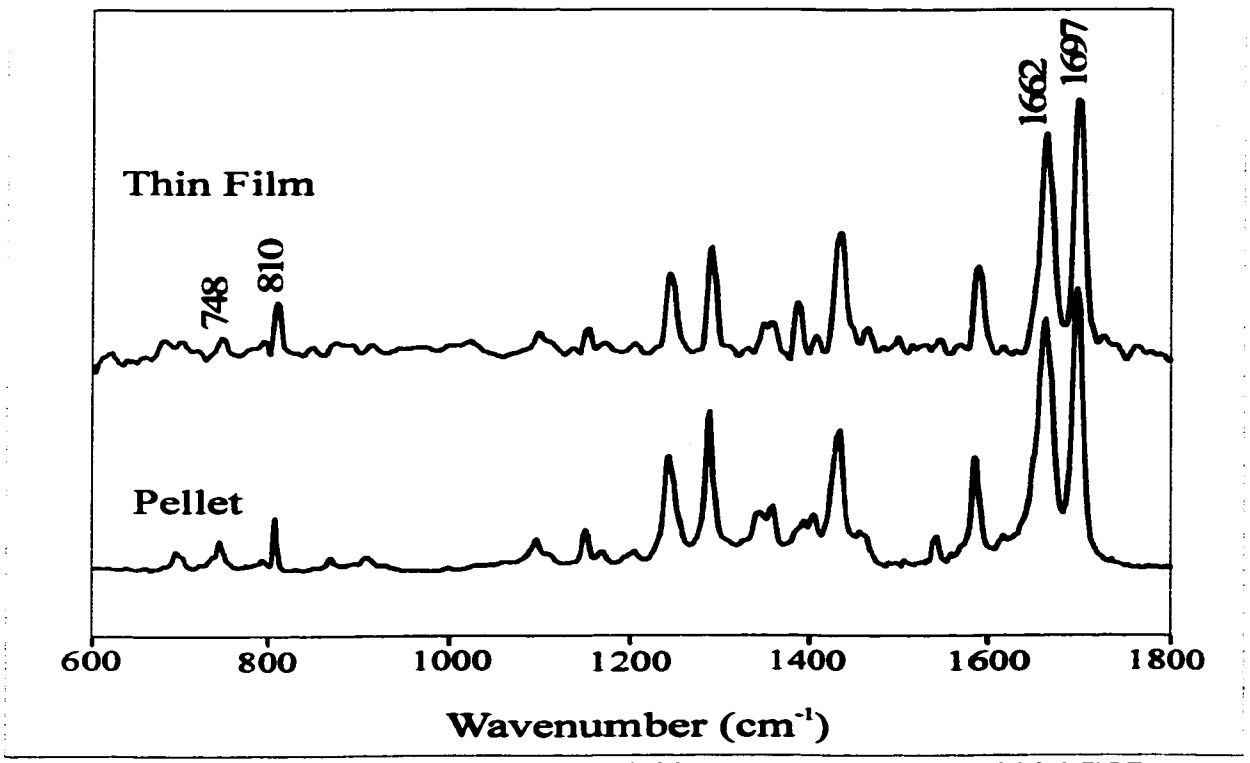

Figure 6.3.2-1: Infrared spectrum of bulk and thin evaporated film of trithiaPTCD.

6.3.3. Molecular Organization

The surface selection rules for molecular orientation are well known [111], and are presented in Chapter 3. The RAIRS spectra of a thin molecular film of trithiaPTCD at room temperature and after annealing are shown in Figure 6.3.3-1.

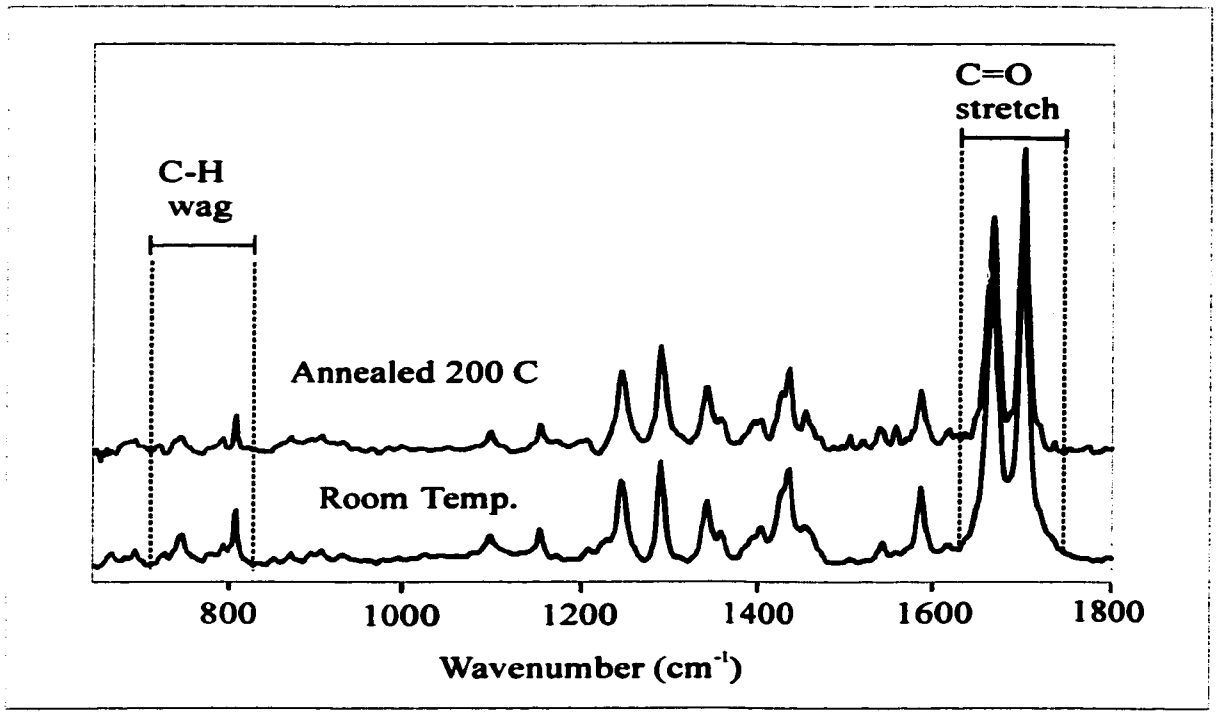

Figure 6.3.3-1: RAIRS of thin films of trithiaPTCD, before and after annealing.

Analysis of the RAIRS spectrum at room temperature indicate a slightly greater intensity for the out-of-plane C-H wagging modes observed at 746 and 819 cm^{-1}, as compared to the reference isotropic KBr pellet. Moreover, the relative intensity of the in-plane C=O stretching vibrational modes at 1662 and 1697 cm^{-1} have also increased slightly relative to the reference, while remaining significantly more intense than the C-H wagging modes. This indicates a preferential head-on tilt molecular orientation. On thermal annealing, the relative intensity of the C-H wagging modes increases slightly while that of the antisymmetric C=O stretching mode at 1662 cm^{-1} decreases relative to the untreated thin film. This suggests that no significant molecular reorientation is induced by thermal annealing and implies the anchorage of trithiaPTCD via Ag-S bonds. However, similar to thioPTCD thin films, this anchorage is not conclusive. Film

morphology studies performed by AFM for thin films of trithiaPTCD both before and after annealing indicate, similar to RAIRS studies, that the morphology of the film changes slightly on thermal annealing, as shown in Figure 6.3.3-2, but not as significant as observed in bisPTCD thin films.

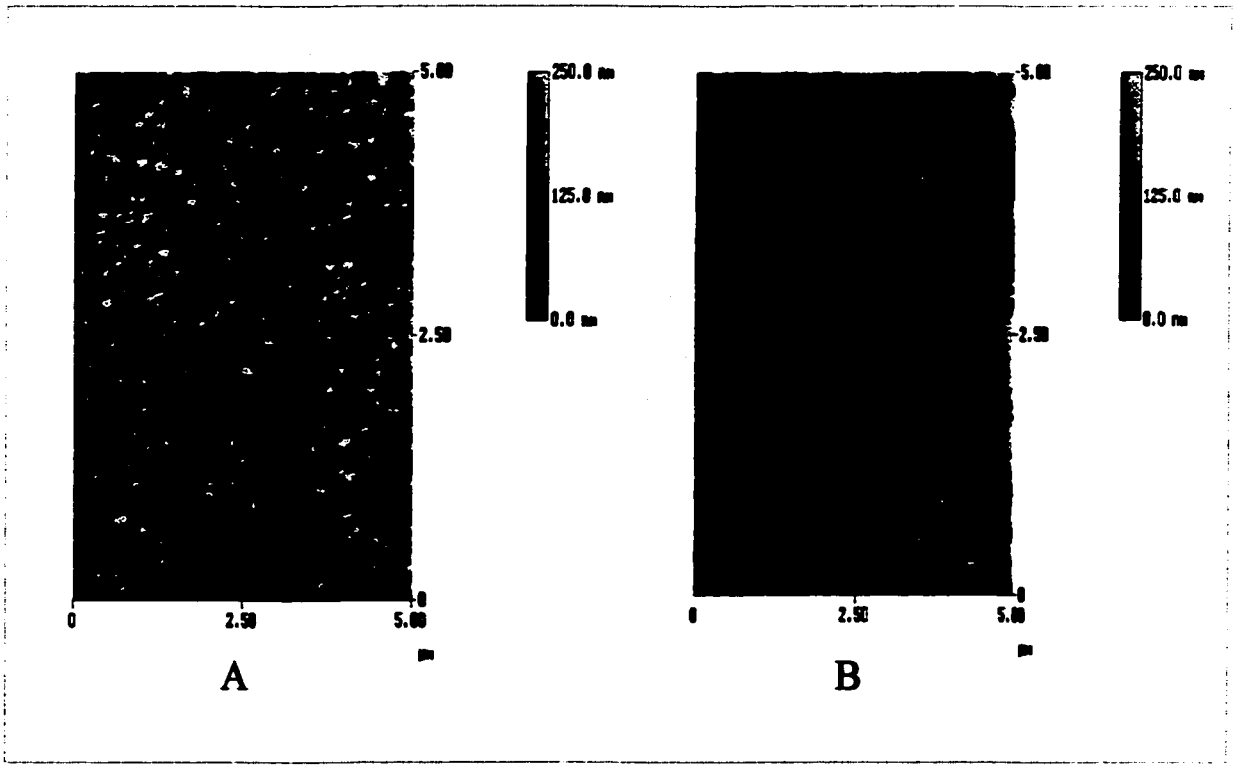

Figure 6.3.3-2: AFM images of thin films of trithiaPTCD, before and after annealing to 200 °C.

6.3.4. FT-Raman and SER(R) S

Selected Raman active vibrational modes for trithiaPTCD are given in Table 6.3.4-1. The off-resonance spontaneous Raman scattering was achieved with the 1064.1 nm laser line, while the SERRS spectrum of a thin molecular film of trithiaPTCD was collected using the 514.5 nm laser line. The FT-SERS spectrum of a monolayer of trithiaPTCD on silver island film was taken with the 1064.1 nm laser line. These spectra are shown in Figure 6.3.4-1.

Table 6.3.4-1: Raman frequencies and relative intensities for trithiaPTCD.

Cal.*	FT-Raman Powder		SERRS 514.5 nm		LB-SERS X nm		Assignment
cm^{-1}	cm^{-1}	FWHM	cm^{-1}	FWHM	cm^{-1}	FWHM	
525	519 (3)	6	525 (4)	26			Ring def.
556	534 (5)	7			539 (41)	41	Ring def.
1071	1088 (3)	5	1082 (2)	28	1065 (25)	74	Ring str.
1110	1115 (5)	15	1106 (3)	27	1119 (8)	23	Ring str.
1248	1241 (1)	6	1251 (4)	65	1248 (8)	25	C-H bend
1268					1268 (8)	23	C-H bend
1324	1321 (35)	14	1319 (21)	31	1321 (58)	57	Ring Str.
1340	1339 (10)	10					Ring str.
1369	1359 (6)	16	1358 (25)	68			Ring str.
1425	1385 (100)	16	1392 (100)	28	1382 (100)	32	Ring Str.
1426			1436 (13)	29			Ring str.
1453	1465 (3)	6	1473 (6)	24	1451 (25)	101	Ring Str.
1524	1512 (9)	10			1519 (17)	33	Ring def.
1558	1550 (7)	11					Ring Str.
1573	1572 (14)	8	1577 (8)	27	1561 (33)	54	Ring str.
1606	1614 (53)	11	1621 (26)	31	1613 (58)	37	Ring str.
1638	1666 (3)	11	1653 (8)	28	1656 (42)	46	Ring str
1642	1675 (4)	10					C=O str.
1714	1699 (25)	13	1698 (6)	31	1701 (50)	32	C=O str.

The relevant and characteristic features of all three spectra are the intense ring stretching vibrations observed at 1321, 1385, 1614 and 1699 cm^{-1}. A comparison of the SERRS spectrum of the thin solid film to the FT-SERS spectrum of the monolayer reveals no apparent change in frequencies. Furthermore, the FT-Raman spectrum of the powdered sample and the SER(R) S spectra of both monolayer and thin evaporated film are similar, with some apparent shifts in frequencies, such as the 1666 cm^{-1} band in the FT-Raman spectrum which is shifted to 1653 and 1656 cm^{-1} in both the SERRS and FT-SERS spectra respectively. Coupled with this shift is the significant increase in the FWHM for thin film and monolayer, an indication of molecular organization and that the trithiaPTCD may be chemisorbed to the substrate. Unfortunately, the elusive Ag-S band was not observed in the 100-300 cm^{-1} region as quoted by other authors [22, 108, 109] and as a result there is no conclusive evidence for chemisorption.

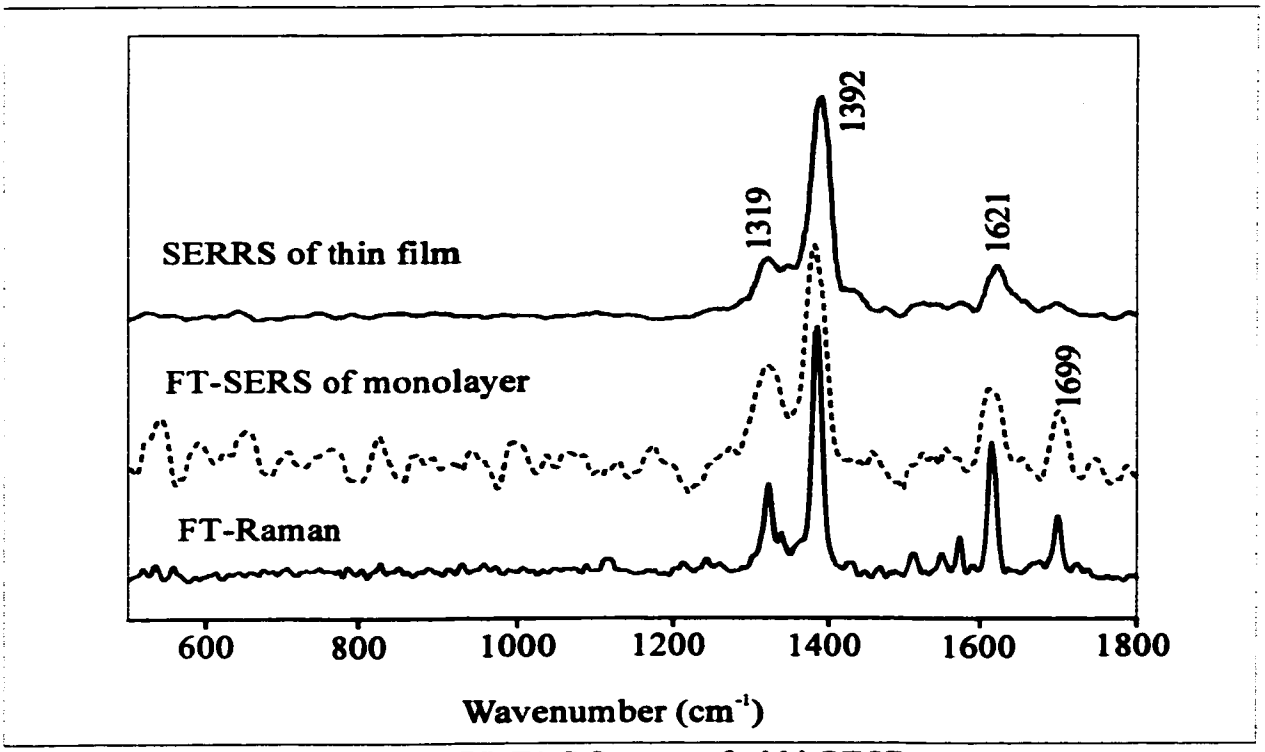

Figure 6.3.4-1: FT-Raman and SER(R) S Spectra of trithiaPTCD.

6.3.5 Summary

Thin solid evaporated films and Langmuir-Blodgett films of a novel material, trithiaPTCD, have been successfully fabricated. Raman and infrared spectroscopy have facilitated vibrational characterization of this material. SERRS and FT-SERS spectra were recorded for the thin films made. Analysis of the thin films by both RAIRS and Raman spectroscopy implies the anchoring of trithiaPTCD to the metal substrates via chemisorption, as evident by AFM studies, frequency shifts and increases in FWHM. However the absence of the Ag-S band in the 100-300 cm^{-1} region contradict this notion. As a result no conclusive evidence was found for the anchoring of trithiaPTCD to metal substrates by an Ag-S bond.

Chapter 7

THIN FILM SPECTROSCOPY AND SERRS IMAGING OF NOVEL N-PROPYLIMIDO-METHYLMERCAPTO PERYLENE DERIVATIVES

Electronic and vibrational characterization

7.1. Introduction

The studies into the possibility of controlling molecular orientation via chemical bonding to the metal substrates by thioPTCD and trithiaPTCD did not produce the expected results normally reported for self-assembly on gold and silver surfaces. The study of sulfur containing PTCD materials was extended to include a new class of perylene derivatives with a sulfur substituent in the alkyl side chain attached to the perylene core chromophore. This new class of perylene dyes, Figure 7.1-1, was characterized and the spectral data and trends attained are compared with those obtained for thioPTCD and trithiaPTCD.

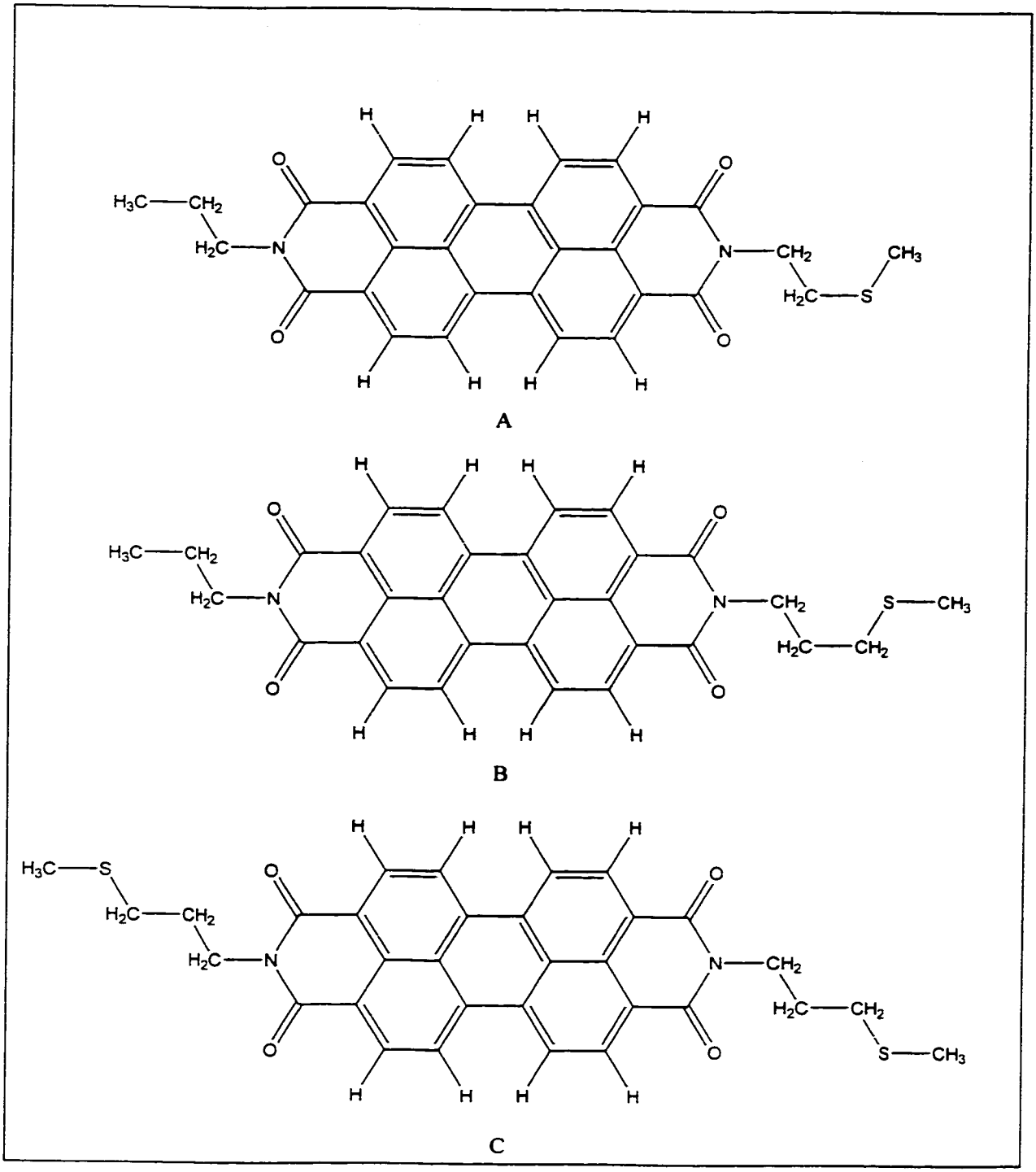

Figure 7.1-1: N-Propylimio -(2-Methylmercaptoethylimido) perylene (A), N-Propylimio -(3-Methylmercaptopropylimido) perylene (B), Bis (methylmercaptopropylimido) Perylene (C).

7.2. N-PROPYLIMIDO-(2-METHYLMERCAPTOETHYLIMIDO) PERYLENE

7.2.1. Electronic Spectra

The absorption and emission spectra of propylimido 2-methylmercaptoethylimido perylene, 2sPTCD, in chloroform are shown in Figure 7.2.1-1. The observed spectra agree well with the pattern observed in the absorption spectra of perylene tetracarboxylic (PTC) derivatives [80, 112].

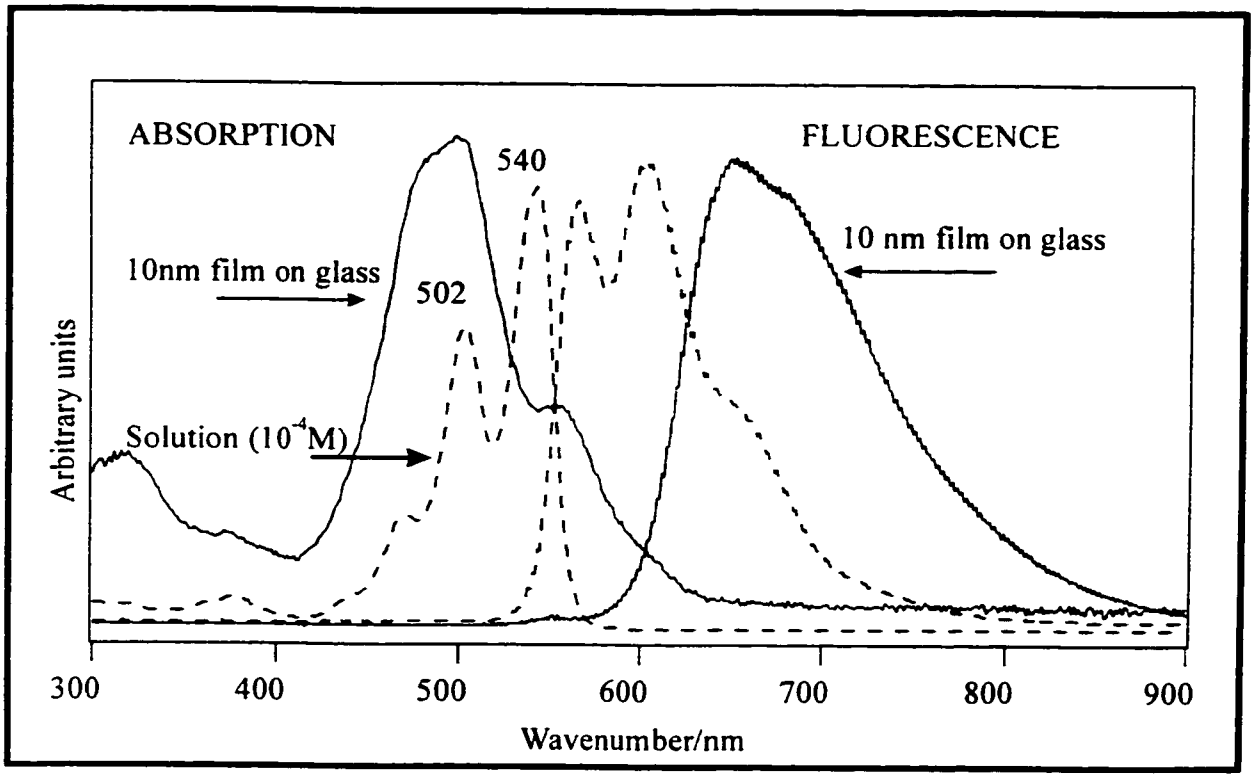

Figure 7.2.1-1: Absorption and fluorescence spectra of the 2sPTCD solution and of a 10 nm vacuum evaporated film on glass.

The observed visible absorption spectrum consists of one electronic transition with the corresponding vibronic structure. The electronic spectrum shows the characteristic structure associated with the transition of the perylene moiety, with the 0-0 band at 540 nm followed by band maxima at 502 and 468 nm. A second electronic

transition was observed at 376 nm. Extinction coefficients were measured in the spectral region where Beer-Lambert law is obeyed and they are collected in Table 7.2.1-1.

Table 7.2.1-1. Experimental extinction coefficients obtained at selected wavelengths.

Band centre/ nm	ε/l mol^{-1} cm^{-1}
540	7.46×10^5
502	4.64×10^5
468	1.73×10^5
376	5.45×10^4

The fluorescence spectra of the same solutions yield a mirror image of the absorption spectrum with maxima at 564 nm, 601 nm and a weak shoulder band at *ca.* 656 nm. The absorption and emission spectra of the 10 nm evaporated film of 2sPTCD on glass are similar to those of the KBr dispersed pellet, and they are also shown in Figure 7.2.1-1. The absorption spectrum of the solid film shows band broadening with the maxima blue-shifted at 496 nm. The emission obtained with the 514.5 nm excitation line is typical of an excimer emitter with a maximum at 653 nm. The observation of a strong excimer emission confirms the ability of these molecules to aggregate and to self organize in the solid state.

7.2.2. Surface-enhanced fluorescence

The fluorescence of dye molecules deposited onto silver island films has several interesting properties that have been the subject of independent studies [113, 114]. The excimer emissions of a 10 nm mass thickness vacuum evaporated film on glass and on

silver island film are shown in Figure 7.2.2-1. From the recorded spectra the SEF enhancement factor is estimated by direct comparison with the emission of the film on glass. The SEF average enhancement was ca. 15. Since the SERRS spectrum is observed in a spectral window where the fluorescence intensity is low, both surface enhanced-spectra are recorded in a single experiment. According to electron microscopy of the silver island film, the average diameter of the islands (assuming spheroidal shape) is ca. 50 nm. The results presented in Figure 7.2.2-1 show that the SEF spectrum is due to aggregates on the surface of the silver islands. There is no evidence of monomer fluorescence and it is concluded that the enhanced spectroscopy presented in this work is that of the large 2sPTCD aggregates formed on silver islands.

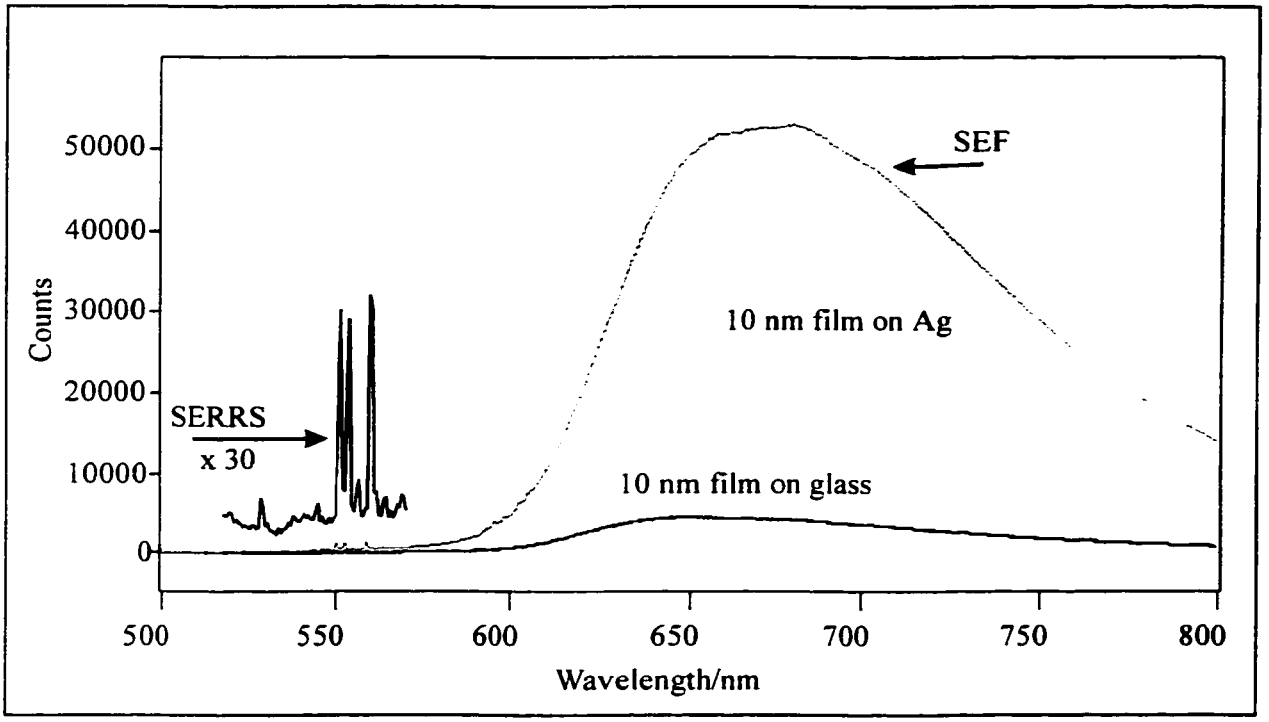

Figure 7.2.2-1: Surface-enhanced fluorescence of a 10 nm mass thickness film of 2sPTCD on silver islands. The SERRS spectrum is amplified by a factor of 30. The fluorescence of the same film on glass is the reference.

7.2.3. Molecular vibrations: Infrared and Raman spectra

Observed wavenumbers in the Raman and infrared spectra of 2sPTCD, their relative intensities and the calculated vibrational spectrum are listed in Table 7.2.3-1. Quantum chemical computations were carried out at 3-21G level of theory using Gaussian98 for Windows and scaled using the 0.8953 factor in Hartree-Fock calculations [115, 116].

Table 7.2.3-1: Observed and calculated Raman and infrared intensities for 2sPTCD.

Calc Freq	Corr. Freq	Calc. IR Int.	Calc. Raman Int.	IR KBr pellet	SERRS 514.5 nm	Raman 633 nm	SERRS 633 nm	Assignment
273	245	2	7		227(2)		277 (vw)	Ring def.
320	288	5	7				298 (vw)	Ring def.
375	338	11	3				333 (vw)	Ring def.
424	382	19	0				353 (vw)	Ring def.
431	388	52	0				374(vw)	Ring def.
443	399	52	2				394 (vw)	Ring def.
485	437	9	38	435(2)	440(1)		434 (vw)	Ring def.
522	470	24	6	476(1)			460 (vw)	Ring def.
531	478	19	6	489(2)	484(1)		483 (vw)	Ring def.
592	532	0	94		544(18)	540(27)	546(14)	Ring breth
645	581	5	12	588(1)	579(5)	579(8)	585(5)	Ring breth
683	615	40	22	604(1)	601(3)			Ring dist
687	618	1	0	614 (2)				Ring dist
700	630	23	37	627(2)	623(1)			S-C str
704	634	9	1				636 (vw)	Ring dist
					641(1)		643 (vw)	Ring dist
					659(1)		653 (vw)	Ring dist
							671 (vw)	Ring dist
775	698	3	79			683(8)	682(5)	N-C wag, ring dist
788	709	6	8				736 (vw)	Ring dist
821	739	4	1	744(13)	760(1)		751(3)	C-H wag
885	797	1	0	793(4)			798 (vw)	Ring dist
889	800	51	0	810(16)				C-H wag
894	804	14	0				806 (vw)	C-H rock
902	812	62	2		817(2)		814 (vw)	C-H rock
908	817						822 (vw)	C-H rock
911	820	49	0				833(3)	C-H rock
957	861			849(1)			839 (vw)	C-H rock
960	864			857(4)		859(5)	851 (vw)	C-H rock
988	889				864(2)		864 (vw)	C-H rock
993	894				912(1)		905 (vw)	C-H rock
1040	936	0	9				930 (vw)	C-H rock
1060	954	24	16				939 (vw)	alkyl C-H wag
1076	969	1	4	973(1)			958 (vw)	alkyl C-H wag
1106	995	42	2		963(3)			C-H wag
1117	1006	13	2	1004(3)				C-H wag
1127	1015	31	14	1027(2)	1033(1)			C-H wag
1177	1059	1	1062	1050(2)			1059 (vw)	C-H wag

1186	1067	0	134					C-H rock
1187	1069	0	7				1071 (vw)	C-H rock
1203	1083	7	3	1081(5)	1086(8)	1087(25)	1080 (8)	C-H rock
1233	1110	12	8	1116(4)	1117(1)	1113(9)		C-H bending
1250	1125	59	0	1128(6)	1131(1)			alkyl C-H bending
1251	1126	167	1	1156(4)	1154(1)			alkyl C-H bending
1285	1156	1	90	1166(4)	1163(1)			C-H bending
1303	1173	117	22	1182(4)	1176(2)			C-H bending
1322	1190	26	2		1204(2)			C-H bending
1358	1222	62	1					C-H bending
1365	1228	15	18					C-H bending
1390	1251	49	3	1246(11)	1244(5)	1248(13)	1254 (14)	C-H bending
1408	1267	37	96	1265(5)	1254(4)			C-H bending
1414	1273	33	0					C-H bending
1421	1279	2	3349					alkyl C-H bending
1426	1284	5	0					
1430	1287	46	3					
1432	1289	335	16	1301(1)	1294(44)	1292(58)	1297 (100)	C-H bend
1446	1301	1	6454		1303(79)	1303(95)		Ring stretching
1459	1313	12	4					C-H wag
1478	1330	498	10					C-H wag, ring breth
1480	1332	139	227					alkyl C-H bending
1488	1339	808	9	1339(34)				C-H bending
1500	1350	19	41	1355(24)		1353(9)	1352 (23)	C-H bending
1502	1352	12	0					C-H bending
1524	1371	50	60	1380(16)	1383 (100)	1378 (100)	1378 (83)	C-H bending
1526	1374	65	39					alkyl C-H bending
1546	1391	159	1					alkyl C-H bending
1550	1395	24	5	1402(22)				alkyl C-H bending
1554	1399	14	82					C-H bending
1571	1413	80	8					C-H bending
1577	1420	0	800					C-H bending

1579	1421	0	526	1439(26)	1437(12)			C-H bending
1625	1462	0	87	1461(3)	1457(15)	1456(19)	1454 (13)	C-H bending
1631	1468	47	30		1471(3)			C-H bending
1645	1480	95	28					C-H bending
1646	1481	57	12	1480(2)	1482(3)			C-H rock
1674	1506	9	27	1507(5)	1502(1)			C-H bending
1749	1574	3	9463		1564(13)	1541(10)	1545 (13)	C=C stretching
1759	1583	421	7	1577(26)	1575(63)	1572(71)	1572 (55)	C=C stretching
1771	1594	422	17	1592(69)	1588(66)	1586(79)	1584 (54)	C=C stretching
1774	1596	0	0					C=C stretching
1776	1599	1	3473		1598(31)	1605(13)	1599 (8)	C=C stretching
1791	1612	0	433	1608(40)	1604(12)			C=C stretching
1860	1674	581	48	1651(56)	1614(8)			C=O stretching
1863	1676	267	99	1660(56)	1659(1)			C=O stretching
1904	1713	686	8	1692(100)	1693(4)			C=O stretching
1908	1717	14	324		1701(7)		1698(6)	C=O stretching

The infrared and Raman spectra are presented in Figure 7.2.3-1 that also includes the calculated infrared and Raman spectral intensities. The experimental spectra were both recorded from a solid state KBr sample. The calculated harmonic spectrum corresponds to a gas phase molecular vibrational spectrum. It can be seen in Figure 7.2.3-1 that using a relatively low level of theory, a qualitatively good agreement is achieved between the observed spectra and the pattern of relative intensities provided by the computed spectra. For instance, the computed Raman spectrum predicts a small number of Raman bands with substantial relative intensity in agreement with observations, with the exception of the 1278 cm^{-1} band. The calculated spectrum predicts

a strong infrared intensity for the carbonyl stretching modes (see Figure 7.2.3-1) and a very weak intensity in the Raman spectrum in full agreement with observations.

The most significant and relevant group frequencies for molecular orientation considerations in 2sPTCD films are both the in-plane carbonyl stretching vibrations and C=C ring stretching vibrations of perylene, and the out-of-plane C-H wagging vibrations. The symmetric and the antisymmetric carbonyl stretching vibrations are observed at 1692 and 1660 cm^{-1} respectively. The strongest in-plane perylene C=C stretching vibrations are observed at 1592 and 1577 cm^{-1}. The out-of-plane vibrational modes with a dynamic dipole moment perpendicular to the perylene plane, the C-H wags, are observed at 810 and 744 cm^{-1}. The molecular organization in a film creates a spatial anisotropy that can be extracted using the change in the relative intensity observed in the spectra of the film recorded in the transmission geometry and in the reflection absorption spectra (RAIRS). The RAIRS spectra of the 20 nm film on smooth silver were recorded. A comparison of the relative intensities of the in-plane and out-of-plane perylene modes does not show any large film anisotropies. It is concluded that the long-range packing often observed in PTCD films, as reported in Chapter 4 [18], is not predominant.

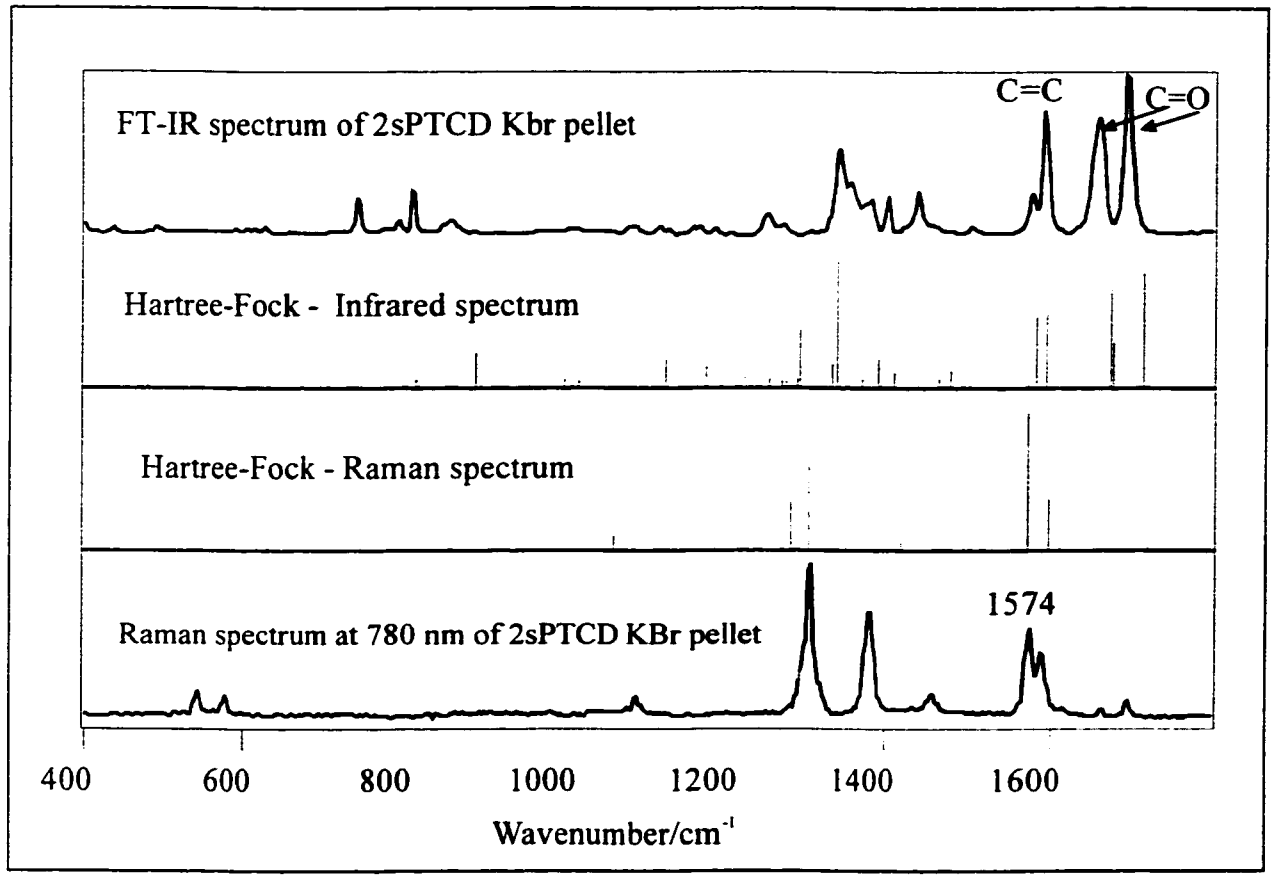

Figure 7.2.3-1: FT-IR and Raman spectra of the 2sPTCD KBr pellet and the corresponding calculated infrared and Raman spectra using the ab initio Hartree-Fock methods.

7.2.4. Surface-enhanced Resonance Raman scattering

The resonant Raman spectra of the pellet and 10 nm thin films were obtained with the 514.5 nm and the 633 nm laser lines. The inelastic scattering excited with the 514.5 nm is observed on the background fluorescence and the baseline corrected RRS spectrum is shown in Figure 7.2.4-1. The SERRS spectrum of a 10 nm vacuum evaporated film onto silver islands is easily recorded with a large signal to noise ratio as shown in Figure 7.2.4-1.

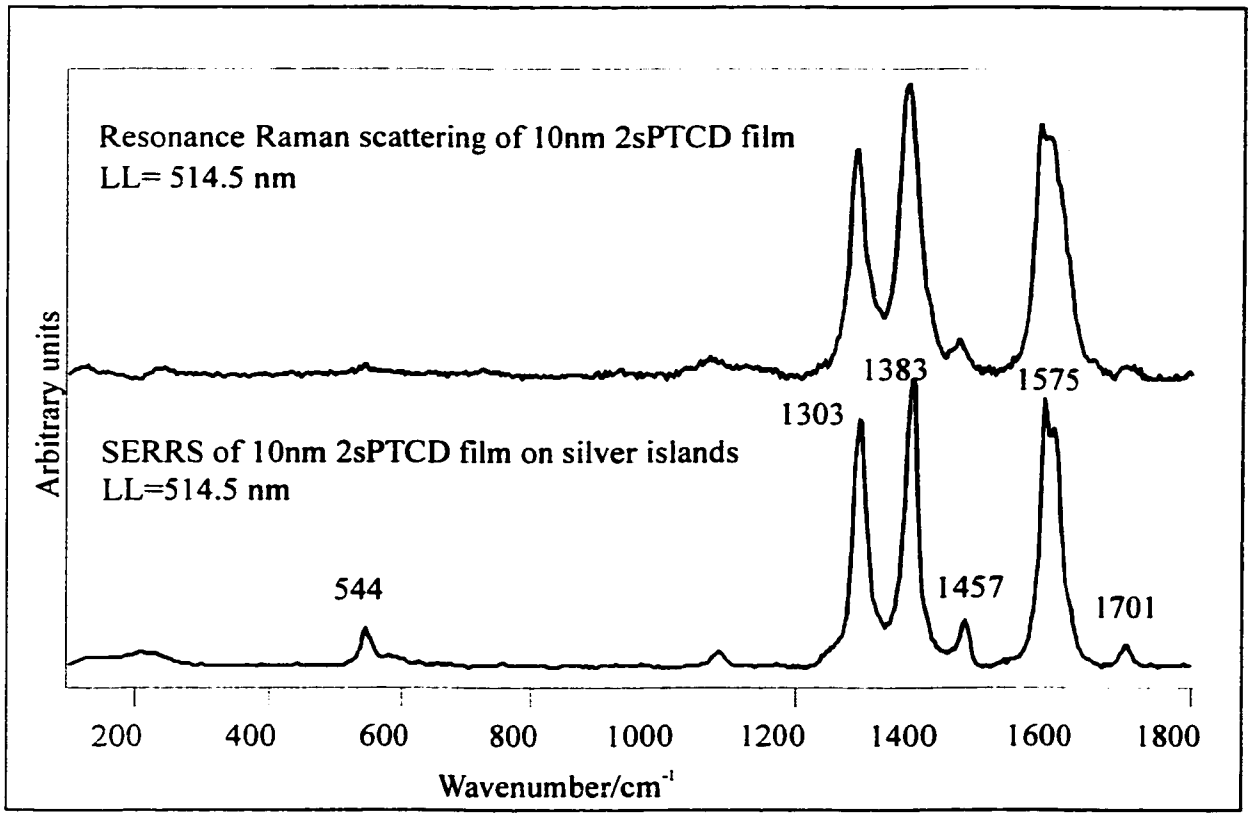

Figure 7.2.4-1: Resonance Raman scattering (baseline corrected) of 2sPTCD solid film at 514.5 nm and SERRS on silver islands. Notice that SERRS and RRS are similar.

A comparison of the resonance Raman and SERRS spectra of the 10 nm film reveals that they are practically identical, with the exception of the surface enhancement

ca. 40; there are no apparent shifts in wavenumbers indicating that the molecular dye (or aggregate) is physisorbed onto the silver substrate. The latter observations also applied to SERRS spectra of the 10 nm film on silver islands obtained with the 633 nm excitation line. The prominent features of both spectra are related to the PTCD chromophore. In the SERRS spectrum, overtones and combinations bands are also observed with considerable intensity and the wavenumbers and assignments are listed in Table 7.2.4-1.

Table 7.2.4-1: Overtones and combinations bands observed in the SERRS spectrum of 2sPTCD excited with the 633 nm laser line.

Observed (cm^{-1})	Overtones and Combinations
3181	1599 + 1584= 3183
3142	1572 x 2 = 3144
2999	1545 + 1454 = 2999
2946	1572 + 1378 = 2950
2863	1572 + 1297 = 2869
2746	1378 x 2 = 2756
2668	1599 + 1071 = 2670
2582	1297 x 2 = 2594
2438	1584 + 864 = 2448
2351	1698 + 653 = 2351
2223	1545 + 682 = 2227
2195	1545 + 653 = 2198
2126	1071 + 1059 = 2130
2024	1352 + 682 = 2034
1968	1599 + 374 = 1973
1933	1352 + 585 = 1937
1847	1572 + 277 = 1849
1734	1254 + 483 = 1737

The SERRS spectrum obtained with the 633 nm laser line featuring the overtone region is shown in Figure 7.2.4-2. There is good agreement between calculated overtones and combinations and observed wavenumbers. It was found that the full-width at half maximum (FWHM) values of overtones and combinations are on average bigger than those of the fundamentals. Although in the present case there is solely the high local symmetry of the chromophore, it should be pointed out that even for highly symmetric molecules, all overtones are Raman active, while combinations are Raman active as the result of Raman active fundamentals and totally symmetric modes.

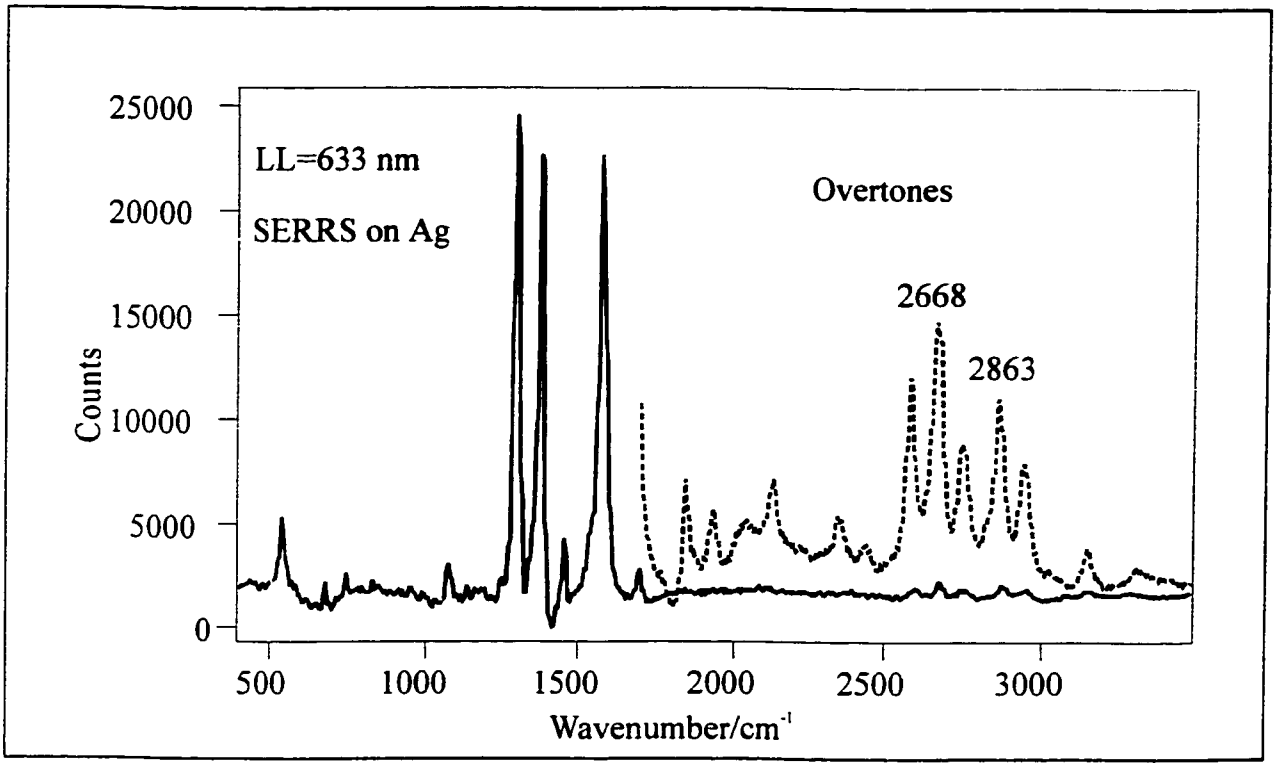

Figure 7.2.4-2: SERRS of 10 nm 2sPTCD film on silver recorded with the 633 nm laser line. The full spectrum is shown with a solid line. The overtone region was recorded separately with longer accumulation time and is shown with dotted line.

7.2.5. SERRS Imaging

Micro-Raman imaging can be generated by recording the spectra point-by-point to produce the line scanning analysis or mapping of areas of the sample. Images can also be obtained by filtering of a particular vibrational wavenumber from the spectrum produced by a defocused laser beam and collecting the light distribution in a wide field or global image. The technique has been applied in SERS studies of Langmuir Blodgett monolayers and self-assembly molecular films [117, 118]. Both point-by-point line mapping and global imaging were used to acquire micro-Raman SERRS images of 10 nm thin films of 2sPTCD on silver island films. Line mapping, area mapping and global imaging were obtained using the 514.5 nm laser line. The point-by-point mapping was recorded using a 2 μm step, 30 μW laser power at the surface of the film and a laser beam focused down to ca. 1 μm^2. The point-by-point line scanning spectra excited with the 514.5 nm laser line and recorded with 2 μm intervals are shown at the top in Figure 7.2.5-1. It can be seen that the intensity of the Raman scattering at each point are similar, an indication of similar average SERRS enhancement across the cross section of the silver island film. Similar results were obtained in the point-by-point area mapping on the same section of the silver island film with the 514.5 nm and the 633 nm laser lines. The latter can be seen in the left bottom corner of Figure 7.2.5-1. The white light coloration is reserved for high intensity of the signal. Since the SERRS spectrum is seen on the background of weak fluorescence, for the generation of the maps a baseline corrected intensity at 1378 cm^{-1} was selected to avoid the fluorescence contribution. The global images were captured using the filtered Raman scattered light of the fundamental vibrational wavenumber at 1297 cm^{-1} (assigned to a perylene ring stretching mode)

excited with the 514.5 nm laser line. Several global field images were taken and a typical 3D image of the 1297 cm^{-1} band is shown on the bottom-right hand side in Figure 7.2.5-1. Both the global imaging and point-by-point area mapping indicate that for a 10 nm mass thickness film a "homogeneous" distribution, within the spatial resolution of the technique, was formed by sublimation of 2sPTCD. The global image gives, however, better display of the "homogeneity" of the SERRS signal on the 40x40 microns surface.

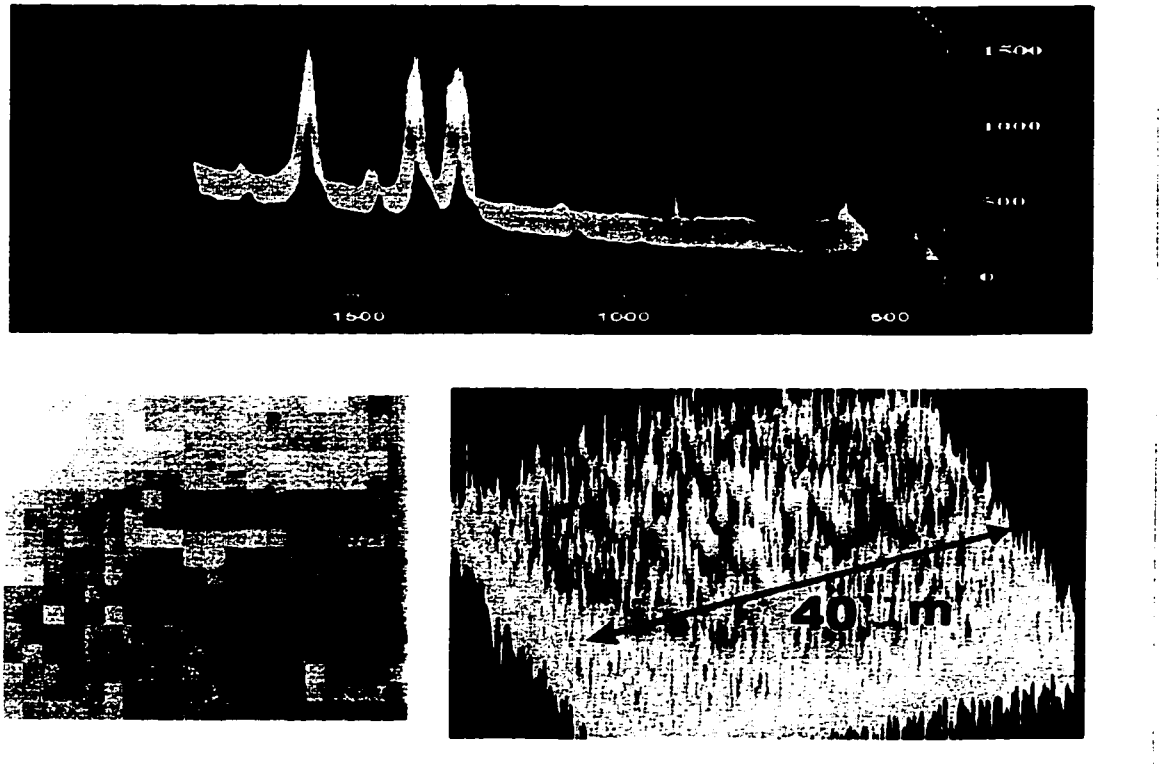

Figure 7.2.5-1: Point-by-point line scanning at the top (excited with 514.5 nm), point-by-point mapping (633 nm) of a ca. 40x40 μm^2 area, and the 3-D global image (at 514.5 nm) generated using the perylene ring stretching vibration at 1297 cm^{-1}.

7.2.6. Summary

The successfull fabrication of thin films of 2sPTCD by sublimation has been established. Films formed onto smooth silver surfaces and IR transparent substrates are

isotropic, i.e. there is no prevalent molecular alignment, which is probably due to the asymmetric ending in the molecule. Global images and point-by-point line mappings indicated that the thin films of the 2sPTCD formed on silver were homogenous. Finally, there is no spectroscopic evidence for a sulfur-metal interaction and the sulfur bond is preserved at the metal-organic interface. It can be concluded that the 2sPTCD is physisorbed on metal substrates.

The interpretation of the molecular vibrations was successfully aided with quantum chemical computations that give, even at low level of theory (3-21G), a fairly good agreement with the observed infrared and Raman spectra.

7.3. N-PROPYLIMIDO-(3-METHYLMERCAPTOPROPYLIMIDO)PERYLENE

This dye is similar in molecular structure to 2sPTCD. It consists of a perylene chromophore with two branching propyl side chains, one of which contains a mercapto-group. The successful fabrication of evaporated thin films of this class of dye has been demonstrated with 2sPTCD. Moreover the main conclusion from spectroscopic studies of 2sPTCD was the formation of physisorbed thin films, rather than the anticipated chemisorption. The perylene derivative, n-propylimido-(3-methylmercaptopropylimido) perylene, 3sPTCD, should confirm the results obtained for 2sPTCD.

7.3.1. Electronic Spectra

The absorption and emission spectra of n-propylimido- (3-methylmercaptopropylimido) perylene in chloroform are shown in Figure 7.3.1-1, and are comparable to those recorded for a similar perylene derivative earlier in the chapter. The electronic spectrum shows the characteristic structure associated with the transition of the perylene moiety, with the 0-0 band at 540 nm followed by band maxima at 503 and 471 nm. A second electronic transition was observed at 379 nm. The extinction coefficients obtained from the Beer-Lambert plot are listed in Table 7.3.1-1. The fluorescence spectra of the same solutions yield a mirror image of the absorption spectrum with maxima at 561 nm, 601 nm and a weak band at *ca.* 651 nm

Table 7.3.1-1: Experimental extinction coefficients obtained at selected wavenumbers.

Band centre/ nm	ε/ l mol^{-1} cm^{-1}
540	7.25 x 10^5
503	4.69 x 10^5
471	1.75 x 10^5
379	5.07 x 10^4

The absorption and emission spectra of the 10 nm evaporated film is also shown in Figure 7.3.1-1. Unlike the absorption spectra of dispersed KBr pellet, the absorption band is split in that of the evaporated thin film. The absorption band maxima for the bulk is at 478nm, whereas for the thin film, one absorption band is blue shifted at 449 nm and the other red shifted at 634 nm. Though the absorption spectrum of the bulk is similar to those previously reported for sulfur containing perylenes, such as 2sPTCD and thioPTCD (Chapter 6), those of the thin solid evaporated films are vastly different. The differences between the thin solid films and pellet spectra may be rationalized due to the molecular stacking and orientational distribution. The broad emission spectrum of the 10 nm evaporated film of 3sPTCD on glass, with a maximum at 682 nm, is similar to those of the bulk. This broad emission band is typical of an excimer and indicates the potential for these molecules to aggregate and self organize in the solid state. In view of the differences in the absorption spectra between the 2sPTCD and 3sPTCD and the results of the RAIRS and transmission infrared spectra (no long-range organization) it is necessary to distinguish here between the short range and the long range organization of these PTCD derivatives. The differences in the electronic absorption spectra have to be

explained in terms of a short-range organization and dipole moment alignment of the molecules in the small aggregates. Clearly the short-range arrangement for 2sPTCD and 3sPTCD is different. A blue shifted electronic absorption with respect to the 0,0 transition in solution is associated with the formation of H-aggregates while the red-shifted absorption would be associated with the J-aggregation [41, 119]. The film absorption of the 3sPTCD shows a "splittting" with a blue and a red absorption band. That is indicative of an intermediate geometry for the alignment of the molecular dipoles.

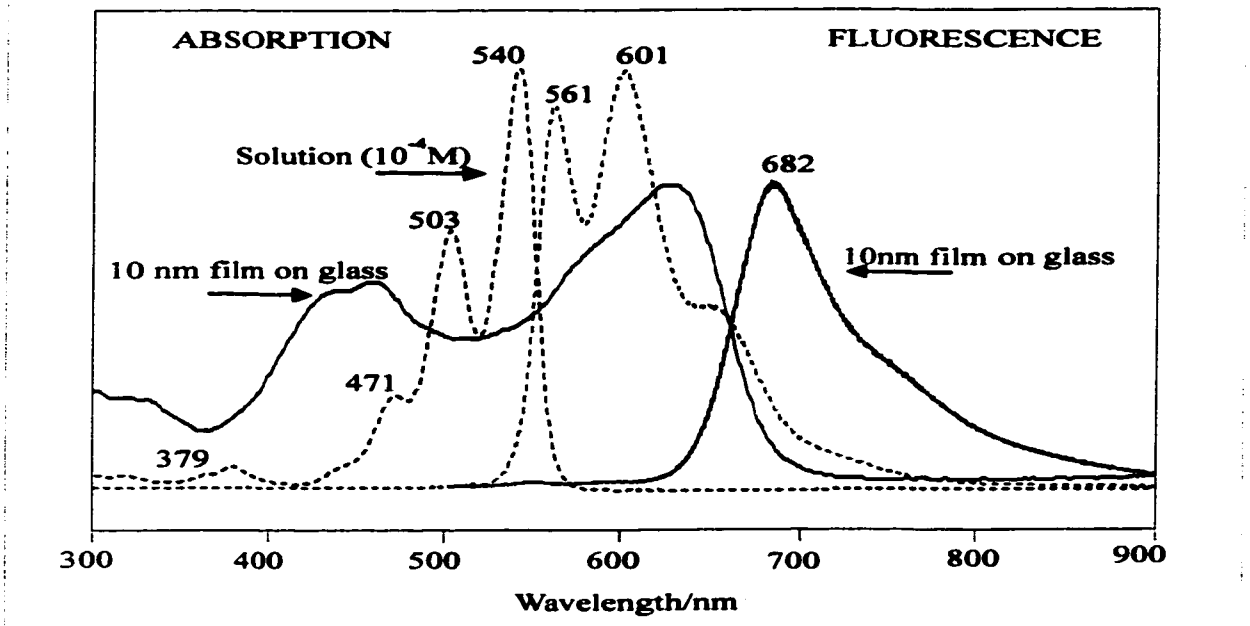

Figure 7.3.1-1: Absorption and emission spectra of a solution and thin evaporated film of 3sPTCD.

7.3.2. Infrared spectra and long range molecular organization

The observed infrared wavenumbers for the isotropic dispersion of 3sPTCD in KBr and RAIRS of 20 nm film on silver mirror are given in Table 7.3.2-1.

Table 7.3.2-1: Infrared intensities and wavenumbers for 3sPTCD.

KBr pellet		RAIRS		Assignment
cm^{-1}	FWHM	cm^{-1}	FWHM	
1771 (2)	7	1764 (4)16		ring breth.
1750 (1)	2			ring breth.
1733 (3)	4			ring breth.
1717 (3)	4	1724 (6)	7	ring breth.
1698 (10)	7			C=O str.
1692 (100)	8	1695 (100)	10	C=O str.
		1676 (4)	2	C=O str.
1656 (98)	12	1658 (62)	10	C=O str.
1636 (2)	9	1628 (6)	6	C=O str.
1615 (2)	3	1606 (11)	30	C=O str.
1592 (52)	8	1593 (53)	8	C=C str.
1577 (14)	8	1578 (19)	20	C=C str.
1558 (4)	4	1563 (11)	6	C=C str.
1540 (3)	5	1549 (15)	11	ring str
1520 (2)	8	1528 (15)	18	ring str
1507 (6)	6	1512 (13)	9	ring str

1497 (1)	4	1500 (6)	4	ring str
1488 (1)	8	1494 (5)	7	ring str
1474 (1)	11	1480 (9)	10	N-C str
1464 (1)	4	1464 (7)	8	C-H bend
1457 (4)	5	1450 (4)	4	N-C, C-C str
1440 (12)	11	1441 (18)	8	ring str
1420 (2)	10	1424 (4)	6	ring str
1403 (12)	6	1403 (21)	8	ring str
1378 (7)	13	1380 (15)	10	ring str
1345 (24)	19	1350 (50)	17	ring str
1301 (1)	9	1300 (2)	12	C-H bend
1287 (1)	9	1282 (2)	14	C-H bend
1257 (7)	11	1258 (3)	8	C-H bend
1244 (5)	12	1244 (3)	7	C-H bend
1182 (2)	11	1180 (4)	16	C-H bend
1158 (2)	11	1157 (3)	11	C-H bend
1123 (1)	16	1126 (2)	20	C-H bend
1081 (2)	10	1081 (7)	11	C-H bend
1051 (1)	20	1061 (4)	23	C-H bend
1014 (1)	13	1016 (4)	28	C-H bend
852 (2)	13	847 (7)	29	C-H bend
810 (7)	5	810 (8)	6	C-H wag
794 (2)	8	791 (5)	28	C-H wag

747 (5)	8	747 (10)	7	C-H wag
667 (1)	3	667 (36)	7	Ring dist.
632 (1)	6	654 (8)	11	Ring dist.
627 (1)	17	609 (4)	26	Ring dist.
499 (1)	8			Ring dist.
435 (1)	8			Ring dist.

Molecular orientation determination may be accomplished by taking into consideration local symmetry arguments as described in Chapter 3. As such, it is reasonable to limit the discussion of normal mode assignment to the characteristic in-plane and out-of-plane vibrations of the PTCD chromophore moiety. The most significant and relevant group frequencies for molecular orientation considerations in PTCD films are both the in-plane symmetric and anti-symmetric carbonyl stretching vibrations, at 1692 and 1656 cm^{-1} respectively, the in-plane C=C ring stretching vibrations of perylene at 1592 and 1577 cm^{-1}, and the out-of-plane C-H wagging vibrations observed at 810 and 747 cm^{-1}. The infrared spectrum of the isotropically dispersed pellet is shown in Figure 7.3.2-1.

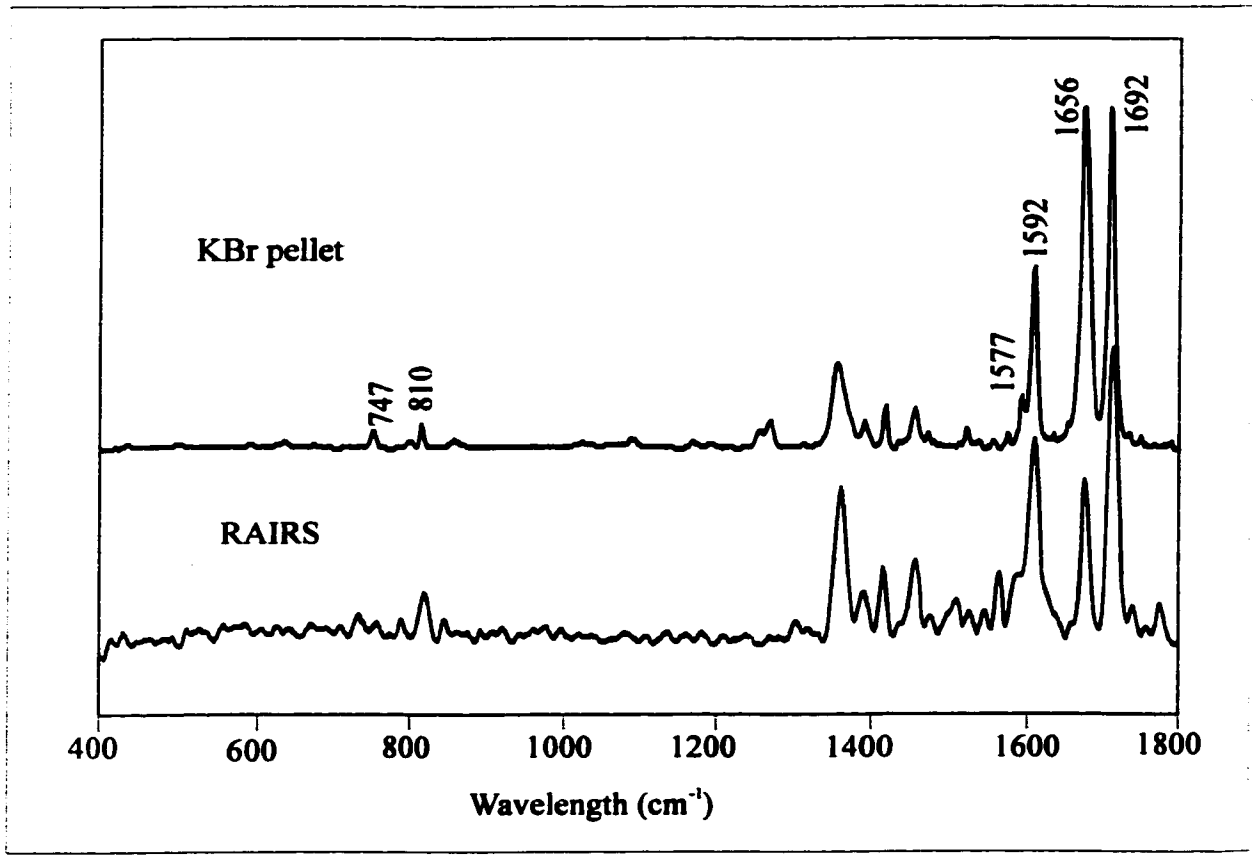

Figure 7.3.2-1: RAIRS spectrum of a thin solid film and infrared spectrum of KBr pellet.

The molecular organization in a film creates a spatial anisotropy that can be extracted using the change in the relative intensity observed in the spectra of the film recorded in the transmission geometry and in RAIRS, as described in Chapter 3. In transmission geometry, unlike that of reflection, the polarization of the incident radiation lies along the substrate's surface and fundamental vibrational modes that generate a change in the dipole moment perpendicular to the substrate's surface will not absorb. Comparison of the reference KBr spectrum, in which there is a random spatial distribution, to the RAIRS spectrum reveals on average a small percentage of molecules with a head-on orientation of the PTCD moiety to the substrate's surface. The

information can be extracted from the RAIRS spectrum, where the out-of-plane C-H wags at 810 and 747 cm^{-1} are relatively less intense than the in-plane carbonyl stretches at 1695 and 1658 cm^{-1}. Also, the relative intensity of the C=C short axis stretch at 1593 cm^{-1}, as well as the symmetric carbonyl stretch at 1695 cm^{-1}, suggests a head-on molecular orientation. The RAIRS spectrum of the 20 nm film is shown in Figure 7.3.2-1. This preferred molecular orientation differs significantly from the molecular orientation as reported in previous chapters for its parent molecule, bis-n-propylimido perylene, and that of thioPTCD where the molecular orientation is head-on and edge-on respectively [18, 120].

A comparison of the RAIRS spectrum to the bulk also indicates no significant shifts in wavenumbers or full widths at half height, a strong indication that the intermolecular interactions are similar and there is no real change in the molecular environment. It is also concluded that in the evaporated films on silver, there is no Ag-S bond formation.

7.3.3. Resonance Raman and surface-enhanced resonant Raman scattering

Selective resonance Raman (RRS), surface-enhanced resonant Raman (SERRS) and surface-enhanced Raman scattering (SERS) wavenumbers and their relative intensities for the pellet and thin solid films of 3sPTCD are shown in Table 7.3.3-1.

Table 7.3.3-1: Raman intensities and wavenumbers for 3sPTCD.

514.5 nm						780 nm		Assignment
RRS (Powder)		RRS (Film)		SERRS		SERS		
cm-1	FWHM	cm-1	FWHM	cm-1	FWHM	cm-1	FWHM	
		1776 (4)	6					Ring brth.
		1747 (7)	2					Ring brth.
		1742 (7)	6					Ring brth.
		1723 (5)	3					Ring brth.
		1711 (3)	20					Ring brth.
1702 (6)	21	1700 (12)	9	1699 (9)	16	1697 (6)	15	C=O str
		1692 (5)	7					C=O str
		1617 (15)	13	1615 (8)	14			C=O str
1606 (25)	31							C=O str

1587	20	1588	19	1588	20	1586	36	ring dist
(57)		(87)		(73)		(36)		
1570	18	1574	11	1573	13	1572	14	C=C str
(72)		(71)		(64)		(49)		
		1529	5	1557	12	1548	25	ring breth.
		(4)		(3)		(8)		
1452	19	1459	12	1457	14	1454	16	ring str.
(11)		(20)		(16)		(13)		
		1398	13					ring str.
		(11)						
1377	27	1382	14	1379	20	1380	13	ring str.
(100)		(100)		(100)		(48)		
		1369	16			1372	33	ring str.
		(26)				(26)		
						1338	28	ring str.
						(30)		
		1306	15					ring str.
		(86)						
1298	27	1295	16	1301	24	1295	27	ring str
(82)		(56)		(90)		(100)		
						1270	13	ring breth.
						(22)		

		1246 (5)	7	1247 (2)	13	1254 (32)	27	C-H bend
						1226 (11)	27	C-H bend
		1171 (10)	2			1197 (7)	22	C-H bend
		1090 (7)	8					C-H bend
1076 (5)	43	1082 (4)	12	1085 (7)	22	1081 (14)	17	C-H bend
						788 (8)	16	ring distor.
						678 (4)	23	ring distor.
		608 (4)	2	615 (1)	22			ring distor.
577 (1)	14	583 (4)	31	581 (3)	30	592 (11)	33	ring brth.
		580 (2)	5					ring brth.
		563 (4)	2					ring brth.
544 (6)	18	544 (20)	14	545 (15)	16	543 (39)	22	ring distor.
522 (1)	11	522 (1)	7					ring distor.
		487 (1)	12					ring distor.
		451 (2)	7					ring distor.

The SERRS and SERS spectra of the 10 nm film on silver islands were obtained with the 514.5 nm and 780 nm excitation lines respectively. The resonant Raman spectra of the pellet and thin film were obtained with the 514.5 nm excitation line and, together with the SERRS spectrum of the thin solid film, are shown in Figure 7.3.3-1. The resonant Raman and SERRS spectra of the 10 nm film appear to be identical with the exception of a x 30 enhancement. This enhancement is much smaller than that observed for n-propylimido-2-(methylmercaptoethylimido) perylene [121].

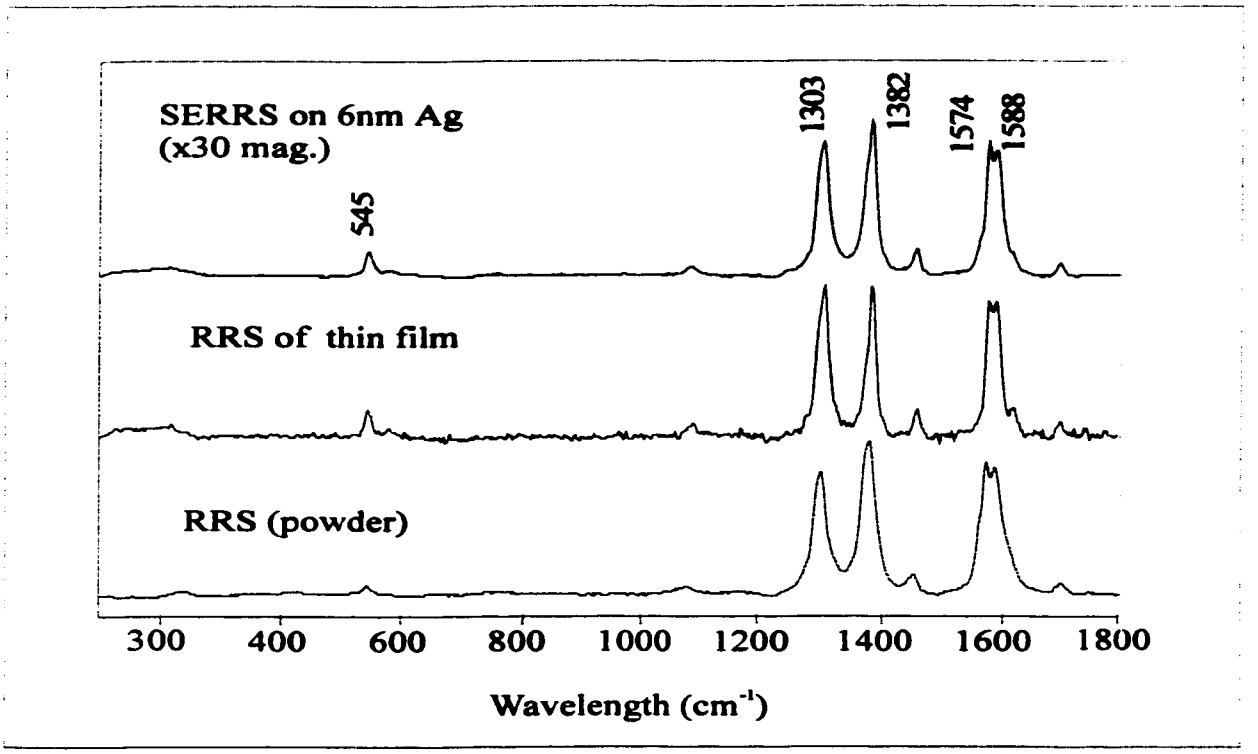

Figure 7.3.3-1: Resonant Raman and SERRS spectra of thin solid films of 3sPTCD.

There are no apparent shifts in wavenumbers or differences in bandwidth indicating that the pigment is physisorbed onto the silver substrate and further suggests that the elusive Ag-S bond is not readily formed, as illustrated for several other members of the perylene tetracarboxylic diamide family reported in previous chapters [18, 120,

121]. The prominent features of both spectra are the ring C=C stretching modes at 1588, 1573, 1379 and 1301 cm^{-1}. A ring distortion mode was also observed at 545 cm^{-1}. The SERS and Raman spectra obtained with the 780 nm excitation line are shown in Figure 7.3.3-2, and are similar to that obtained with the 514.5 nm laser line.

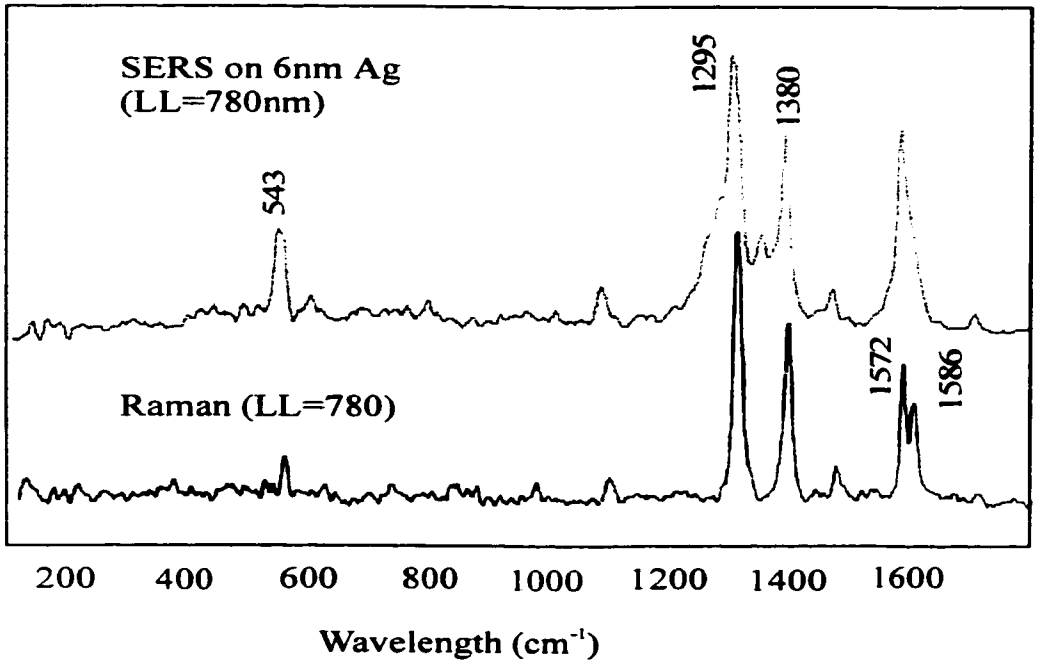

Figure 7.3.3-2: Raman and SERS spectra of a thin film of 3sPTCD.

7.3.4. SERRS Imaging

The two distinct concepts of Raman imaging, global imaging and point-by-point line and area mapping, are illustrated for thin evaporated films of 3sPTCD on silver island films. Line mapping and global imaging were obtained using the 514.5 nm laser line. The global images were captured using the filtered Raman scattered light of the fundamental vibrational wavenumber at 1301cm^{-1}, corresponding to a C=C ring stretch. The SERRS spectrum is seen on the background of a weak fluorescence. Consequently, for the mapping a baseline corrected intensity was selected to avoid the contributions

from fluorescence. The global field image was taken from a 40 μm^2 area and a typical 3D image of the 1298 cm^{-1} band (Figure 7.3.4-1a) is shown in Figure 7.3.4-1. The global image indicates a homogeneous distribution of the film on substrate. Similarly, the point-by-point line scan map (Figure 7.3.4-1b), with a 1μm step, is also shown in Figure 7.3.4-1. It should be noted that the x-cross section of the line scan is a typical SERRS spectrum of 3sPTCD on 6 nm silver, as should be expected.

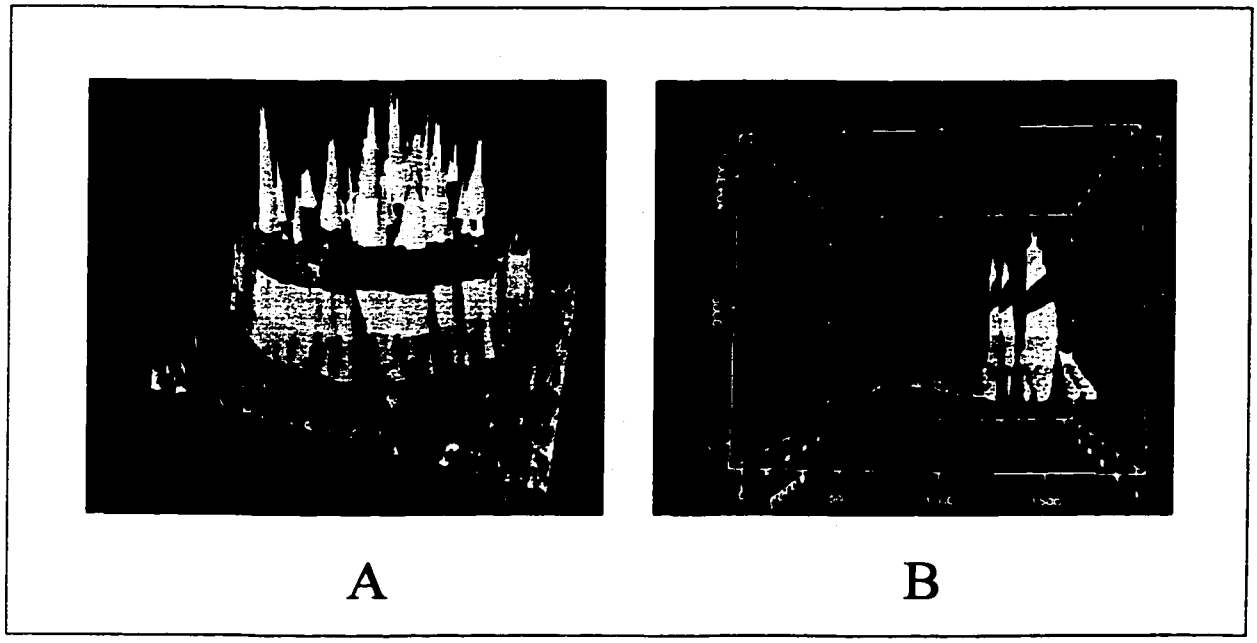

Figure 7.3.4-1: Global image (A) and point by-point line scan map (B) of a thin solid film of 3sPTCD.

7.3.5. Summary

Thin films of 3sPTCD were successfully fabricated. Vibrational analysis indicates 3sPTCD is physisorbed to metal substrates and has a head-on molecular orientation. RRS and SERRS spectra of 3sPTCD were recorded and a SERRS enhancement of 30 observed. Global images and point-by-point line mappings revealed that the thin films of the 3sPTCD formed were homogenous.

7.4. BIS (METHYLMERCAPTOPROPYLIMIDO)PERYLENE

Spectroscopic characterization and investigative studies of bis-(methylmeracptopropylimido) perylene , Figure 7.1-1, revealed similar traits to other members of the family of alkyl-thiol perylene derivatives. The electronic spectra of 2(3s)PTCD is shown in Figure 7.4-1. The absorption spectrum of the thin solid film resembles that of 2sPTCD, however the maxima is blue shifted to 470 nm.

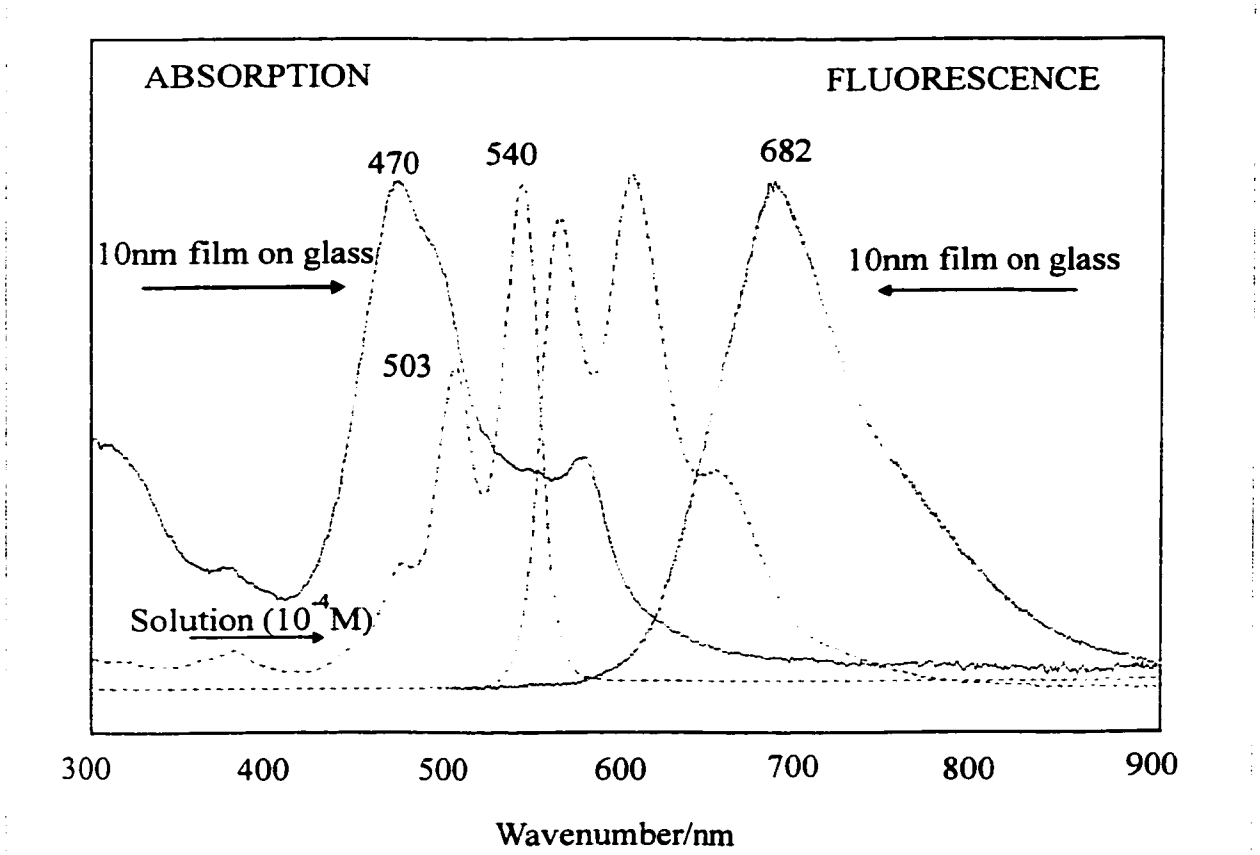

Figure 7.4-1: Electronic and emission spectra of 2(3s)PTCD solution and of a 10 nm vacuum evaporated film on glass.

Molecular orientation studies revealed a head-on orientation similar to 3sPTCD and the RAIRS spectrum of a thin solid film and infrared spectrum of a KBr pellet of

2(3s)PTCD are shown in Figure 7.4-2. A comparison of the two spectra indicates physisorption of the molecule onto the substrate.

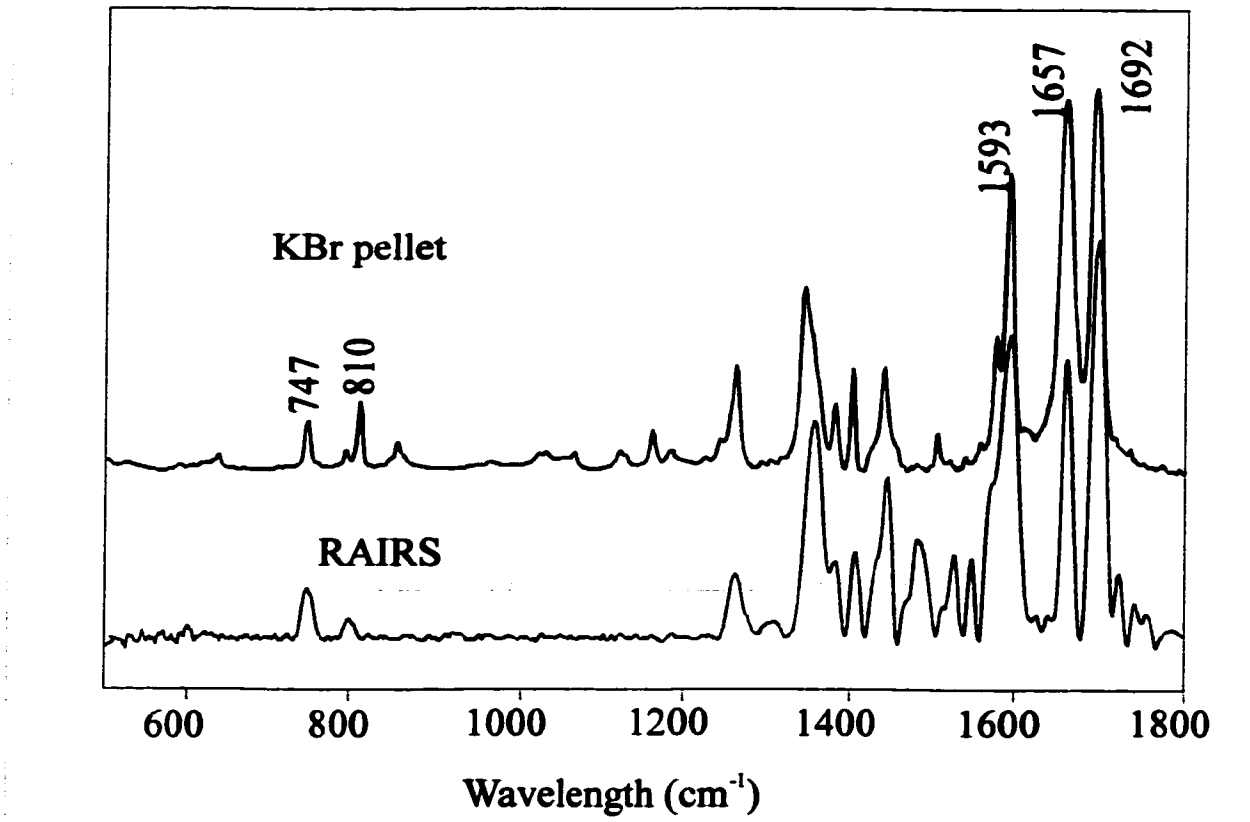

Figure 7.4-2: RAIRS and infrared spectra of a thin solid film and KBr pellet of 2(3s)PTCD respectively.

The resonant Raman and surface enhanced Raman spectra of 2(3s)PTCD taken with the 514.5 nm laser line is shown in Figure 7.4-3. Similar to the infrared spectra, a comparison of the Raman spectrum to the surface enhanced Raman spectrum reveals no band shifts and the full width at half maximum for both spectra are approximately the same, evidence for physisorption of the molecule on the substrate. Furthermore, the spectra resemble both the RRS and SERRS spectra of 3sPTCD.

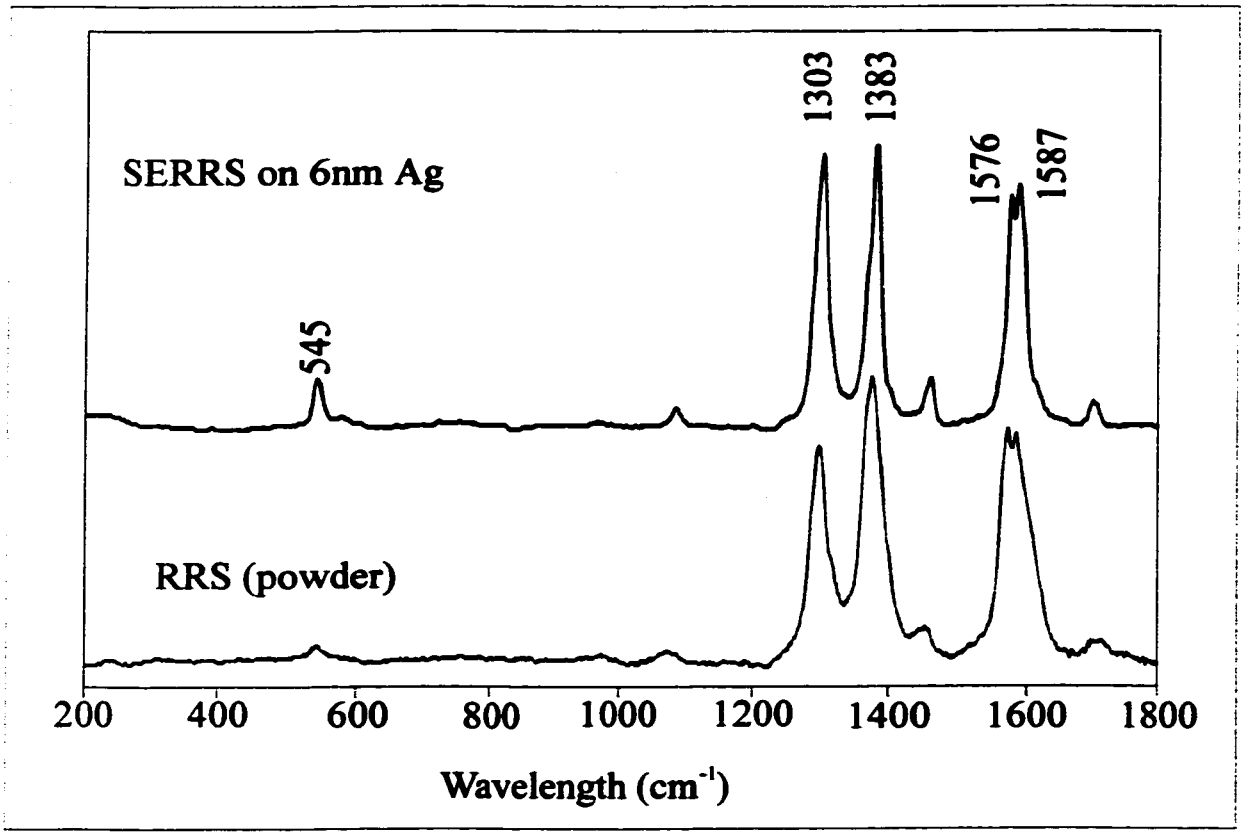

Figure 7.4-3: Resonant Raman and SERRS spectra of 2(3s)PTCD.

SERRS imaging is shown in Figure 7.4-4 (A). The global image was captured using the filtered Raman scattered light of the fundamental vibrational wavenumber at 1301 cm^{-1} (assigned to a perylene ring stretching mode) excited with the 514.5 nm laser line. The global image indicates a homogeneous distribution of the film on the substrate, similar to that reported for both 2sPTCD and 3sPTCD. The baseline corrected point-by-point line scan is also shown in Figure 7.4-4 (B) and the cross section of the line scan, Figure 7.4-4 (C), is a typical SERRS spectrum of 2(3s)PTCD.

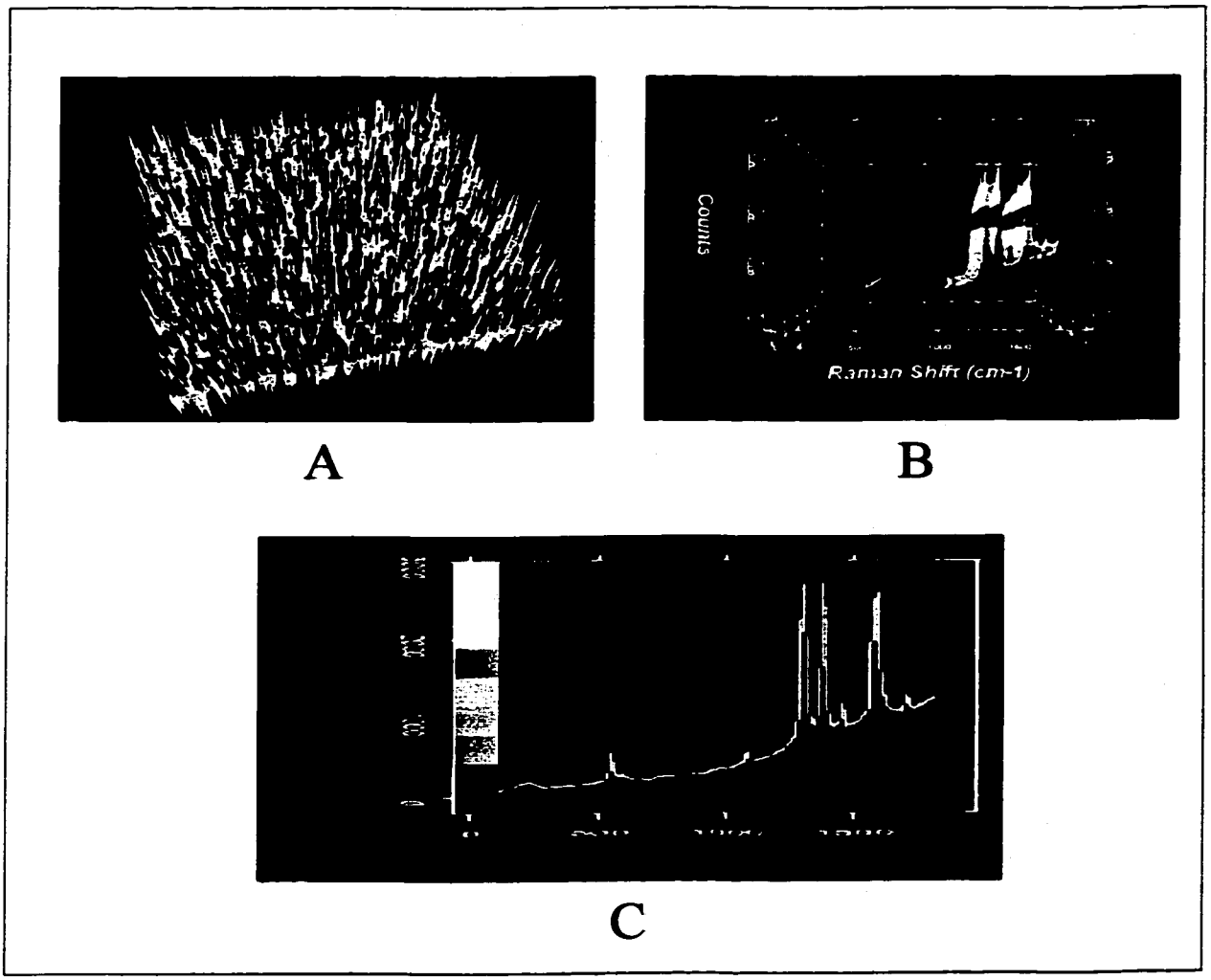

Figure 7.4-4: Global image (A), point-by-point line scan (B) and cross-section of a line scan of a thin film of 2(3s)PTCD.

Chapter 8

SURFACE ENHANCED RAMAN SCATTERING AND SERRS IMAGING OF PERYLENE-PHTHALOCYANINE MIXED FILMS

Spectroscopic characterization and imaging of mixed films

8.1. Introduction

The motivation for the study of mixed films and their applications in thin film devices has been given in Chapter 1. Here, the results of the spectroscopic analysis of codeposited metal phthalocyanine (MPc)-perylene tetracarboxylic derivatives (MPc-PTCD) mixed films are presented. The specific molecular structures of the dyes discussed here are presented in Figure 1.

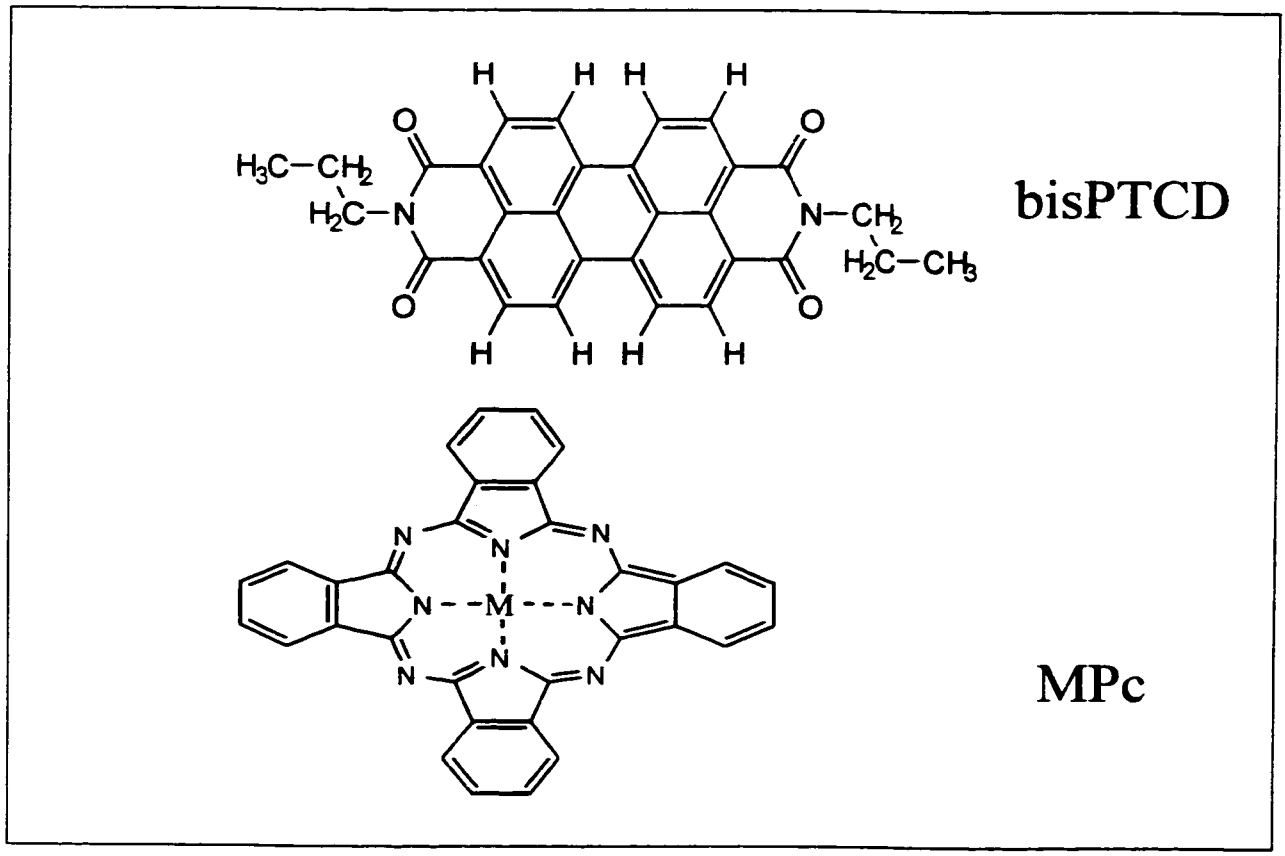

Figure 8.1-1: Molecular Structure of bis (n-propylimido) perylene and metal phthalocyanine, where M=Co or Cu.

8.2. Plasmon resonance of coated silver films

A basic requirement for SERS is the absorption of light by the rough surface in the spectral region of the laser excitation. The plasmon absorption spectrum of a 6 nm

silver island film coated with 10 nm of CuPc is shown in Figure 8.2-1. For comparison, silver films with the same mass thickness of 6 nm coated with CoPc and with co-evaporated mixed film of CuPc/bisPTCD and CoPc/bisPTCD are plotted in Figure 8.2-1.

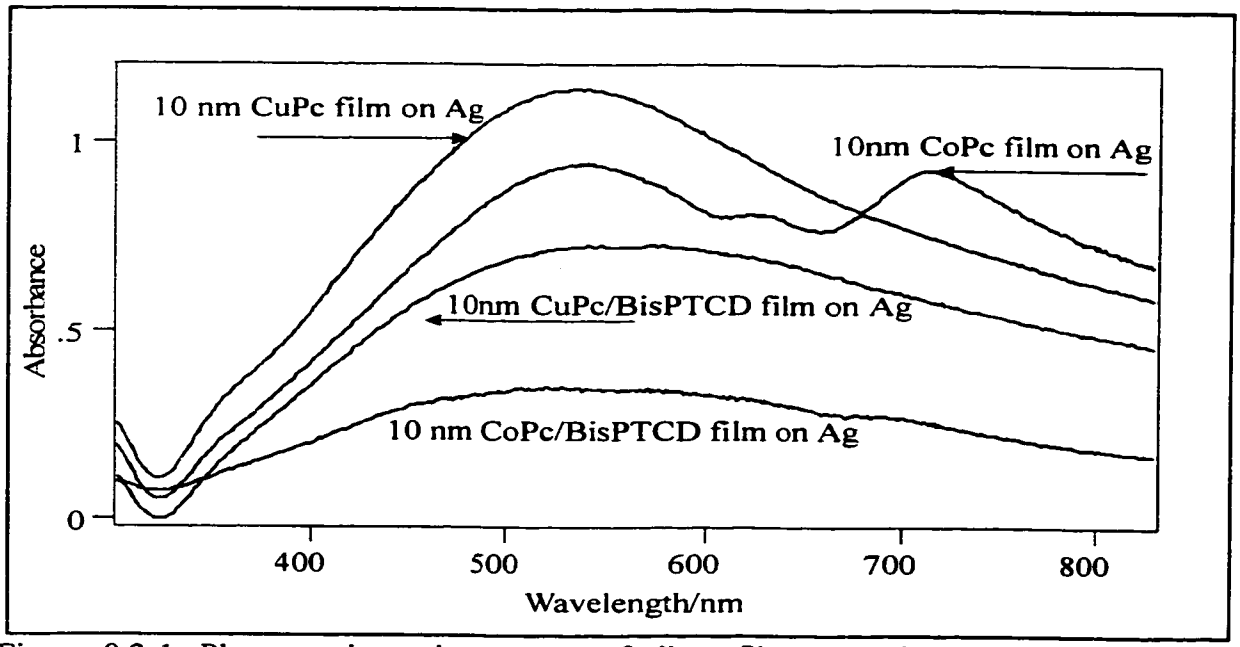

Figure 8.2-1: Plasmon absorption spectra of silver films coated with, CuPc, CoPc and with mixed films of CoPc and CuPc/bisPTCD.

It is observed that the CoPc film changes the plasmon absorption and the CoPc spectrum is clearly superimposed onto the Ag plasmon. The same holds for the CoPc/BisPTCD mixed film coating where the decrease in absorbance is evident if compared with neat silver film. Since the electromagnetic enhancement is proportional to the plasmon absorption, from these results it can be concluded that to maximize the SERRS enhancement, organic overcoatings of less than 10 nm mass thickness should be used.

8.3. Surface Enhanced (Resonance) Raman of Metal-Phthalocyanine

The 514.5 nm and the 633 nm laser lines are in resonance with the region of maximum plasmon absorption while the 780 nm laser line is on the tail of the plasmon.

The molecular absorption spectrum of bisPTCD consists of one electronic transition with a strong broad absorption band in the 500-600 nm region as shown in Chapter 4 [18]. Therefore for bisPTCD, the 514.5 nm laser line produces the resonant Raman effect and for bisPTCD on silver, the surface-enhanced resonance Raman scattering (SERRS) is obtained. The MPc molecules in the solid state absorb in the 500-700 nm region [122] and all three laser lines used could be in resonance or pre-resonance with the molecular electronic absorption spectrum. The 780 nm laser line produces pre-resonance Raman scattering that explains the differences in the CoPc and CuPc spectra at 780 nm and those obtained with 514.5 or 633 nm excitations lines. The latter is illustrated for CoPc in Figure 8.3-1, where the SERRS spectra obtained with all three laser lines are shown.

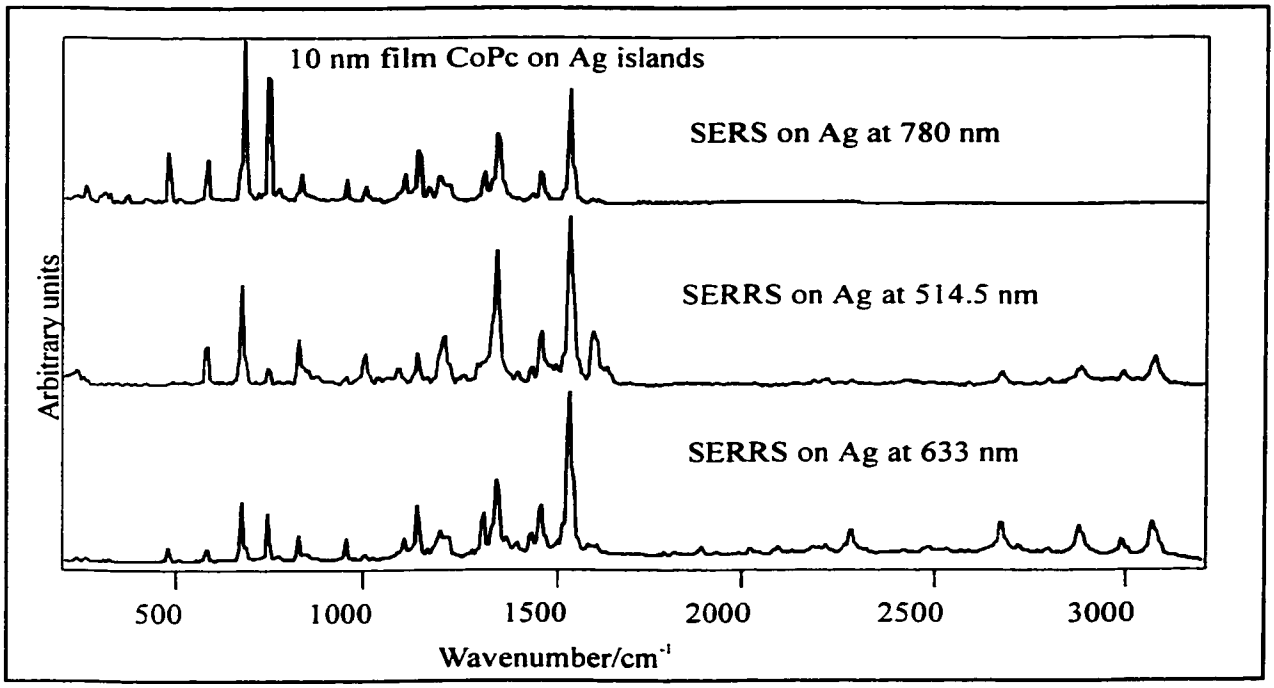

Figure 8.3-1: SER(R)S of a 10 nm CoPc film evaporated onto silver islands (6 nm mass thickness) recorded with three laser lines.

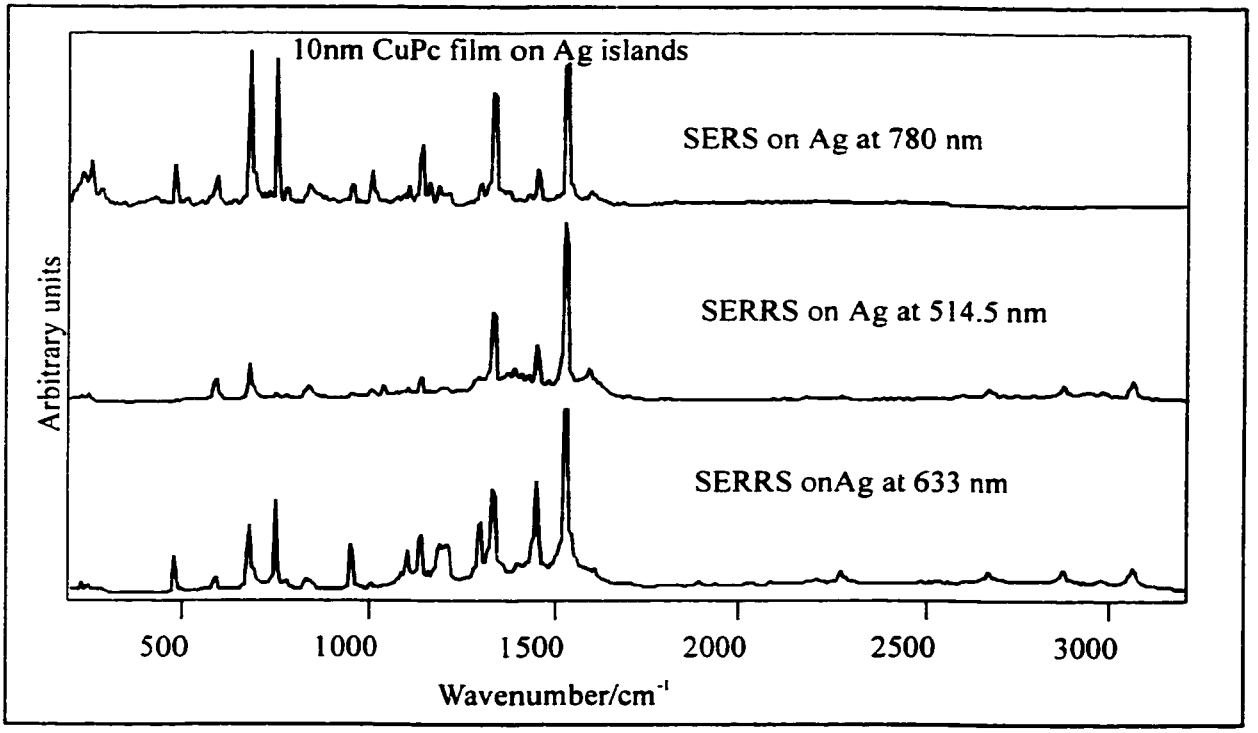

Figure 8.3-2: SER(R)S of a 10 nm CuPc film evaporated onto silver islands (6 nm mass thickness) excited with three laser lines.

It can be seen that the SERRS spectrum obtained with the 633 nm laser line contains overtone and combination modes with the strongest relative intensity. Similar results are obtained for the SERRS spectra of CuPc as can be seen in Figure 8.3-2. The observed vibrational wavenumbers are listed in Tables 8.3-1 and 8.3-2 respectively.

Table 8.3-1: CoPc. Characteristic fundamental vibrations, overtones and combination wavenumbers (cm^{-1}). RRS spectra recorded at 633 nm with two different laser powers.

	633 nm 20 μW	Overtones and combinations	633 nm 2 mW	Overtones and combinations	Assignment
η_1	1542vs	3083vs $2\eta_1$	1531vs	3062m $2\eta_1$	C=N aza str
η_2	1464s 1454sh	2996m $\eta_1+\eta_2$	1456m	2985w $\eta_1+\eta_2$	Pyrrole stretch
η_3	1341m	2884s $\eta_1+\eta_3$	1335s	2869m $\eta_1+\eta_3$	Isoindole str
η_4	1307m		1304m		Isoindole str
η_5	1137m	2680s $\eta_1+\eta_5$	1137m	2669m $\eta_1+\eta_5$	Pyrole stretch
η_6	1108w		1105w		C-H bend
η_7	958m		956m		
η_8	749m	2292s $\eta_1+\eta_8$	748m	2280m $\eta_1+\eta_8$	Ring str
η_9	682s	2225m $\eta_1+\eta_9$	680s	2212w $\eta_1+\eta_9$	Macro br
η_{10}	592m		592m		Benzene radial
η_{11}	483m	2023w $\eta_1+\eta_{11}$	483m	2014w $\eta_1+\eta_{11}$	Ring def
η_{12}	238w		238m		Co-N str
η_{13}	198w	1739w $\eta_1+\eta_{13}$	194m	1725w $\eta_1+\eta_{13}$	Ring def

Table 8.3-2: CuPc - Characteristic fundamental vibrations, overtones and combination bands observed in the RRS spectra obtained with the 633 nm laser line.

RRS	633 nm 20 μW	Overtones and combinations	633 nm 2 mW	Overtones and combinations	Assignment
	cm^{-1}		cm^{-1}		
η_1	1530 s	3059 vs $2\eta_1$	1517 vs	3034 m $2\eta_1$	C=N aza str.
η_2	1451 m	2981 m $\eta_1+\eta_2$	1443 s	2962 vw $\eta_1+\eta_2$	Pyrrole stretch
η_3	1341 m	2872 s $\eta_1+\eta_3$	1333 s	2852 m $\eta_1+\eta_3$	Isoindole stretch
η_4	1305 w		1303 m		Isoindole stretch
η_5	1141 w	2672 s $\eta_1+\eta_5$	1140 m	2658 w $\eta_1+\eta_5$	Pyrrole stretch
η_6	1107 w		1106 w		C-H bending
η_7	952 m		950 m		
η_8	746 m	2276 m $\eta_1+\eta_8$	744 s	2262 w $\eta_1+\eta_8$	Ring stretch
η_9	679 s		676vs		Macro breathing
η_{10}	592 m		592 m		Benzene radial
η_{11}	482 m		480 m		Ring deformation
η_{12}	232 m		232 m		Cu-N stretch

The overtones and combinations of the CuPc have been reported before [123]. The study of the CuPc and CoPc overtones and combinations including the effects of the incident laser power on the observed spectra is reported here [123]. A change in the RS and RRS spectra of both materials was observed when the laser power illuminating the sample was increased from a few microwatts to a total of two milliwatts. The correlatation between the local heating initiated by the laser beam with the observed frequency shifts was investigated. Several fundamentals show a significant red shift with increasing laser power. For example, a laser power of 20 micro watts measured at a sample of CoPc gives inelastic scattering at 1543 cm^{-1} for the C=N aza mode, but a laser beam of 2 mW at the sample gives a Stoke's C=N aza band at 1532 cm^{-1}. The laser effect is observed with all the laser lines. The changes in the fundamentals, due to the changing of the energy density of the laser beam at the sample, are reflected in the overtone and combinations, Tables 8.3-1 & 8.3-2 for CoPc and CuPc respectively. The wavenumbers have been numbered in decreasing order. The assignment of the C=N aza mode means that there is an important contribution of this group of atoms to the molecular vibration at that wavenumber. In summary, this is the first report on the change in the wavenumber of CoPc and CuPc related to the effect of the laser power at the microcrystalline sample.

8.4. Raman and surface-enhanced (resonance) Raman scattering of mixed films

Assignment of the characteristic vibrational wavenumbers for bisPTCD has been previously reported in chapter four [18]. The SERS and SERRS spectra of bisPTCD/CoPc on Ag obtained with the 514.5 nm and 780 nm excitation lines are shown in Figure 8.4-1.

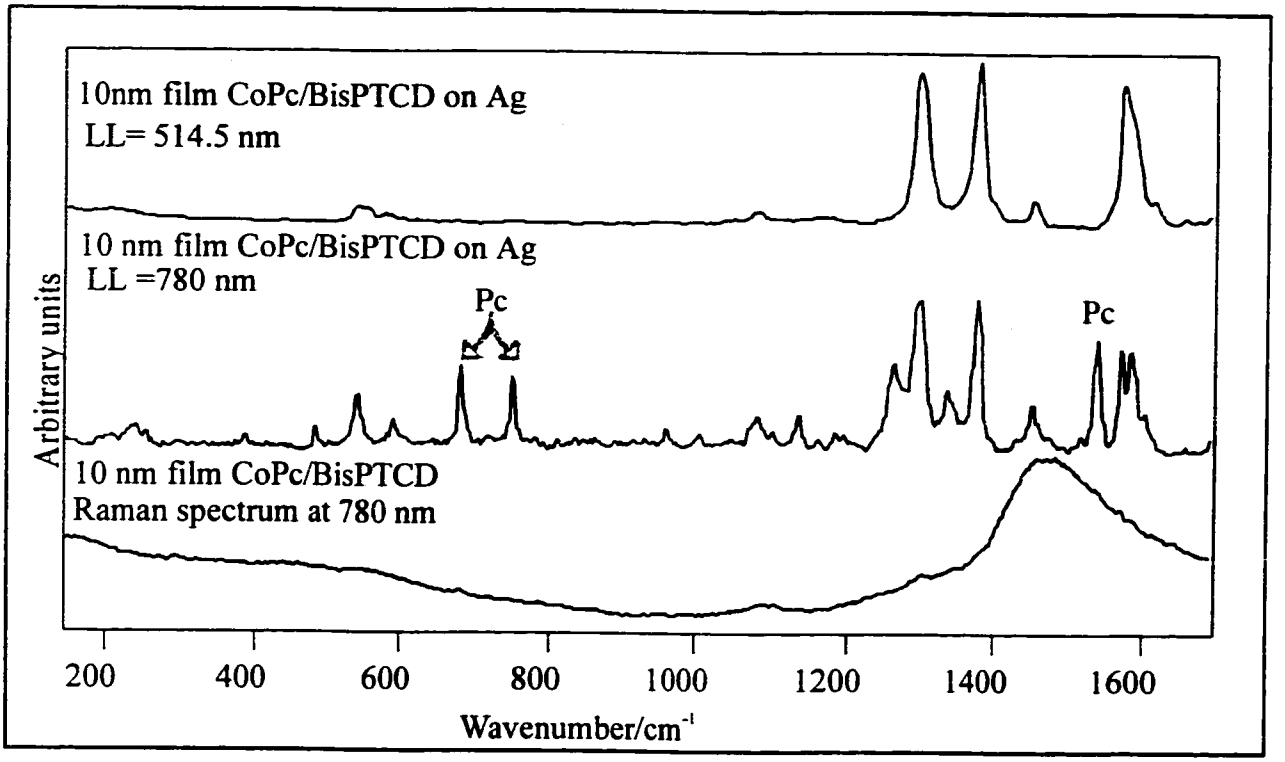

Figure 8.4-1: SER(R)S of CoPc/bisPTCD/Ag mixed film obtained with the 514.5 nm and the 780 nm laser lines.

The spectrum obtained with the 780 nm laser line of the mixed film deposited on glass (without silver) is also shown in Figure 8.4-1 to outline the fact that fluorescence from the film completely masks the Raman scattering of the neat mixed film. The SERRS spectrum of the mixed film at 514.5 nm, a laser line in full resonance with the electronic absorption of bisPTCD, is mainly that of the bisPTCD with four prominent perylene ring stretches at 1589, 1574, 1381 and 1301 cm^{-1}. The 1301 cm^{-1} band has the largest relative intensity that is in contrast with the RRS spectrum of the neat bisPTCD where the 1372 cm^{-1} band is the strongest. The SERS spectrum of bisPTCD/CoPc obtained with the 780 nm excitation line shown in Figure 8.4-1 reflects the mixture, and contains the perylene ring stretches and deformation bands as observed in the SERRS and RRS with the 514.5

nm laser line as well as some intense bands observed at 1541, 1341, 749 and 682 cm^{-1} corresponding to characteristic vibrational modes of CoPc as discussed above.

Notably, the observed bands of CoPc correspond to the solid phase detected at low laser power and low temperatures [123]. The latter observation support the assumption of a CoPc formed by smaller aggregates since the mixing process hinders the formation of large stacks.

The SERRS spectrum of the bisPTCD/CuPc mixed film at 514.5 nm is again that of prominent perylene ring stretches at 1589, 1574, 1381 and 1301 cm^{-1}. The SERS spectrum of the mixed film obtained with the 780 nm laser line is given in Figure 8.4-2. The SERS spectrum of the CuPc on silver islands at 780 nm is also presented for comparison. The main molecular vibrations of CuPc in the mixed film are observed at 1528, 1340, 746 and 677 cm^{-1}. Therefore, the CuPc and CoPc mixed film render similar spectroscopic results with one peculiar difference in the relative intensity of the 1528 (1541) and 1341 cm^{-1} bands. In CuPc mixed film the 1341 cm^{-1} band is stronger than the 1528 cm^{-1} band in dissension with what is observed in the neat film of CuPc at 780 nm. However, the CoPc mixed film maintains the same relative intensity of the 1541 vs. 1341 cm^{-1} bands as observed in the neat film SERS.

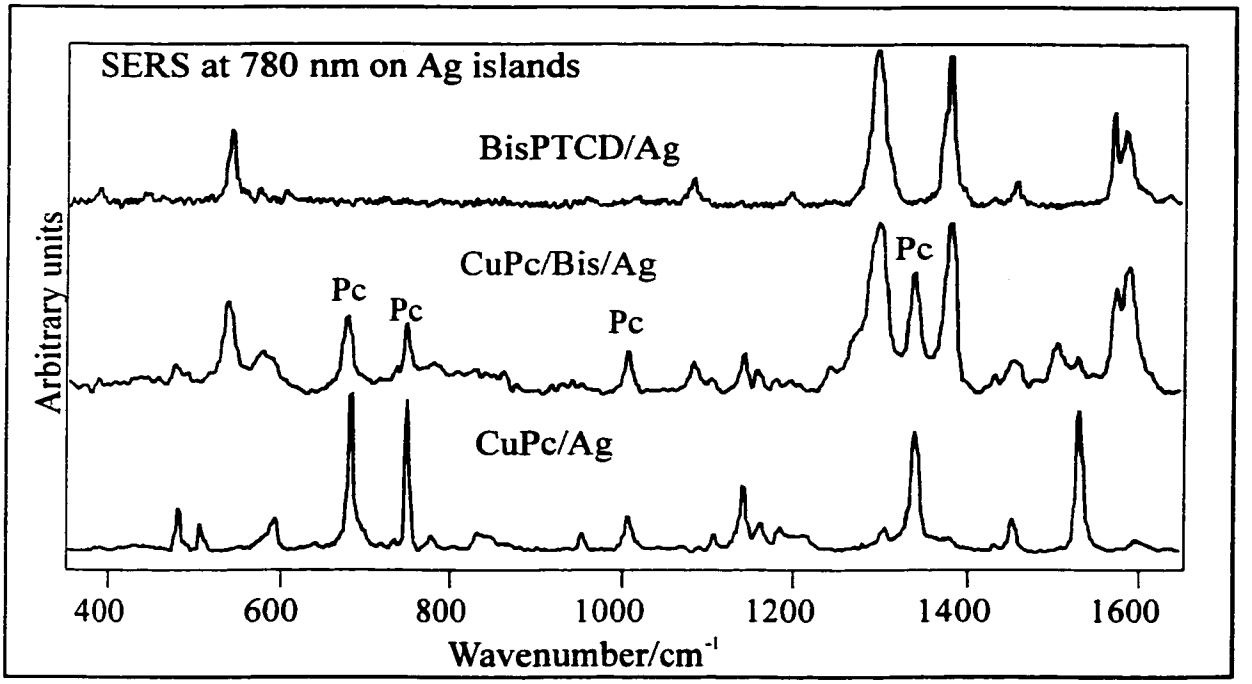

Figure 8.4-2: SERS of CuPc/bisPTCD/Ag mixed film obtained with the 780 nm laser line. CuPc and bisPTCD/Ag are also included.

Mixed films of bisPTCD/CuPc of increasing mass thickness were fabricated and the spectra for 10, 20 and 200 nm mass thickness films on silver islands are presented in Figure 8.4-3. The 780 nm laser line was used. With increasing thickness of the co-evaporated mixed film, the phthalocyanine molecular vibrations become more prominent and at 200 nm mass thickness the bisPTCD spectrum is hardly noticeable. However, the wavenumber of the CuPc fundamentals and their full width at half height (FWHH) remain unchanged. The latter results can only be explained on the basis of a much larger cross section of the CuPc RRS scattering compared with the bisPTCD cross section at 780 nm excitation. For thin coatings the elctromagnetic enhancement makes possible the observation of both spectra. However, for a mass thickness of 200 nm, the contribution

from the surface enhancement strongly decreases with distance, while the RRS scattering from the CuPc increases with thickness.

In summary, for a 10 nm mass thickness film, the SERS spectra taken with the 780 nm laser line contain more phthalocyanine character than the SERRS spectra taken with the 514.5 nm line. The difference in spectral characteristics between the spectra is explained by the fact that the 514.5 nm laser line falls in the absorption region of the perylene moiety. Therefore, the resonant Raman vibrational spectrum of the perylene derivative in the mixed film would be readily observed when the excitation line is 514.5 nm. On the other hand, the phthalocyanine absorption -Q band- occurs between 600 and 700 nm and pre-resonant Raman would be favored with the excitation line at 780 nm.

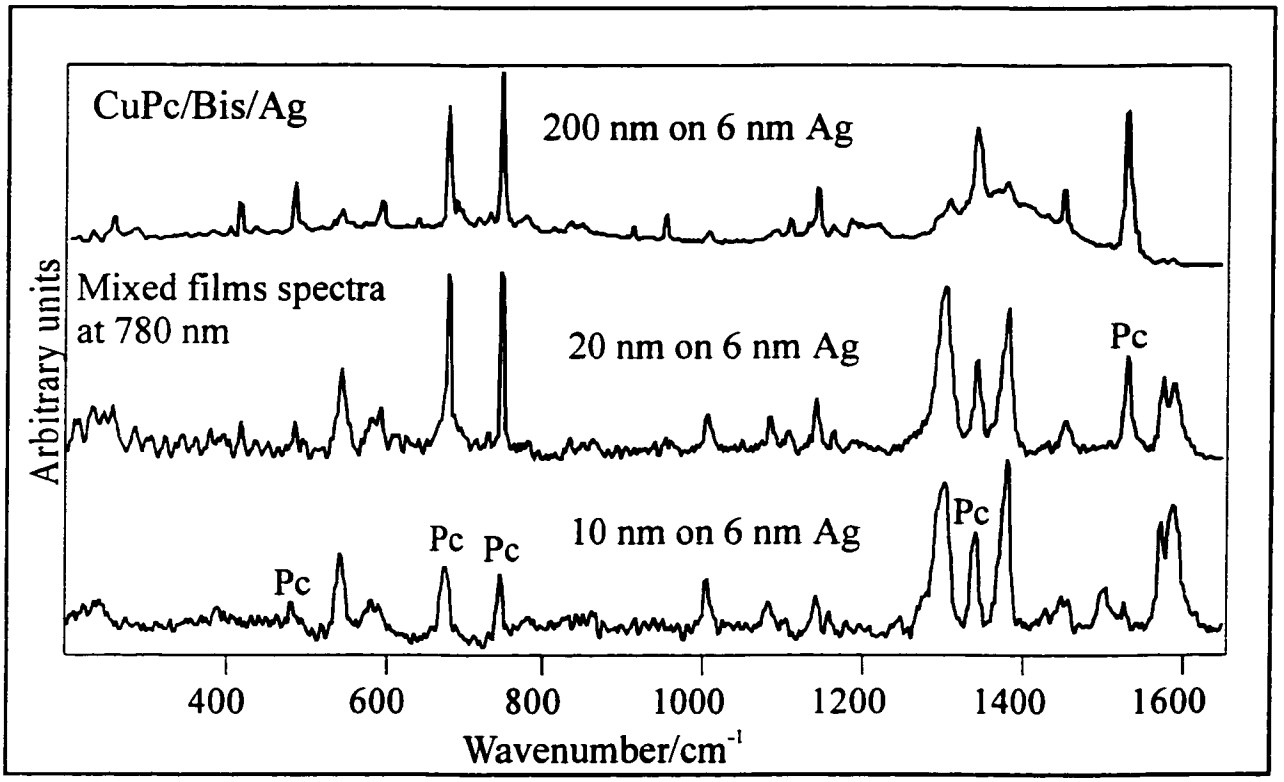

Figure 8.4-3: SERS of three CuPc/bisPTCD/Ag mixed film samples with varying thicknesses of the mixed organic layer: 10 nm, 20 nm and 200 nm mass thickness of CuPc/bisPTCD co-evaporated onto silver islands.

8.5. SERRS imaging

The present investigation is the first report on mapping and global imaging techniques applied to mixed films using SERRS. It is now known that defocusing the laser beam over a large area, as needed to obtain global images, presents a challenge to obtain quality images in micro-Raman. It is shown here that both point-by-point area mapping and global images are easily obtained using the SERRS signal from mixed films of bisPTCD/CoPc and bisPTCD/CuPc on silver island films. The excitation line used in the experiment was the 514.5 nm laser line. The global images from the mixed film samples were captured using the filtered Raman scattered light of the fundamental vibrational wavenumber at 1297 cm^{-1} as shown in Figure 8.5-1. The SERRS spectrum is seen on the background of a weak fluorescence. Consequently, for the point-by-point mapping, a baseline-corrected intensity has been selected to avoid the contributions from fluorescence.

Several global field images were taken from a 40 μm^2 area and a typical image is given in Figure 8.5-1. The SERRS signal, bright coloration in Figure 8.5-1, gives the two-dimensional distribution of bisPTCD in the mixed film deposited onto silver islands. The bisPTCD/CuPc mixture presented a more homogeneous distribution of the bisPTCD in the film. Under the conditions of the present experiments, the CoPc mixed film were found to have a higher degree of phase separation, i.e., lower degree of mixing compared to the CuPc/bisPTCD films.

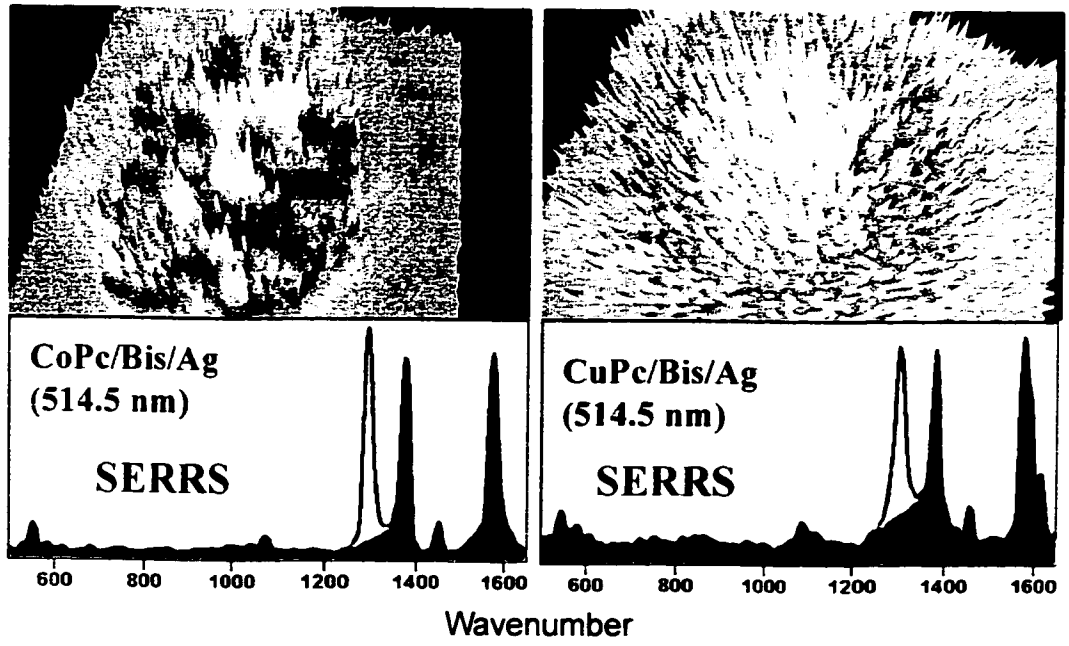

Figure 8.5-1: Global image and line cross-section of a point-by-point area mapping of CoPc and CuPc/bisPTCD mixed films. The vibrational band selected for the filter spectrum is highlighted.

8.6. Summary

The spectra of Pc/PTCD mixed film can be probed with laser lines that can bring to the forefront any of the components: 514.5 nm for PTCD and 633 nm or 780 nm for the Pc materials. The RRS, SERS and SERRS spectra of CuPc and CoPc materials have been recorded. The overtone and a progression of combinations for the 1528 cm^{-1} (CuPc) or 1541 cm^{-1} (CoPc) are observed in the RRS and SERRS excited at 633 nm. Using low laser power it was found that the intensity of the overtone and the progression of combinations is higher than that of the fundamental vibrational modes.

A good mixing or phase separation can be probed using wide field global images using the filter spectrum of the component for which the spatial imaging is recorded.

Based on the global images taken using the SERRS signal of bisPTCD in the mixed films, it was found that the bisPTCD/CuPc film forms a more homogeneous mixed film than the bisPTCD/CoPc film. The global imaging using SERRS is shown to be a powerful analytical tool to study degree of mixing within the spatial resolution of Raman-microscopy (1 μm^2).

Chapter 9

MOLECULAR PROPERTIES AND FILM STRUCTURE OF PERYLENE-PHTHALOCYANINE MIXED THIN SOLID FILMS EXTRACTED FROM SURFACE ENHANCED (RESONANCE) RAMAN SCATTERING AND IMAGING

Interpretation of molecular behavior in mixed films

9.1. Introduction

In the previous chapter, the successful fabrication of mixed films of bisPTCD and M-phthalocyanine was demonstrated. The main conclusion from Chapter 8 was that co-evaporation of the two dyes provides a viable technique for mixed-film fabrication. Further, at the submicron level, global SERRS imaging permits the conclusion that CuPc/bisPTCD mixing is more uniform than that of bisPTCD and CoPc. In this chapter, the study of mixed films and their molecular spectra for a series of co-evaporated films of bisPTCD or thioPTCD with metal phathlocyanines of the C_{4v} and D_{4h} point group is presented. The SERRS chemical imaging of the bisPTCD and thioPTCD mixed films is used to extract the degree of phase separation at the micron level resolution. The effect of the mixing on the molecular environment of the dyes is analyzed following the trends in the full width at half maximum (FWHM) values and in the vibrational band center of the most characteristic fundamentals.

9.2. BisPTCD-Pc Mixed Films

9.2.1. *Absorption and Fluorescence*

The reference absorption spectrum of a thin solid film of bis (N-propylimido) perylene (bisPTCD) evaporated onto KBr substrate (Figure 9.2.1-1), in which strong absorption signals were observed at 376, 469, 502 and 545 nm, was discussed in Chapter 4 [18]. Similarly, the reference absorption spectrum of a thin solid film of thio-bis (n-propylimido) perylene (thioPTCD) is given in Chapter 6 [120]. From the spectra it can be seen that the 514.5 nm laser line is in resonance with the region of maximum absorption and would give rise to resonant Raman scattering (RRS) dominated by characteristic bands of the perylene moiety. Correspondingly, a surface-enhanced Raman scattering

(SERRS) effect is obtained for bisPTCD and thioPTCD deposited on silver islands if excited with the 514.5 nm laser line. Both the 633 and 780 nm laser lines are off-resonance with the absorption band of bisPTCD and thioPTCD and would excite the spontaneous Raman spectrum (RS), or surface enhanced Raman scattering spectra (SERS) on silver substrates. The MPc molecules in the solid state absorb in the 500-700 nm region [122], as a result characteristic SERRS and RRS spectra of MPc molecules were achieved by excitation with the 633 nm laser line while SERS and RS were facilitated with the 514.5 and 780 nm laser lines.

A comparison of the electronic absorption maxima of 10 nm mixed bisPTCD-Pc films to the absorption maxima of a 10 nm bisPTCD film, with respect to each phthalocyanine constituent revealed a particular trend. The absorption spectrum of the bisPTCD-Pc mixed films showed characteristic band structure of both PTCD and Pc species. The Soret band of the phthalocyanine moiety, appearing in the 320-340 nm region in the mixed films, overshadowed the secondary electronic absorption of bisPTCD observed at 376 nm in pure bisPTCD films. The 0,2 band of bisPTCD in CoPc mixed films (Figure 9.2.1-1) were relatively similar to that observed in pure bisPTCD films at 469 nm, while this band appeared red shifted in bisPTCD/ClInPc mixed films (Figure 9.2.1-2) and blue shifted in bisPTCD mixed films of H_2Pc, ZnPc (Figure 9.2.1-1), CuPc and ClGaPc. The band corresponding to the 0-1 electronic transition of the perylene moiety was not observed in any of the mixed films studied, however upon deconvolution of the spectra the band was extracted from bisPTCD mixed films of ClInPc, CoPc, H_2Pc and ZnPc. This 0,1 transition band of bisPTCD appeared to be red-shifted in mixed films of bisPTCD/ClInPc (Figure 9.2.1-2) and bisPTCD/CoPc (Figure 9.2.1-1), while blue

shifted in bisPTCD mixed films of H_2Pc and ZnPc (Figure 9.2.1-1), to that observed at 502 nm in the pure bisPTCD films.

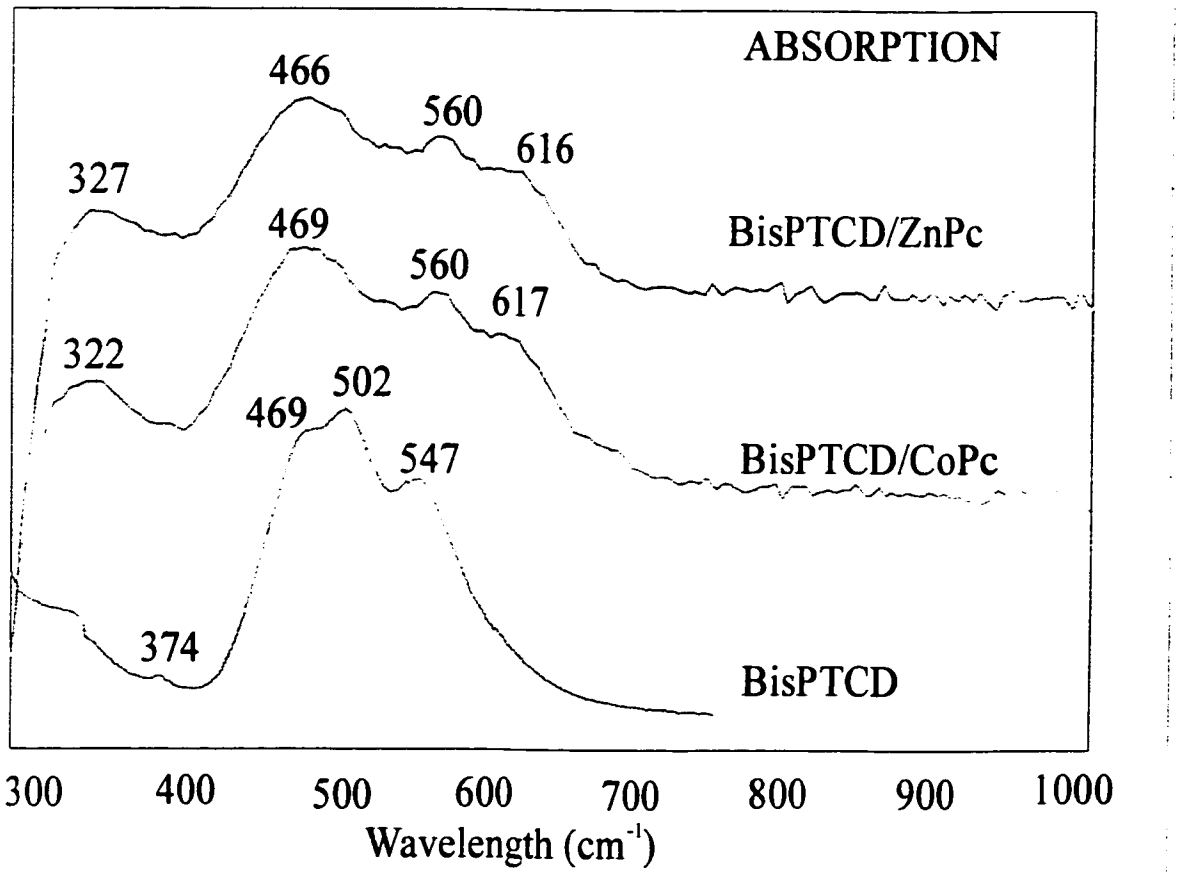

Figure 9.2.1-1: Absorption spectra of 10 nm thin films of bisPTCD and mixed films of bisPTCD/CoPC and bisPTCD/ZnPc.

The 0,0 electronic transition of bisPTCD observed in the pure bisPTCD films at 547 nm appeared red shifted in the absorption spectra of all the mixed films. The characteristic phthalocyanine Q-band is observed in the 600-700 nm spectral region of absorption spectra of the mixed films investigated, one exception being the bisPTCD/ClInPc mixed film in which it was red-shifted to 703 nm (Figure 9.2.1-2).

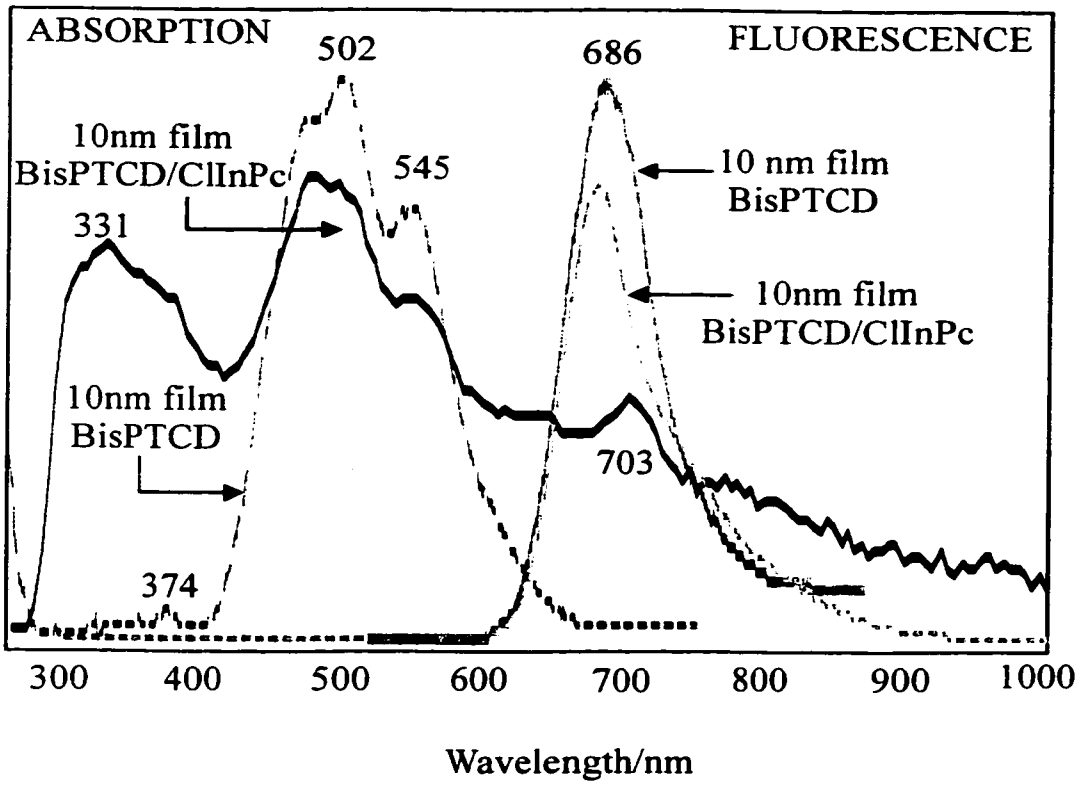

Figure 9.2.1-2: Electronic absorption and electronic spectra of 10 nm thin films of bisPTCD and bisPTCD/ClInPc.

For SERRS spectral and image studies, silver island films were coated with bisPTCD-Pc mixed films and neat PTCD and phthalocyanine materials. The effect of the coating on the silver plasmon absorption band maxima of silver island films revealed specific trends. In the case of the bisPTCD mixed films of ClInPc (Figure 9.2.1-3) and ClGaPc, the silver plasmon was red shifted to those observed in silver films coated with 10 nm thin films of pure ClInPc and ClGaPc respectively. Whereas, in the case of the planar phthalocyanines: CoPc, CuPc, H_2Pc and ZnPc, the silver plasmon of the mixed films was unshifted to that in the respective silver plasmon films coated with pure phthalocyanine films. All plasmon bands observed in the mixed films were broad and structureless.

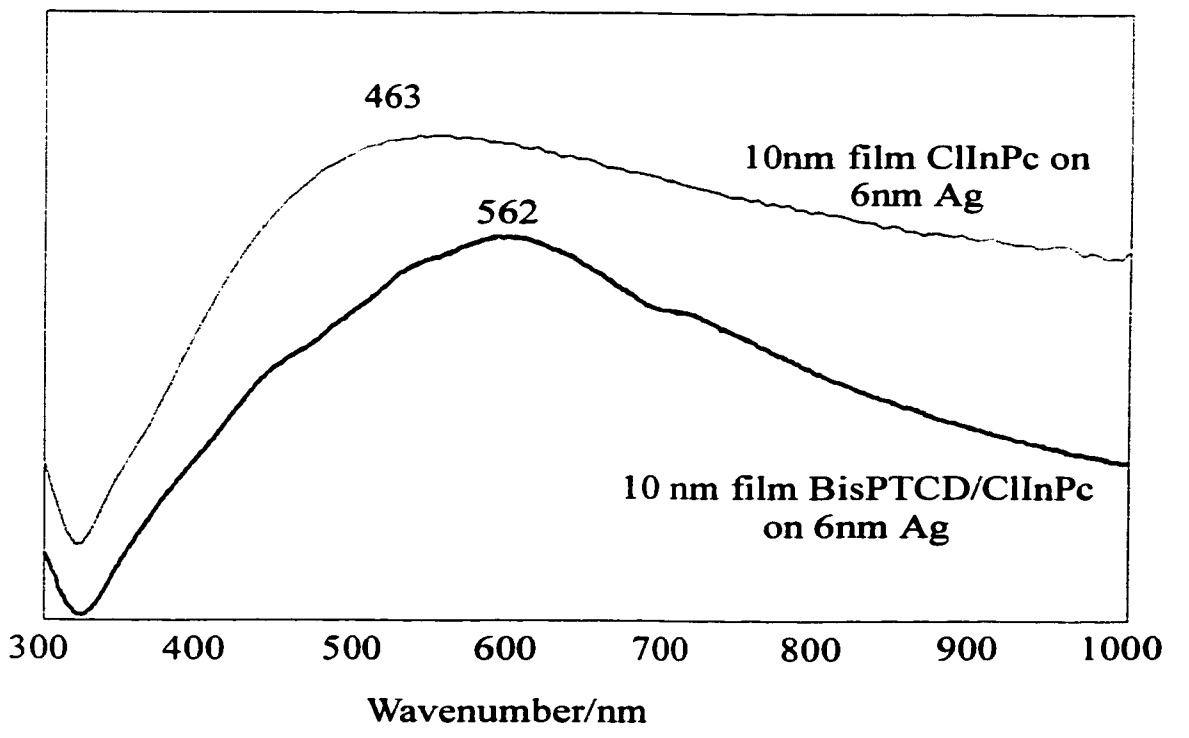

Figure 9.2.1-3: Electronic absorption of the silver plasmon of 10 nm thin solid films of ClInPc and bisPTCD/ClInPc.

The emission spectra of thin solid films of bisPTCD and thioPTCD have been discussed in Chapters 4 and 6 respectively [18, 120]. The characteristic broad excimer emission was observed at 686 nm for a thin solid film of pure bisPTCD, as shown in Figure 9.2.1-2. The emission spectrum of 10 nm bisPTCD/ClInPc thin solid film is also shown in Figure 9.2.1-2. A comparison of the excimer emission observed for all bisPTCD-Pc mixed films studied to that of pure thin films of bisPTCD indicated a blue shift in the emission maxima, with the exception of bisPTCD/ZnPc in which the maxima was red-shifted to 715 nm. A secondary, unresolved, red shifted emission band was also observed in all bisPTCD mixed films. Furthermore, the emission spectra were broad, structureless and their maxima were Stokes-shifted relative to the absorption origin of the

respective mixed films. These characteristics are indicative of excimer formation in crystalline thin films of perylene [124, 125].

9.2.2. Raman and Surface enhanced Raman Scattering

The vibrational spectra of metallophathlocyanines and metal free phthalocyanine have been assigned. [126-129]. Similarly, the vibrational analysis of bisPTCD and thioPTCD is reported in Chapters 4 and 6 respectively [18, 120]. BisPTCD is a member of the perylene tetracarboxylic 3,4,9,10- dimide (PTCDI) family. Using local symmetry arguments the discussion on the vibrational assignments bisPTCD can be restricted to that of its parent PTCDI, a simplification that allows the discussion and extraction of important molecular information. PTCDI is a planar molecule of 40 atoms. It has 114 internal degrees of freedom and belongs to the D_{2h} symmetry point group. There are 57 Raman active and 49 infrared active vibrations. Since PTCDI is a planar molecule there are 77 in-plane vibrations, 46 bending and 68 stretching vibrations. The number of molecular vibrations of each reducible representation and their vibrational band assignment are given in Table 9.2.2-1 [125, 130] Since PTCDI is a large planar molecule, it is reasonable to assume that the change in the polarizabilty of the ellipsoid due to the out-of-plane vibrational modes is relatively small. As such, the B_{2g} and B_{3g} vibrational modes would be have low intensity and the most intense Raman bands in the Raman spectra are dominated by the A_g and B_{1g} modes [131]. The small number of observed Raman vibrational frequencies for the PTCDI moiety are summarized in Table 9.2.2-1.

Table 9.2.2-1: Irreducible representation and molecular vibrations of PTCDI.

Representation	Number	Raman	Characteristic Vibrational bands	Assignment
A_g	20	α_{xx}, α_{yy},α_{zz}	358, 551, 797 982, 1105, 1296 1370, 1574	In-plane
B_{1g}	19	α_{xy}	366, 1301, 1378 1582	In-plane
B_{2g}	11	α_{xz}	421, 625, 889, 752	Out-of-plane
B_{3g}	7	α_{yz}	452, 626, 960	Out-of-plane
A_u	8			Out-of-plane
B_{1u}	11			Out-of-plane
B_{2u}	19			In-plane
B_{3u}	19			In-plane

The RRS and SERRS spectra of the 10 nm mixed film of bisPTCD/ClInPc were obtained with the 514.5 nm laser line and are presented in Figure 9.2.2-1. The RRS spectrum was observed on a weak fluorescence background, as a result to avoid contributions from fluorescence the spectrum was baseline corrected using the Galactic Industries GRAMS/32^{TM} C software. The most intense bands observed are due to the perylene moiety. The low frequency fundamental at 542 cm^{-1} is the perylene ring deformation vibration. The C-H bend is observed at 1084 cm^{-1}, while perylene ring stretches appear at 1291(sh.), 1302, 1378 and 1456 cm^{-1}. The perylene C=C stretches and

the C=O stretches are observed at 1572 and 1586 cm^{-1}, and 1697 cm^{-1} respectively. The SERRS spectrum obtained for this mixed film is similar to that of the RRS spectrum. The fundamental frequencies of the perylene chromophore observed in both the RRS and SERRS have relatively the same frequency, indicating that the PTCD moiety is physisorbed on to the silver island substrate. Furthermore, differences in relative intensities may be explained within the framework of the SERS selection rules, as explained in Chapter 6.

The RS spectrum of the 10 nm mixed film of bisPTCD/ClInPc taken with the 780 nm laser line is presented in Figure 9.2.2-1. It becomes apparent, on comparing the RRS and RS spectra of this mixed film, that the RS spectrum contains characteristic bands of both ClInPc and bisPTCD. In the RS spectrum, the most intense characteristic vibration belonging to ClInPc moiety was observed at 1416 cm^{-1}, while that of perylene at 1577, 1435, 1354, 1298, 1081 and 532 cm^{-1} respectively. It is of particular interest to note that the perylene ring stretch appearing as a shoulder at 1291cm^{-1} in the RRS spectrum becomes one of the most intense bands in the SERRS spectrum. This may be due to the packing as observed in the α-perylene polymorph [131].

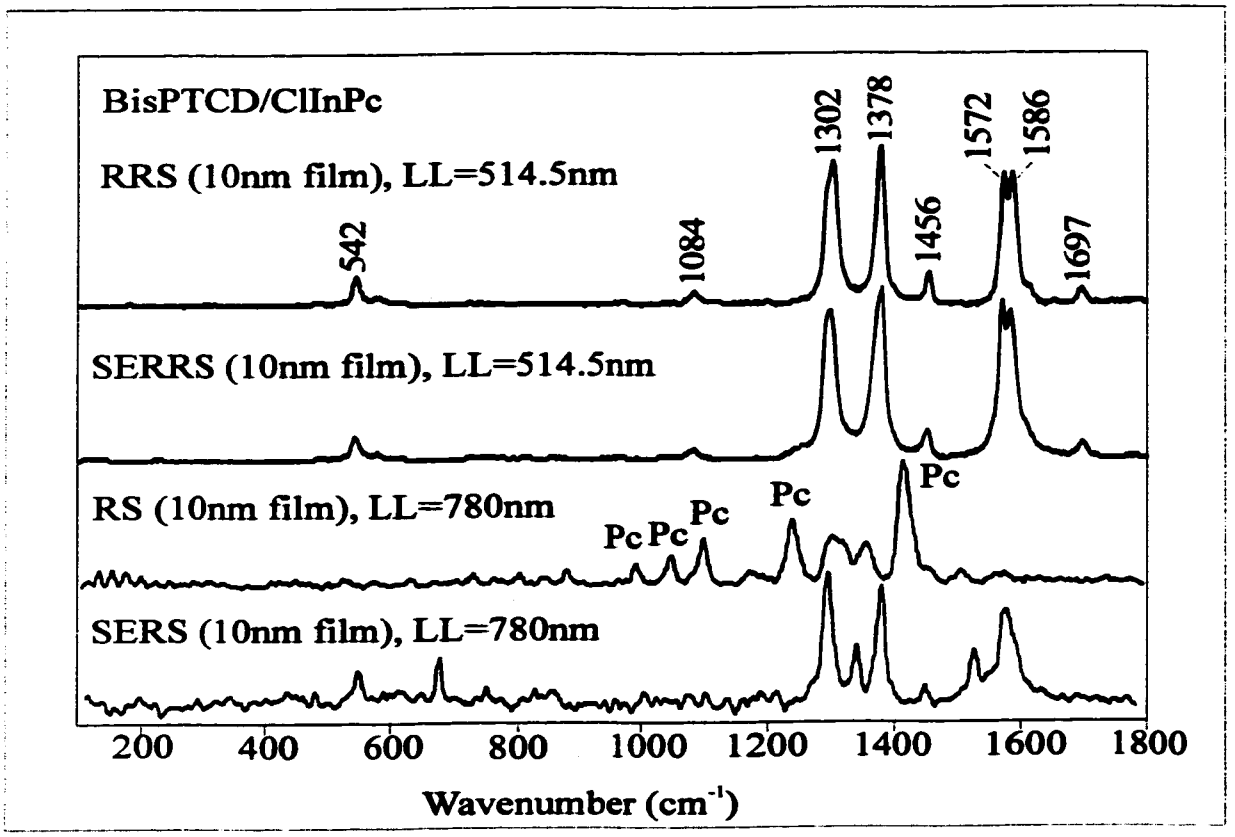

Figure 9.2.2-1: SER(R)S, RRS and Raman scattering spectra of thin solid films of bisPTCD/ClInPc.

The SERS spectrum of the 10 nm bisPTCD/ClInPc mixed film, obtained with the 780 nm line, is also shown in Figure 9.2.2-1. Similar to the RS spectrum, it consists of a combination of MPc and perylene chromophore vibrations. The discussion of the SERS (780 nm) spectrum is restricted to the characteristic vibrations of the perylene moiety in order that the influence of the MPc on the molecular properties of bisPTCD in the mixed film may be analyzed. The predominant perylene bands in the SERS (780 nm) spectrum are observed at: 1689,1594, 1576, 1439, 1379, 1295 and 531cm^{-1}. Taking the 531 cm^{-1} band as reference and normalizing the other perylene bands in the spectra with 531 cm^{-1}, a comparison of the SERS (780 nm) to the RS spectra of bisPTCD/ClInPc mixed films

indicate an increase in the relative intensities of four in-plane ring stretching vibrations, in particular that of 1577 cm^{-1}. The full width at half maximum (FWHM) of the characteristic vibrations in the SERS (780 nm) spectrum remained constant for all vibrational bands with respect to the 531 cm^{-1} vibrational band. In the RS spectrum, however, the FWHM doubles for the 1354 and 1435 cm^{-1} bands with respect to the 531 cm^{-1} band. This indicates the presence of doublets, though not evident in the spectrum due to band overlap. Vibrational band shifts were also observed for the 1354 cm^{-1} (1379 in SERS) and 1702 cm^{-1} (1689 in SERS) bands, which may be accounted for by considering the contributions from the overlayer of bisPTCD molecules that were adsorbed to the silver islands.

An increase in the relative intensity of four perylene ring stretching vibrations: 1291, 1378, 1456 and 1572 cm^{-1}, was observed on comparison of the SERRS spectrum to the RRS spectrum of the bisPTCD/ClInPc mixed film, when the vibrational band at 542 cm^{-1} was used as the internal reference. On the contrary, the relative intensities of the C-H bend and C=C stretching vibrational bands, at 1084 and 1586 cm^{-1} respectively, decreased in the SERRS spectrum with respect to the RRS spectrum. A comparative analysis of the FWHM bandwidths shows that the bandwidth of the 1295 cm^{-1} vibrational band in the SERS (780 nm) spectra doubles relative to that in the RRS spectrum, and indicates the presence of doublets. It should be concluded that the two well-defined vibrational bands at 1291 and 1302 cm^{-1} in the RRS, merge to form the broad band at 1295 cm^{-1} in the SERRS spectrum.

Applying this method of analysis to 10 nm bisPTCD/MPc mixed films, it becomes apparent that the influence of MPc on the molecular properties of bisPTCD in

the mixed films is significant. The relative intensity of RS is greater than the RRS for the 1081, 1298, 1354 and 1435 cm^{-1} vibrational bands of the perylene moiety for all mixed films, bisPTCD/ZnPc having the greatest difference in relative intensities. For the ring stretching vibrations at 1577 and 1598 cm^{-1}, the RRS has greater relative intensity than the RS for bisPTCD-Pc mixed films containing ClInPc, ClGaPc, CoPc and CuPc, the exception being H_2Pc and ZnPc where RS is more intense than the RRS for the 1577 cm^{-1} band. The C=O stretching vibration at 1702 cm^{-1} was only observed for mixed systems containing ClInPc, ClGaPc, CoPc and H_2Pc. Of these systems, the RS relative intensity for this band was greater than the corresponding RRS band for ClInPc, CoPc and H_2Pc. Similarly, a comparison of the change in FWHM of the observed bands for RS and RRS spectra of bisPTCD-Pc films indicates that the RS spectra for the mixed films have on average more bands than the RRS spectra. This is exemplified in Figure 9.2.2-2 for mixed films of bisPTCD-Pc.

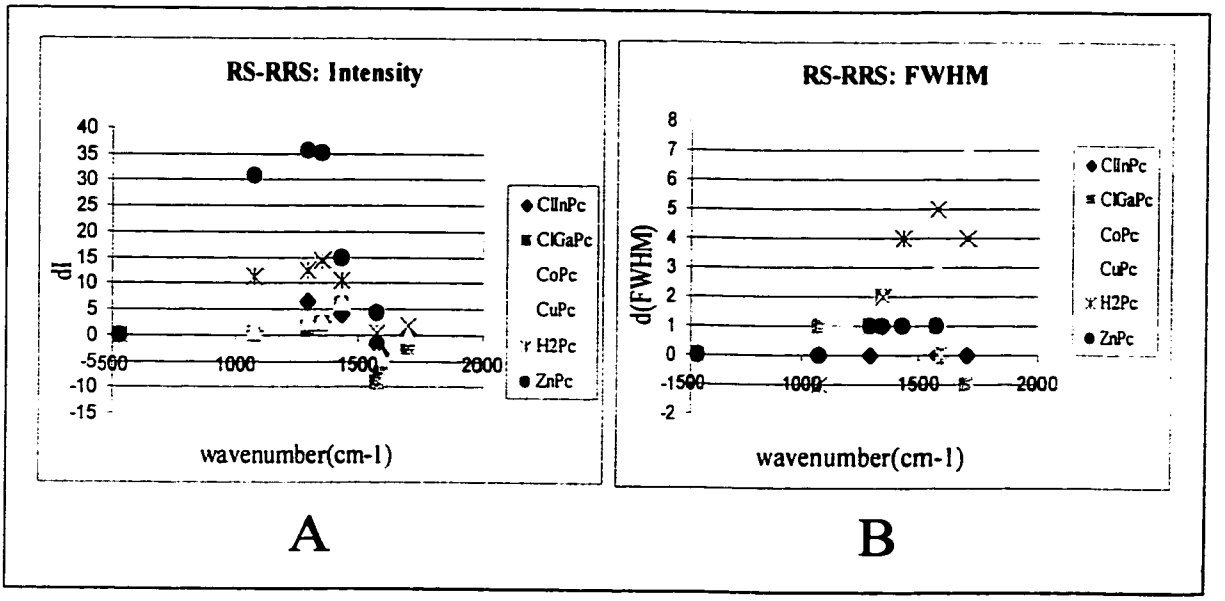

Figure 9.2.2-2: Relationship of the changes in relative intensities (A) and FWHM (B) for characteristic perylene wavenumbers in RS as compared to that in RRS spectra.

The changes in relative intensities and FWHM between the RRS and SERRS spectra (Figure 9.2.2-3A & 9.2.2-3B) and RS and SERRS spectra (Figure 9.2.2-3C & 9.2.2-3D) for mixed films of bisPTCD-Pc are shown in Figure 9.2.2-3. The changes in relative intensities and FWHM between the RS and SERRS spectra of pure bisPTCD films are shown in Figure 9.2.2-4 for comparison. As is evident from figures 9.2.2-3 and 9.2.2-4, the relationships between the RS and SERRS intensities and FWHM for the mixed films appear to follow that of the pure 10 nm bisPTCD thin film.

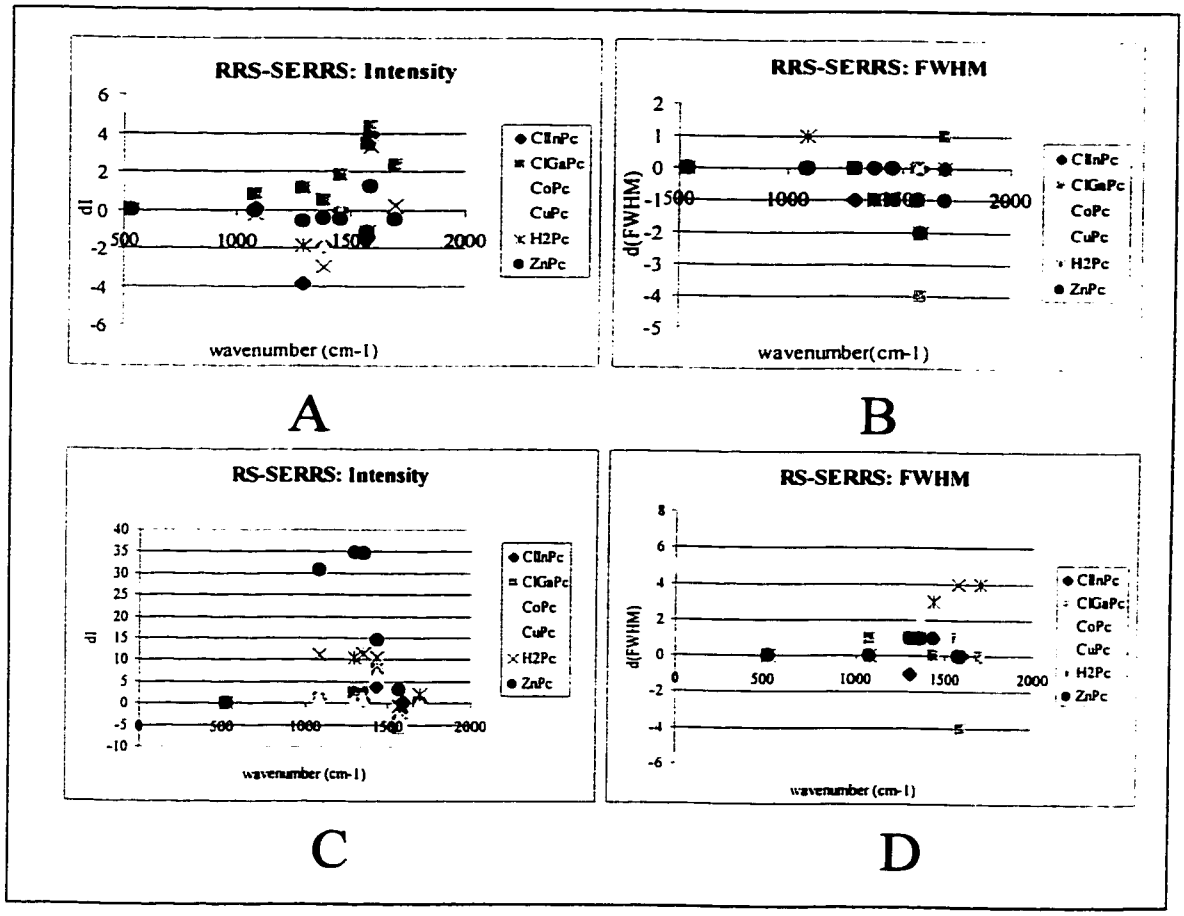

Figure 9.2.2-3: Relationships of the changes in relative intensities and FWHM of characteristic perylene wavenumbers for RRS-SERRS (A, B) and RS-SERRS (C, D) spectra of bisPTCD-Pc mixed films.

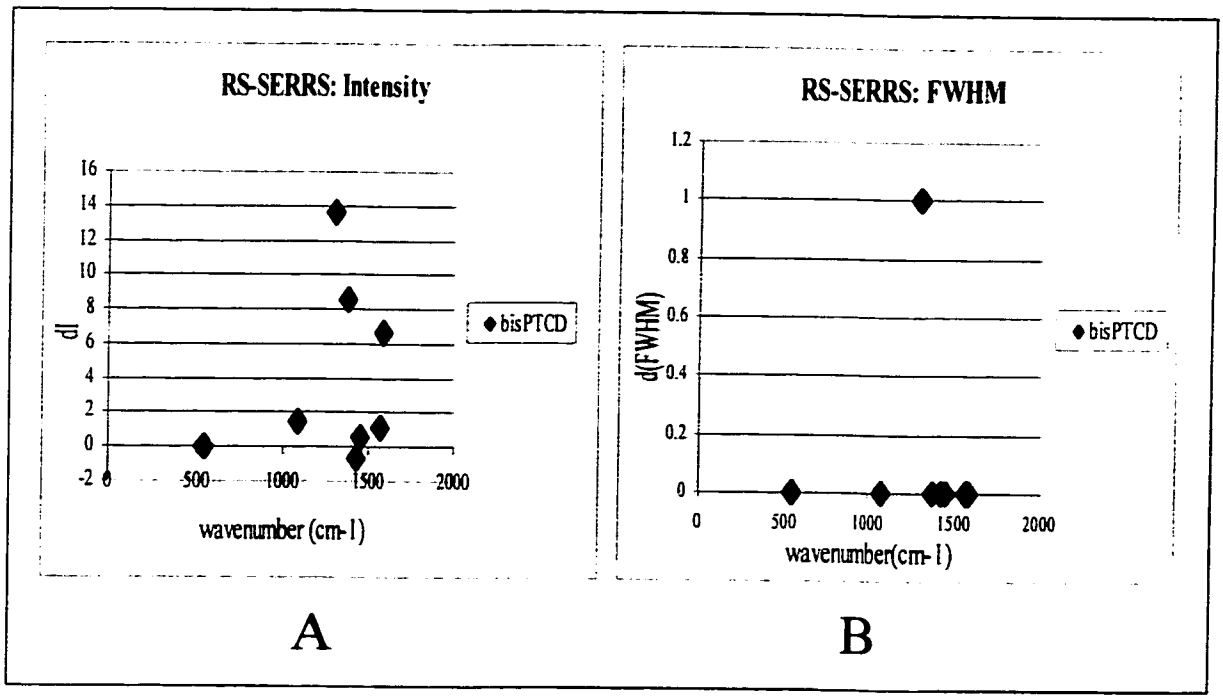

Figure 9.2.2-4: Relationship of the changes in the relative intensities (A) and FWHM (B) for RS and SERRS spectra of thin films of bisPTCD.

9.2.3. SERRS Imaging of bisPTCD-Pc Mixed films

Point to point line scanning, area mapping and global SERRS images from the surface of 10 nm mixed thin films of bisPTCD and various phthalocyanine derivatives on silver island films were obtained using the 633 nm laser line. The bisPTCD chemical global images from an ca. 40 μm^2 area of mixed film samples were captured using the filtered Raman scattered light of the fundamental vibrational wavenumber at 1302 cm^{-1}. The phthalocyanine images were recorded using the 676 cm^{-1}. Typical images are shown in Figure 9.2.3-1 for a mixed film of bisPTCD and ClInPc. In Figure 9.2.3-1A the SERRS signal gives the two-dimensional distribution of bisPTCD in the mixed film on silver islands. Similarly in Figure 9.2.3-1B, a two-dimensional distribution of ClInPc in the mixed film on silver islands is shown. The SERRS spectrum is seen on the background of a weak fluorescence. Consequently, for the point-by-point area mapping a

baseline-corrected intensity was selected to avoid the contributions from fluorescence, Figure 9.2.3-1C. The images from the bisPTCD/ClInPc film present a homogeneous distribution for both the bisPTCD and ClInPc components in the film. Homogeneity is used here with the caveat of the spatial resolution of the technique. It could be said, for example, that according to the global imaging, there is a homogeneous distribution of aggregates of both the bisPTCD and ClInPc materials.

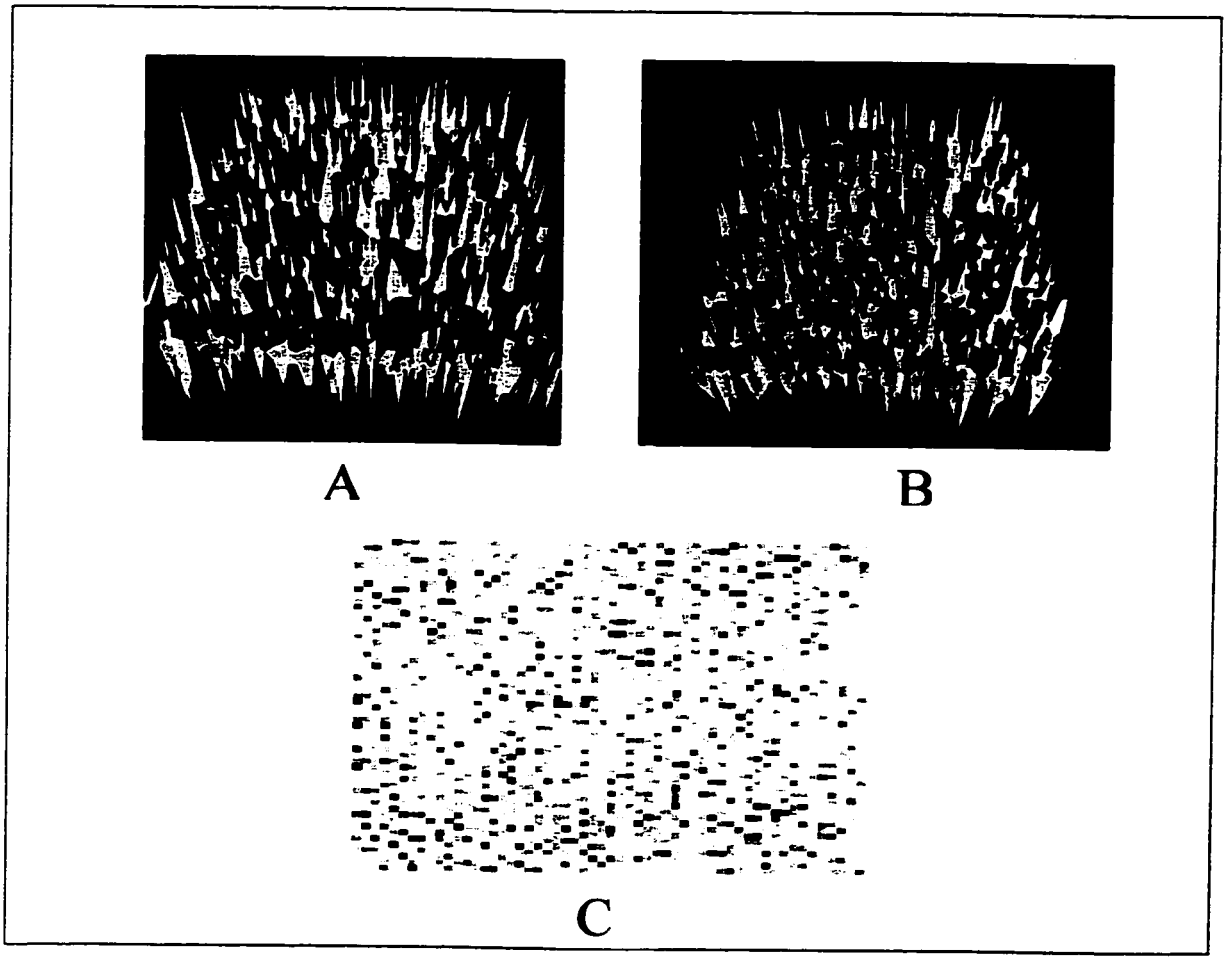

Figure 9.2.3-1: Global field images of a 10 nm bisPTCD/ClInPc mixed film showing the distribution of perylene (A) and phthalocyanine (B). Point-by-point area map for bisPTCD/ClInPc mixed film (C).

The global image analysis for bisPTCD-Pc mixed films with other phthalocyanines reveals that there is on average a homogeneous distribution of both perylene and phthalocyanine in mixed films of CuPc and ClGaPc. However for mixed films of bisPTCD/CoPc, bisPTCD/H_2Pc and bisPTCD/ZnPc the phase separation of these materials is clearly distinguished with micrometer resolution, i.e., the distributions of perylene and phthalocyanine were not "homogenous".

The point-to-point line mapping of a 10 nm mixed film of bisPTCD/ClInPc is shown in Figure 9.2.3-2. The cross section of the line scan is a typical SERRS spectrum of mixed film on 6 nm silver and is also shown in Figure 9.2.3-2.

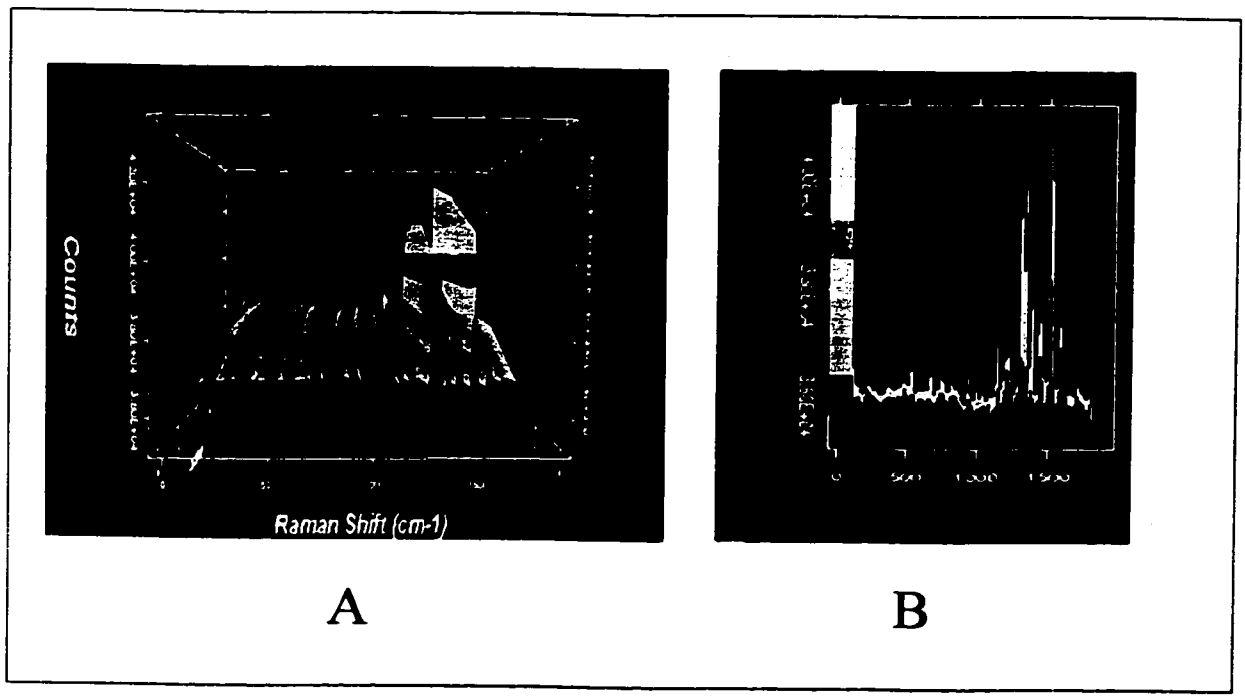

Figure 9.2.3-2: Point-to-point line scan (A) and cross section of the line scan (B) for a 10 nm mixed film of bisPTCD/ClInPc.

9.2.4. Summary

Mixed films of bisPTCD and various phthalocyanines were successfully fabricated by vacuum co-evaporation. The electronic absorption and emission studies of

the mixed films suggest that in these materials there is a potential for energy transfer between bisPTCD and MPc. The energy transfer in similar materials has been documented [132]. In the case of bisPTCD, the emission band is in the same spectral region of the characteristic Q-absorption band of phthalocyanines.

By studying the trends in characteristic vibrational band values for the PTCD moiety in the mixed films, it was concluded that bisPTCD was physically adsorbed to the substrate. Furthermore, intermolecular interaction between bisPTCD and MPc was minimal since the bisPTCD vibrational bands and FWHM retained their values on mixing with numerous and varied phthalocyanine dyes. This conclusion is also supported by the fact that the trends observed for the perylene characteristic vibrational bands in the mixed films follow those in the pure bisPTCD films. This suggests that the molecular and packing arrangement found in pure bisPTCD films are somehow present in the mixed films. The global image analysis of the mixed bisPTCD-MPc films reveal on-average a homogeneous distribution of both perylene and phthalocyanine for mixed films of bisPTCD/ClInPc, bisPTCD/ClGaPc and bisPTCD/CuPc. On the other hand, global images of bisPTCD mixed films of CoPc, ZnPc and H_2Pc indicated phase separation. Since the spatial resolution of the image technique is ca. 1 μm^2, the clarification of homogeneous is within that resolution limit. At the same time there is no direct spectroscopic evidence of molecular mixing in the co-evaporated films.

9.3. ThioPTCD-Pc Mixed Films

9.3.1. Absorption and Fluorescence

The important issue here is the presence of the sulfur atom attached to the perylene ring and its effect on the mixed-film formation ability with the same Pc molecules used in the case of bisPTCD. The absorption spectrum of a thin solid film of thioPTCD, evaporated on KBr disc, contains absorption bands characteristic of the perylene moiety that were observed at 449, 480 and 519 nm, shown in Figure 9.3.1-1. A comparative analysis of the electronic absorption maxima of the 10 nm thioPTCD-Pc mixed films to that of a 10 nm thioPTCD thin film indicates that the thioPTCD-Pc mixed films absorption spectra contain the characteristic absorption bands of both the perylene and phthalocyanine species. The phthalocyanine Soret band was observed in the 300-390 nm spectral region for all thioPTCD-Pc mixed films. In all the thioPTCD-Pc mixed films investigated the 0,2 vibronic transition band, characteristic of the perylene moiety, appeared red shifted relative to that observed in thin solid films of neat thioPTCD at 449 nm, with the exception of thioPTCD/ClGaPc and thioPTCD/ClInPc (Figure 9.3.1-1) in which this band was blue shifted. The 0,1 transition band of the perylene chromophore was observed only in thioPTCD mixed films of ClInPc, CoPc, CuPc and ZnPc, and all were red-shifted compared to the 0,1 band in thin films of pure thioPTCD observed at 480 nm, with the exception of thioPTCD/ClInPc in which it was blue-shifted. The perylene 0-0 electronic transition band was observed in all thioPTCD mixed films and appeared red shifted to that of the characteristic 0-0 band of the pure thioPTCD observed at 519 nm. The exceptions to this trend were mixed films of thioPTCD/ClInPc and thioPTCD/ZnPc in which the transition band was blue shifted. Surprisingly the

characteristic phthalocyanine Q-band was only observed in thin mixed films of thioPTCD/ZnPc at 688 nm. It is important to notice the changes in the absorption spectra that confirm its dependence on the long-range structure of the film. A similar phenomenom is responsible for the changes observed in the absorption spectra of phthalocyanines induced by solvents. The absorption spectrum of thioPTCD/ClInPc mixed thin film is shown in Figure 9.3.1-1.

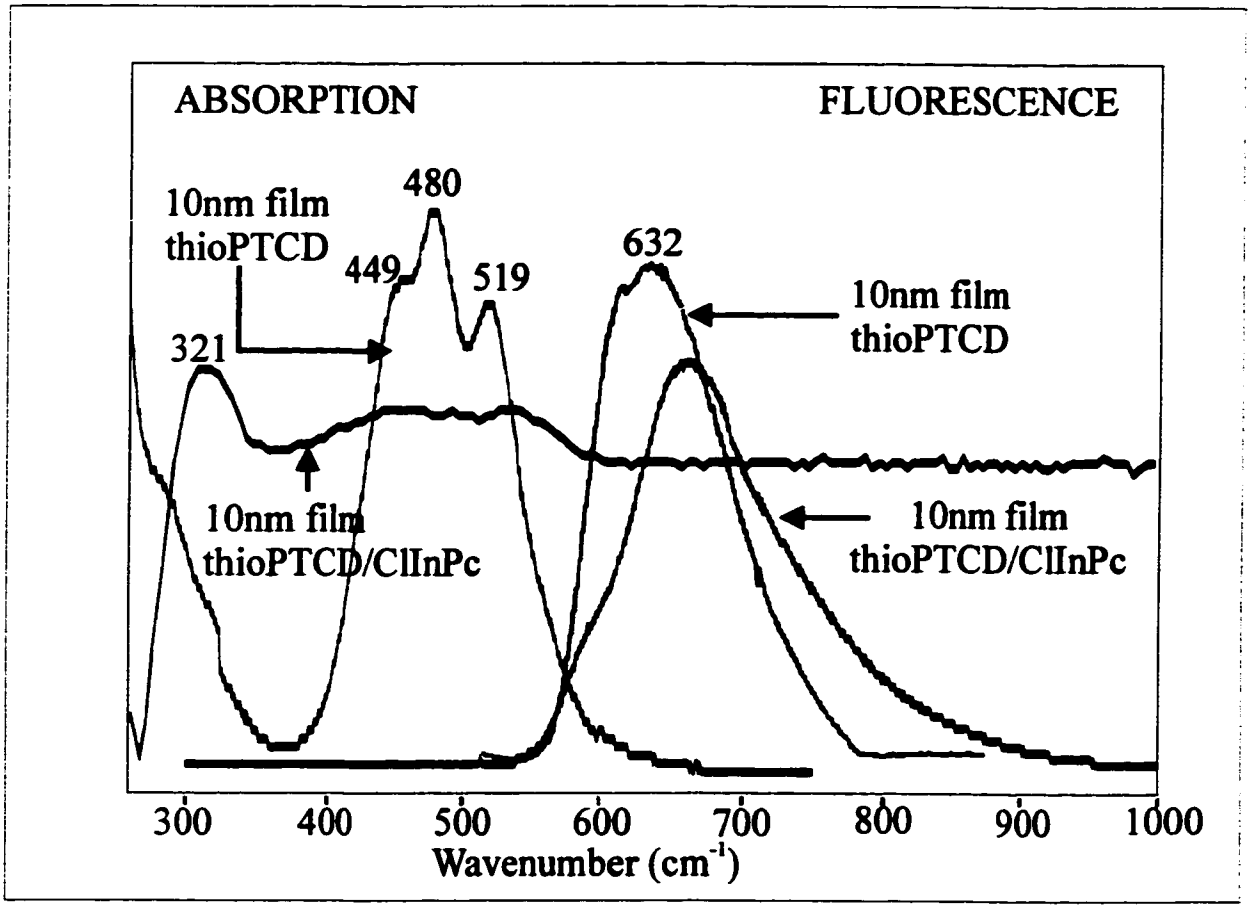

Figure 9.3.1-1: Electronic absorption and emission spectra of thin films of thioPTCD and thioPTCD/ClInPc.

The fluorescence spectrum of thin solid films of thioPTCD shows the typical broad emission band centered at 632 nm, as seen in Figure 9.3.1-1. The emission spectra of all thioPTCD-Pc mixed films investigated had maxima that were red shifted to that observed for thin films of pure thioPTCD at 632 nm. The emission spectrum of thioPTCD/ClInPc thin film is shown in Figure 9.3.1-1.

A broad structure-less silver plasmon absorption band was observed for all silver island films coated with mixed films of thioPTCD-Pc studied, with the exception of thioPTCD/ZnPc. The plasmon maxima of silver island films coated with thioPTCD mixed films containing ClGaPc, ClInPc, CoPc and CuPc appeared red shifted to that observed in silver island films coated with the respective pure phthalocyanine films. The absorption spectra of the silver plasmon of silver island films coated with both ClInPc and thioPTCD/ClInPc are shown in Figure 9.3.1-2. Unlike other thioPTCD mixed films studied, the silver absorption plasmon of silver islands films coated with thioPTCD/ZnPc (Figure 9.3.1-2) contained unresolved bands characteristic of both perylene and phthalocyanine. On deconvolution of the absorption spectrum of the mixed film of thioPTCD/ZnPc on silver, the perylene absorption bands were observed at 465 and 522 nm, while the phthalocyanine bands were at 354, 594 and 672 nm.

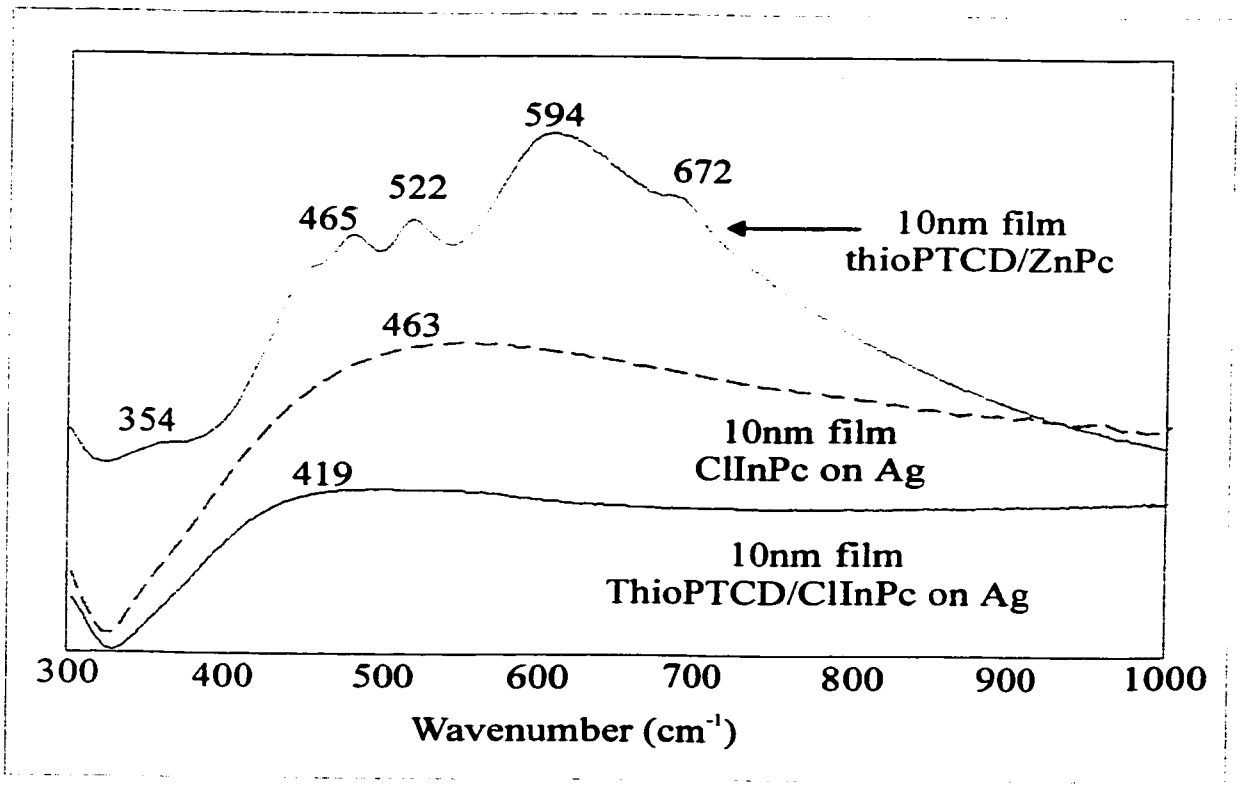

Figure 9.3.1-2: Electronic absorption of the silver plasmon of thin solid films of ClInPc, thioPTCD/ClInPc and thioPTCD/ZnPc.

9.3.2. Raman and Surface enhanced Raman

Similar to the discussion of the Raman and surface enhanced Raman spectra of bisPTCD, the analysis of the Raman spectra of thioPTCD-Pc mixed films is confined to the vibrational bands of the perylene moiety as to gauge the influence the MPc molecule on the molecular properties of thioPTCD. The thioPTCD/ClInPc mixed system is taken here as a study case representative of the other system and is used as a reference point for discussion.

The RRS and SERRS spectra of the mixed film thioPTCD/ClInPc were obtained with the 514.5 nm laser line and are presented in Figure 9.3.2-1. As in the bisPTCD/ClInPc mixed film, the most intense bands observed are attributed to the

perylene moiety at 553, 1075, 1255, 1388, 1449, 1579, 1596 and 1695 cm^{-1} respectively. The vibrational assignments of these bands have already been reported in a Chapter 6 [120]. The SERRS spectrum of the mixed thioPTCD/ClInPc film mimics that of the RRS spectrum, with no relative shifts in frequencies alluding to the absence of a strong interaction of the dyes with silver. The RS of the mixed film of thioPTCD/ClInPc taken with the 780 nm laser line is presented in Figure 9.3.2-1. The RS spectrum of the mixed films contains characteristic frequencies of both thioPTCD and ClInPc, and like the bisPTCD/ClInPc film the most intense perylene vibrations are observed at 526, 1047, 1298, 1354, 1433 and 1569 cm^{-1}. Normailizing the spectra with the ring distortion band of the perylene moiety at 526 cm^{-1}, an analysis similar to that performed for the bisPTCD-Pc mixed films was done on the collected Raman spectra. A comparison of the RRS to the RS spectra of thioPTCD/ClInPc films, indicates a splitting of the ring stretching vibration at 1569 cm^{-1} in the RS spectrum to two bands at 1579 and 1596 cm^{-1} in the RRS spectrum. The presence of a doublet at 1569 cm^{-1} in the RRS spectrum is further supported by the FWHM values, which is twice the width of the 526 cm^{-1} band. The SERS spectrum of the mixed film, obtained with the 780 nm line, is also shown in Figure 9.3.2-1. The SERS (780 nm) spectrum is similar to the RS spectrum, and the perylene bands are observed at: 1699,1622, 1579, 1440, 1397, 1314, 1082 and 547 cm^{-1}. A comparison of the RS to SERS (780 nm) spectra of thioPTCD/ClInPc mixed films indicates an increase in the relative intensities of the C-H bending vibration at 1047 cm^{-1} and the ring stretching vibrations at 1298 and 1433 cm^{-1}. Moreover, in the SERS (780 nm) spectrum the full width at half maximum (FWHM) remained constant for all vibrational bands with the exception of 1440 and 1579 cm^{-1}, for which it doubles for the

1440 (indicating overlapping bands) and halves for the 1579 cm^{-1} bands (hinting at the disappearance of an overlapping band).

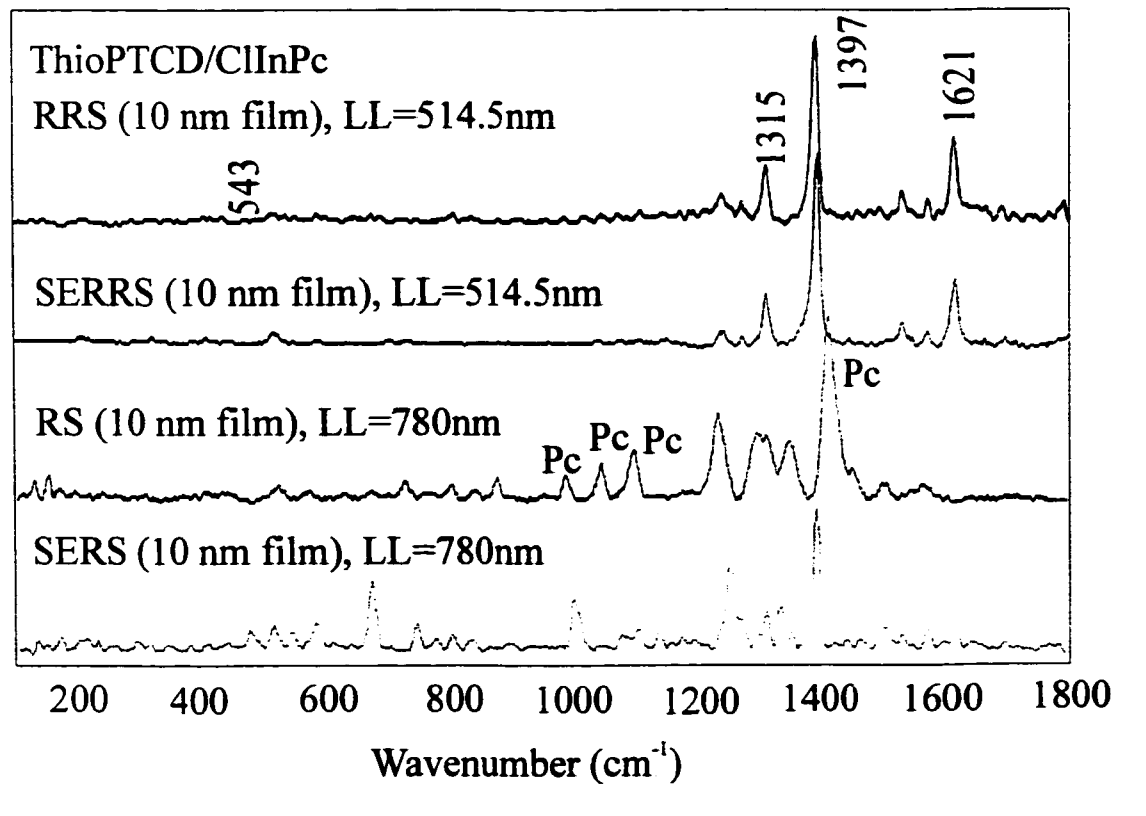

Figure 9.3.2-1: SER(R)S, RRS and Raman scattering spectra of thin solid films of thioPTCD/ClInPc.

A comparative analysis of the SERRS spectrum to the RRS spectrum of thioPTCD/ClInPc mixed films indicates an increase in the relative intensity of the perylene ring stretching vibration at 1255 cm^{-1} and the C=C stretching vibration at 1596 cm^{-1} for the SERRS spectrum. The relative intensities of the C-H bending vibration at 1075 cm^{-1} and ring stretching vibrations at 1388, 1449 and 1579 cm^{-1} decreased in the SERRS spectrum with respect to the RRS spectrum. Investigation of the FWHM

bandwidths reveals no apparent change, with the exception of the 1255 and 1388 cm^{-1}, where they increase and decrease respectively in the SERRS spectrum when compared to the RRS spectrum.

A similar approach in analysis was utilized for the other thioPTCD/MPc mixed films studied. Comparative to the bisPTCD/ClInPc mixed film, the influence of MPc on the molecular properties of thioPTCD in the mixed films is greater, though less defined. This trend is evident in all the thioPTCD-Pc systems investigated. The most noteworthy system is the thioPTCD/CoPc mixed films, in which there are huge relative intensity deviations when comparing the RRS to SERRS and the RS to RRS spectra. Surprisingly, comparison of the RS to RRS spectra of thioPTCD/CoPc mixed films reveals no change in FWHM. Comparisons of the changes in relative intensities and FWHM between the RRS and SERRS (Figure 9.3.2-2A & 9.3.2-2B) and the RS and RRS spectra (780 nm, Figure 9.3.2-2C & 9.3.2-2D) of the 10 nm thioPTCD-Pc mixed films are shown in Figure 9.3.2-2. Comparisons of the changes in relative intensities and FWHM between the RS and SERRS spectra of the thioPTCD-Pc mixed films (Figure 9.3.2-3A & 9.3.2-3B) and that of a pure 10 nm thioPTCD thin film (Figure 9.3.2-3C & 9.3.2-3D) are shown in Figure 9.3.2-3. As with the bisPTCD-Pc systems, the RS-SERRS data from the mixed films appear to follow the same trend as observed in the RS-SERRS data of the pure thioPTCD thin film. In the case of the resonance Raman spectra, the differences between the intensities of the neat films against the mixed film can be due to the observed changes in the electronic absorption induced by mixing as explained above.

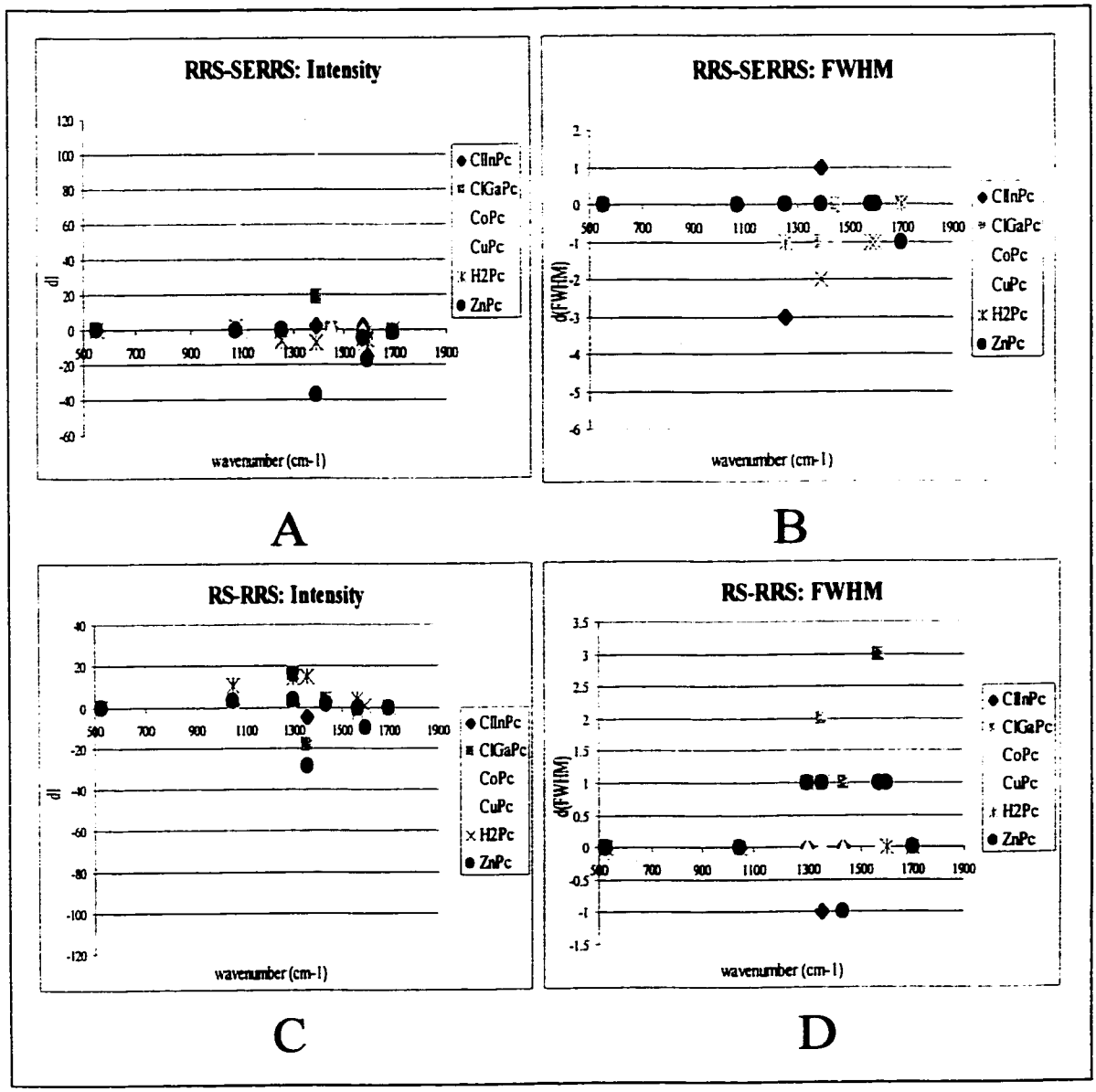

Figure 9.3.2-2: Relationship of the changes in relative intensities and FWHM of characteristic perylene wavenumbers between the RRS and SERRS spectra (A, B) and between the RS and RRS (C, D) spectra of thioPTCD-Pc mixed films.

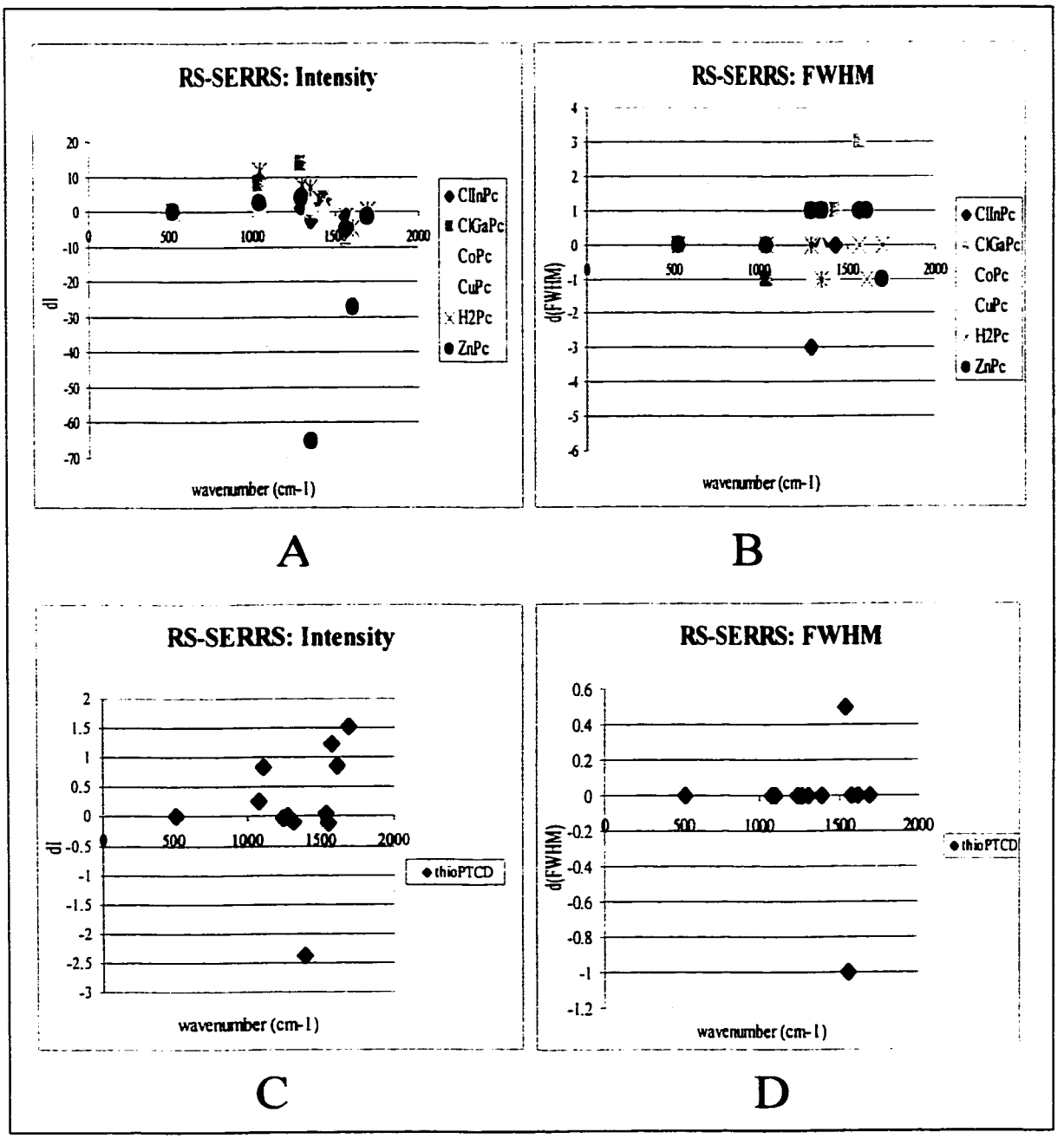

Figure 9.3.2-3: Relationship of the changes in relative intensities and FWHM of characteristic perylene wavenumbers between the RS and SERRS spectra of thioPTCD-Pc mixed films (A, B) and pure thioPTCD film (C,D).

9.3.3. SERRS Imaging of thioPTCD-Pc Mixed films

The global images of thioPTCD-Pc on silver island films were obtained using the 633 nm laser line and captured using the filtered Raman scattered light of the fundamental vibrational wavenumber at 1302 cm^{-1}, for perylene, and 676 cm^{-1}, for phthalocyanine. The global images of a 10 nm thin film of thioPTCD/ClInPc mixed film, exhibiting the distribution of perylene (Figure 9.3.3-1A) and phtahlocyanine (Figure 9.3.3-1B) in the film is shown in Figure 9.3.3-1. The thioPTCD/ClInPc film presents a homogeneous distribution (within a micrometer resolution) of both the thioPTCD and ClInPc in the mixed film.

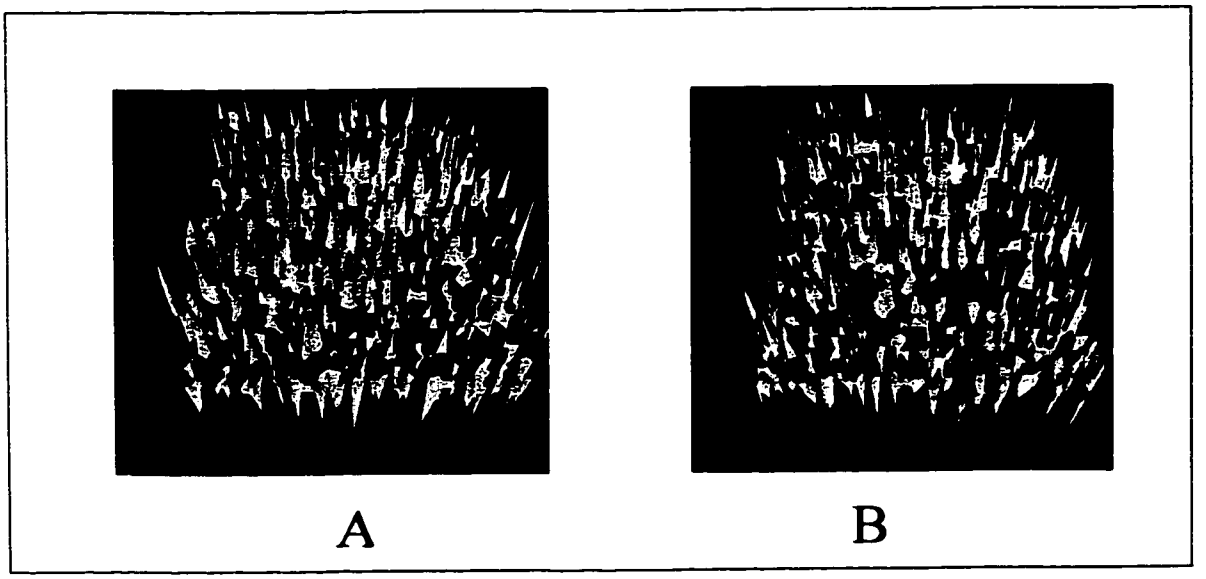

Figure 9.3.3-1: Global field images of a 10 nm ThioPTCD/ClInPc mixed film showing the distribution of perylene (A) and phthalocyanine (B).

Similarly, global images of thioPTCD mixed films of ClGaPc and CuPc exhibited a homogenous distribution of both perylene and phthalocyanine in the films. While in the mixed films of thioPTCD/CoPc, thioPTCD/H_2Pc and thioPTCD/ZnPc the phase

separation in the distributions of perylene and phthalocyanine can be distinguished. This lack of homogeneity is more pronounced in the thioPTCD-Pc films than comparative bisPTCD-Pc thin films and indicates a greater degree of phase separation of thioPTCD and phthalocyanine in the thioPTCD-Pc mixed films investigated.

The point-to-point line scan and area map of a 10 nm thin film of thioPTCD/ClInPc taken with the 633 nm laser is given in Figure 9.3.3-2. The cross section of the line scan is also shown in Figure 9.3.3-2 and is the SERRS spectrum of the thioPTCD/ClInPc mixed film on 6 nm silver islands.

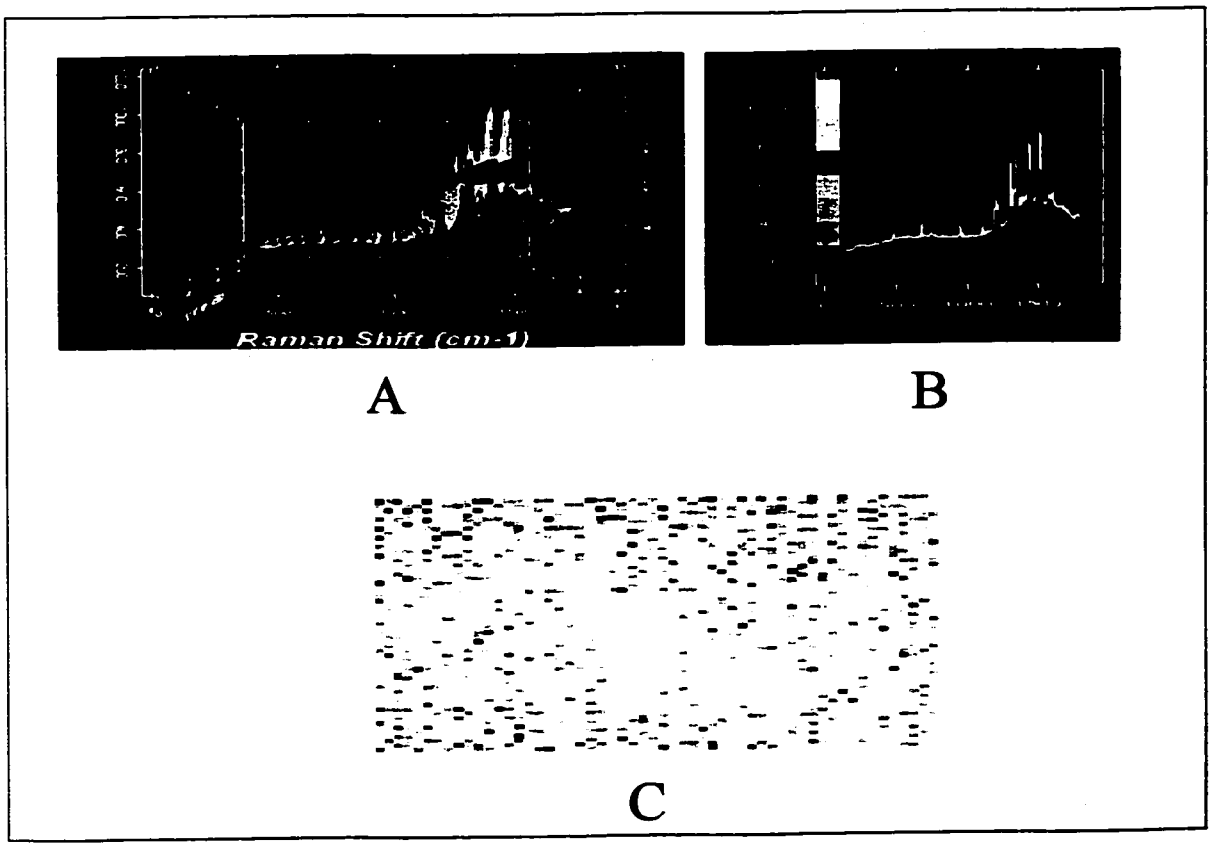

Figure 9.3.3-2: Point-to point line scan (A) and cross-section (B) of thioPTCD/ClInPc mixed film. Point-to-point area map of thioPTCD/ClInPc mixed film (C).

9.3.4. Summary

In summary, mixed films of thioPTCD and phthalocyanine can be fabricated successfully using co-evaporation. The spectral properties of these thioPTCD -Pc mixed films: RS, RRS and SER(R)S have been probed here for the first time. The Raman spectra progress from a predominantly perylene characteristic to reflect that of the film mixture as the laser lines are scanned from 514.5, 633 to 780 nm respectively. Investigation of the band positions and bandwidths of characteristic perylene bands in the mixed films indicate that both dyes do not inetract strongly with the silver surface. Moreover, the mixing affects the electronic absorption of the dyes and correspondingly changes are seen in the RRS or SERRS spectra compared to the neat films of phthalocyanine or thioPTCD. The global images of the mixed thioPTCD-MPc films reveal an on-average homogeneous distribution of both perylene and phthalocyanine for mixed films of bisPTCD/ClInPc, bisPTCD/ClGaPc and bisPTCD/CuPc. Homogeneous here does not mean molecular mixing. In fact, the images indicate mixing of aggregates of each material rather than molecular mixing. Global images of thioPTCD mixed films of CoPc, ZnPc and H_2Pc indicated a good degree of phase separation, as was also found in some of the mixed films of bisPTCD-Pc.

UV-VIS absorption and fluorescence emission spectra of the thioPTCD/ZnPc mixed films indicates the possibility of energy transfer between thioPTCD and ZnPc, since the emission band of pure thioPTCD overlaps the zinc phthalocyanine Q-absorption band at 688 nm.

Chapter 10

CONCLUSIONS

The work presented in this thesis can claim three main contributions. The factors that may allow one to control the molecular organization in PTCD films, preparation and characterization of mixed PTCD/Pc films and the application of SERRS imaging as an analytical technique for phase separation studies are shown.

The successful fabrication of submicron thin molecular films of six novel perylene tetracarboxylic acid derivatives by vacuum evaporation was demonstrated. Fabrication of thin molecular films was also achieved by Langmuir Blodgett techniques. The electronic absorption, emission and vibrational spectra were obtained to provide a complete spectroscopic characterization of the thin solid films. The well-suited reflection-absorption infrared spectroscopy was applied to determine the molecular orientation in the fabricated films. The molecular orientation of bisPTCD in thin films on Ag was shown to be head-on relative to the substrate, as extracted from the surface selection rules provided by RAIRS. Thermal annealing induces a molecular re-orientation and the perylene tetracarboxylic ring becomes oriented face-on to the substrate. Encapsulation studies suggest that molecular re-orientation is initiated through penetration of the thin molecular film by small polar molecules that interact with the polar moieties of bisPTCD. The change in morphology under annealing was also affirmed by AFM investigations.

In an attempt to control molecular orientation of other perylene derivatives in thin molecular films, a new class of thio-derivatives was developed and investigated. Both thioPTCD and trithiaPTCD have sulfur atoms incorporated into the backbones of the perylene chromophore. RAIRS studies indicated that thioPTCD is oriented edge-on to the substrate, whereas trithiaPTCD maintains a head-on tilted orientation. Raman scattering

and SERS data suggest that both molecules are physisorbed onto silver island films. Surface-enhanced infrared (SEIR) spectra were also obtained for thin solid films of thioPTCD, and enhancement factor of 5 and 10 for island films on tin and silver respectively, were demonstrated. The fabrication of a mixed Langmuir Blodgett monolayer consisting of thioPTCD and arachidic acid was successful and surface enhanced resonance Raman spectra and SERRS line scanning for this monolayer are reported.

Thio-perylene derivatives that contained sulfur atoms in the alkyl chains of the perylene chromophore were also investigated in addition to thioPTCD and trithiaPTCD. A predominant head-on molecular orientation relative to the substrate was found in the molecular organization of thin solid films of at least two of the three thio-derivatives, 3sPTCD and 2(3s)PTCD. Preferential molecular orientation is not as evident in 2sPTCD and suggests that long-range packing is not predominant in thin films of this dye. SERRS studies of the thin molecular films of these materials also showed that the molecules were physisorbed onto the substrate. SERRS imaging and mapping of the thin films on silver island films were obtained by defocusing ca. 1 mW of laser power on a 40 μm^2 surface area. The feasibility of SERRS global imaging with low laser powers is demonstrated here and later applied to mixed films studies.

Thin molecular mixed films of bisPTCD and MPc (M = Co or Cu) co-deposited onto several substrates were characterized using SERS (LL = 780 nm) and SERRS. SERRS spectroscopy allows selective characterization of each component by tuning the incident wavelength into the resonance absorption of the dye. The latter was achieved using the 514.5 nm laser line to display the perylene chromophore and the 633 nm line

for the phthalocyanine component. It is shown that using SERRS imaging phase separation studies (degree of mixing studies) in mixed films is a powerful analytical technique. The technique applied to bisPTCD/CoPc shows a lower degree of mixing relative to mixed films of bisPTCD/CuPc.

In the course of the investigation, the resonance Raman spectroscopy of CoPc and CuPc provided some interesting data on overtones and progressions of combinations bands in thin films of the neat materials.

Since the spectroscopic data on mixed films is very limited, the trends associated with surface enhanced resonance Raman scattering and imaging of mixed thin solid films of perylene and phthalocaynine were investigated within a series of PTCD-MPc combinations. For mixed films of bisPTCD-MPc, electronic spectra indicate that there is a potential for energy transfer between the perylene and phthalocyanine chromophores. A study of the progression of characteristic perylene chromophore bands in the mixed films with SERS reveals that bisPTCD is physisorbed to the substrate and there is minimal molecular interaction between perylene and phthalocyanine. Raman global imaging and mapping showed a homogenous distribution of both PTCD and MPc for mixed films of bisPTCD/ClInPc, bisPTCD/ClGaPc and bisPTCD/CuPc.

Mixed films of thioPTCD and MPc, displayed similar characteristics to that of mixed films of bisPTCD-MPc. Mapping the characteristic vibrational bands of the thioPTCD chromophore in the mixed films, similar to that of bisPTCD-MPc films, showed that thioPTCD is physisorbed to the substrate with minimal molecular interaction between constituents of the mixed films. Furthermore, Raman global images of the

mixed films revealed a higher phase separation in mixed films of thioPTCD/CoPc, thioPTCD/ZnPc and thioPTCD/H_2Pc.

REFERENCES

[1] K.-Y. Law, *Chem. Rev. 93* (1993) 429.

[2] B. Gregg, *J. Phys. Chem. 100* (1996) 852.

[3] H. G. Lohmannsroben, H. Langhals, *Appl. Phys. B 48* (1989) 449.

[4] B. Elvers, J. Arpe, W. Gerhartz, , *Vol. 20*, VCH Publishers, New York 1992.

[5] H. Yanagi, N. Tamura, S. Taira, H. Furuta, S. Douko, G. Schnurpfeil, D. Wohrle, *Mol. Cryst. Liq. Cryst. Sci. Technol. A 267* (1995) 435.

[6] C. W. Tang, S. A. Van Slyke, *Appl. Phys. Lett. 51* (1987) 913.

[7] M. K. Debe, *J. Vac. Sci. Technol. 21* (1982) 74.

[8] R. Aroca, A. K. Maiti, Y. Nagao, *J. Raman Spectrosc. 24* (1993) 227.

[9] J. D. Joannapoulos, R. D. Meade, J. N. Winn, *Photonic Crystals: Molding the Flow of Light*, Princeton University Press, New Jersey 1995.

[10] P. S. Vincett, Z. D. Popovic, C. McIntyre, *Thin Solid Films 82* (1981) 357.

[11] D. Smith, *Thin Solid Film Deposition, Principles and Practice*, McGraw-Hill Inc., New York 1995.

[12] A. Schmidt, T. J. Schuerlein, G. E. Collins, N. R. Armstrong, *J. Phys. Chem. 99* (1995) 11770.

[13] T. Schmitz-Hubsch, T. Fritz, R. Staub, A. Back, N. R. Armstrong, K. Leo, *Surface Science 437* (1999) 163.

[14] V. Shklover, F. S. Tautz, R. Scholz, S. Sloboshanin, M. Sokolowski, J. A. Schaefer, E. Umbach, *Surface Science 454-456* (2000) 60.

[15] J. R. Sheats, H. Antoniadis, M. Hueschen, W. Leonard, J. Miller, R. Moon, D. Roitman, A. Stocking, *Science 273* (1996) 884.

[16] P. E. Burrows, V. Bulovic, S. R. Forrest, L. S. Sapochak, D. M. McCarty, M. E. Thompson, *Appl. Phys. Lett. 65* (1994) 2922.

[17] H. Aziz, Z. Popovic, S. Xie, A.-M. Horr, N.-X. Hu, C. P. Tripp, G. Xu, *Appl. Phys. Lett. 72* (1998) 756.

[18] A. Kam, R. Aroca, J. Duff, C. P. Tripp, *Chem. Mater. 10* (1998) 172.

[19] H. Aziz, Z. Popovic, C. P. Tripp, N.-X. Hu, A.-M. Horr, G. Xu, *Appl. Phys. Lett. 72* (1998) 2642.

[20] B. H. Loo, *Chem. Phys. Lett. 89* (1982) 346.

[21] C. J. Sandroff, D. R. Herschbach, *J. Phys. Chem. 86* (1982) 3277.

[22] Y. H. Yim, K. Kim, M. S. Kim, *J. Phys. Chem. 94* (1990) 2552.

[23] D. Lamoen, P. Ballone, M. Parrinello, *Phys. Rev. B. 54* (1996) 5097.

[24] H. Hirose, A. Khan, V. Aristov, P. Soukiassian, V. Bulovic, S. R. Forrest, *Phys. Rev. B 54* (1996) 748.

[25] Y. Hairma, K. Yamashita, H. Ishii, K. Seki, *Thin Solid Films 366* (2000) 237.

[26] L. F. Veiros, J. Morgado, *Mol. Cryst. Liq. Cryst. 333* (2000) 259.

[27] J. C. Conboy, E. J. C. Olsen, D. M. Adams, J. Kerimo, A. Zaban, B. A. Gregg, P. F. Barbara, *J. Phys. Chem. B. 102* (1998) 4516.

[28] C. W. Tang, *Appl. Phys. Lett. 48* (1986) 183.

[29] S. R. Forrest, L. Y. Leu, F. F. So, W. Y. Yoon, *J. Appl. Phys. 66* (1989) 5908.

[30] J. Danzinger, J.-P. Dodelet, P. Lee, K. W. Nebesny, N. R. Armstrong, *Chem. Mater. 3* (1991) 821.

[31] M. Hiramoto, H. Fujiwara, M. Yokoyama, *Appl. Phys. Lett. 58* (1991) 1062.

[32] U. Beckers, O. Stenzel, S. Wilbrandt, U. Falke, C. von Borczyskowski, *J. Phys. Condens. Matter 10* (1998) 1721.

[33] A. Schmidt, L.-K. Chau, V. S. Valencia, N. R. Armstrong, *Chem. Mater. 7* (1995) 657.

[34] Rudiono, F. Kaneko, M. Takeuchi, *Appl. Surface Sci. 142* (1999) 598.

[35] T. Kudo, M. Kimura, K. Hanabusa, H. Shirai, *J. Porphyrins and Phthalocyanines 2* (1998) 231.

[36] H. G. Kjaergaard, B. R. Henry, *J. Phys. Chem. 99* (1995) 899.

[37] J. J. Cox, T. S. Jones, *Surface Science 457* (2000) 311.

[38] K. Petritsch, R. H. Friend, A. Lux, G. Rozenberg, S. C. Moratti, A. B. Holmes, *Synthetic Metals 102* (1999) 1776.

[39] M. K. Debe, *Progress in Surface Science 24* (1987) 1.

[40] G. Exarhos, N. Hess, *J. Raman Spec. 27* (1996) 765.

[41] R. Aroca, E. Johnson, A. Maiti, *Appl. Spec. 49* (1995) 466.

[42] K. Akers, R. Aroca, A. M. Hor, R. O. Loufty, *Spectrochim. Acta 44A* (1988) 1129.

[43] R. K. Chang, T. E. Furtak, *Surface Enhanced Raman Scattering*, Plenum Press, New York 1982.

[44] S. Nie, S. R. Emory, *Science 275* (1997) 1102.

[45] K. Kneipp, Y. Wang, R. R. Dasari, M. S. Feld, *Appl. Spec. 49* (1995) 780.

[46] G. Roberts, , Plenum Press, New York 1990.

[47] G. L. Gaines Jr., *Thin Solid Films 68* (1980) 1.

[48] G. L. Kovacs, P. S. Vincett, J. H. Sharp, *Can. J. Phys. 63* (1985) 346.

[49] G. Munger, R. M. Leblanc, *Rev. Sci. Instrum. 51* (1980) 710.

[50] J. DeSaja, *M.Sc. Thesis Dissertation*, University of Windsor, Windsor, Ontario 1996.

[51] D. Battisti, *Ph.D. Thesis Dissertation*, University of Windsor, Windsor, Ontario 1992.

[52] F.-L. F. B. Manual, (1987) .

[53] L. Eckertova, *Physics of thin Films*, Plenum Press, New York 1986.

[54] D. A. Skoog, J. J. Leary, *Principles of Instrumental Analysis*, Saunders College Publishing, New York 1992.

[55] www.varianinc.com/osi/us/products/cary50.htm, .

[56] P. W. Atkins, *Quanta-A Handbook of Concepts*, Oxford University Press, Oxford 1991.

[57] R. Inc., , Renishaw Inc. 2000.

[58] B. D. T. Manual, , Bomem Inc. 1986.

[59] C. P. Tripp, M. L. Hair, *Appl. Spec. 46* (1992) 100.

[60] D. A. Guzonns, M. L. Hair, C. P. Tripp, in D. R. Scheuing (Ed.): *Fourier Transform Infrared Spectroscopy in Colloid and Interface Science* 1990.

[61] J. T. Yates, T. E. Madey, *Vibrational Spectroscopy of Molecules on Surfaces*, Plenum Press, New York 1987.

[62] R. L. McCreery, *Raman Spectroscopy for Chemical Analysis, Vol. 157*, John Wiley & Sons Inc., New York 2000.

[63] G. Binnig, C. F. Quate, C. H. Gerber, *Phys. Rev. Lett. 56* (1986) 930.

[64] S. Alexander, L. Hellemans, O. Marti, J. Schneir, V. Elings, P. K. Hansma, M. Longmire, J. Gurley, *J. Appl. Phys. 65* (1989) 164.

[65] G. Binnig, D. P. E. Smith, *Rev. Sci. Instrum. 57* (1986) 1688.

[66] R. S. Howland, , Park Scientific Instruments 1993.

[67] J. E. Griffith, G. L. Miller, C. A. Green, D. A. Grigg, P. E. Russell, *Rev. Sci. Instrum. 62* (1991) 2167.

[68] H. Ximen, P. E. Russell, *Ultramicroscopy 42* (1992) 1526.

[69] http://spm.aif.ncsu.edu/tutorial.htm, .

[70] J. M. Duff, A. M. Hor, R. O. Loufty, A. R. M. Eleryk, *Chem. Functional. Dyes 2* (1992) 564.

[71] Y. Nagao, *Prog. in Org. Coatings 31* (1997) 43.

[72] C. W. Tang, *US Patent 4,281,053*, US 1981.

[73] B. A. Gregg, J. Sprague, M. W. Peterson, *J. Phys. Chem. B 101* (1997) 5362.

[74] L. Alcacer, J. Morgado, R. T. Henriques, M. Almeida, *Synthetic Metals 70* (1995) 1093.

[75] M. Hiramoto, T. Imahigashi, M. Yokoyama, *Appl. Phys. Lett. 64* (1994) 187.

[76] J. R. Ostrick, A. Dodabalapur, L. Torsi, A. J. Lovinger, E. W. Kwock, T. M. Miller, M. Galvin, M. Berggren, H. E. Katz, *J. Appl. Phys. 81* (1997) 10.

[77] H. Yanagi, Y. Toda, T. Noguchi, *J. Appl. Phys. 34* (1995) 3808.

[78] R. M. Hochstrasser, *Can. J. Chem. 39* (1961) 451.

[79] R. M. Hochstrasser, *J. Chem. Phys. 40* (1964) 2559.

[80] M. Adachi, Y. Murata, S. Nakamura, *J. Phys. Chem. 99* (1995) 14240.

[81] D. Weiss, R. Kietzmann, J. Mahrt, B. Tufts, W. Storck, F. Willig, *J. Phys. Chem. 96* (1992) 5320.

[82] M. Adachi, Y. Nagao, *Chem. Mater. 11* (1999) 2107.

[83] A. K. Dutta, K. Kamada, K. Ohta, *Langmuir 12* (1996) 4158.

[84] T. Maki, H. Hashimoto, *Bull. Chem. Soc. Jpn. 25* (1952) 411.

[85] T. I. Solomentseva, V. I. Rogovik, T. A. Chibisove, V. F. Traven, B. I. Stepanov, *Zh. Org. Khim. 22* (1986) 1050.

[86] J. Duff, A. M. Hor, A. R. Melnyk, D. Teney, *SPIE Hard Copy and Printing Materials, Media and Process 1253* (1990) .

[87] E. Spietschka, H. Troster, *US Patent 4,709,029*, US 1987.

[88] H. Troster, *Dyes and Pigments 4* (1983) 171.

[89] W. B. Cheston, *Elementary theory of Electric and Magnetic Fields*, John Wiley and Sons, New York 1964.

[90] S. A. Francis, A. H. Ellison, *J. Opt. Soc. Am. 49* (1959) 131.

[91] H. Pickering, H. Eckstrom, *J. Phys. Chem. 63* (1959) 512.

[92] R. G. Greenler, *J. Chem. Phys. 44* (1966) 310.

[93] O. Heavens, *Optical Properties of Thin Solid Films*, Dover Publications Inc., New York 1991.

[94] D. Halliday, R. Resnick, *Fundamentals of Physics*, John Wiley and Sons, New York 1991.

[95] G. W. Poling, *J. Colloid Interface 34* (1970) 365.

[96] A. S. Davydov, *Quantum Mechanics*, Pergamon Press 1965.

[97] M. Born, E. Wolf, *Principles of Optics*, Pergamon Press, Oxford 1975.

[98] J. C. Decius, R. M. Hexter, *Molecular Vibrations in Crystals*, McGraw-Hill, New York 1977.

[99] A. Kam, R. Aroca, J. Duff, *Proceedings of the XVth International Conference on Raman Spectroscopy*, John Wiley and Sons, Pittsburgh 1996.

[100] E. Johnson, R. Aroca, *Langmuir 11* (1995) 1693.

[101] A. K. Maiti, R. Aroca, Y. Nagao, *J. Raman Spectrosc. 24* (1993) 351.

[102] E. Lifshitz, A. Kaplan, E. Ehrenfreund, D. Meissner, *J, Phys. Chem. 102* (1998) 967.

[103] S. Rodriguez-Llorente, R. Aroca, J. Duff, *Spectrochimica Acta A 55* (1999) 969.

[104] A. Hartstein, J. R. Kirtley, J. C. Tsang, *Phys. Rev. Lett. 45* (1980) 201.

[105] R. Aroca, S. Rodriquez-Llorente, *Asian J. Phys. 7* (1998) 391.

[106] M. Osawa, K. Ataka, K. Yoshii, Y. Nishikawa, *Appl. Spectrosc. 47* (1993) 1497.

[107] R. Aroca, B. Price, *J. Phys. Chem. 101* (1997) 6537.

[108] G. A. Bowmaker, L. C. Tan, *Aust. J. Chem. 32* (1979) 1443.

[109] T. H. Joo, M. S. Kim, K. J. Kim, *J. Raman Spectrosc. 18* (1987) 57.

[110] S. D. Evans, T. L. Freeman, T. M. Flynn, D. N. Battchelfelder, A. Ulman, *Thin Solid Films 244* (1994) 778.

[111] M. Moskovits, *J. Chem. Phys. 77* (1982) 4408.

[112] R. Mercadante, M. Trsic, J. Duff, R. Aroca, *J. Mol. Struc. (Theochem.) 394* (1997) 215.

[113] J. Kummerden, A. Leitner, H. Brunner, F. R. Aussenegg, A. Wokaun, *Mol. Physics. 80* (1993) 1031.

[114] P. J. Tarcha, J. DeSaja-Gonzalez, S. Rodriguez-Llorente, R. Aroca, *J. Appl. Spectrosc. 53* (1999) 43.

[115] A. P. Scott, L. Radom, *J. Phys. Chem. 100* (1996) 16502.

[116] M. W. Wong, *Chem. Phys. Lett. 256* (1996) 391.

[117] R. Aroca, C. J. L. Constantino, *Langmuir 16* (2000) 5425.

[118] X. M. Yang, D. A. Tryk, K. Ajito, K. Hashimoto, A. Fujishima, *Langmuir 12* (1996) 5525.

[119] E. Johnson, R. Aroca, *Applied Spectrsocopy 49* (1995) 472.

[120] A. Kam, R. Aroca, J. Duff, C. P. Tripp, *Int. J. Vib. Spectrosc. [www.ijvs.com] 4* (2000) 6.

[121] A. Kam, R. Aroca, J. Duff, *Submitted to Chemistry of Materials* (2000) .

[122] M. J. Stillman, T. Nyokong, *Phthalocyanines: Properties and Applications*, VCH Publishers Inc., New York 1989.

[123] R. Aroca, N. Pieczonka, A. P. Kam, *J. of Porphyrins and Phthalocyanine 5* (2001) 25.

[124] K. Akers, *M.Sc. Thesis Dissertation*, University of Windsor, Windsor, Ontario 1987.

[125] R. M. Hochstrasser, C. A. Nyi, *J. Chem. Phys. 72* (1980) 2591.

[126] C. Jennings, R. Aroca, A. M. Hor, R. O. Loufty, *Anal. Chem. 56* (1984) 2033.

[127] R. Aroca, G. J. Kovacs, *Surface Enhanced Raman Spectroscopy in Vibrational Spectra and Structure.*, Elsevier, Amsterdam 1991.

[128] R. Aroca, Z. Q. Zeng, J. Mink, *J. Physics and Chemistry of Solids 51* (1990) 135.

[129] A. Napier, R. A. Collins, *Thin Solid Films 248* (1994) 166.

[130] F. Ambrosino, S. Califano, *Spectrochimica Acta 21* (1965) 1401.

[131] K. Akers, R. Aroca, A. M. Hor, R. Loufty, *J. Phys. Chem. 91* (1987) 2955.

[132] E. Johnson, R. Aroca, *Can. J. Chem. 69* (1991) 1728.

VITA AUCTORIS

Alicia Patricia Kam was born in Port-Of-Spain, Trinidad, on the 9th June 1974. She attended Dunross Preparatory Primary School. At the age of 12 years, she attended Providence Girl's Catholic School and then at 14 years attended St. Joseph's Convent High School, where she completed both O'Level and A'Level examinations.

In 1992, she moved to Montreal Quebec, Canada, where she enrolled in the Chemistry Program at McGill University and graduated with a Bachelor's of Science in 1995. Upon graduation, she took a Research Assistant Position at the McGill Pulp and Paper Research Centre for six months. In the winter of 1996, she enrolled at the University of Windsor, Windsor Ontario, Canada as a Ph.D. graduate student. She has since been conducting research in the Materials and Surface Science Group in the Department of Chemistry and Biochemistry, under the supervision of Dr. Ricardo Aroca.

LIST OF PUBLICATIONS

- A.P. Kam, R. Aroca, J. Duff, Perylene Tetracarboxylic-Phthalocyanine mixed thin solid films. Surface enhanced resonance Raman Scattering Imaging Studies. Chemistry of Materials (*submitted*)

- A. Kam, R. Aroca, J. Duff, Spectroscopic Characterization and SERS of a Novel Thio-derivative of Perylene: n-propylimido- (2-methylmercaptoethylimido) perylene. Materials Chemistry (*submitted*)

- R. Aroca, N. Pieczonka, A.P. Kam, Surface enhanced scattering and SERS imaging of phthalocyanine mixed films. Journal of Porphyrins and Phthalocyanines, 2001, 5, 25

- A. Kam, R. Aroca, J. Duff, C.P. Tripp, Thin solid films and surface enhanced vibrational spectra of Thio-bis (n-propylimido) perylene. Int. Journal of Vibrational Spectroscopy, 2000, 4(2), 6

- A. P. Kam, R. Aroca, J. Duff, C.P. Tripp, The role of water in the molecular re-orientation on thermal annealing of Bis (n-propylimido) perylene films. Langmuir, 2000, 16(3), 1185-1188.

- A. Kam, R. Aroca, J. Duff, C.P. Tripp, Evolution of the molecular organization in Bis (n-propylimido) perylene films under thermal annealing. Chemistry of Materials, 1998, 10(1), 172-176.

- Dr. D.G. Gray and Alicia Kam, Chiral Properties of Thin Wood Sections, Holzforchung, 1997, 51(1), 1-5.

CONFERENCES

PRESENTATIONS

- A. Kam, R. Aroca, J. Duff, C.P. Tripp, "The Spectroscopic Characterization, Langmuir Blodgett Films and Chemisorption on Metal Surfaces of a Novel Perylene Derivative: Thio-bis (n-propylimido) perylene".
  44th International Conference on Analytical Sciences and Spectroscopy (ICASS), Kingston, Ontario, Canada, August 1998

- A. Kam, R. Aroca, J. Duff, C.P. Tripp, "Solid State Morphology of Thin Solid Films on thermal annealing"
  43rd International Conference on Analytical Sciences and Spectroscopy (ICASS), Montreal, Quebec, Canada, August 1997.

POSTERS

- A. Kam, R. Aroca, J. Duff, "Spectroscopic Characterization and SERS of novel thio-derivatives of perylene tetracarboxylic acid".
  FACSS, Vancouver, British Columbia, Canada, October 1999.

- A. Kam, R. Aroca, J. Duff, C.P. Tripp, "Evolution of Three Bis-Tetracarboxylic Acid Anhydride Derivatives Under Thermal Annealing".
  CSC National Conference, Windsor, Ontario, Canada, June 1997.

- A. Kam; R. Aroca, J. Duff, "Resonance and Surface Enhanced Resonance Raman Spectra of Thio-Perylene Derivatives"
  ICORS, Pittsburgh, Pennsylvania, United States, August 1996.